CREEP BEHAVIOUR OF SOIL NAIL WALLS IN HIGH PLASTICITY INDEX (PI) SOILS

A Dissertation

by

MOHSEN MAHDAVI KHARANAGHI

Submitted to the Office of Graduate and Professional Studies of
Texas A&M University
in partial fulfillment of the requirements for the degree of

DOCTOR OF PHILOSOPHY

Chair of Committee,	Marcelo Sanchez
Committee Members,	Jean-Louis Briaud
	Stefan Hurlebaus
	Christopher C. Mathewson
Head of Department,	Robin Autenrieth

December 2015

Major Subject: Civil Engineering

Copyright 2015 Mohsen Mahdavi Kharanaghi

ABSTRACT

An aspect of particular concern in the soil nail wall manual and construction guideline, Geotechnical Engineering Circular No. 7 on Soil Nail Walls, is the creep behavior of soil nail systems in high-plasticity clays. This research is aimed to gain a better understanding of the long-term behavior of the soil nail walls in fine-grained soil with plasticity index more than 20. Experimental and numerical investigations are performed in this Ph.D. work in the context of a research project funded by Texas Department of Transportation (TxDOT).

Field investigation consisted of pullout tests at the National Geotechnical Experimental Site (NGES) at Texas A&M University; and instrumentation, monitoring and testing at the actual soil nail wall project. The tests at NGES-TAMU were focused on effect of load level on creep behavior of soil nails in a natural clay deposit with high plasticity. The tests were conducted on 10 existing anchors (installed in 1991), 16 new vertical soil nails installed in this research, and 6 sacrificial soil nails installed during the construction of an actual soil nail wall. This wall corresponded to a new project of an excavation wall in an embankment fill, in which 9 permanent soils nails were instrumented with the aim of monitoring the long term behavior of the wall and performance of the nails in high plasticity clays.

Complementary laboratory tests to learn about the creep behavior of clays involved in this research were performed at TAMU using the samples gathered from the field.

The main goal of the numerical modeling was to calibrate the constitutive models using the information gathered from the laboratory and pullout tests; and also to simulate the long-term behavior of the actual soil nail. FLAC3D was adopted in this research.

Monitoring the actual soil nail wall and the numerical modeling results revealed that the maximum horizontal deformation of the wall due to the creep of the wall for one year after the construction is less than 10% of the horizontal deformation of the wall soon after the construction. According to GEC#7, the horizontal deformation of the wall after construction usually increases up to 15% compared to the deformation observed soon after construction. As a results of this movement (i.e. due to the post-construction creep movement of the wall), additional tension load is developed in the nails. The maximum additional load in the nail one year after the construction is 50% of the axial load in the nails at the end of the construction for the bottom third of the wall. Even with additional 50% axial load, the axial load in the nails at the bottom third of the wall is less than 30% of the maximum pullout capacity of the nails.

DEDICATION

I dedicate my dissertation to my father, whose words of encouragement and support were my main source of energy and patience; to my wonderful mother, who's my main source of love and warm-heartedness; to my brothers, who's my main source of believing in a bright and great future.

ACKNOWLEDGMENTS

I am sincerely grateful to many people who helped me to complete this strenuous journey. First of all, I would like to express my cordial gratitude to my committee chair and academic advisor, Dr. Marcelo Sanchez for providing me with opportunities and shaping my career, and for his precious guidance, encouragement, and support throughout the course of this research. I would like to extend my gratitude to my committee member, Dr. Jean-Louis Briaud, who was always there to assist me in my work, answer my questions, and guide me in the right direction. I would like also to thank Dr. Stefan Hurlebaus and Dr. Christopher Mathewson for their guidance and support throughout this research. Additional thanks go to Dr. Hurlebaus for his extreme effort in instrumentation the soil nail wall.

Great thanks also go to Pooyan Razi, Reza Keshavarz, Mehdi Mohammadrajabi, Mohammad Aghahadi, Ghassan Ackrouch, Masoud Darabi, and Niloofar Hosseini (for her cooking lessons) for being great friends and for making my time in College Station unforgettable.

Last, but not least , I also would like to extend my gratitude to Texas Department of Transposition (TxDOT) and Texas Transportation Institute (TTI), which supported this research.

TABLE OF CONTENTS

Page

LIST OF FIGURES

Page

LIST OF TABLES

Page

1. INTRODUCTION

1.1. Background

Soil nailing is a convenient and economical stabilization method for the reinforcement of existing soil or excavation by installing threaded steel bars into cuts or slopes as wall construction progress from top down. In this technique, the first step to create a stable soil mass is to install grouted bars in the soil. The nailing process creates a single block of earth able to hold-back its overburden during the excavation. Afterwards, a layer of shotcrete is applied and bearing plates are installed before a final facing is put in place to complete the soil nail wall (FHWA, 1998). Construction sequence of soil nail wall system is illustrated in Figure 1-1.

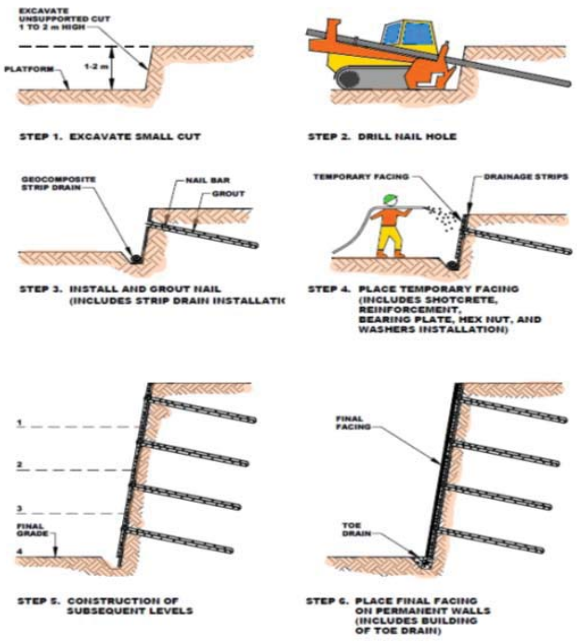

Figure 1-1. Soil nail wall sequence (after GEC#7, 2003)

Soil nail walls are becoming very popular in the US because it has been shown that soil nail walls are technically feasible, flexible, easy to modify, rapid and cost-effective alternative to conventional retaining walls used in top-to-bottom excavations in temporary and permanent applications (GEC#7, 2003). Soil nail walls have been generally used for temporary retaining structures. However, the use of soil nail walls as a permanent structure has increased substantially in the last few years (GEC#7, 2003).

In 1985, a National Research Project, Clouterre (i.e. clou=nail, terre=soil), was devised to construct a full-scale soil nail wall, taken to failure. Clouterre lies in the fact that three fully instrumented experiments involving soil nail walls were built and monitored from construction to failure. The objective of the Clouterre project was a better knowledge of the behavior of soil nail walls, determination of the limitations of the method, and an elaboration in the design recommendation. (Plumelle et all., 1990). These five years of research led to publish a French Specifications entitled Recommendations Clouterre 1991. In 1993, Federal Highway Administration (FHWA) sponsored an English version of this recommendation. In 1996, FHWA published a design manual of soil nail wall, manual for design and construction monitoring of soil nail walls. This manual was then revised in 1998. In November 2003, the FHWA published an updated version of the manual published in 1998, which is known as "Geotechnical Engineering Circular No. 7".

1.2. Motivation

An aspect of particular concern in the "Geotechnical Engineering Circular No. 7 on Soil Nail Walls" is the creep behavior of the soil nail systems in high plasticity Index (PI) clays. Since there were not enough information on creep behavior of soil nail systems

in high PI clay, this matter was addressed in this manual based on some practices in fine-grained soil with PI more than 20 which exhibited unfavorable creep. Potential issues associated with the construction of soil nail walls in high PI clay are included in this manual for fined-grained soil with Plasticity Index (PI) more than 20. Obtaining a better understanding of the behavior of soil nail walls in fine-grained soil is the main motivation of this research.

1.3. Objectives

A quite large number of observations can be found in GEC#7 for projects involving soil nail walls in high PI clays. However, for projects in Texas dealing with high PI clays, Texas Department of Transportation (TxDOT) has successfully limited the bond strength of the soil nail to a "safe" load level, reducing the potential of creep behavior and the associated long term deformations. The validation of a design approach for soil nail walls in those types of profiles is necessary because high PI clays are very common in Texas. Furthermore, a relatively new application of soil nailing that is becoming very popular in Texas is related to the construction of the "Texas Turn Around". In these applications, soils nails are commonly used in the constructions of walls under piled bridge abutments.

In general terms, when dealing with soil nail walls in high PI clays two main different issues can be associated with creep effects:

A. Problems associated with local (or internal) effects related to creep behavior of nails. These issues are related to effect of creep on the bonding strength between the grouted nails and the clay.

B. Problems associated with the long term behavior of the creeping soil mass. The lateral movement of the soil mass that may occur due to the creep of clay will be reflected in an increase in the load in the nails.

1.4. Research Approach

To address the problem associated with load level on creep behavior of the nails, pullout tests were performed to gain a better understanding of creep behavior of soil nails in high plasticity clay (PI>20), and determine the effect of load level on creep behavior in these type of soil. These pullout tests consisted of tests on existing anchors installed in 1991 at National Geotechnical Experimentation Site, the Texas A&M University (NGES-TAMU) clay site. In addition, 16 vertical soil nails were installed in context of this research at NGES-TAMU clay site to conduct the pullout test with different load protocol and creep tests at different load levels. Furthermore, 6 sacrificial nails were installed at different heights of actual soil nail wall (i.e. emergency slope repair project at Beaumont district) to perform the pullout test at different confining stresses and determine the creep load threshold for the permanent nails.

To address the problem associated with the creep behavior of the soil mass, emergency slope repair project at Beaumont district was instrumented and monitored under the operation condition (i.e. service load) for period of 15 months after construction. The PI of the embankment material is around 50; which made this project a very attractive option for the field tests and monitoring. Horizontal movements of the wall, load distribution in the nails, service load in the nails, load change in the nails due to the excavations during construction, and due to the creep after the construction, nail loads at

the wall face, and change in temperature and water content of the embankment were obtained after monitoring the wall.

Finally, to thoroughly investigate the creep behavior of soil nail wall in high plasticity clay, this research combined experimental and numerical studies. A number of computational tools were used to investigate the performance of soil nail walls in high-plasticity clay. FLAC 3D was used to simulate the time-dependent (creep) behavior of soil nail wall during and after construction. The advantages of using FLAC3D in this research are multiple, among others: it is a well-known and validated code for geotechnical problems involving excavations, it allows the modeling of soil nails, a large variety of creep models are available in this software (e.g. eight creep models). The numerical code was used in the following possible analysis:

- Effect of sacrificial nail on the axial load of the production nails around it;
- Wall design/verification;
- Simulation and model calibration against the data collected in the field;
- Parametric study to cover the various cases.

Furthermore, once the numerical model was validated (using, e.g., the field data), it was used to study the behavior of soil nails walls exploring other scenarios, for example: different geometries, and ground conditions.

1.5. Significance of This Research

A good understanding of the creep behavior of soil nail wall in high PI clay, allow to use the soil nail walls in larger variety of problem involving fine-grained soil with high plasticity. It is expected that the final outcome of this research will expand and enhance

the current knowledge related to the behavior soil nails wall in high plasticity clays, and possibly will help to provide future guidelines for designing soil nail wall in high plasticity clay. The underlying aim of this research is to gain a better understanding of the time dependent behavior of soil nail wall in high plasticity clay.

1.6. Dissertation Organization

This dissertation is organized into seven sections. Section one provides the introduction and identifies the problem statement, objectives, motivations, and the significance of this research. Section two covers the literature review on the soil nail wall. This section provides the fundamentals of the creep behavior of the soil, different models to predict the creep behavior, case studies and observation of using soil nail wall as the stabilization method in high plasticity clay.

The third section presents the instrumentation design of the pullout test at National Geotechnical Experimental Site (NGES) at Texas A&M University, and instrumentation and long-term monitoring of the TxDOT project (i.e. emergency slope repair project at the Beaumont district). The instrumentation is a crucial component of this research because the data gathered from the experiments is used to gain a better understanding of the problem, and it is the basic information to calibrate the numerical models.

Section four of this dissertation is related to the loading tests at the National Geotechnical Experimental Site (NGES) at Texas A&M University and all the related activities. Two different kinds of tests were performed. Tests on existing anchors installed more than 20 years ago (with a very well-known load history), and tests on newly constructed soil nails are in the context of this research included in this section. These tests

mainly focus on studying the effect of the load level on creep behavior of soil nails in HP clays. Furthermore, all the activities at NGES are presented in this section.

Section five focuses on the instrumentation and long-term monitoring of the TxDOT soil nail wall located at the Beaumont district. The field investigations comprise two main activities; I) long-term monitoring; and II) load tests on the sacrificial nails. The main objective of the long-term monitoring is to study the creep behavior of the soil nail wall under the operational condition (i.e. service load). Horizontal movements of the wall, load distribution in the nails, service load in the nails, load change in the nails due to the excavations during construction, and due to the creep after the construction, nail loads at the wall face, and change in temperature and water content of the embankment will be obtained at the end of monitoring. To gain a better understanding of the creep behavior at different load levels, creep tests are performed at different load levels on the sacrificial nails. Since the ultimate pullout capacity and the service load of the permanent nails depend on the nail position, installing and testing the sacrificial nails at different heights are relevant.

Section six includes the numerical modeling. The main goal of the modeling is to calibrate the constitutive models using the information gathered from the laboratory and pullout tests; and also to simulate the long-term behavior of the actual soil nail at the Beaumont project and validate the model outputs with the data from wall monitoring. Once the numerical model is validated, parametric study is performed to study the behavior of soil nails walls exploring other scenarios, for example: different geometries,

and ground conditions. In addition, results of the simulation and model calibration of the unconsolidated undrained triaxial tests are presented in this section.

Section Seven concludes this research work and possible future works in this area are suggested.

2. LITERATURE REVIEW

2.1. Introduction

The concept of combining passive steel reinforcement and shotcrete started in the earliest 60's with the stabilization of rock slopes. The use of passive (i.e. no post-tensioning) steel reinforcement in the rock followed by the application of reinforced shotcrete is also a key component of the well-known and widely used New Austrian Tunneling method. The first application of soil nailing was implemented in 1972 for a railroad widening project near Versailles, France (GEC#7, 2003). Soil nails were used to stabilize an 59 ft. high slope consisting of sandy soil. This method proved to be more cost-effective, while at the same time cut down the construction time when compared to other conventional support methods.

One of the first contributions reporting the application of soil nailing in the US is related to its use to support a 45 ft. deep foundation excavation in dense silty sands. The project was related to the expansion of a Hospital in Portland, Oregon, in 1976 (FHWA, 1998). The first nailed walls were built in Texas in the mid to late 80's (Galvan, 2012). Figure 2-1 illustrates the usage of retaining walls by TxDOT. This chart is based on statistical data collected from August 2010 through September 2011 (Galvan, 2012). Over the past year approximately 500,000 L.F. of soil nail was installed on TXDOT projects.

Drilled soil nails are the most popular in the US. They consist of a steel bar placed in a pre-drilled hole and then grouted. The basics elements of a soil wall are presented in Figure 2-2, showing the main components for a zone near the nail head (GEC#7, 2003).

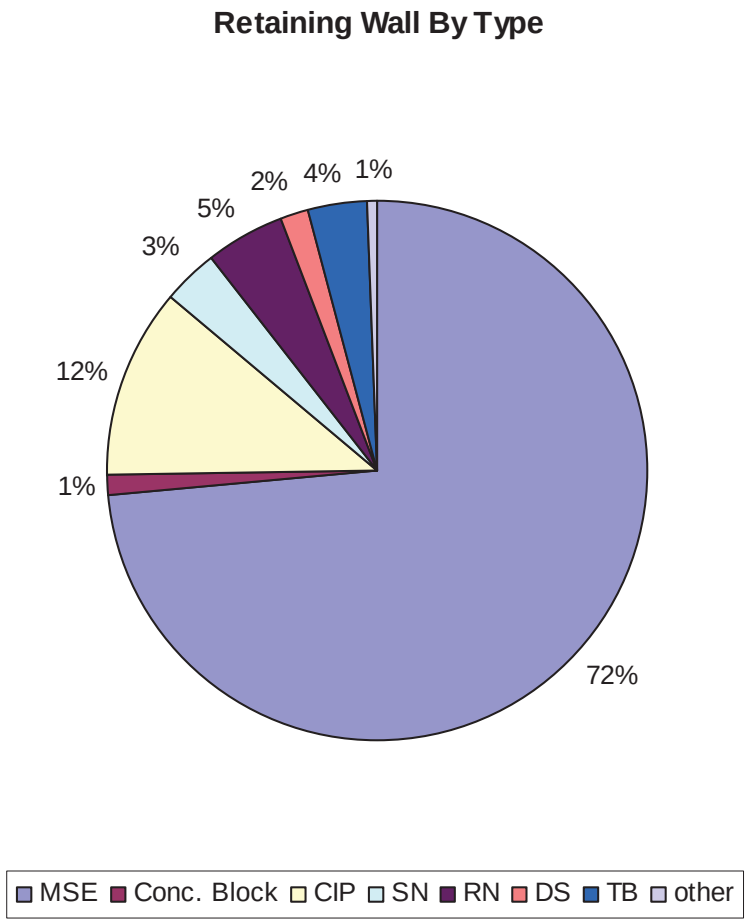

Figure 2-1. Retaining walls used by TxDOT from 08/2010 through 09/2011 (after Galvan, 2012)

Soil nails are passive elements because they are not mechanically pre-tensioned after installation (Tuozzolo, 2003). This is a difference respect to tieback anchors. During the process of excavation the earth mass supported by the soil nails tends to deform laterally and the nails are loaded (generally) in tension.

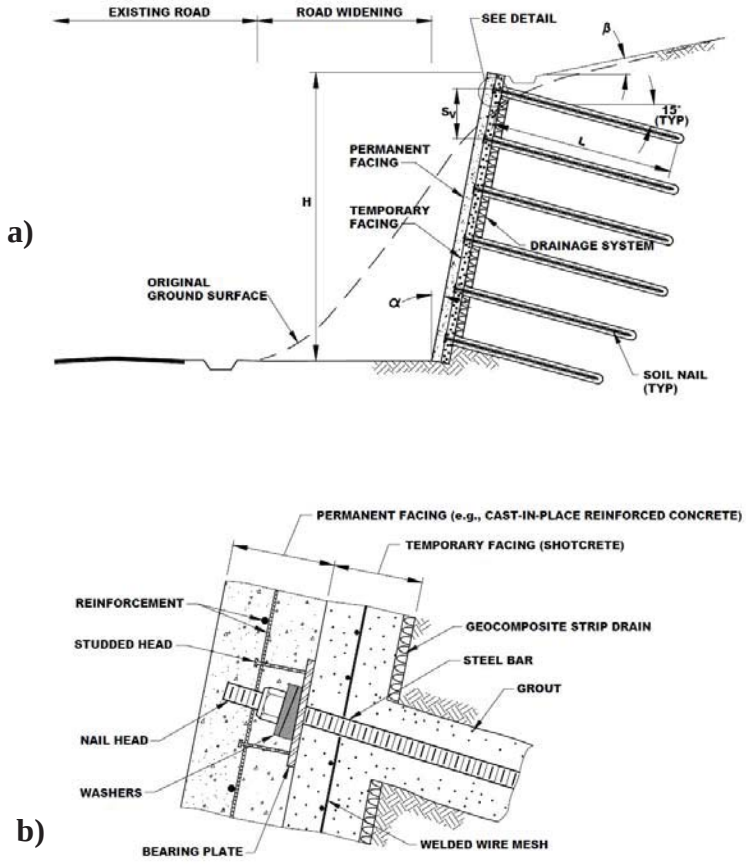

Figure 2-2. Typical cross-section of a soil nail wall, b) detail of the nail head (after GEC#7, 2003)

In this problem two main zones can be distinguished: i) the active zone, and ii) the passive zone (or resistant zone). As is illustrated in Figure 2-3, a potential failure surface separates the active and resistant zones (Geoguide 7, 2008). The active zone is the region in front of the potential failure surface, where it has a tendency to detach from the soil-nailed system. The passive zone is the region behind the potential failure surface, where

it remains more or less intact. The soil nails act to tie the active zone to the passive zone (Geoguide 7, 2008). It is important to bear in mind that the two zones configuration is a very simplified model generally adopted in limit equilibrium analyses. One limitation of this kind of analysis is that they do not account for the deformation of the soil nail system.

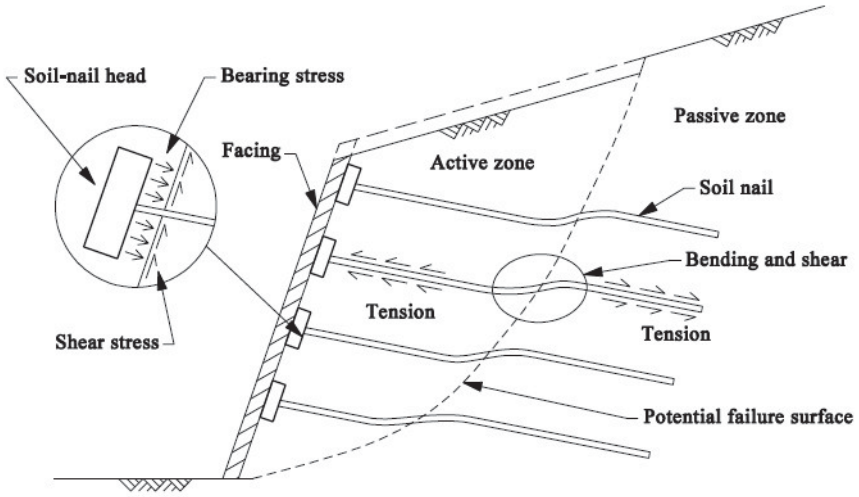

Figure 2-3. The two-zone Model of a Soil-nailed System (after Geoguide 7, 2008).

The actual nail-ground interactions are much more complex, and the forces developed in the soil nails are influenced by many factors. Those factors include, amongst others: the mechanical properties of the soil nails (e.g. tensile strength, shear strength and bending capacity); the inclination and orientation of the soil nails; the shear strength of the ground; the relative stiffness of the soil nails and the ground; the friction between the soil

nails and the ground, the size of soil-nail heads; and the nature of the slope facing (Geoguide 7, 2008).

Figure 2-4 presents schematically the typical sequence of construction for a soil nail wall using solid steel nail bars (GEC#7, 2003).

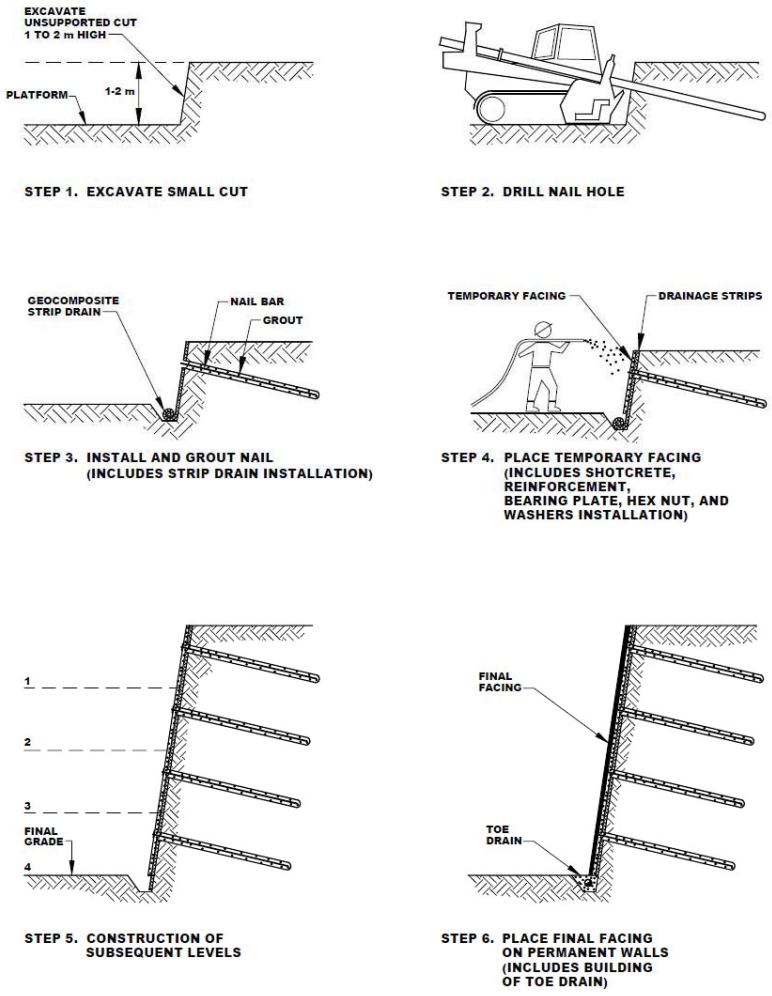

Figure 2-4. Typical Soil Nail Wall Construction Sequence (after GEC#7, 2003).

An aspect of particular concern in the "Geotechnical Engineering Circular N° 7 on Soil Nail Walls" (GEC#7, 2003) is the creep behavior of soil nail systems in high-plasticity (HP) clays (i.e. Plasticity Index (PI) >15), and the associated long term deformations. A quite large number of observations can be found in GEC#7 for projects involving soil nail walls in HP clays. The validation of a design approach for soil nail walls in those types of profiles is necessary because HP clays are very common in Texas. Furthermore, a relatively new application of soil nailing that is becoming very popular in Texas is related to the construction of the "Texas Turn Around". In this applications soils nails are commonly used in the constructions of walls under piled bridge abutments (Figure 2-5).

Figure 2-5. Typical soil nail wall solution in a "Texas Turn Around" (after Galvan, 2012).

2.2. Usage of Soil Nail Walls in Texas and TxDOT Design Method

As mentioned in Section 2.1, soil nail walls have been regularly used as possible solutions for the construction of temporary and permanent retaining walls in Texas. Table 2-1 provides information on the wall usage by TxDOT (Galvan, 2012).

Table 2-1. Wall Usage by TxDOT. August 2010 through September 2011 (after Galvan, 2012)

Wall Type	Area (ft^2)	%
MSE	3,196,417	72
Concrete block (no r/f)	47,791	1
Cantilever drilled shaft	72,286	2
Soil Nailed	146,793	3
Rock Nailed	197,216	5
Tied-back	161,827	4
Spread footing	505,019	12
Other	22,389	1

TxDOT uses this kind of solution in project involving a variety of soil types including many walls in high-plasticity clays. They are used for cuts only, in project with restricted areas (both overhead and laterally) and with adequate room for nails (Galvan, 2012). Furthermore, soil nails are generally used in the construction of unimpeded turn-around lanes under bridges where such lanes were not planned in the first place (Briaud and Lim, 1997). This is an innovative way of making the traffic flows easier in large

urban areas. This is achieved by moving the embankment slope in front of the abutment under the bridge and nailing the soil between the piles that support the abutment (Figure 2-6). The slope is typically 15 ft. meters high with a 2- horizontal to 1-vertical slant. The 30 ft. width, which is freed by this technique, gives ample room for the turn-around lane.

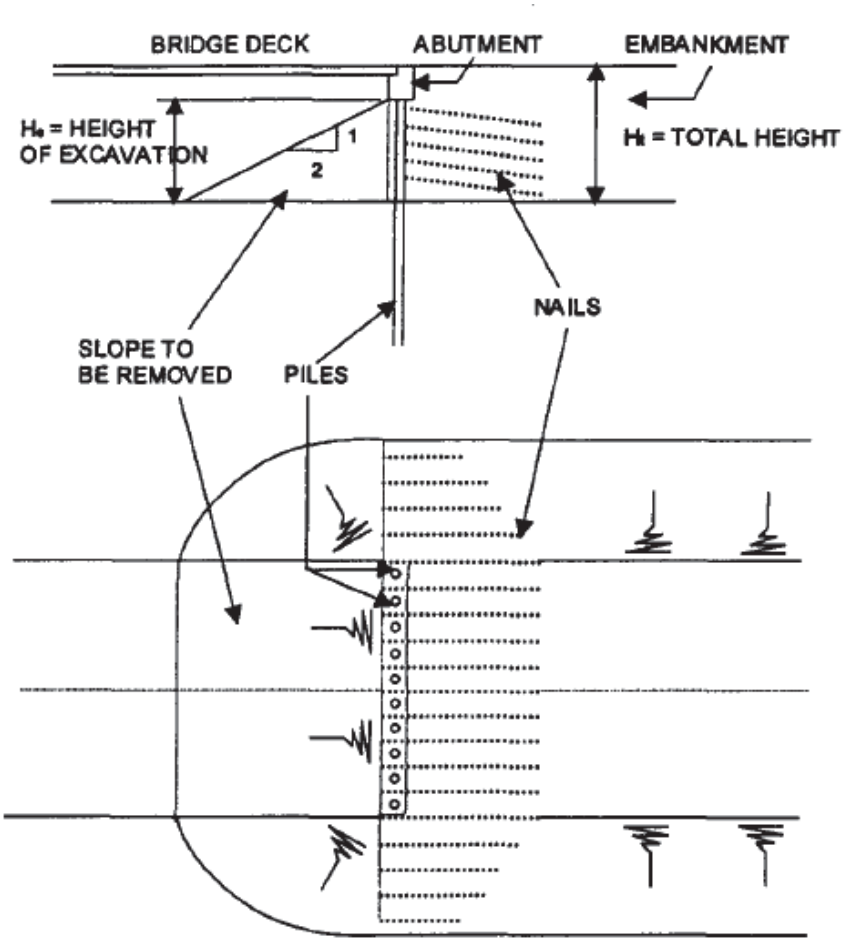

Figure 2-6. Soil-Nailed Wall under Polled Bridge Abutment (after Briaud and Lim, 1997).

Such kind of solution based on soil-nailed walls under piled bridge abutments represent a relatively new application of soil nailing that has become quite common in Texas and other states in US. In Texas, the design of such soil nail walls in existing embankments generally involves the presence of HP clays. Figure 2-7 presents the cross-section of a typical soil nail wall for an existing bridge, and a picture of a typical unimpeded turnaround. The basic information required for the design of such kind of project involving soil nail wall is (Galvan, 2012):

- Soil borings through zone to be nailed
- Cross-sections normal to wall face
- Existing bridge plans
- Roadway alignments, including tie-in to existing bridge

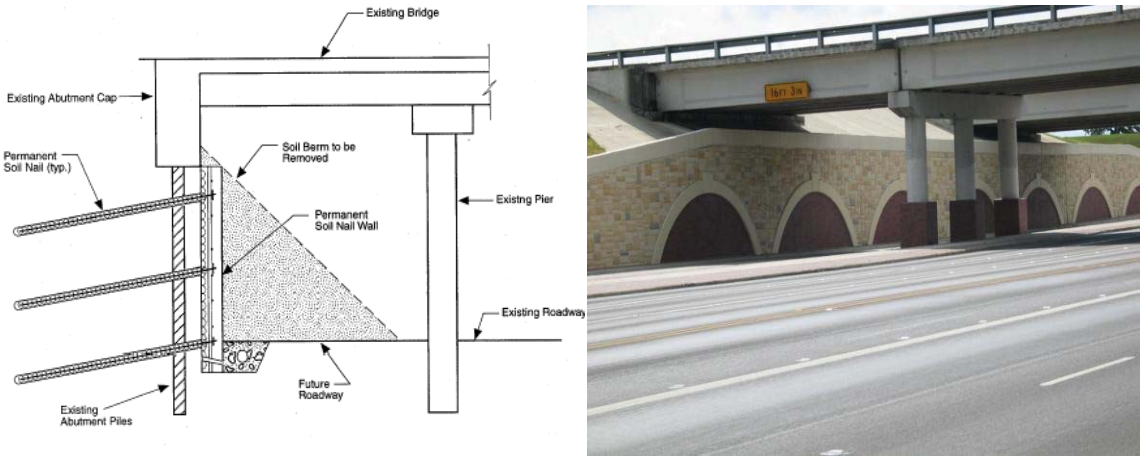

Figure 2-7. Typical soil nail wall cross section for existing bridge (after Galvan, 2012).

2.3. Guide to Soil Nail Design and Construction – Geoguide 7

The Geoguide 7 presents the recommended standard of good practice for the design, construction, monitoring and maintenance of soil-nailed systems in Hong Kong (Geoguide 7, 2008). This Geoguide summarizes the experience gained from the use of the soil nailing technique in Hong Kong, including the main findings coming from related technical works recently developed. This guideline cares specially about the effect of creeping on the stability and serviceability of the excavation, in particular if the soil nails are designed to carry sustained loads.

For soil nails designed to carry sustained loads and bonded in the soil mass, a creep test should be carried out to determine the susceptibility of the soil nails to long-term creep. Figure 2-8. illustrates the load-deformation cycle of a creep test as part of a pullout test. The procedure for a creep test is similar to the one for the pullout test except that only one loading cycle is required. T_{DL1} should be the allowable pullout resistance provided by the bond length of the cement grout sleeve of the test soil nail (Figure 2-8). T_{DL2} is the intermediate test load for a pullout test. T_{DL2} should be T_{DL1} times the factor of safety against pullout failure at soil-grout interface (FSG). The soil nail should be loaded from the initial load (T_a) to the creep test load (T_c). In creep tests T_c is coincident with T_{DL2}. The creep period should be considered to begin when T_c is applied. The load should be maintained for 60 minutes for deformation measurement. During the creep period, the measurement should be taken at time intervals of 1 minute, 3, 6, 10, 20, 30, 40, 50 and 60 minutes.

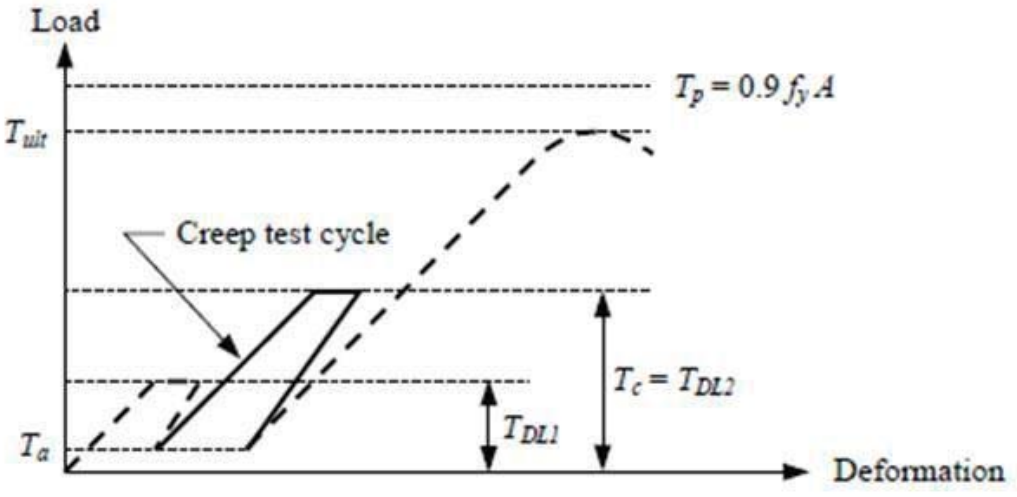

Figure 2-8. Schematic diagram of load-deformation cycle of a creep test as part of pullout test (after Geoguide 7, 2008).

A test soil nail should be considered acceptable when: *i*) the difference of soil nail movements at 6 minutes and 60 minutes during the creep period does not exceed 2 mm or 0.1 % of the bond length of the test soil nail; and *ii*) the overall trend of creep rate (i.e., soil nail movement/log time) is decreasing throughout the creep period. In the event that the acceptance criteria cannot be met by any of the creep tests, the design bond strength of the soil nails, which the creep test represents, should be reviewed and revised as needed.

2.4. Recommendations Clouterre 1991 – France

This recommendation have been compiled from studies performed by the French National Project "Clouterre" (Clou=nail, terre=soil) carried out from 1986 to 1990. Details about this work can be found in: Recommendations Clouterre, 1991; and Plumelle et al. (1990). The originality of the project Clouterre lies in the fact that three

fully instrumented experiments involving soil nail walls were built and monitored from construction to failure. The results of the clouterre program have been very useful to understand better the behavior of soil nail system. They have been published and constituted the basis for the soil-nailing design approach adopted in France. It was translated to English and printed by the Federal Highway Administration (FHWA) as report N^{o} FHWA-SA-93-026.

This recommendation states that the soil nail technique does not generally perform well in very plastic, clayey soils and very sensitive soils, particularly where there is a relatively low unit skin friction value between the soil and the inclusion. Two different kinds of pullout tests are contemplated: controlled displacement test (constant speed), and controlled force test (creep steps). With the controlled displacement pullout test, it is possible to determine the maximum pullout force (T_L), the residual force, as well as the value of the initial slope of the force displacement curve. With controlled force test, the critical creep tension (T_C) and eventually the limit tensile force (T_L) can be measured. Results from a wide number of controlled force tests in Clouterre project have allowed the development of correlations between T_L and T_C. (i.e. $k = T_L/T_C$) k values are summarized in Table 2-2.

Table 2-2. Magnitude of $k=Tl/T_C$ as a function of the type of soil and the installation method (after Recommendation Clouterre, 1991)

		$k = T_y/T_c$
GRAVITY INJECTION	Sands	1.2
	Clays	1.3
	Marls and Chalks	1.3
DRIVING	Sands	1.4

The test type known as "controlled force test" was used for creep experiments. The nail is gradually subjected to a pull-out force, which increase up to the estimated pull-out force T_{LE}. This is the nail's pullout tension estimated on the basis of geotechnical data or based on the contractor's experience. In practice is usually assessed from the controlled displacement pullout test; which is always carried out first. This force must be lower than $0.6T_G$ (i.e. the elastic limit of the reinforcement), so as to limit creep in the steel. The first loading step is applied at 0.2 T_{LE}. The displacement measurements are taken at each loading steps and performed at the following time intervals, t_0: 1 minute, 2, 3, 4, 5, 8, 10, 15, 20, 25, 30, 45, 60 minutes. Successive loading steps are applied every $0.1T_{LE}$ and are maintained during 60 minutes, except for the $0.7T_{LE}$ loading step, which is maintained for 3 hours. It is important to highlight that the creep tests were performed at constant load, a load cell was used to measure the applied load. The jack pressure was adjusted to guarantee that force required for a given loading step was actually applied.

The results were plot in decimal logarithmic scale for the time and arithmetical scale for the displacement. Typical creep curves of the pullout tests performed in this project are shown in Figure 2-9 (note that in this Figure $T_{max} = T_{LE}$). In this plot the slope α characterizes the creep curve and it can be calculated for each load step (as shown in Figure 2-9). It can be observed that for the first loading steps, the creep curves are straight lines and α (and so the creep rate) gradually increase with the load level. At higher loads, the creep curves are no longer straight lines. This experimental evidence confirms what was discussed in previous sections about the concept that creep rate in nails strongly depends on stress level. Very small creep rates were observed when the load acting in the nail was small.

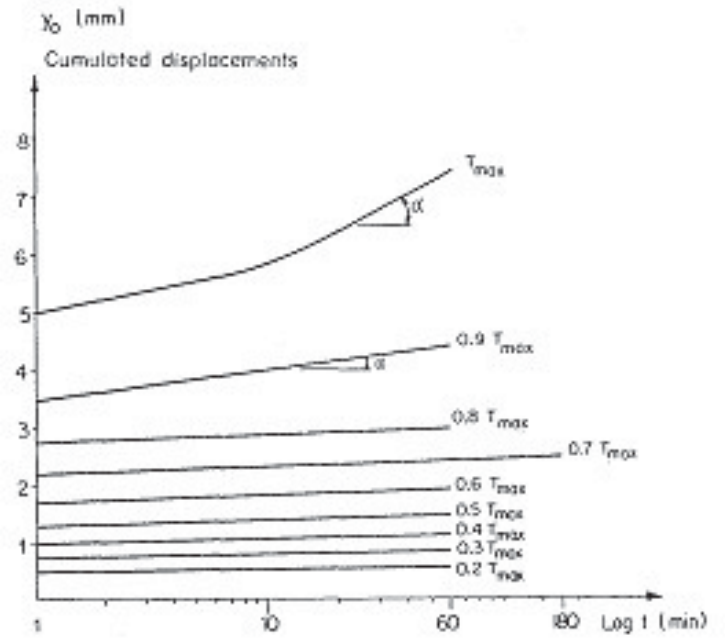

Figure 2-9. Creep curves of a pullout test (after Recommendation Clouterre, 1991).

Another useful way to present the information from the creep tests is by plotting the results as shown in Figure 2-10. From this plot, the critical creep tension T_C can be obtained. T_C corresponds to the last loading step before the curve bends. T_c' corresponds to the intersection of the two straight lines fitting the experimental data (generally $T_c \cong 0{,}9\ T_c$').

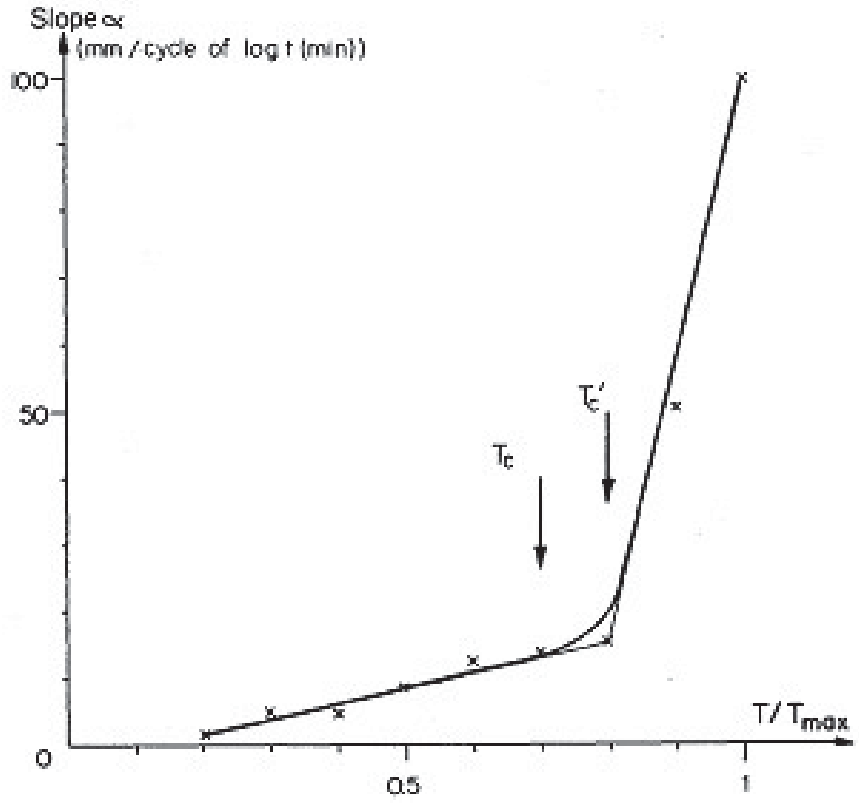

Figure 2-10. Determination of critical creep tension (after Recommendation Clouterre, 1991).

2.5. Creep Behavior of Soils

The general case of creep in soils is characterized by the three main steps shown in Figure 2-11 (Vyalov, 1986) as follows:

A. Step I: is related to a primary creep (δ^{I}); characterized by an attenuated deformation with a decreasing rate of deformation ($d\delta/dt$). The duration of this stage is generally very short.

B. Step II: known as secondary creep (δ^{II}) takes place at a constant deformation rate.

C. Step III: is associated with a tertiary creep (δ^{III}); characterized by a non-attenuated deformation, with an increasing rate of deformation.

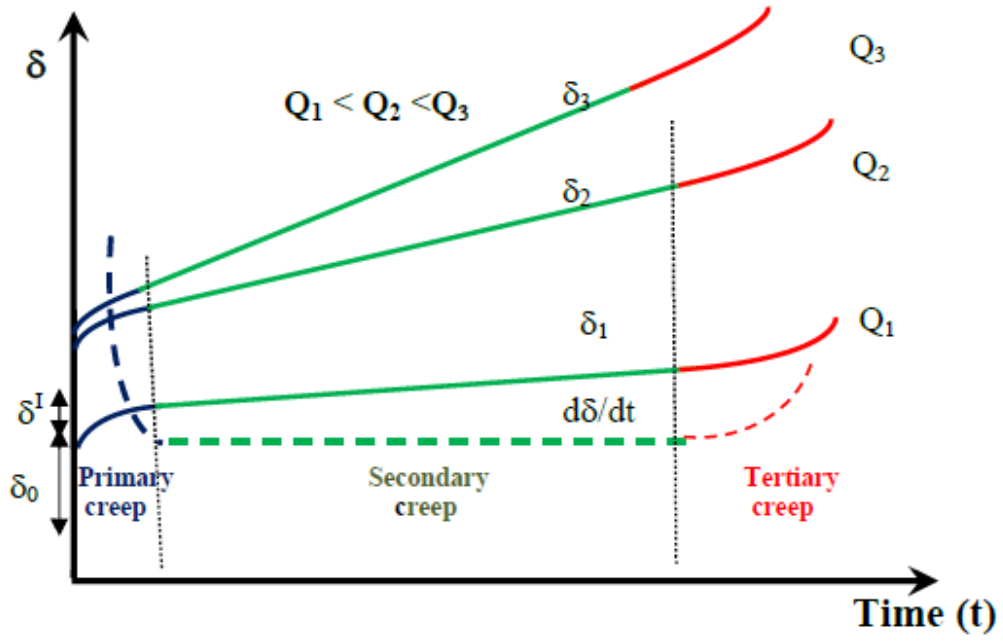

Figure 2-11. Three main steps associated with creep in soils (after Vyalov, 1986)

The actual configuration of these curves will depend on, amongst others: soil type, stress level, water content and temperature. Load level ('Q') has a predominant effect on creep behavior. Figure 2-11 illustrates the effect of different load levels (Q_1, Q_2, and Q_3) on creep. As suggested by Vyalov (1986), the different steps quoted above are generally associated with changes in the clay fabric that take place during creep (Figure 2-12). In this conceptual model is assumed that the soil fabric is composed by clay particles, aggregates and pores.

Before loading, the orientation of the clay particles and aggregates is random. Once the load is applied, stress concentration occurs near the aggregates (at the contact points), bonds are broken and the particles tend to be oriented in the direction of the load. At this point the material starts to creep at an increasing rate. Generally the breaking of the bonds starts at the weakest point of the soil structure. Therefore, after some re-arrangements of the soil particles, the soil structure tends (generally) to a more stable skeleton (obviously, this condition will depend on dry density and strength of the material). If the stress level is low, the new re-arrangement of the soil particles is capable of equilibrating the external load, and so the movement is attenuated in time and, under certain circumstances, the creep may eventually stop. This step corresponds to what is known as primary creep.

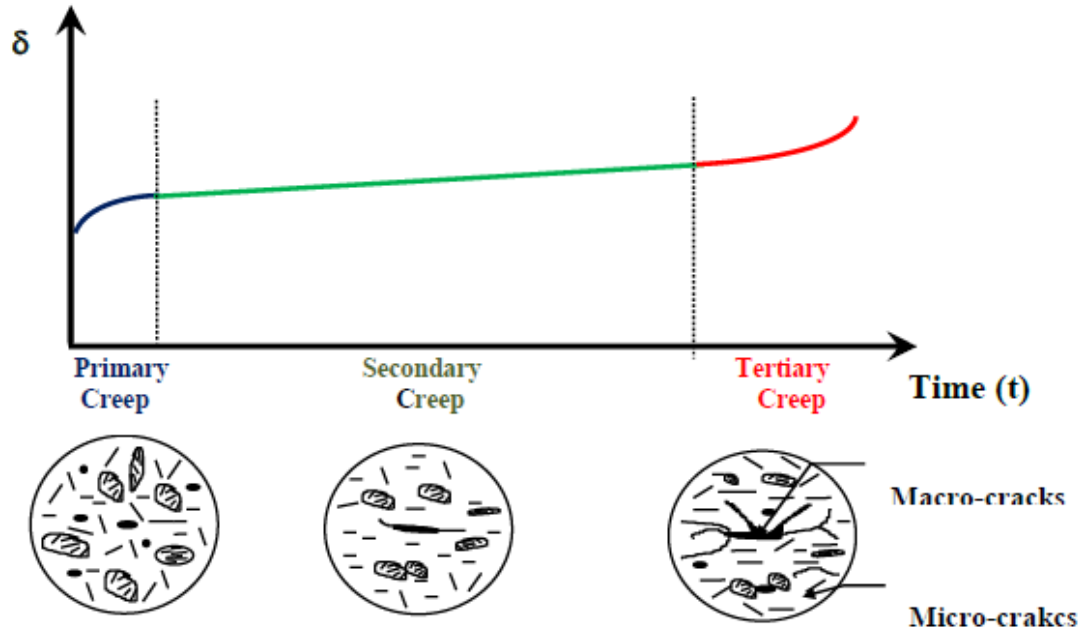

Figure 2-12. Changes in the soil fabric during creep (after Vyalov, 1986)

However, if the stress level is such that after the initial re-arrangement of the soil particles (described above) the modified soil structure cannot equilibrate external stresses, the material will continue creeping. This step corresponds to the secondary creep, where the re- arrangement and re-orientation of the soil particles take place at a constant creep rate. It could happen that after important deformations some micro-cracks may develop. Those micro-cracks affect the strength of the soil, leading to a stage of non-attenuated strain rate with the big changes in the soil structure and with the formation of macro-cracks.

A proper geotechnical design must prevent tertiary creep to be developed at any time of the earth-structure lifetime. It has also to assure that the constant creep rate (i.e.

Step II) is below the maximum one established in the guidelines. The total deformation at a given time can be calculated as the instantaneous deformation (δ_0), plus the one related to Step 1 (δ^I), plus the strain rate associated with Step II ($d\delta^{II}/dt$) times the elapsed time (Δt). This is because the (short) time related to 'Step I' is generally disregarded.

$$\delta = \delta_0 + \delta^I + d\delta^{II}/dt \times \Delta t \qquad (2.1)$$

Note that the graphs presented in Figure 2-11 and Figure 2-12 are very general and aimed at explained the basics of creep in soils and the main patterns of behavior typically observed in soils. In practice, it is quite common to plot creep tests in semi-log scale (i.e. displacements versus log time) or log scale (i.e. log displacement versus log time); as it is explained below.

Similar behavior and stages can be anticipated in the problem to be studied in this project. It is important to bear in mind that the creep movement of the soil nail can be regarded as the sum of different contributions, amongst others: creep of the steel nail, the progressive (relative) movement of the grout, and the creep of the soil itself.

The creep behavior of soils has been a matter of especial interest in geotechnical engineering, different models have been proposed in the last few years. As an example of a creep law, the model proposed by Pestana and Whittle (1995) is briefly introduced below.

Pestana and Whittle (1995) proposed a nonlinear compression model for freshly deposited cohesionless soils that assumes that specimens loaded from different formation densities approach a unique response at high stresses. This limiting

compression curve (*LCC*) is characterized by a linear relationship in log (*e*) – log(σ') space

$$\log(e) = -\rho_c \log(\frac{\sigma_v'}{\sigma_{vz}'}) \tag{2.2}$$

where ρ_c= compressibility index; and σ'= reference effective stress at unit void ratio (e=1.0).

Pestana and Whittle (1998) proposed later on a simple extension of the compression model to account for time-dependent creep deformations. The *LCC* regime is characterized by parallel isochronous compression lines, which are analogous to the secondary compression models for cohesive soils

$$\log(e) = -\rho_c \log\left[\frac{\sigma_v'}{\sigma_{vr}'(t_{ref})}\right] - \rho_a\left(\frac{t}{t_{ref}}\right) \tag{2.3}$$

Where ρ_a is a creep rate coefficient that characterizes the rate of deformation at constant vertical effective stress in the *LCC* regime, and t_{ref} is a reference time.

Sanzeni et al. (2012) used Pestana and Whittle (1998) model to study the compression and creep behavior of Venice Lagoon Sands. The compression test procedures included: i) 1D compression at a strain rate 1.0% per hour to a maximum vertical effective stress of 2.0 MPa; ii) drained creep for a period of 24 hours at the maximum stress; iii) unloading at strain rate -0.5% per hour. Figure 2-13 presents some comparisons in term of creep strain between experimental observations and model predictions (4). As it can be observed in this figure, quite good results were obtained with this model.

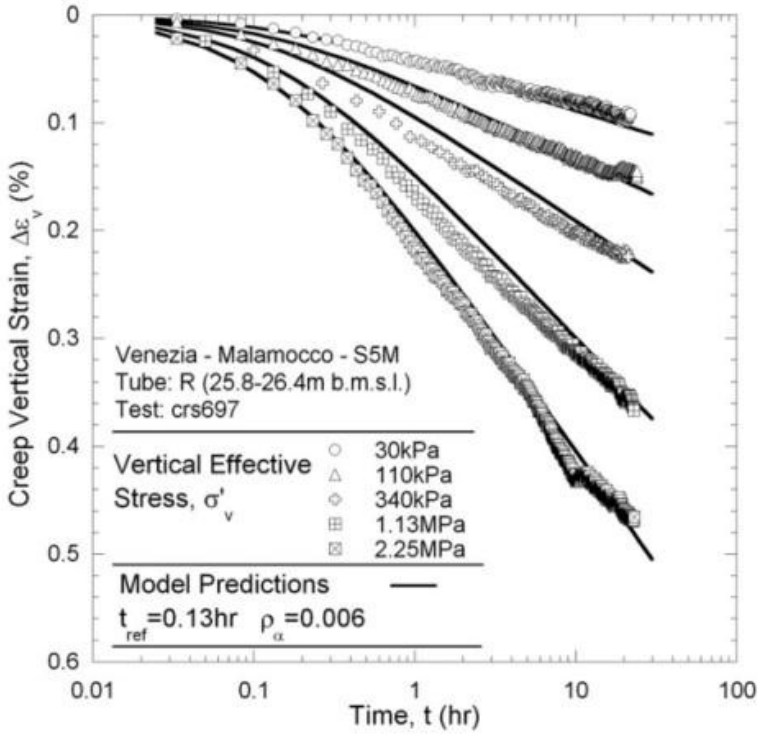

Figure 2-13. Comparison between experimental creep rate and model results (after Sanzeni et al. 2012)

Briaud and Garland (1985) proposed the rate effect model to predict the time-dependent behavior of soils. The model can be expressed as follows:

$$\frac{s}{s_1} = \left(\frac{t}{t_1}\right)^n \tag{2.4}$$

where the settlement s_1 is the value of settlement " s " observed at a time t_1 = 1 minute (after the beginning of a load step); and "n" is the creep exponent which is considered a soil property. Typical n values range from 0.005 to 0.03 for sands and 0.02 to 0.08 for clays.

Briaud and Gibbens (1999) used this model to interpret the data from five large spread footing field test. The testing procedure consisted of applying the load in increments equal to one-tenth of the estimated footing capacity. Each load step lasted 30 minutes or 24 hours. The load settlement curve is shown in Figure 2-14 As it can be seen, important creep settlements took place during the time that the load was kept constant.

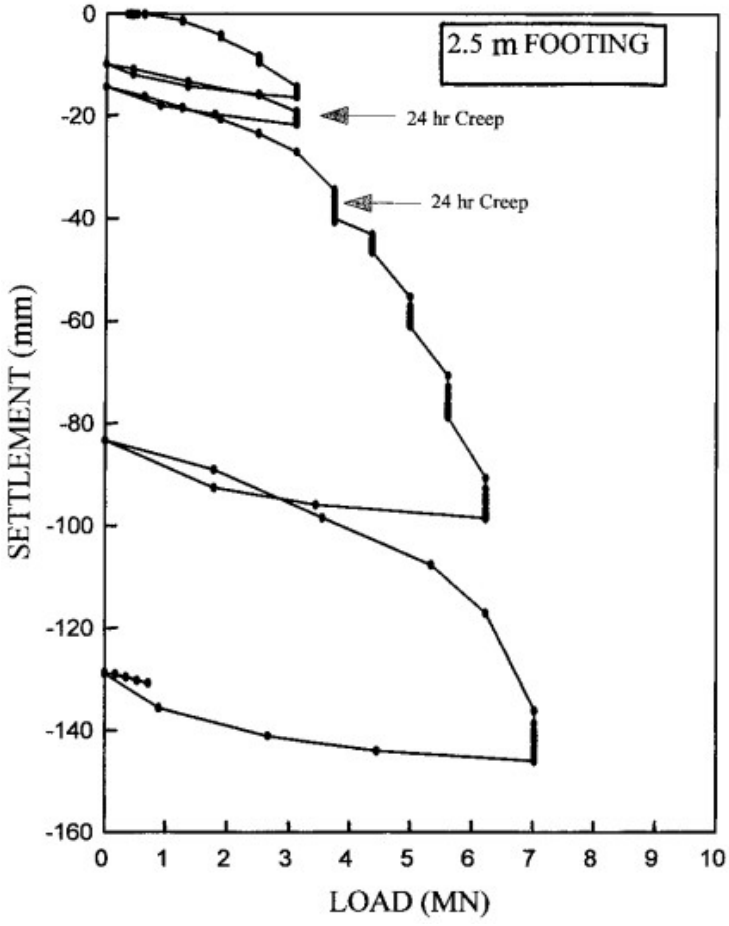

Figure 2-14. Load-settlement curve (after Briaud and Gibbens, 1999).

The creep curves for different load steps and different load levels are shown in Figure 2-14. Figure 2-15 (a) shows the creep curve for 30 minutes load steps. These results show the strong dependency of the creep rate on the applied load. Figure 2-15(b) present the results of test obtained for the 24 hours load step.

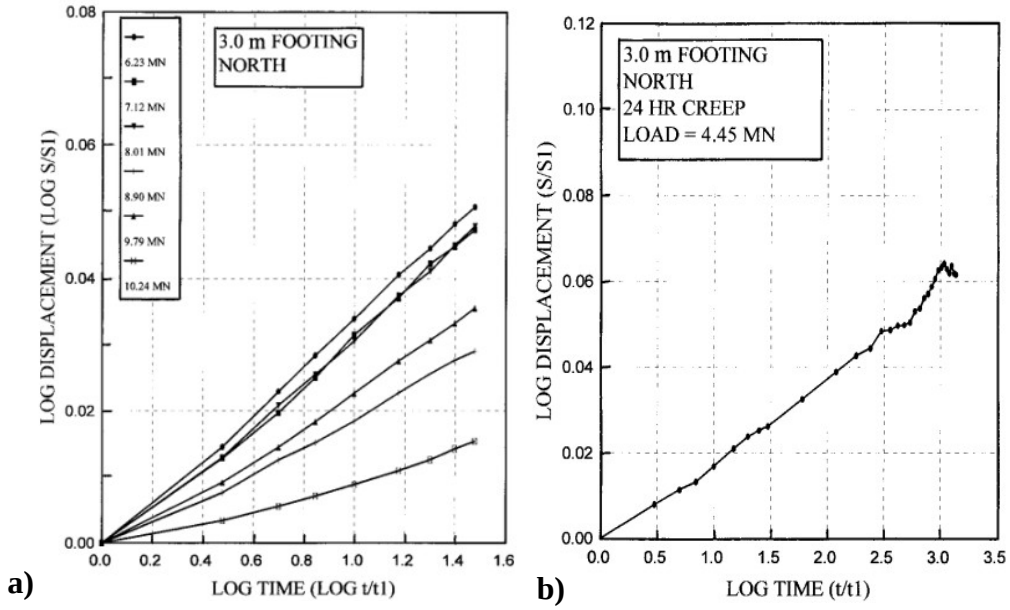

Figure 2-15. a) Creep curves for 30 minute load steps, and for b) 24 hour load steps (after Briaud and Gibbens, 1999).

As for the creep behavior of soils under deviatoric loads, there is less information compared with the contributions related to creep behavior of soils under volumetric or oedometric conditions. In general terms it can be said that the study of

the creep behavior in geotechnical engineering has been quite intensive for problems involving rock salt and frozen soils (e.g. Eckardt, 1982).

Perhaps one of the more relevant contributions related to the creep behavior of clays is the work by Briaud et al. (1998). They were the first ones that mentioned that creep will cut across the hump of the stress strain curve. This means that failure may be induced before reaching the peak stress, by creep, if the deviatoric load is hold constant at a relatively high stress level. This phenomenon can be explained better looking at Figure 2-16, in which it can be observed that when the creep test (represented with the empty triangular symbols) is performed at a high deviatoric stress (but below the peak stress), the stress-strain curve will follow the path of the gradual failure; crossing (nearly horizontal) below the stress-strain curve obtained in the standard test (represented by the dark triangular symbols) and reaching failure at large strains.

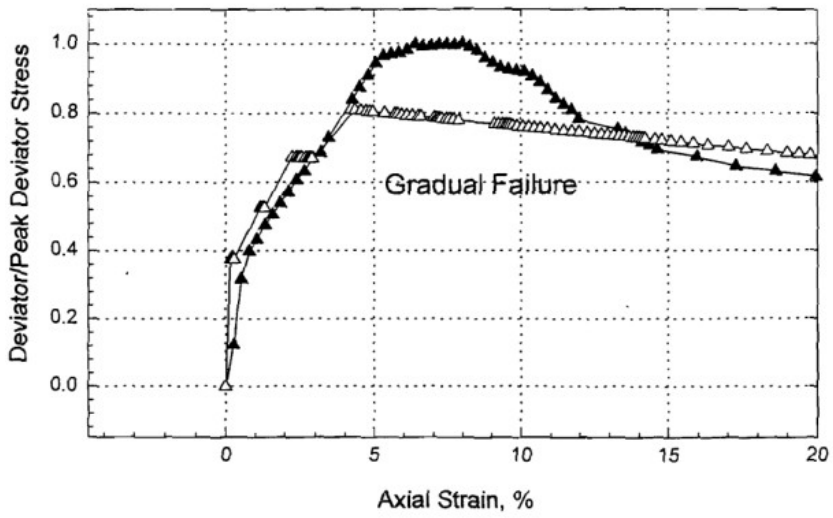

Figure 2-16. Failure under constant load (after Briaud el at., 1998)

Hunter and Khalili (2000) and Dornfest et al. (2007) both proposed similar models also based on the concept of "cutting across the hump" to explain the creep behavior in over- consolidated clays. The scheme in Figure 2-17 (a) presents the idealized creep failure model showing that when the constant stress is higher than the critical state stress, it will start to creep (onset of tertiary creep). The stress-strain curve will cut across the hump, until merging with the stress-strain curve of the standard triaxial test.

Figure 2-17 (b) presents what could happen in different situations, for example, if the stress is kept constant at a point like A, the creep path will be 'A' to 'B'. In Dornfest et al. (2007) it is explained other possible paths when creep tests start at lower stress level, as 'C' and 'F'.

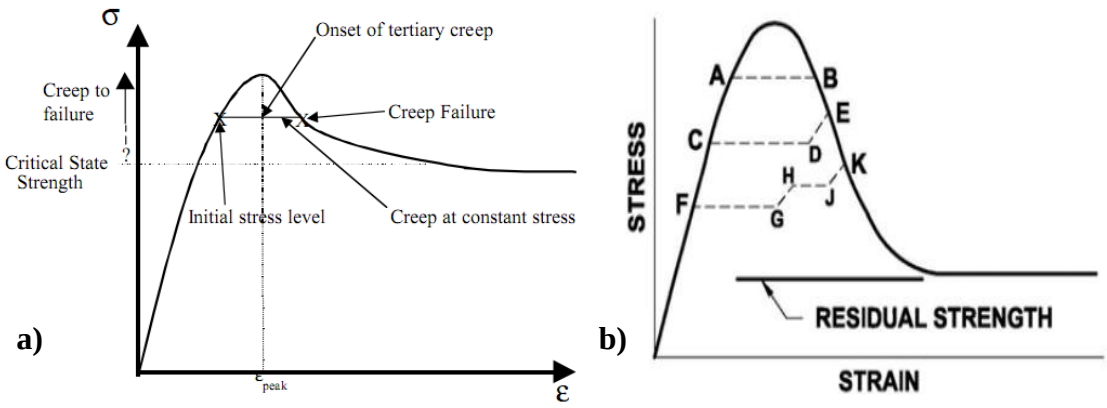

Figure 2-17. a) Scheme showing soil failure during creep tests (after Hunter and Khalili, 2000); b) idealized stress-strain curve for over-consolidated clay and creep test paths (after Dornfest et al., 2007),

In Hunter and Khalili (2000) results of drained creep tests performed in different clay types are presented. The aim of those tests was to prove the concept of "cutting across the hump". For example, Figure 2-18 shows some typical results from this paper in terms of the ratio between the axial strain and axial strain at peak stress (in constant strain rate triaxial test) versus axial strain rate. The results are presented for tests performed at different ratios between the stress at which the creep test is performed and the peak stress. In this figure it can be observed that when the ratio is not that high, the axial strain rate is decreasing tending to very small values. However, when the stress ratio is high, the axial strain rate is increasing. This means that the displacements are also increasing and the sample will fail.

Most of the laboratory tests that focus on creep behavior of soils under deviatoric load are triaxial CD test (e.g. Hunter and Khalili, 2000). Other stress paths have been used, but they are not very popular, for example typical results from triaxial CU tests performed by Martinez- Vasques and Diaz-Rodriguez (2009) are presented in Figure 2-19.

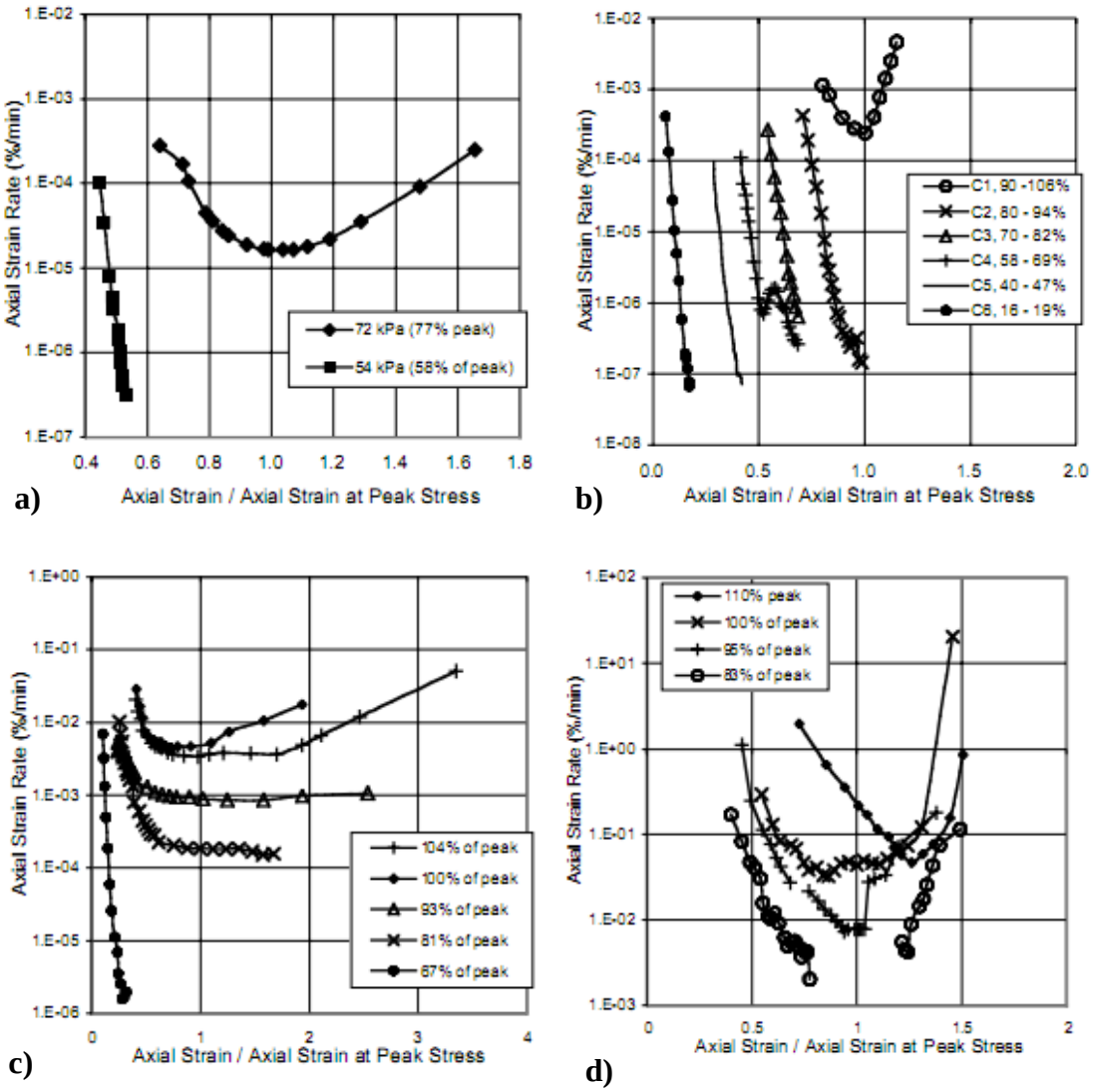

Figure 2-18. Drained Creep test results on different clays: a) Drained creep tests on Nicolet clay b) Drained creep tests on London clay c), Drained creep tests on Saint Alban clay d), Drained creep tests on Umeda clay (after Hunter and Khalili, 2000)

In relation to the duration of the creep tests in the laboratory, different strategies have been adopted in the past. For typical laboratory tests, creep stages (i.e. time during which the load is kept constant) of 24 hours have been generally adopted. For example,

the creep tests performed on Venice Lagoon sands last 24 hours (Figure 2-13, Sanzeni et al., 2012). There has been however some exemptions. For example the creep stages of the CU triaxial tests carried out by Martinez-Vasques and Diaz-Rodriguez (2009) lasted over 10,000 minutes (one week). The soil studied in this work was an undisturbed lightly over-consolidated clay.

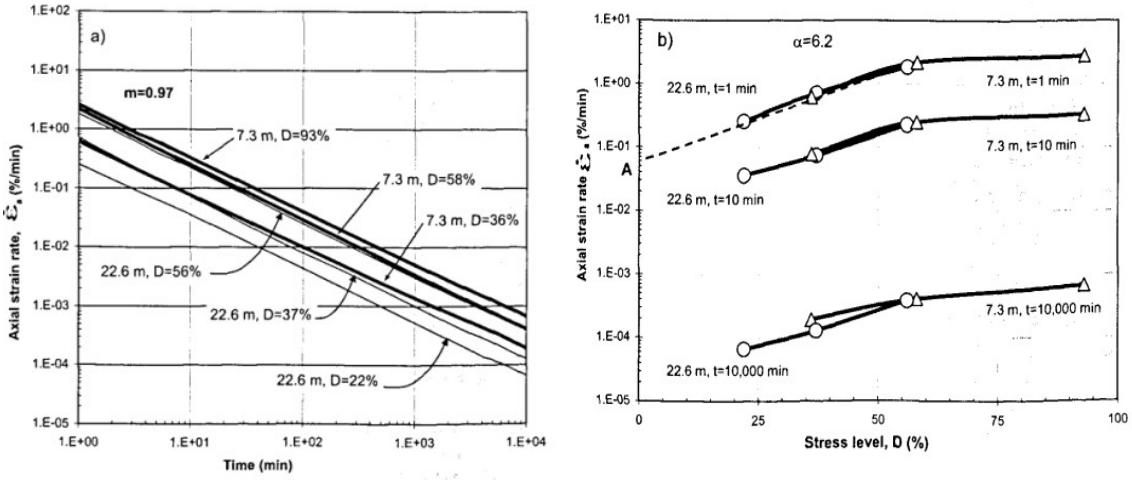

Figure 2-19. Results of triaxial CU test on Mexico City soils (after Martinez-Vasques and Diaz- Rodriguez, 2009)

Figure 2-19 shows that for a given stress level, the longer the time, the smaller the axial strain rate is. It also shown that for a given duration of the creep test (e.g. t=10,000 minutes), as the stress level increases, the axial strain rate also increases. This observation indirectly shows that creep will be more relevant at high stress level.

As for the field investigations, different timespans for the creep tests have been adopted. For example, Briaud and Gibbens (1999) held the load for 30 minutes (at most) in each load step. From those experiments they proposed the power law model). Figure 2-20 presents results of creep tests on anchors performed by Ostermayer (1975), in which the load was hold for 100~1000 minutes at different load levels. It can be observed that when the load is higher than 515 kN, the displacement versus the time (semi-log) is no longer a line, and the displacement starts to increase more when compared with the behavior at low load level.

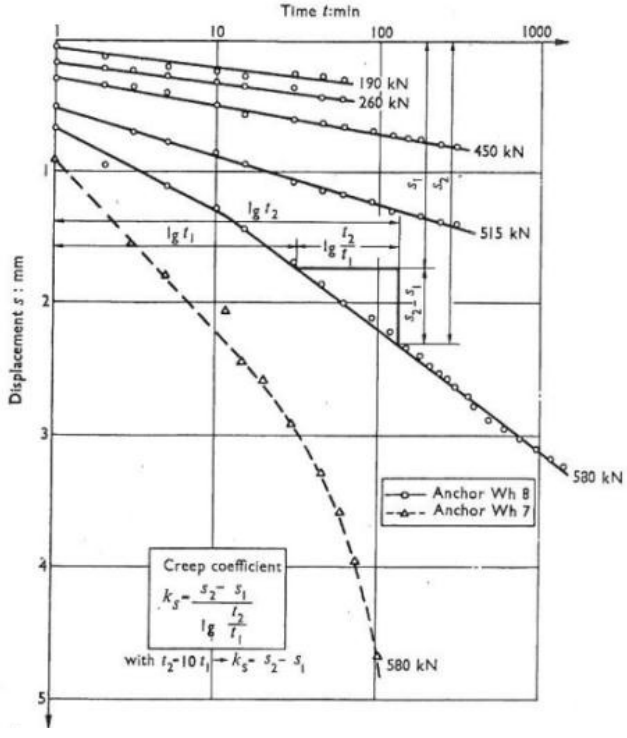

Figure 2-20. Time-displacement curves for various loading steps on anchors (after Ostermayer, 1975)

An important number of contributions have focused on the creep behavior of anchors (e.g. Briaud et al., 1999; Ludwig et al., 1984 and 1985; Ostermayer, 1975; and Weatherby, 1982 and 1998). Weatherby (1998) presents the apparent earth pressure diagrams to design the permanent ground anchor walls based on the research performed on two full-scale wall sections, four model-scale walls and ten large-diameter ground anchors installed in a fine- grained soil.

Ludwig et al, (1984 and 1985) studied load tests performed on instrumented tiebacks anchored in a variety of cohesive soils. A series of cyclic loads was applied to the tieback. The peak load of each successive load cycle was greater than its predecessor. At the end of each load cycle, the load was released to a nominal alignment load. In the creep tests, the peak load of each load cycle was held constant for periods range from 10 minutes to 10,000 minutes. The result of creep test in anchor is illustrated in Figure 2-21 These curves show that the creep behavior is dependent on load level. In the low load level the creep rate is almost zero. As the load level increases the creep rate is increases. Figure 2-22 shows that for a load higher than 70 to 80 percent of the ultimate load, the residual anchor movement increase rapidly.

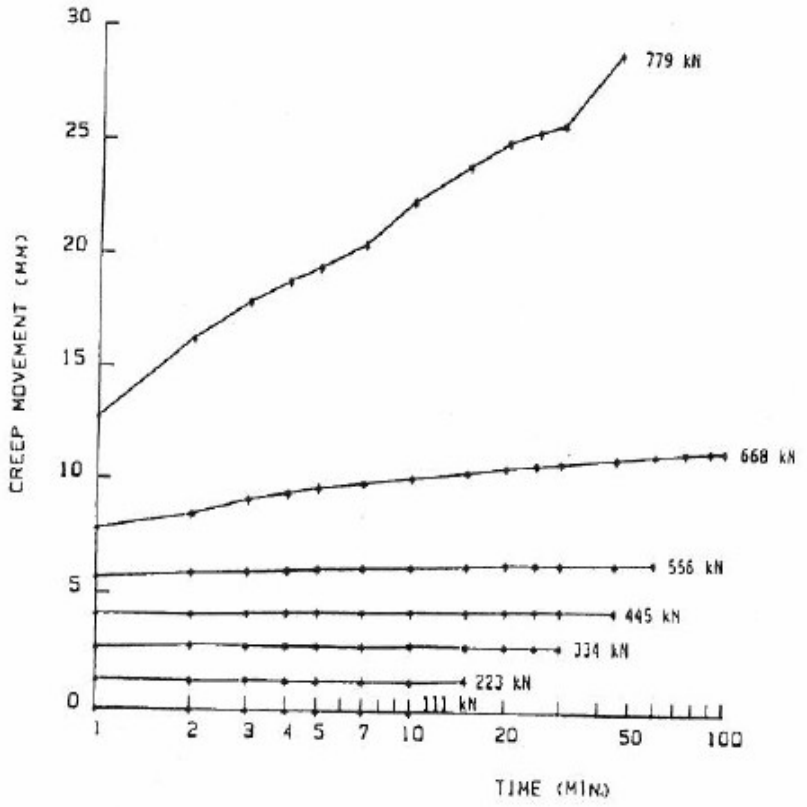

Figure 2-21. Typical creep curves of straight-shafted tieback anchored in cohesive soils (after Weatherby, 1982).

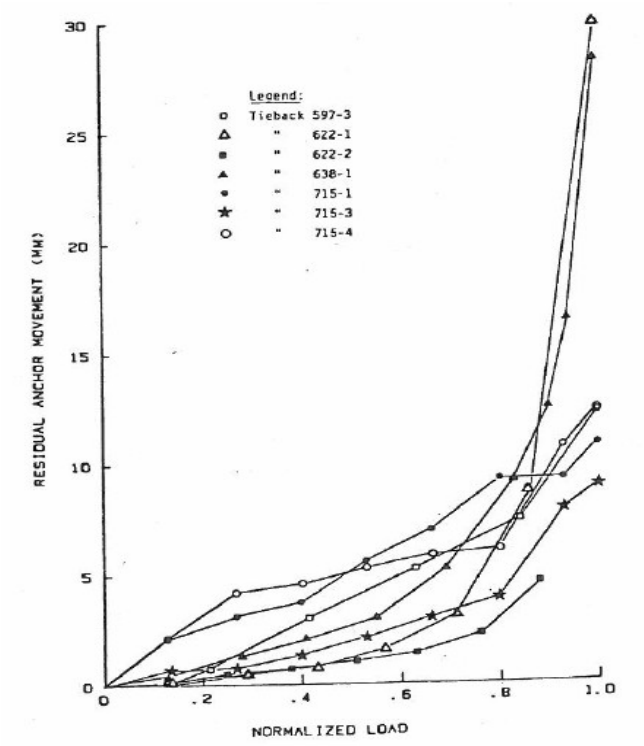

Figure 2-22. Residual anchor movement. Normalized load curves of several straight-shafted tiebacks anchored in different cohesive soils (after Weatherby, 1982).

2.6. Pull-Out Tests, Field Experiments and Monitoring of Soil Nail Walls

Pull out devices to perform tests in the laboratory under controlled conditions have been developed to gain a better understanding of the key processes associated with the transfer of load between the soil and the nail (e.g. Chu and Yin, 2005; Yin et al. 2009; and Su et al. 2008). Figure 2-23 shows a schematic representation of the pull-out test device and a picture of the device taken during a test.

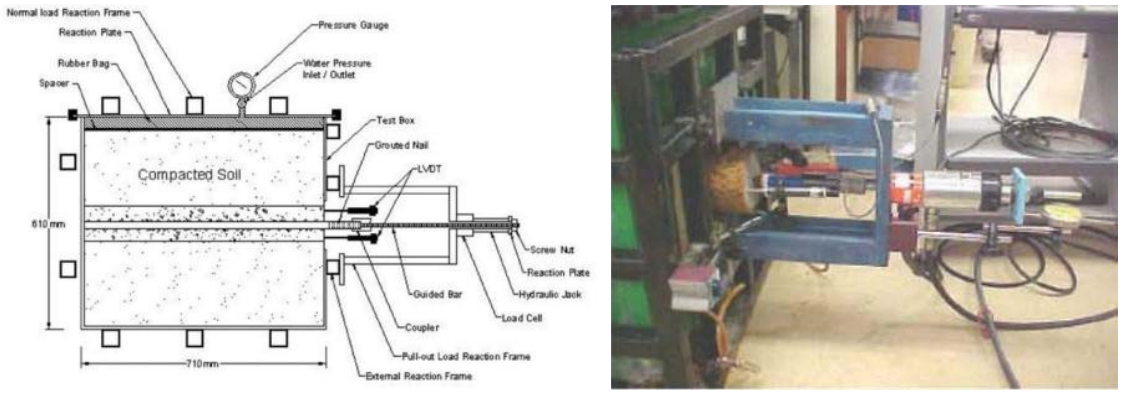

Figure 2-23. Laboratory soil nail pull out test apparatus: a) schematic representation and b) picture of the device during testing (after Chu and Yin, 2005).

This kind of devices allows studying practically of all the possible factors related to soil nail behavior; as for example: degree of saturation, overburden pressure, and grouting pressure. For example, Figure 2-24 shows that the pullout shear strength decreases as the degree of saturation increases.

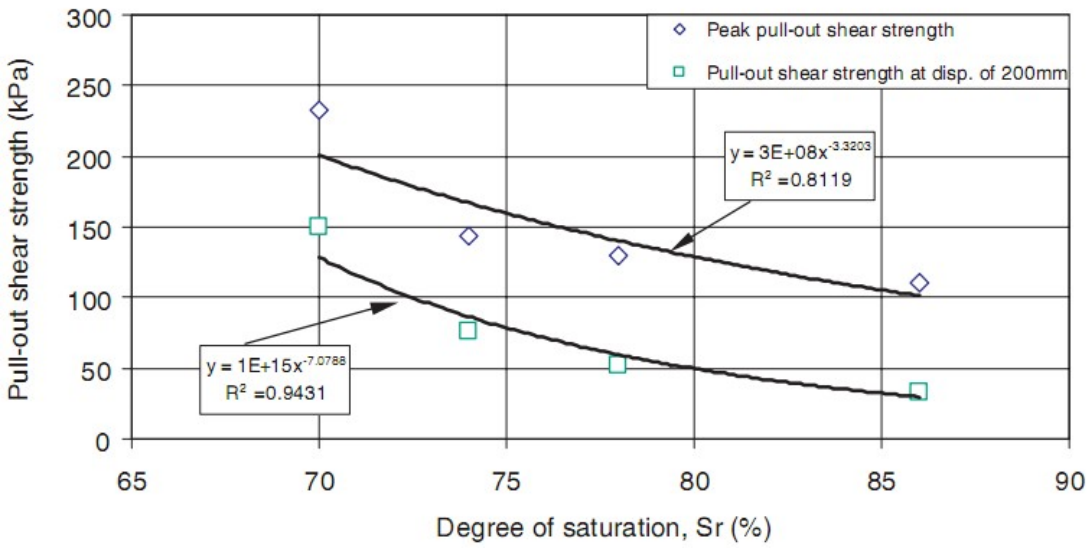

Figure 2-24. Correlation between degree of saturation and pull-out strength (after Yin and Sun, 2006).

Li et al. (2008) presents results obtained from a full scale test involving soil nails in a loose fill slope. The inclination of the slope was 33° respect to the horizontal. The slope was 9 meters wide and 4.75 meters high. The grouted nails were arranged in two rows of five nails per row, following a square grid of 1.5 meter x 1.5 meter. The nails were installed with an inclination of 20° respect to the horizontal (Figure 2-25).

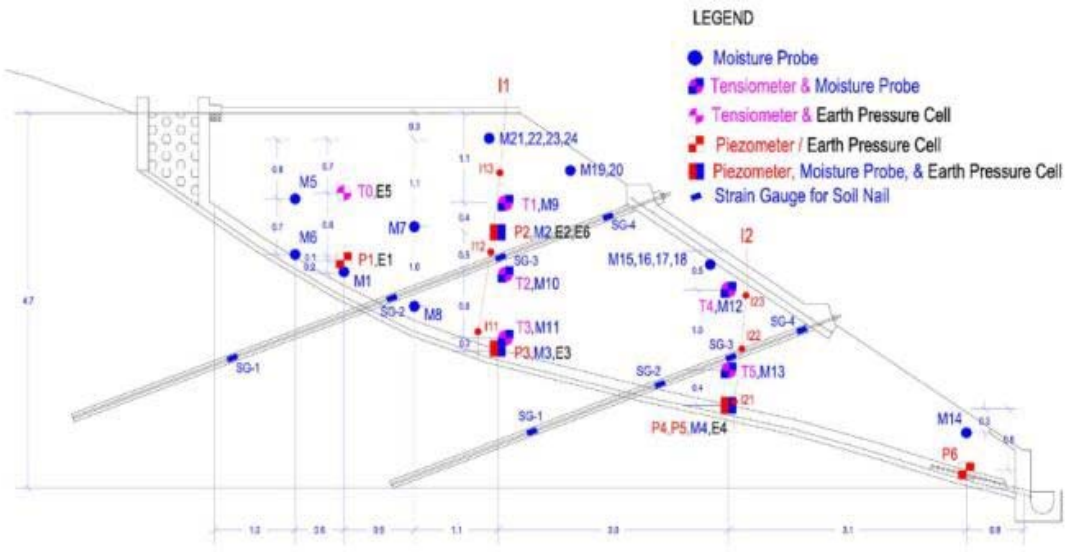

Figure 2-25. Arrangement of instruments for a tested soil nail wall (after Li et al., 2008)

Various instruments were installed to monitor the performance of the soil nail wall. The monitoring was performed for about 6 months. Then the wall was subjected to loading and wetting. Figure 2-26 shows the surcharge applied and the wetting of slope. In addition, Figure 2-26 shows some typical results gathered from this test related to development of earth pressure during loading. As expected, the earth pressure increases as the slope is loaded.

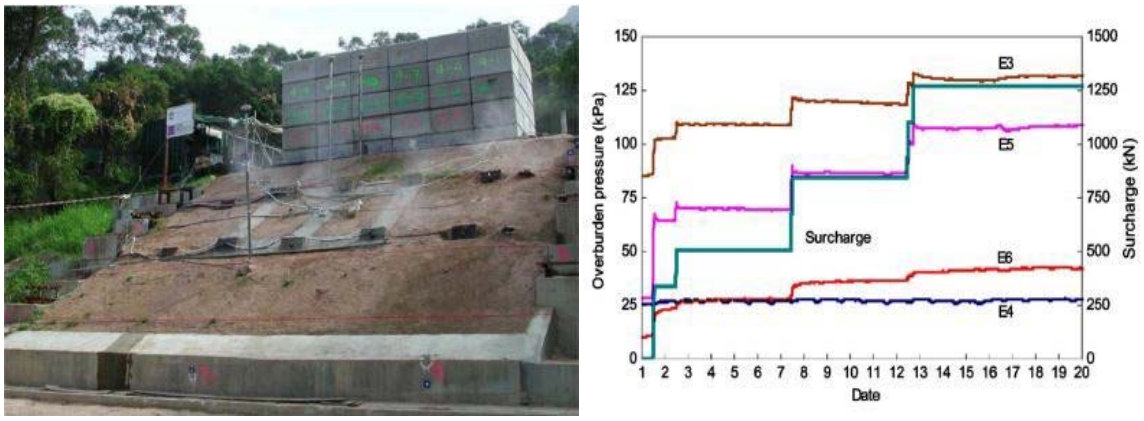

Figure 2-26. Soil nail slope with surcharge (after Li et al., 2008)

Figure 2-27 presents the variations of suction, pore pressure and displacement during wetting. The slope was initially unsaturated and became fully saturated at the end of the wetting stage (wetting II) with the measurements of positive pore pressure. At that time, the more important displacements took place. Figure 2-27 shows the development of the load taken by the nails in different positions during wetting. It can be observed that the load in the nails increased slightly after the first wetting (wetting I) and considerably during the second wetting (wetting II) when significant displacements were observed. It is clear from this study that the soil suction plays a crucial role in the creep behavior of the soil nail walls.

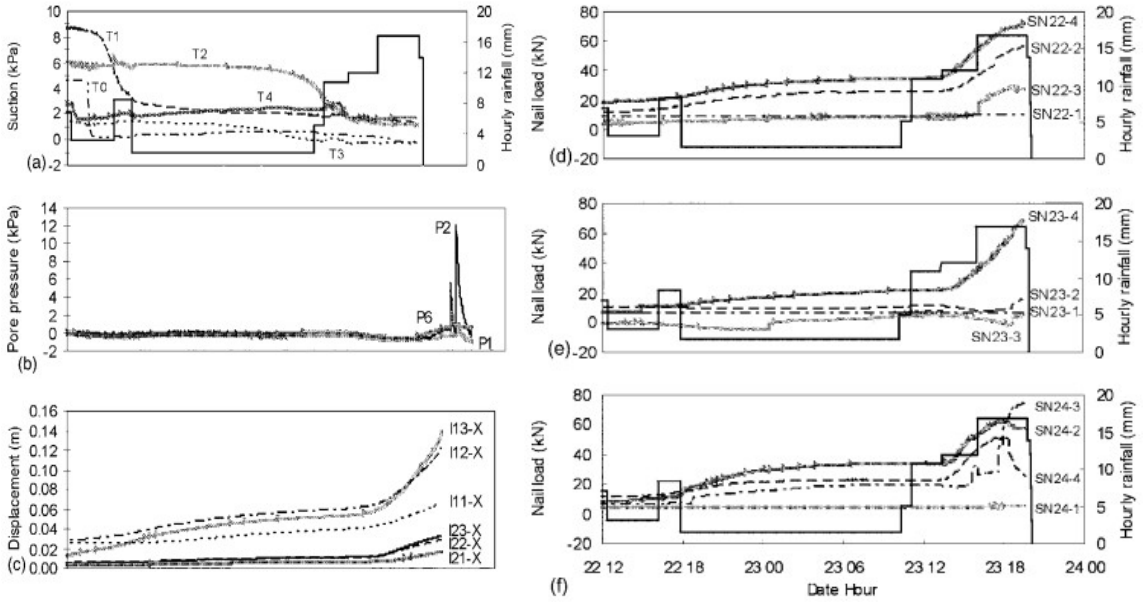

Figure 2-27. Measured deformations and pore pressure during wetting and the associated response of nails (after Li et al., 2008)

Turner and Jensen (2005) reports the results of the monitoring campaign of a soil nail system constructed for the stabilization of an active landslide in Wyoming (Figure 2-28). A datalogger was used to gather the information from the strain-gauges. A solar panel and a battery were adopted for the power supply. Two slope inclinometer casings were also installed to track the deflections of the slope. The monitoring of this soil nail wall was very useful to assess the service conditions of the wall and check the method used in the design. This project allowed a better understanding of how the different components of the soil nail system interact under actual field conditions.

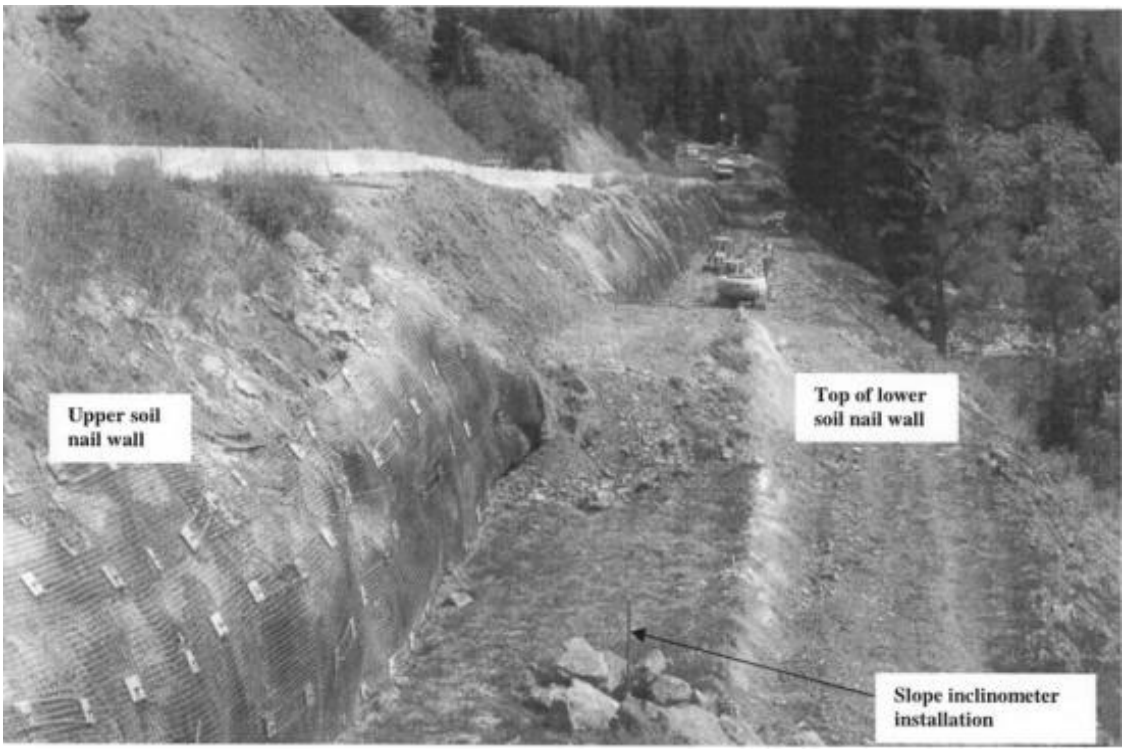

Figure 2-28. Picture of an instrumented soil nail wall (Turner and Jensen, 2005)

The Dublin Port Tunnel project is another successful case in which the instrumentation played a crucial role to gain a better understanding on the behavior of soil nail walls. Full details about this case study can be found in Menkiti and Long, 2008. The instrumentation was composed by: strain gauges; piezometers (at 4, 8, and 12m depth); inclinometer; surface-mounted prism for detecting slope face movements, and settlement markers at the slope crest. The strain gauges (installed only in some selected nails) were installed in a way that it was possible to measure the influence of vertical bending. The strain gauges were also equipped with thermistors to measure the temperature at each instrument location (Figure 2-29).

Menkiti and Long (2008) concluded that nails work in tension mainly and that the influence of bending is marginal. The instrumentation also assisted to understand better the acting loads during installation and excavation. It was observed that the more significant loads acting in the nail were related with the drilling and nailing of the lift immediately below and not with the excavation (as it is generally assumed in the design current methods). It was also detected that the upper nails were the ones that developed the highest forces (while most design methods assume that the maximum bond capacity develop at depth).

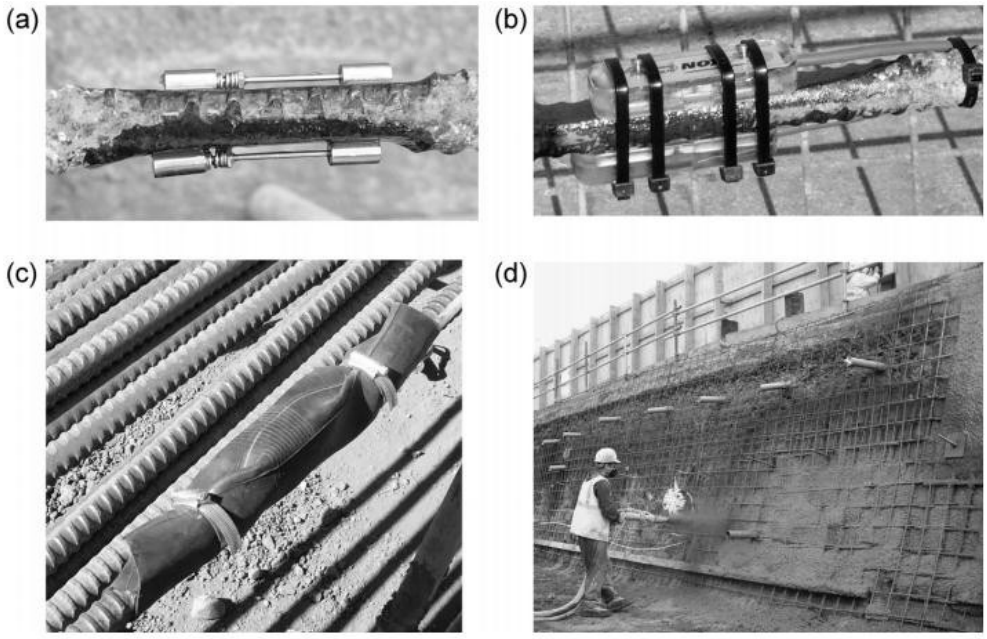

Figure 2-29. Attached the strain gauges (after Menkiti and Long, 2008)

In these two works (i.e. Turner and Jensen, 2005; and Menkiti and Long, 2008) there are no much details about the long term or creep behavior of the soil nail systems. Based on the information gathered from the monitoring of the soil nail walls, these two contributions (i.e. Turner and Jensen, 2005; and Menkiti and Long, 2008) agree in the idea that the guidelines (and methodology) used for the design of these two walls resulted in conservative designs.

2.7. Modeling of Soil Nail Walls

Numerical modeling of soil nail walls is often carried out to assess the performance and stability of the retaining system. Global stability analyses of soil nail walls is approached by using limit equilibrium software specifically developed for the design of soil nail walls. The two computer programs most commonly used in the United States for the analysis and design of soil nail walls are SNAIL and GOLDNAIL. A limitation of both computer codes is that they are not able to analyze composite failure surfaces, which might be applicable when multiple soil layers with dissimilar strengths exist (e.g. FHWA GEC#7).

Another limitation inherent to numerical codes based on limit equilibrium method is that they cannot assess the performance of soil nail walls in term of deformations or load distribution in the nails.

A good example of the numerical analysis of soil nailed system using different pieces of software corresponds to the study of the soil nail wall constructed and instrumented at National Geotechnical Experimentation Site (NGES) at the University of Amherst, Massachusetts. The wall was built in a moderately plastic varved clay. After

construction the wall was over excavated up to failure. The lateral deformations of the wall were monitored during this process. The data gathered during the test showed that the deformation of the wall occurred mainly at the face of the wall. It was also observed that as one move away from the face of the wall, the deformations decrease significantly. Furthermore, the more significant lateral deformations of the wall were concentrated above the first row of the nails. Oral and Sheahan (1998) back analyzed the wall by using three software packages used to determine the global factor of safety for the soil nail wall. The results of these analyses are shown in Table 2-3.

These three very popular pieces of software computed values of the factor of safety (F.S.) between 1.00 and 1.17. However, the actual wall reached failure (i.e. F.S. less than 1). It is important to bear in mind that those analyses have a number of assumptions and important limitations (e.g. 2D conditions, simplified soil and nails models, nails working only in tension); so some discrepancies between the actual observed behavior and the numerical predictions may be expected. For example, the failed wall did experience some 3D effects due to its limited length. Furthermore, the deformation pattern and lack of nail pullout, indicated nail bending as one of the reinforcement mechanism.

Table 2-3. Results from stability analysis of the wall (after Oral and Sheahan, 1998)

GoldNail	F.S.= 1.148 at 5.6 m (18.4 ft) with a base angle of 29°
Shen	F.S. against sliding through toe : 1.00 F.S. against deep seated rotation: 1.64
Snail	F.S.= 1.172 at 5.5 m (18 ft) Lower failure plane : 39.8° length 5.7 m (18.7 ft) [a] Upper failure plane : 65.8° length 2.7 m (8.8 ft) [a]

[a] Angles of orientation for failure wedge.

Numerical modeling using FLAC were carried out to assess the lateral movement of a 20 meters soil nailed wall. The soil nail wall was built in a high plasticity clay, with SPT over 20 blow-counts in the city of Zagreb (Maric, 2001). In order to assess the performance of the soil nail wall, the deformation of the wall were monitored from May to November 2000. The maximum horizontal displacement was 2 mm, while the numerical modeling prediction for this magnitude was 20 mm. Overall; these results demonstrate that the calculations should account for a wide range of modes of behavior when assessing the loading effects during service. It was also clear that special attention should be given to 3D effects. It is important to highlight that from October 2000, no extra deformations in this wall have been measured. This can mean that creep effects are not relevant in this high plasticity clay.

The performance of soil nail walls depends on the interaction between the soil, nails and facing. Additionally many other parameters affect the performance of soil nail walls, for example: nail inclination, method of installing nail, grouting and construction.

Finite Element Methods (FEM) programs such as Plaxis (Singh and Babu, 2010), FLAC (Briaud 1997, Maric 2001) and Abaqus (Barrows 1994) have been used to assess the performance of the soil nail walls. These programs can predict horizontal and vertical deformation of the wall and also can calculate the load distribution in the nails.

PLAXIS 2D has been found to be an appropriate tool for evaluating the behavior of the soil- nailing walls and many researcher have used it to simulate the soil nail walls (e.g. Shiu et al., 2006; Fan and Luo 2008; Singh and Babu, 2010; Akhavan et al., 2011). In 2009, Plaxis bulletin published the work by Babu and Singh (2009), which focus on the impact of different elements on the modeling of soil nail walls. The Mohr-Colum (MC) model was used to simulate the soil behavior. In 2010 this study was extended (Singh and Babu, 2010) and three different soil models: namely MC-model, Hardening Soil (HS) model and HSsmall model, were used to simulate the soil behavior. In this work it was investigated the influence of the different soil models on the predictions of the: i) base heave of excavation; ii) lateral displacements of the wall; and iii) global stability. In soft soils, the bottom of excavation is generally at risk of heaving. The MC model predicted approximately twice base heave in front of the soil nail wall than HS and HS small model.

Up to 60% of the construction, the lateral displacement at the top of the wall predicted by the MC model is higher than the displacement predicted by HS model and HSsmall model. However, between the 60% of the construction and the completion of the wall, the MC model predictions are approximately half of the amount than the predicted by HS model and HSsmall model. These observations may be attributed to

the following two reasons: a) with the progression of the construction stages, cumulative plastic strains in the soil nail system increase and thereby reduce the stiffness of the retained soil mass significantly, and b) the assumption of the linear elastic pre-failure behavior of the soil in MC-model. Lateral displacement with different soil models are shown in Figure 2-30.

Another relevant conclusion of this work is that different soil models do not have mayor effect on the global stability of the soil nail wall, and the analyses performed for the period after the end of the construction to the same factor of safety was reached, regardless the type of the soil model adopted. Furthermore, the three soil models analyzed predicted similar responses of axial force developed in soil nails during the construction stages. The hardening soil model is suitable for all soils but not account for viscous effects, i.e. creep and stress relaxation. Plaxis has specific creep model, that is called “Soft Soil Creep Model”; but it is certainly not recommended for use in excavation (Plaxis manual, 2012).

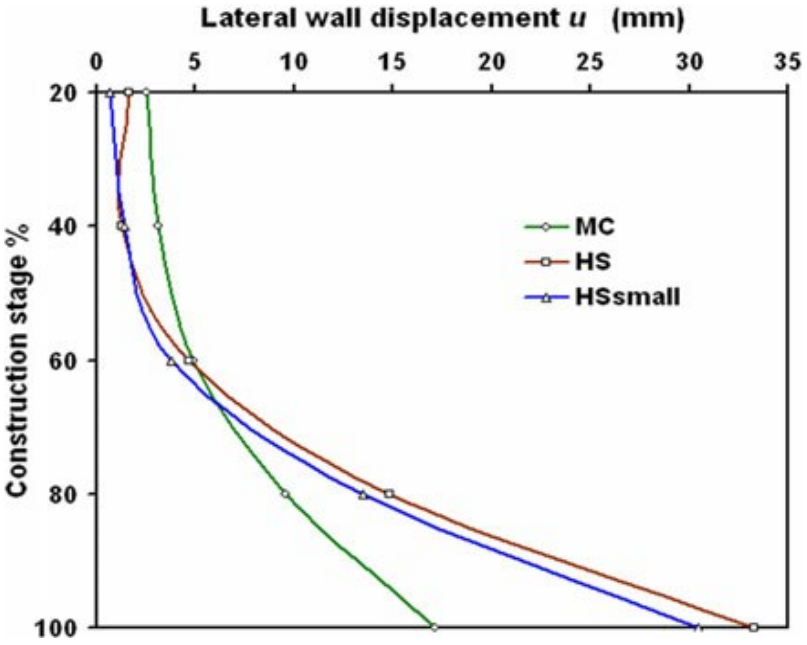

Figure 2-30. Lateral displacement of soil nail wall with construction (after Singh and Babu, 2010)

As mentioned before, finite element analyses allow the calculation of the load take by the nails. For example, in Plaxis program it is possible to use geogrid elements or plate elements. Geogrid elements do not account for the bending stiffness of nails, and the nail elements have axial stiffness only. On the other hand, the plate elements have both: axial and bending stiffness. In order to considerate the bending stiffness, Singh and Babu (2010) simulated two series of 10 meter height soil nail walls using Plaxis 2D. One series use the plate to simulate nail elements and for the other one adopted the geogrid elements were adopted. Figure 2-31 shows the axial load distribution along nails length for both plate elements and geogrid elements. This information is very important because inform about the nail service load.

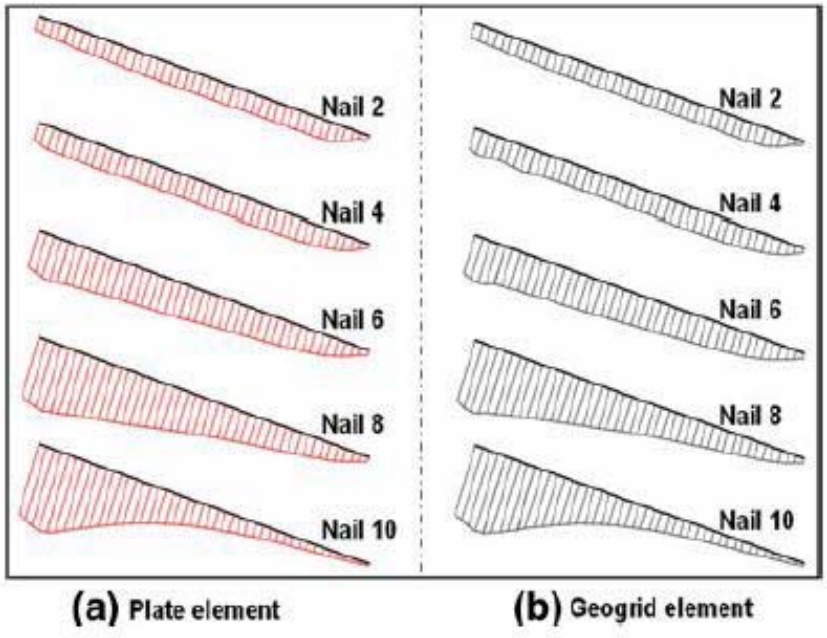

Figure 2-31. Variation of axial force along nail length (after Singh and Babu, 2010)

In this work contributions related to creep in soils have been reviewed and discussed. There are very large number of papers and reports dealing with the behavior of soils, especially for oedometric conditions. Several constitutive models have been proposed and implemented in FEM codes, but just a few of them have been applied successfully to reproduce the creep behavior in excavations. From the numerical point of view, pieces of software based on limit analysis are more common for the study of stability of soil nail walls. However they are not capable of simulating creep or long term behavior.

Case studies dealing with instrumentation and monitoring of soil nail walls have also been discussed. No problems associated with creep have reported in these

contributions. In fact there are not evidences, or reported cases, of actual soil nail walls in high plasticity clays that had fail or have been damage due to creep related issues. From the bibliography review, it is also clear that increases in soil moisture (or decrease in soil suction) can trigger creep or viscous effects. From this review, it is clear that creep rate in soils strongly depend on stress level.

3. INSTRUMENTATIONS DESIGN AND INSTALLATION

3.1. Introduction

The instrumentation is a crucial component of this project because the data gathered from the experiments was used to gain a better understanding of the problem. Furthermore, this is the basic information to calibrate the numerical models and to revisit current design guidelines. The design of the instrumentation is oriented to two main activities related to; i) soil nail tests, and ii) long term monitoring of the TxDOT site. These two activities require different kind of sensors and instruments. The aim of this section is to present the main devices adopted for this research.

As for the loading tests, Geotechnical Engineering Circular N˚ 7 on Soil Nail Walls" (GEC#7, 2003), GEC#7 establishes that soil nails are load tested in the field to verify that the nail design loads can be carried without excessive movements and with an adequate factor of safety. The creep test could be done as part of the ultimate test, or verification test, or proof tests. It is performed by holding the load for a specific period of time while the displacements at nail head are monitored.

According to GEC#7 the basic set-up for pull-out test consists of the three main components illustrated in Figure 3-1, as follows:

i. A center-hole hydraulic jack and hydraulic pump to apply a test load to a nail bar, Two dial gauges mounted on a tripod or fixed to a rigid support that is independent of the jacking set-up and wall to measure the movement of the nail head and

ii. A center-hole load cells is used to monitor the applied load during creep test while the hydraulic jack pump is incrementally adjusted (GEC#7, 2003). This allow performing creep tests in which the load is keep constant at the steps load defined in the test protocol.

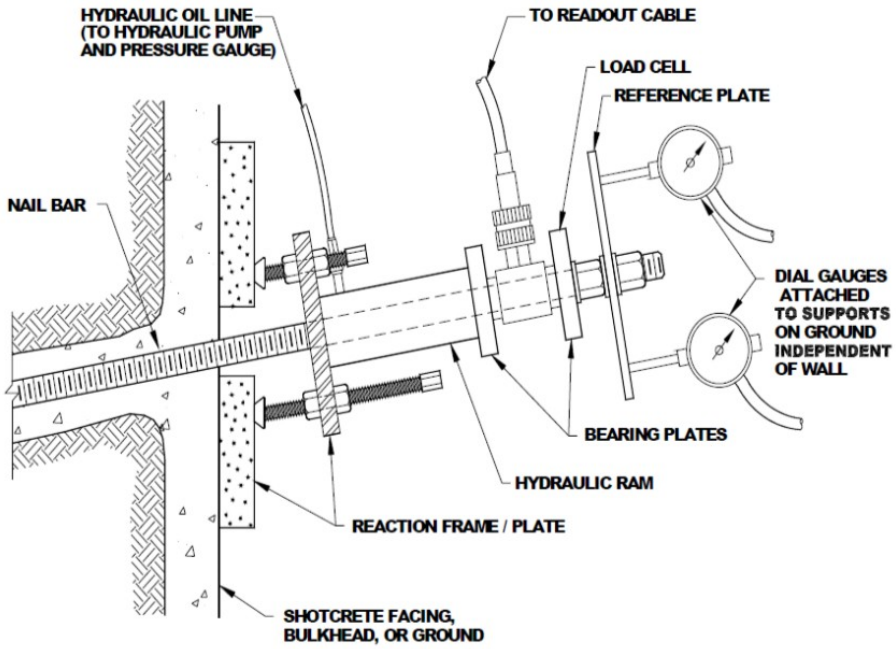

Figure 3-1. Soil Nail Load Testing Setup (after GEC#7, 2003)

In addition to this basic information proposed for the load tests in the GEC#7, this research is also aimed at learning about the distribution of stresses in the nails. Strain gauges (glued to the steel bar) can be used to measure the stresses in the nail.

In relation to the long term monitoring of the actual soil nail wall, the basic instrumentation suggested in GEC#7 is presented in Figure 3-2. The instrumentation for the long term duration of the soil nail wall is divided in two main components: soil nail wall instrumentation and nails instrumentation. In the following these components will be defined. As for the wall instrumentation, the more relevant magnitude to monitor is the wall deflection, alongside the horizontal and vertical wall movements. In relation to the nail instrumentation the more relevant parameters to study are: the load in the soil nails (at different positions) and the load in the nail head. An additional aim of this research is to measure the changes in water content (and or suction) to explore the impact of moisture on creep rate.

Out presents the main magnitudes to be measured in this research (i.e. loads, displacements, deflection, soil moisture and stresses); the devices that can be used to control/measure those parameters (i.e. jacks, load cells; strain gauges, linear variable differential transducers (LVDTs), string potentiometer, slope inclinometers, photogrammetry targets, sensor probes and strain gauges) and the experimental activities (i.e. load tests and long term monitoring) in which those devices may be used.

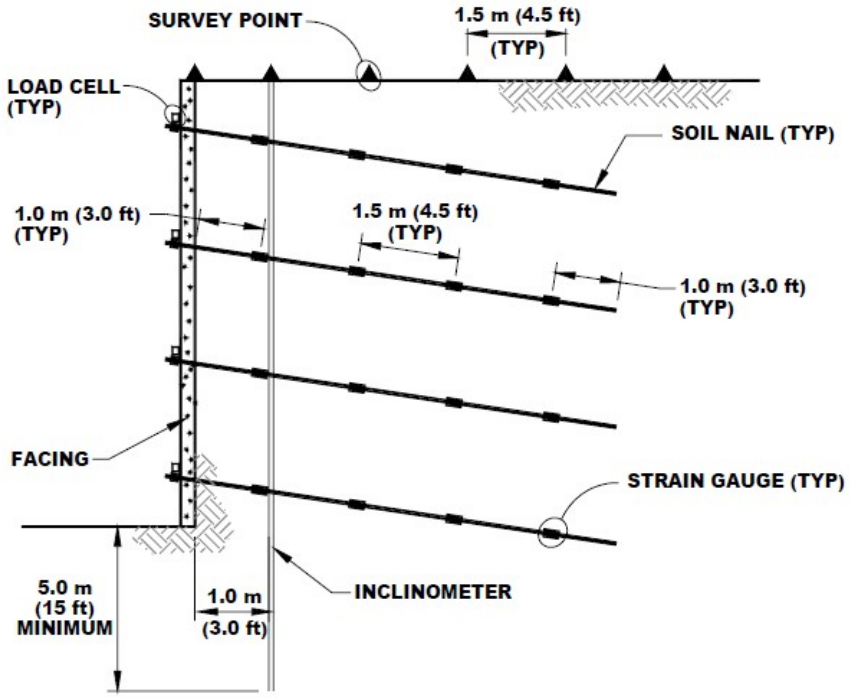

Figure 3-2. Typical soil nail wall instrumentation (after GEC#7, 2003)

To support the experimental campaign, other devices are necessary, such as data acquisition and power supply. Two different type of power supply are anticipated: i) generator to be used during the load test (i.e. a 5kW Honda); and ii) solar panel to provide power (around 20W) for long term monitoring. In the following section the general aspects of sensors described above are briefly presented.

Table 3-1. Soil Nail research: magnitudes to be measured, devices to be used and tests to be carried out

Magnitude	Instrument	Test
Load	Hydraulic jack	Nail load
	Load cell	Nail load
		Long term monitoring
Displacement	Dial gauge	Nail load
	LVDT	
	String potentiometer	Long term monitoring
	Survey	
Deflection	Slope inclinometer	Long term monitoring
	Tiltmeter	
Soil Moisture	Water content probe	Long term monitoring
Stress	Strain gauge	Nail load Long term monitoring

3.2. Instruments and Testing Design

For the each one of the different devices presented in Table 3-1 there are different options that can be adopted, in general terms, two main functional systems can be distinguished: the traditional ones based on voltage measurements; and (relatively) new systems based on the vibrating wire technology to make the measurements. In voltage measurements systems the parameter to be measured is transmitted via the gauge base (electrical insulation) to the resistance wire (or foil) in the gauge. As a result, the fine wire experiences a variation in the electrical resistance. The variation of the electrical resistance is proportional to the parameter to be measured. For example, a strain-gauge

is constructed by bonding a fine electric resistance wire to an electrical insulation base. A crucial component of this system is the perfect bonding between the gauge and the material to be tested.

The vibrating wire system is based on the fact that the resonant frequency of vibration of a tensioned steel wire depends on the tension in the wire. This principle is used in a number of configurations for the measurement of load, pressure, force, strains, temperature, and tilt. A characteristic of vibrating wire sensors is their long-term stability. The advantage of this kind of sensors over the voltage ones lies mainly on the sensor output, which is a frequency rather than a voltage. Frequencies can be transmitted over long cables (i.e. thousands of meters), without significant degradation of the signal caused by variations in cable resistance. The variation in resistance may arise from water penetration, temperature fluctuations, contact resistance or leakage to ground. This factor results in sensors which exhibit a good long-term stability and which are convenient for long-term measurements in adverse environments .

3.2.1. Hydraulic Jack

As mentioned in Section 3.1 a central hole hydraulic jack was used for the pullout test of the new nails and existing anchors. The hydraulic jack and the associated pump was used as shown in Figure 3-1. Picture in Figure 3-3 illustrate the setup typically used in this kind of tests. Due to the different load capacity of the nails and anchors contemplated in this research, two different hydraulic jacks were used. It has been estimated that a 50 tons central hole hydraulic jack was used for the new nails and a 175 tons was necessary for testing the existing anchors.

Figure 3-3. Picture showing a nail load test performed in inclined soil nails.

3.2.2. Load Cell

The load cell is a transducer that consists of a cylinder of high strength steel with a series of electrical resistance strain gauges connected around the periphery as a Wheatstone bridge, which usually consists of four strain gauges. In this way the transducer can compensate for unevenly distributed loads. The load cells are also compensated for temperature variations typically found during normal operating environments. Via a multi-core sheathed cable the load cell can be connected to a direct portable readout, switched terminal units or a data logging system. They are manufactured with a central hole to accommodate nails and anchors (Figure 3-4).

In this research the load cell was used in two different activities: i) to measure the applied load during the nail and anchor load tests (as illustrated in Figure 3-1); and ii) to measure the load at the head of the nail during the long term monitoring (as showing in Figure 3-2).

Figure 3-4. Central hole load cell (Geokon)

Two different load cells was used in this research: i) the Geokon (3000–500kN) for the soil nail load tests (at both NGES and TxDOT sites) and the long term monitoring of the soil nails; and ii) the Geokon (3000–1500kN) to be used in the tests involving the existing anchors. Note that this last cell, able to work at higher loads, is necessary because the maximum load on the anchors is much higher than the one on nails.

3.2.3. Dial Gage

Dial gauges was used to record (manually) the displacements to be measured during the soil nail test. They will measure the relative displacement of the nail respect to a (fix) reference plate. Figure 3-1 illustrates the way in which relative displacements was measured during the load tests.

A dial gauge also known as ‘dial test indicator’ and/or ‘lever arm test indicator’ and/or ‘finger indicator’ are very popular devices in geotechnical laboratory investigation to measure displacements. In fact a dial gauge measures angular displacement and not linear displacement. Linear distance can be correlated to the angular displacement based on the correlating variables. If the cause of movement is perpendicular to the finger, the linear displacement error is acceptably small (within the display range of the dial). Contact points of the dial gauges are generally build with a standard spherical tip of 1, 2, or 3mm diameter.

3.2.4. Slope Inclinometer

Slope inclinometers provide significant quantitative data associated with the deflection or inclination along a borehole. This device is perhaps the more common one use to measure lateral movement of earthworks or structures. It also provides the pattern of deformation and the zone of potential failure. As mentioned before, in this research it was used to measure horizontal deflections of soil nail wall. This technique requires the installation of an inclinometer casing in a borehole that passes beside the structure to be monitor (in this case the soil nail wall). The boreholes are typically located at around 3 ft.

from the face of the wall and at minimum depth of around 15 ft. below the foundation of the soil nail wall (see Figure 3-2).

This research will use the DGSI inclinometer manufactured by Slope Indicator Company. The main components of this device are presented in Figure 3-5, as follows:

A. The traversing inclinometer probe, which is the standard device for surveying the casing. The traversing probe obtains a complete profile because it is drawn from the bottom to the top of the casing; and

B. The portable readout, which is used to record the surveys obtained with the portable probe. Advance readouts store readings in solid-state memory, eliminating pencil, paper, and transcription errors, and transfer the data to a computer for processing

The inclinometer allows recording the deflection of the entire profile (in depth) at given times. In order to use this technique it is necessary to drill a vertical borehole and insert the inclinometer casing. The inclinometer probe is then made to pass through the entire length of the hole, taking readings at fixed predetermined depths from the top surface. During the process, two accelerometer probes sense the inclination of access tube in two planes at right angles to each other.

Figure 3-5. Portable inclinometer

The high level voltage output from the probe is directly proportional to the sine of the angle of inclination of the long axis of the probe from vertical. A set of initial base reading is taken at given depths within the gage well. This forms the reference datum. All subsequent readings are taken over a period of time at identical depths, thereby indicating rate, magnitude, and direction of lateral deformation. This inclination is displayed in terms of angular or horizontal displacement (deviation) on the electronic readout equipment at the ground level with the operator. Provided that one end of the access tubing is known to be fixed, it is possible to obtain a complete profile of the gage well by taking a succession of readings. By comparing these profiles, the horizontal displacement of the gage well at different depths over a period of time may be determined.

3.2.5. Tiltmeter

The tiltmeter is an instrument that allows for the measurement of the inclination of an object. It responds to the local acceleration of gravity 'g'. Tilmeter output is determined by the mass distribution of the earth. This instrument allows tracking the (continuous) variation of the inclination in time at fixed positions.

The operational principle can be shown with tools commonly used in carpentry. A plumb-bob orients itself along the direction of gravity, and then defines the local vertical. Alternatively, a fluid bubble, contained by a tube, will determine one of the loci of directions, orthogonal to gravity, which constitute the local "level". For this kind of instrument there are different options in the market, which depend mainly on the chosen manufacturer. The "Cline Lab Inc. 100010-02" tiltmeter was used in this research (Figure 3-6).

Figure 3-6. Tiltmeter

3.2.6. Water Content Probes

There are different techniques to estimate the amount of water in the soil. The more popular devices are based on the measurement of the dielectric constant. This constant is a measure of the capacity of a non-conducting material, such as soil mixture, to transmit electromagnetic waves and it is define as the ratio of the permittivity of a substance to the permittivity of free space. The dielectric constant of water (i.e. around 80 at 20 °C) is so much greater than solid particles (between 2 and 6) and air (around 1). This is because the water molecule has a dipole moment and so water can be polarized. Consequently, the contribution of water to the overall soil mixture dominates the soil dielectric constant. This implies that relatively small changes in the quantity of water have large effects on the soil dielectric constant. Using this relationship, the water content can be determined with a calibration model relating soil dielectric constant to the volumetric water content.

Two approaches are typically used to measure the dielectric constant of soil mixture and estimate the volumetric water content: time domain reflectometry (TDR) and frequency domain reflectometry (FDR).

In this research the water content probe was used to elanr abiout the moisture content at different depths. In parallel the soil retention curve (or Soil Water Characteristic Curve SWCC) that correlated soil moisture with suction will be determined in the lab. In this way the distribution of water content and suction was determined at different depths at different times of the year.

3.2.7. Strain Gages

A strain gauge (or strain gage) is a sensor that measures the strain of an object. The most common type of strain gauge consists of an insulating flexible backing which supports a metallic foil pattern (Figure 3-7). The gauge is attached to the object by a suitable adhesive. As the object is deformed, the foil is deformed, causing its electrical resistance to change. This resistance change, usually measured using a Wheatstone bridge, is related to the strain by the quantity known as the gauge factor. Basically, this sensor converts force, pressure, tension, weight, etc., into a change in electrical resistance which can then be measured. Strain-gauges are widely used for physical force measurement in mechanical, marine, aircraft and civil engineering.

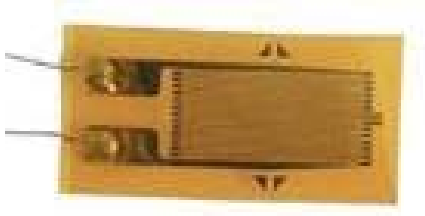

Figure 3-7. Strain Gages

The principles used in construction of the strain gauges can be used as the basis for classifying them into the following four groups: mechanical, optical, electrical, and acoustical. In this research mechanical strain gauges was used, based on a full- bridge configuration with four strain-gauges. This configuration is the recommended one. This

disposition guarantees a linear relationship, while the others not. Quarter-bridge and half-bridge circuits provide an output (imbalance) signal that is only approximately proportional to applied strain gauge force. Linearity, or proportionality, of these bridge circuits is best when the amount of resistance change due to applied force is very small compared to the nominal resistance of the gauge(s). With a full-bridge, however, the output voltage is directly proportional to applied force, with no approximation (provided that the change in resistance caused by the applied force is equal for all four strain gauges). Moreover, by using full bridge strain it is compensated both for bending (by installing at both side of nail) and for temperature (by installing one perpendicular to the main one).

The more common strain gauges used in the literature are Geokon Model VK-4100 vibrating wire strain gauges (ODOT, 1999) and Geokon Model VCE-4200 vibrating wire strain gauges (ODOT, 1999), Geokon VK-4100/4150 strain gauges (Menkiti and Long, 2008). In this research the UFCA-5-11 strain gauges from Tokyo Sokki Kenkyujo Co. Ltd. (TML), and Geokon model 4100 vibrating wire strain gauges are chosen to use in the field test.

3.2.8. Data Acquisition System

The data acquisition system is used to read the data from instruments and storage it. The following basic components are necessary: data logger, solar panel, battery and modem. A brief explanation of them is presented as follows.

Data Logger

The data logger to be used in this research is Campbell Scientific CR1000. Figure 3-8 shows the adopted device. This system has worked very well in previous TTI research, and so it has been adopted for this research. Some of the positive aspects of this device are as follows:

1) Serial communications with serial sensors and devices supported via I/O port pairs. It supports all of devices used in this research.
2) Solar panels and batteries was required. It I possible to use this power supply with CR1000.
3) Compatible with channel expansion peripherals allowing expanding the system Up to 32 channels if necessary (by default it has 16 channels).

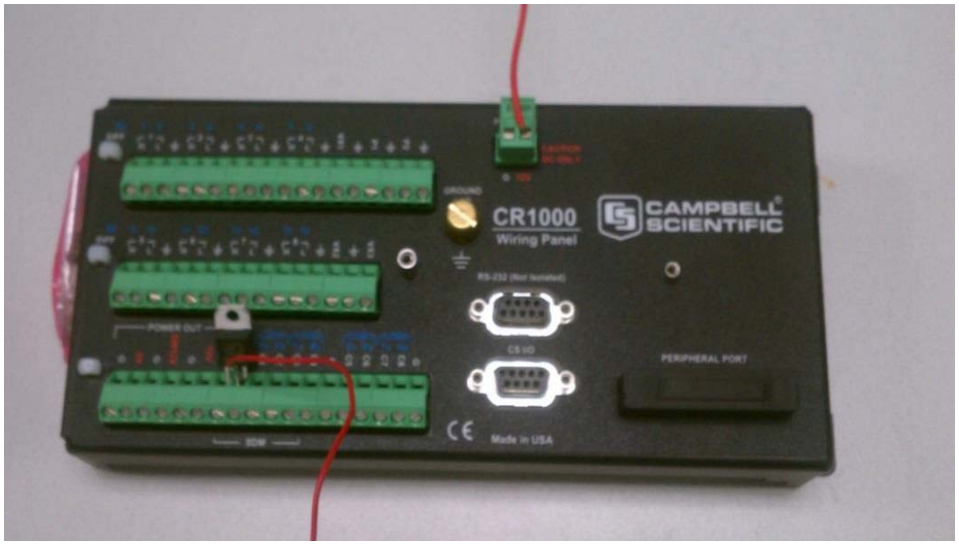

Figure 3-8. CR1000 data logger

Solar Panel

In this research Campbell Scientific SP10-10W solar panel was used for the power supply. Figure 3-9 shows the device to be used in this research. It supplies electrical power in locations where ac power is unreliable, expensive, or not available.

Figure 3-9. SP10-10W solar panel

Battery

Campbell Scientific PS100 rechargeable power supply was used in this research. The PS100 provides a 12-Vdc, 7-Ahr rechargeable power supply. The rechargeable battery can be trickle-charged from ac or from an external solar panel. Figure 3-10 shows the device described above.

Figure 3-10. PS100 rechargeable power supply

4. TESTS AT NGES-TAMU CLAY SITE

4.1. Introduction

Creep behavior in soils is closely related to the stress level. However, GEC#7 associates creep behavior directly with the presence of high Plasticity clays, regardless of the load level. To determine the effect of load level on creep behavior of soil nails, pullout test were performed at NGES-TAMU clay site. Two different kinds of tests were performed. Tests on existing anchors installed more than 20 years ago (with a very well-known load history), and tests on new soil nails constructed in the context of this research. These tests mainly focus on studying the effect of the load level on creep behavior of soil nails in HP clays.

This section describes test site characteristics including the location of the test site, existing anchors and new soil nails layout. In context of this research, soil samples were collected from different boreholes and laboratory tests were performed. Brief presentation of laboratory tests is included in this section. All the activities related to existing anchors installed in 1991, background and results of the tests in 1991 and 1997 are presented in section 4.3, while section 4.4 covers the load test set-up, and results of the pullout tests on new nails.

4.2. NGES-TAMU Clay Site Characteristics

4.2.1. Test Site

The location of test site for the new nails and existing anchors is at “NGES-TAMU clay site’ (Figure 4-1), which covers about 5500 m^2 at the end of “Runway 4” located on the Texas A&M University Riverside campus (4.2).

Figure 4-1. Location of test site (NGES-TAMU clay site) on Google map

Figure 4-2. Location of test site (NGES-TAMU clay site) on Riverside Campus

New nails were installed very close to the existing anchors. Detailed layout of new nails is shown in Figure 4-3. Seven boreholes were drilled by Terracon Consultants Inc. The aim was sampling the soil at the testing location, to perform then the laboratory investigation to gather the basic properties of the soil at this location. The positions of these boreholes (BH1 and BH7) are also indicated in Figure 4-3. Figure 4-4 illustrate the location of the existing anchors.

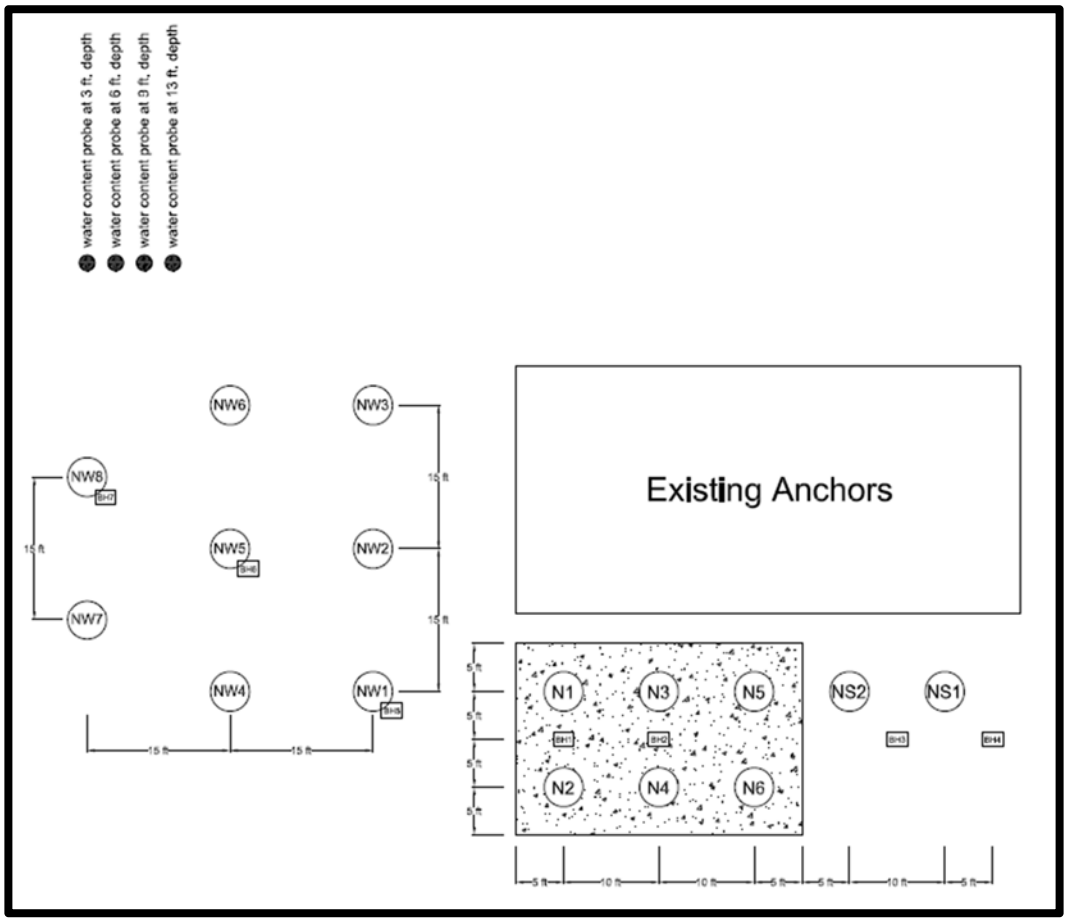

Figure 4-3. Layout of nails and boreholes

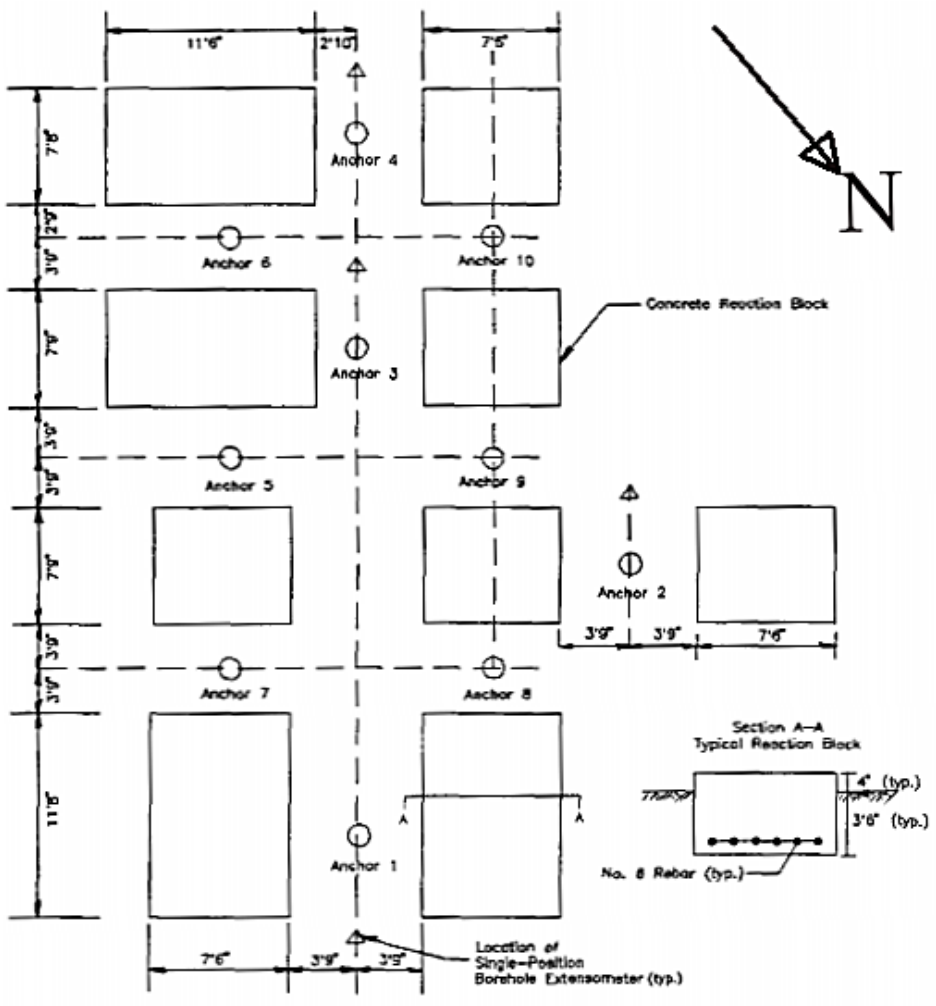

Figure 4-4. Location of anchors and spread footings (after Powers, 1993)

4.2.2. Soil Properties

A large number of tests have performed at NGES-TAMU clay site in the last few decades (e.g. Briaud, 1998). Figure 4-5 shows a large view of the zone with the location of the more relevant test performed in 90's.

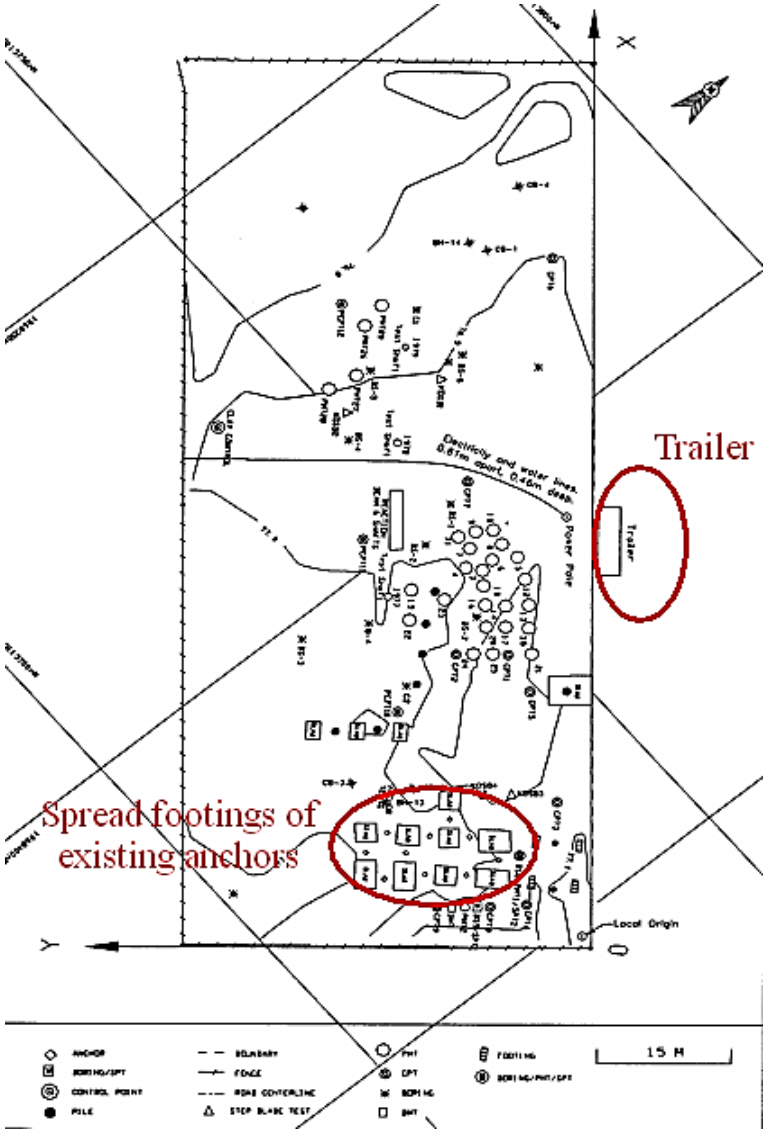

Figure 4-5. Previous tests done at the NGES-TAMU clay site (after Briaud et al., 1998)

The stratigraphy of the NGES-TAMU clay site is illustrated in Figure 4-6, as described by Briaud (1998) “the clay site is underlain by four distinct layers. The clay unit at the surface is very uniform in thickness down to about 18 ft. (5.5 m) in depth below the

surface. Below the clay, the sand unit is variable in thickness and averages 3 ft. (1 m). The third unit, another clay unit, generally reaches around 21 ft. (6.5 m) below the surface and continues to a depth of approximately 42 ft. (12.5 m). The fourth unit continues to a depth greater than 165 ft. (50 m)."

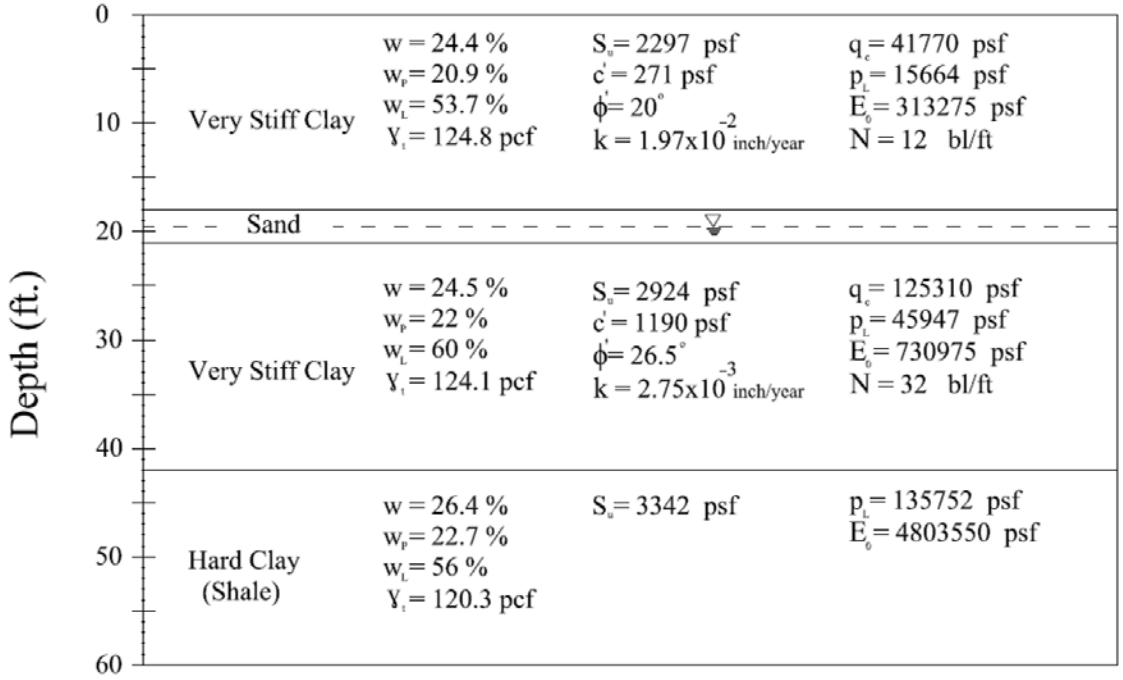

Figure 4-6. Stratigraphy and soil properties of the NGES-TAMU clay site (after Briaud et al., 1998)

The summary of soil properties from laboratory tests and field tests are shown in Figure 4-7 and Figure 4-8 (Briaud, 1998).

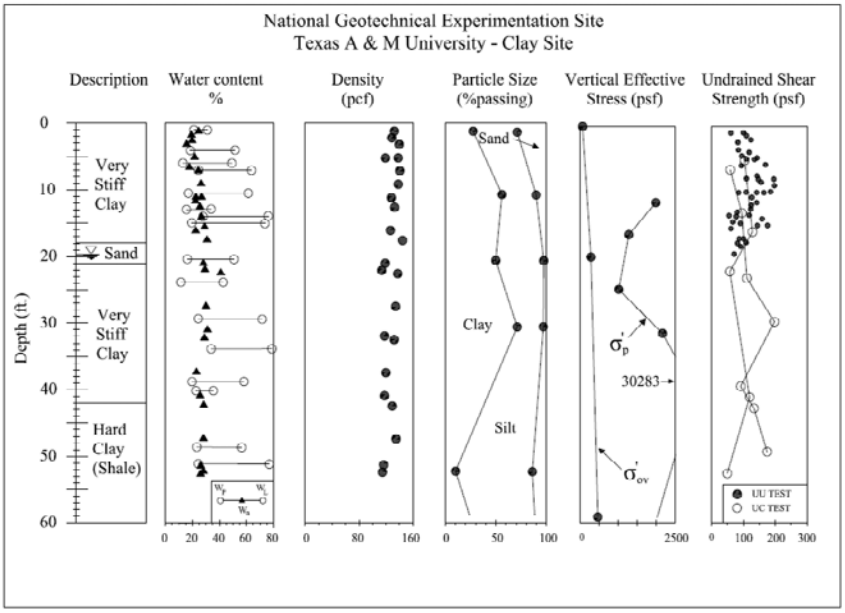

Figure 4-7. Soil properties from laboratory tests at NGES-TAMU clay site (after Briaud et al., 1998)

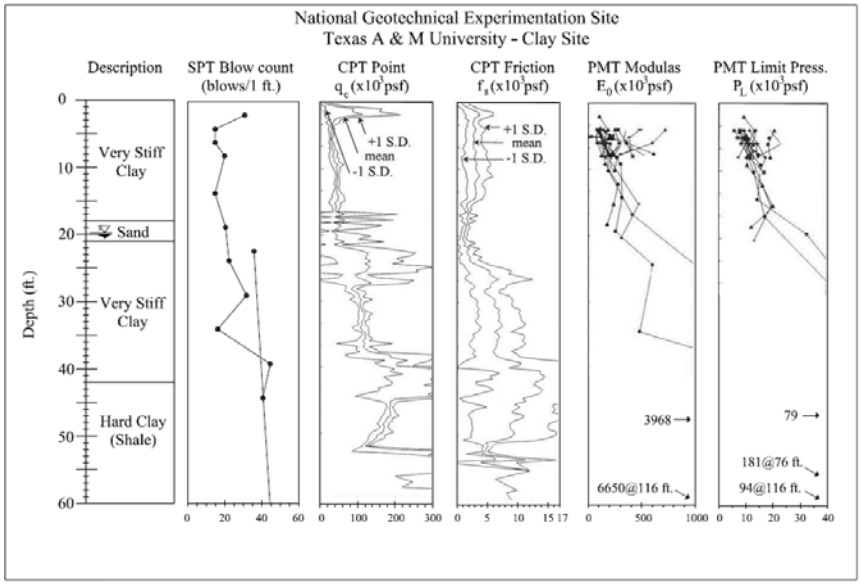

Figure 4-8. Summary of soil properties from field tests in NGES-TAMU clay site (after Briaud et al., 1998)

Table 4-1 (Briaud, 1998) and Table 4-2 (Powers, 1993) present the soil properties that had been used to design existing anchors. This information was used in this research to the preliminary design the soil nail length and test load protocol.

Table 4-1. Soil properties of layers (after Briaud et al., 1998)

Soil properties	**0~21 ft. clay**	**23.8~41 ft. clay**	**Clay shale**
Water content	$w = 24.4\%$	$w = 24.5\%$	
Plastic limit	$w_p = 20.9\%$	$w_p = 22\%$	
Liquid limit	$w_l = 53.7\%$	$w_l = 65.5\%$	
Natural unit weight	$\gamma_t = 124.8\,pcf$	$\gamma_t = 124.1\,pcf$	
Undrained shear strength	$S_u = 2298\,psf$	$S_u = 2924.6\,psf$	
Cone penetrometer tip resistance	$q_c = 41780\,psf$	$q_c = 125340\,psf$	
Pressuremeter limit pressure p_L	$p_L = 16712\,psf$	$p_L = 45958\,psf$	$p_L = 135785\,psf$
SPT blow count	$N = 32 blows/1 ft.$	$N = 32 blows/1 ft.$	
Ratio of E_0 over p_L	$E_0 / p_L = 25$	$E_0 / p_L = 16$	$E_0 / p_L = 230/6.5 \approx 35$

It is interesting to note that a ratio between the modulus E_0 over the limit pressure P_L around 12 (i.e. E_0/P_L ~12) would be expected for a normally consolidated clay. The

clay between ground level and 21 ft. is judged to be highly over-consolidated. However, based on the same ratio, it is considered that the clay between 24 and to 41 ft. is moderately over-consolidated.

Table 4-2. Summary of SPT, CPT and laboratory data to design existing anchors (after Powers, 1993)

	Laboratory tests				Atterberg limits			In situ tests						
									CPT8			CPT9		
Depth (ft)	Soil type (USCS)	Unit weight (pcf)	Moisture content (%)	S_u (psi)	Liquid limit (%)	Plastic limit (%)	Plasticity index	SPT (blows/ft)	Q_s (tsf)	Q_c (tsf)	F_r (tsf)	Q_s (tsf)	Q_c (tsf)	F_r (tsf)
5	CH	125	23.9	12.5	51	18	33	9	0.8	10	8	1.5	18	8.3
10		122	23.6	11.5				11	1	18	5.6	0.9	20	8.3
15	CH	129	29.3	18	77	27	49	16	1.1	20	5.5	2	40	4.5
20		129	29.7	12.2				16	1.5	220	4.7	0.5	10	5
25	CL	127	24.2	18.6	43	11	32	27	2	50	4			
30		122	29.5					35	3.5	60	5.8	1.3	63	2.1
35	CH	119	29.6	18.3	84	34	50	31	2.7	61	4.4	1.2	62	1.9
40		122	27.3	19.7				44	3.4	90	3.8	1	82	1.2

In context of this research, laboratory tests are performed to obtain soil properties and shear strength of the soil. The water content (Figure 4-9) is quite constant from ground surface to depth 10ft, then gradually increases by 30% at depth 18ft (which is the bottom of nails). The unit weight (Figure 4-10) is around 125 pcf. Soil is considered to be fully saturated ($S_r \geq 85\%$) even if the ground water level is at the depth 18ft (Figure 4-11), and is high PI clay (Figure 4-11). Shear strength profile of the soil obtained from triaxial test and direct shear test is shown in Figure 4-13.

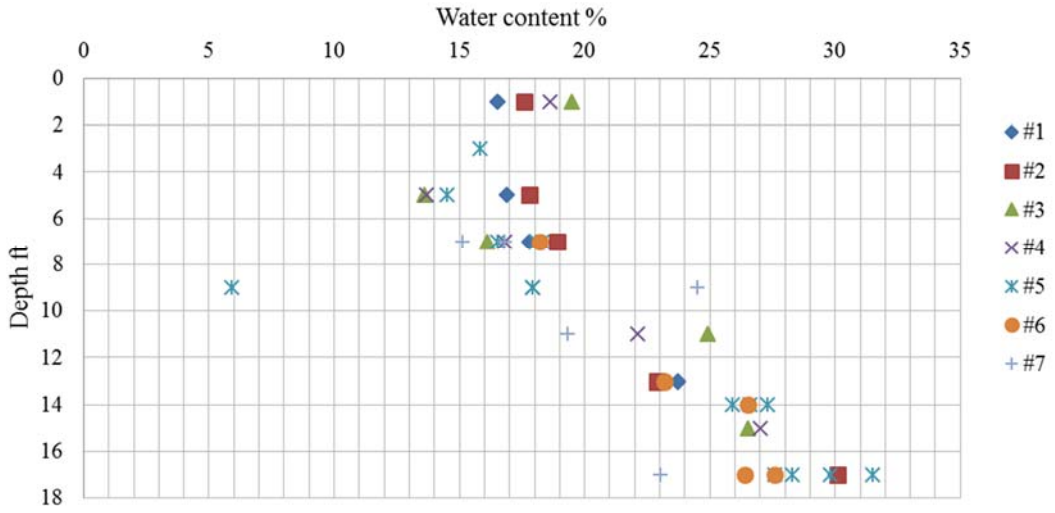

Figure 4-9. Water content profile with depth

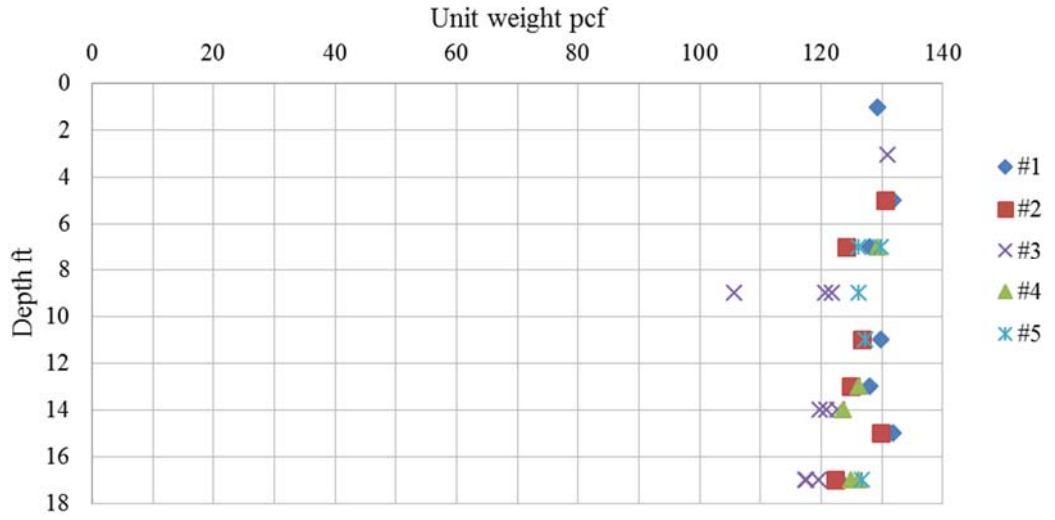

Figure 4-10. Unit weight profile with depth

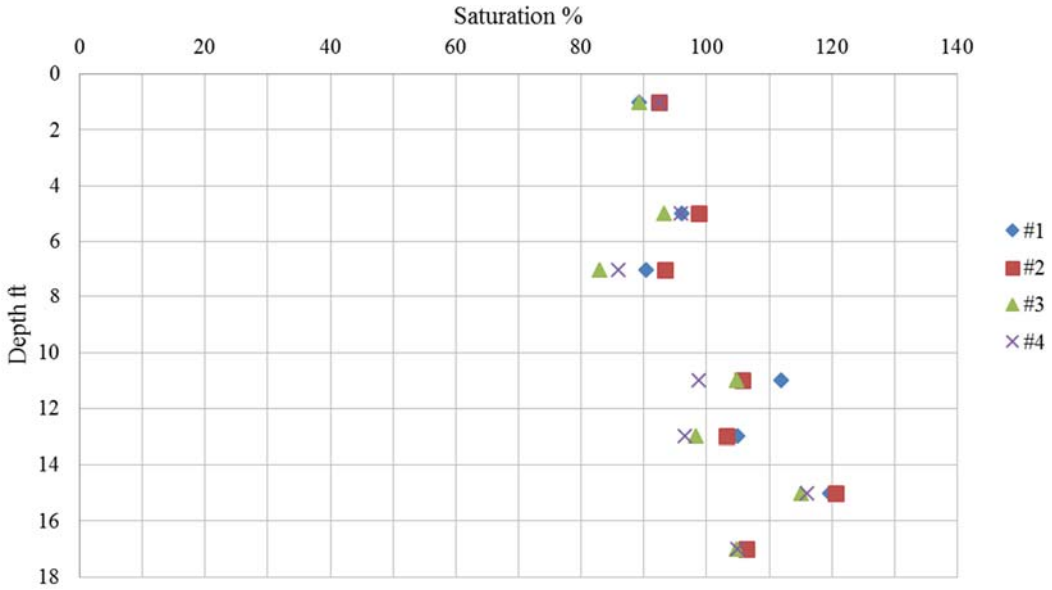

Figure 4-11. Saturation profile with depth

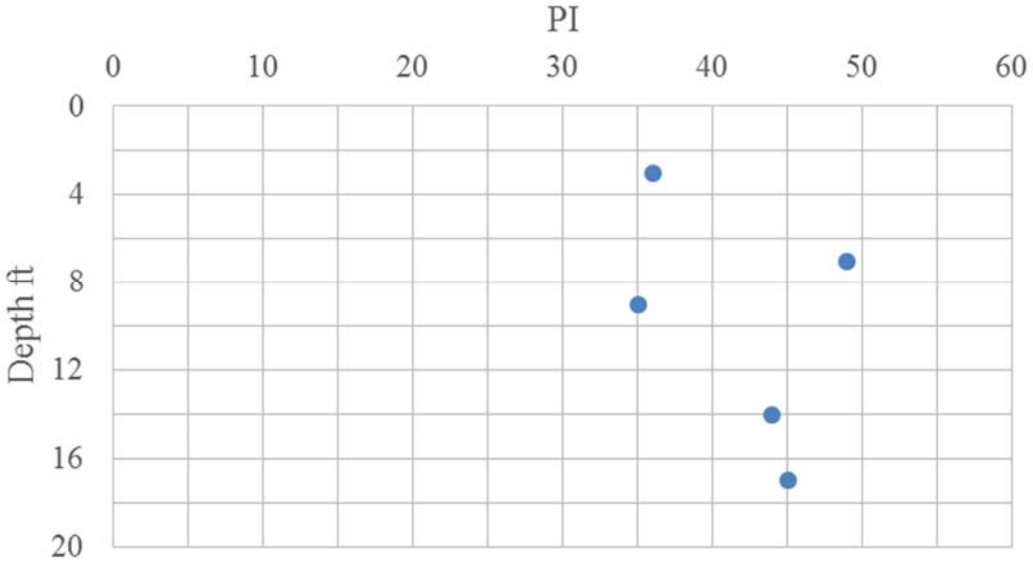

Figure 4-12. PI profile with depth

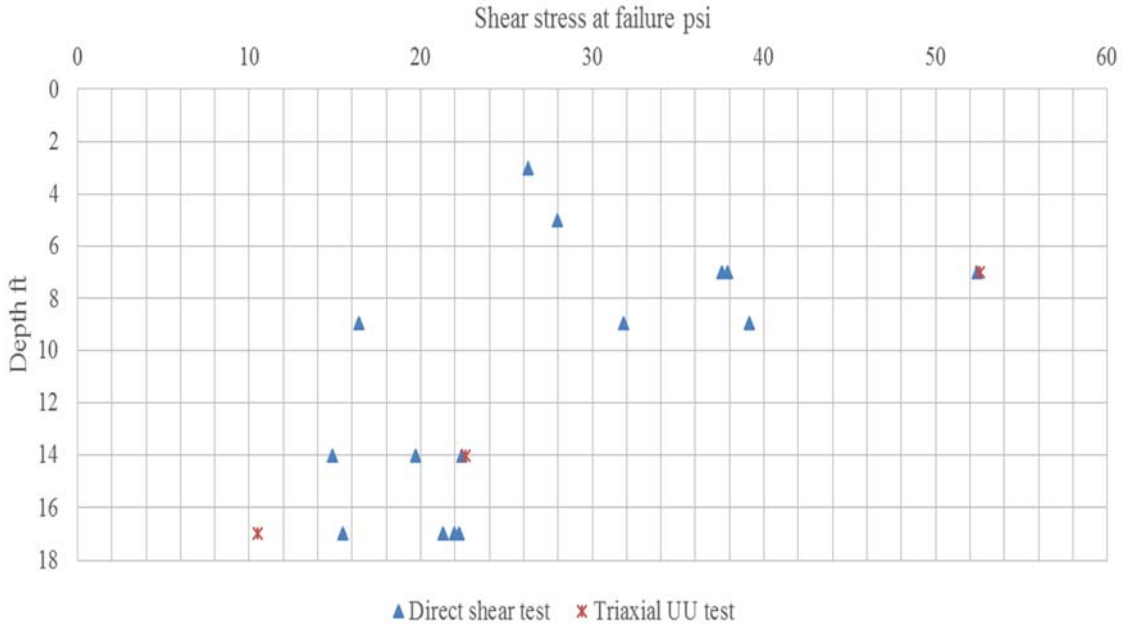

Figure 4-13. Soil strength profile in different depth

4.3. Tests on Existing Anchors at NGES-TAMU Clay Site

This section deals with the retesting of the existing anchor at NGES-TAMU. The aim of this activity is to design the instrumentation and loading protocol for the new nails. In addition, it was a great opportunity to retest the anchors to study the creep behavior after 23 years of installation. First, a summary of the previous research on existing anchors in NGES-TAMU at the clay site will be introduced as background information. Afterwards, the tests set-up, load protocol and results of the load tests in July 2013 (during this research) will be presented. Results of new tests will be compared to the results of the tests in 1991 and 1997.

4.3.1. Introduction to Previous Research on Anchors at NGES-TAMU Clay Site

Ten anchors were constructed at the NGES located on the Texas A&M University Riverside campus. Those anchors were initially load tested in 1991 and then retested in 1997 (Figure 4-14).

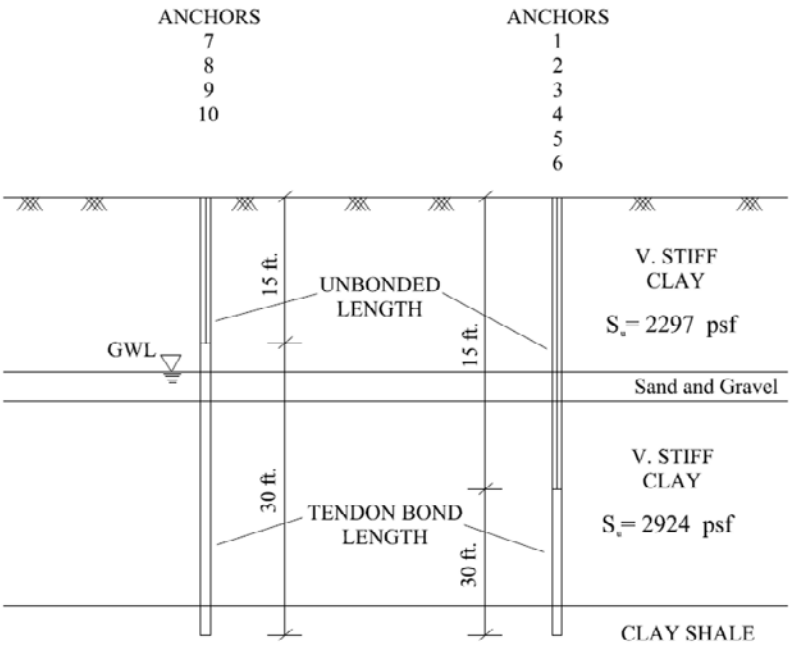

Figure 4-14. Stratigraphy and anchors specifications (after Briaud et al., 1998)

All anchors were embedded 45.2 ft. (13.8m) in the clay deposit, going through the four soil layers as shown in Figure 4-14. A total of 68 instruments were installed in the bonded lengths and at the beginning of the unbonded lengths of the six anchors. The installation of the 10 anchors and the subsequent load testing took place from Nov. 1990

to Jul. 1991. The load tests were tension or uplift tests performed by pulling on the anchors with a hollow hydraulic jack with the capacity of 385.8 kips (175 tons) (Figure 4-15).

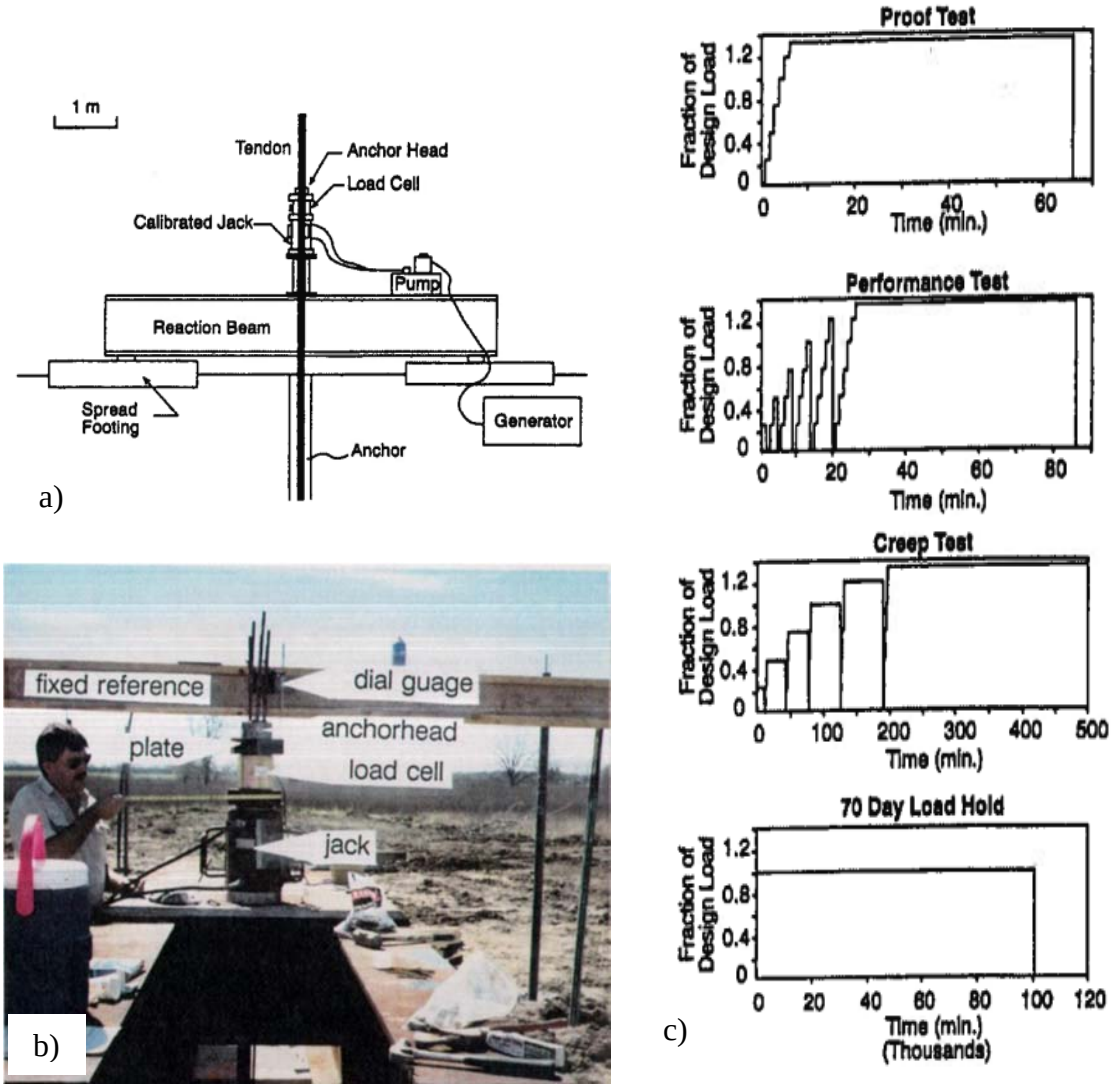

Figure 4-15. a) Load test setup (after Briaud et al., 1998); b), Photo of pullout test (after Powers, 1993); c) Load history for four load test types (after Briaud et al., 1998)

4.3.2. Test Details of Previous Research on Anchors

There are three main aspects to pay attention respect to the previous test results on anchors:

a) The ultimate load on each anchor;

b) The difference of ultimate load between tests in 1991 and tests in 1997;

c) The creep load threshold of each anchor.

The ultimate load (or failure load) on each anchor tested in 1991 is shown in Table 4-3 (Powers, 1993). The failure load is defined as the load at which the residual movement reached 1 inch (Powers, 1993). In all the cases, the residual movement did not reach 1 inch and the failure load was estimated by manual extrapolation (Powers, 1993).

Table 4-3. Predicted ultimate capacity of anchors tested (after Powers, 1993)

Anchor	Type of Test						Dates(s) of tests	Maximum Test Load (kips)	Failure Load (kips)	Load @ 0.08 inches/ log cycle	Stiffness (kips/in)	Stiffness @ 0.5" (kips/in)	Creep Rate @ Max. Load (inches/ log cycle)	Creep Rate @ Fail. Load (inches/ log cycle)
	Proof		Performance		Creep									
	Initial loading	Final loading	Initial loading	Final loading	Initial loading	Final loading								
1					*		4/8/91 - 4/10/91	174	208	—	549	354	0.050	0.146
						*	7/14/91 - 7/16/91	177	291	—	671	416	0.009	0.042
2					*		4/10/91 - 4/12/91	197	262	—	732	407	0.050	0.162
						*	7/12/91, 7/13/91	198	325	—	1203	473	0.034	0.181
3	*						4/4/91	236	*****	—	842	*****	0.021	*****
		*					7/10/91	249	*****	—	1264	*****	0.030	*****
4			*				4/3/91	179	222	174	657	363	0.103	0.301
				*			7/9/91	176	376	—	1237	502	0.029	0.285
5	*						3/26/91	134	*****	—	1034	*****	0.009	*****
		*					3/26/91	226	243	206	10346	375	0.473	0.662
6			*				3/20/91	133	133	—	526	247	0.017	0.017
				*			3/20/91	132	135	—	12300	271	0.025	0.025
7					*		3/8/91, 3/11/91	153	180	158	623	303	0.094	0.154
						*	3/18/91, 3/19/91	186	188	164	1144	339	0.231	0.244
8					*		3/6/91, 3/7/91	169	147	144	164	84	0.436	0.128
						*	3/7/91	176	167	167	2239	312	0.310	0.072
9					*		3/27/91	149	247	—	853	338	0.050	0.103
						*	3/27/91, 3/28/91	149	286	—	5605	414	0.044	0.357
10					*		3/21/91	177	177	161	533	326	0.300	0.300
						*	3/22/91	176	172	155	9436	328	0.500	0.409

Anchors 1, 2, 7, and 8 were retested on August 1997, and results of the 1991 and 1997 ultimate loads are compared in Table 4-4. It can be observed that the gain on ultimate load was at least 20% regardless whether there was a hold load on the anchor (as for example for anchor 1= 117.5 kips (523kN), or anchor 2 = 136 kips (606kN)) or not (as for the anchors 7 and 8) (Briaud et al., 1998). The ultimate load for each anchor was defined as the load obtained for a residual displacement of one-tenth of the anchor diameter (B/10). Alternatively the ultimate load was also defined as the load measured for a total displacement of B/10 plus the elastic elongation of the unbounded length of the anchor (the maximum load applied divided by extrapolated ultimate load > 0.8) (Briaud et al., 1998).

Table 4-4. Comparison of 1991 and 1997 ultimate loads (after Briaud et al., 1998)

Anchor Number	Date Installed	Date Tested	Capacity (kN)	Date Tested	Capacity (kN)	Date Tested	Capacity (kN)
1	1-16-91	4-9-91	867	7-15-91*	978(?)	8-30-97	1245
2	1-16-91	4-11-91	1080(?)	7-13-91*	1156(?)	8-30-97	1255
7	12-19-90	3-7-91	801	3-18-91	738	8-30-97	1090
8	12-19-90	3-7-91	747	3-7-91	738	8-30-97	1060

Note: All capacities correspond to a residual movement of 25 mm.
*Denotes capacity after 70-day load-hold test.
(?) Capacity calculated by extrapolating load-movement curve.

Examining Figure 4-16 and Figure 4-17 it can be observed that a creep load threshold exists and that below the threshold load the creep rate is very small. On the contrary, it can be observed that for loads above this threshold load, the creep rate is much larger (Briaud et al., 1998).

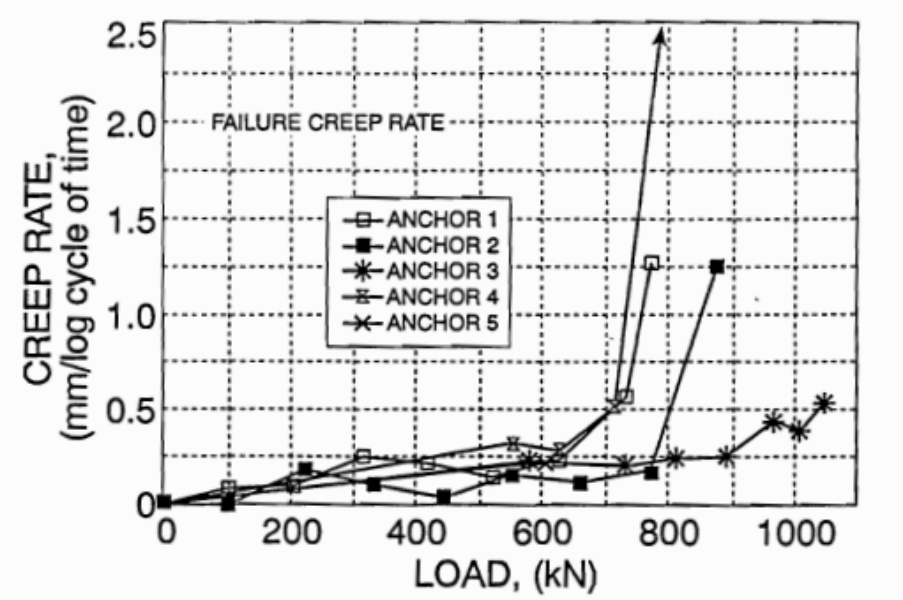

Figure 4-16. Creep rate vs. load curves for first loading on 4.6m bonded length tested in 1991 (after Briaud et al., 1998).

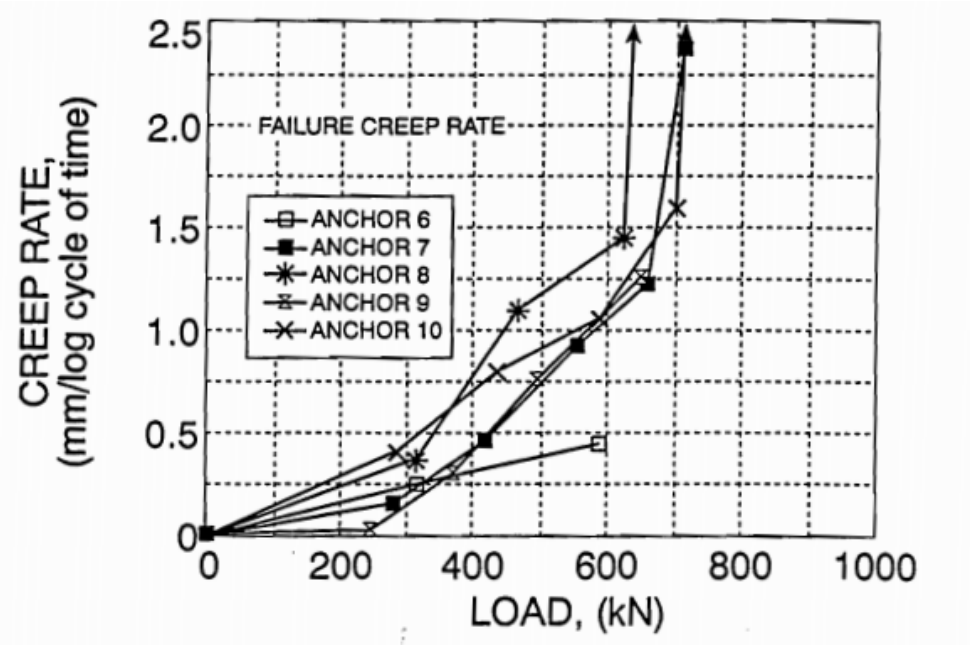

Figure 4-17. Creep rate vs. load curves for reload on 9.2m bonded length tested in 1991 (after Briaud et al., 1998)

The comparison of tests results of anchor 1, 2, 7, and 8 in 1991 and in 1997 shows that there is gain of 20% (at least) on strength (Briaud et al., 1998). In context of this research, pullout tests were performed to check the current ultimate load of the anchor (i.e. how much the strength has increased or decreased since 1997).

4.3.3. Details of Tests on Anchors in Context of this Research (July 2013)

Anchors 1, 2, 3, 4, 7, 8, 9 and 10 were retested in July 2013 after 23 years of installation. These anchors were constructed and tested at NGES-TAMU clay site in 1991. During the tests on anchors 3 and 4, tendons of these anchors failed at 238 kips due to erosion and the tests were stopped. Figure 4-18 shows the failure of the tendons for these

anchors. Load tests set-up used to retest the anchors is shown in Figure 4-19. It consists of reaction beam, hollow hydraulic jack, load cell, anchor head and dial gauges. Load protocol and results of pullout tests will be presented as follows.

Figure 4-18. Failure of anchors 3 and 4 tendons during the test at 238 kips

Figure 4-19. Load test set-up in July 2013, a) Photo of pullout test; b) Place the reaction beam; c) load cell and dial gauges

Load Test Protocol

Verification tests with creep steps were conducted on anchors 1, 2, 3, 4, 7, 8, 9 and 10. In the verification test, load steps with duration of 10 minutes was applied and the movement of anchor head was recorded at 1, 2, 3, 5, 6 and 10 minutes after the load applied. If the creep movement exceeded than 0.04 in, for 10 minutes reading, the load was held for 60 minutes and the movement of anchor head was recorded at 20, 30, 50 and 60 minutes also. Figure 4-20 illustrates the load test protocol for the anchors.

Tested anchors in 1991 and 1997 did not failed, and the ultimate pullout capacity of the anchors reported in previous researches were estimated by manual extrapolation (Table 4-4). Therefore, to obtain the ultimate pullout capacity, loading steps were increased and the anchors were loaded until the failure reached. The increment for each load step was 26 kips.

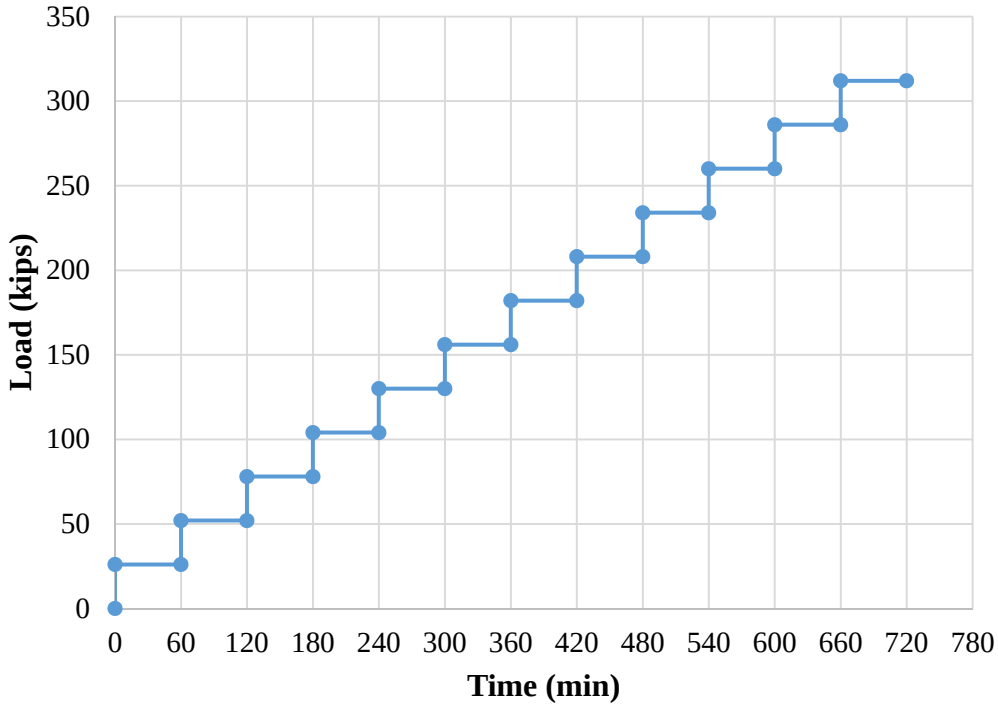

Figure 4-20. Load sequence for pullout test on existing anchors in July 2013

Total, Elastic and Residual Movement

During the test, the anchors were incrementally loaded until failure occurred. Total movement is defined as the measured movement of the anchorhead during the test. Total movement consists of elastic movement and residual movement. Elastic movements are the recoverable movements when the anchor is unloaded (i.e. the anchor load is reduced from a test load to an alignment load). Residual movements are non-recoverable movements measured when the anchor is unloaded (FHWA, 1998). Figure 4-21 to Figure 4-28 illustrate the total, elastic and residual movements versus test loads on tested anchors.

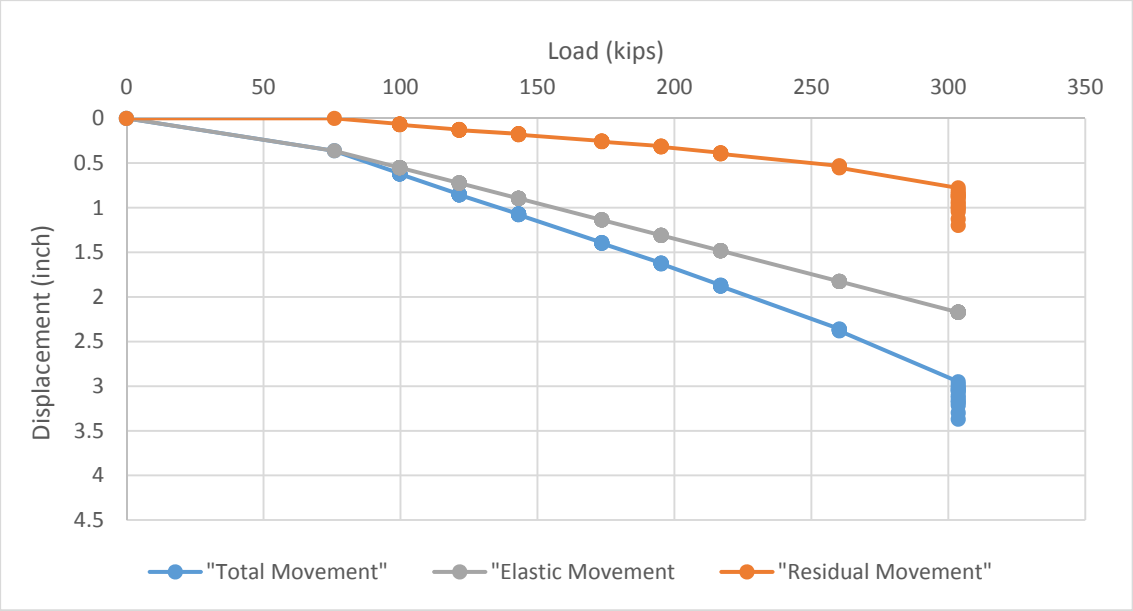

Figure 4-21. Load-Displacement for anchor 1

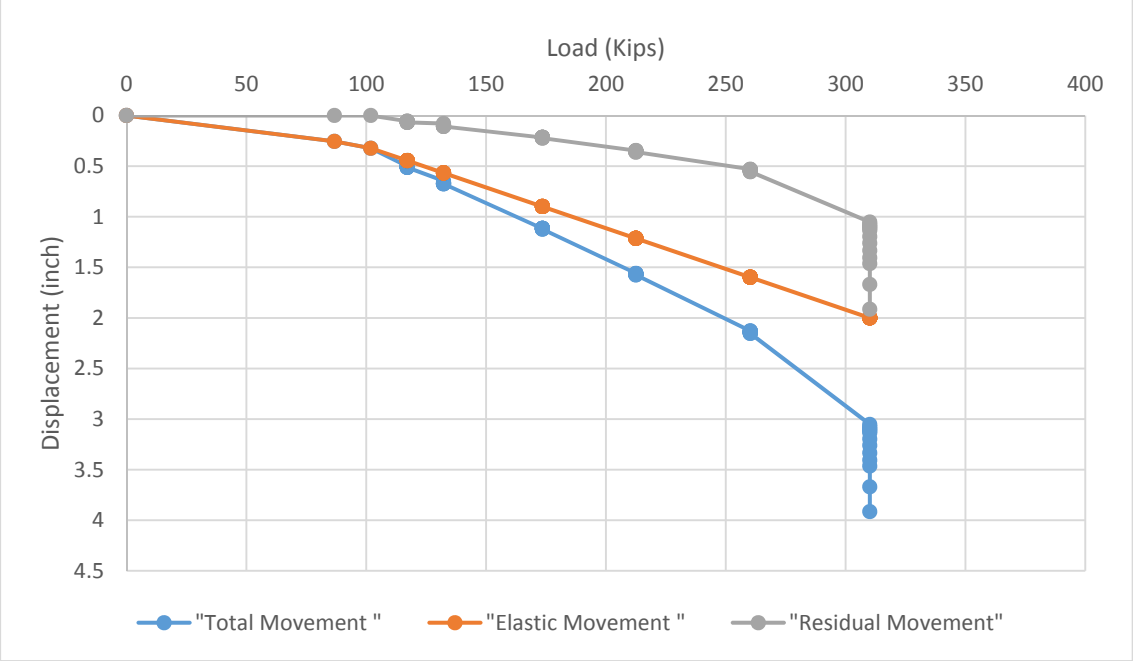

Figure 4-22. Load-Displacement for anchor 2

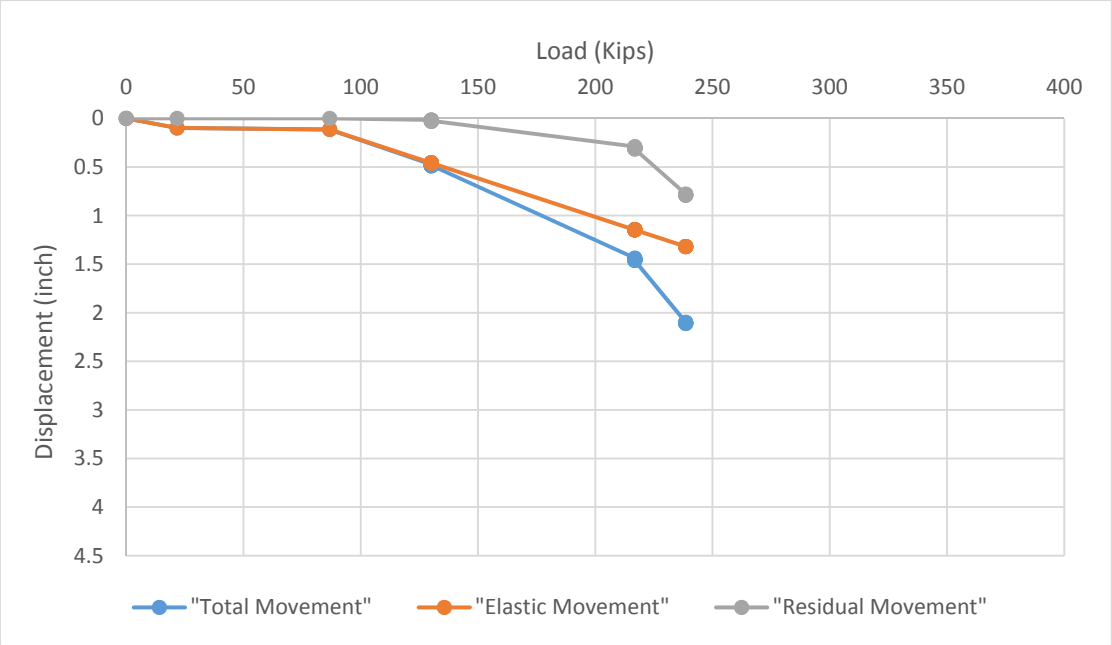

Figure 4-23. Load-Displacement for anchor 3

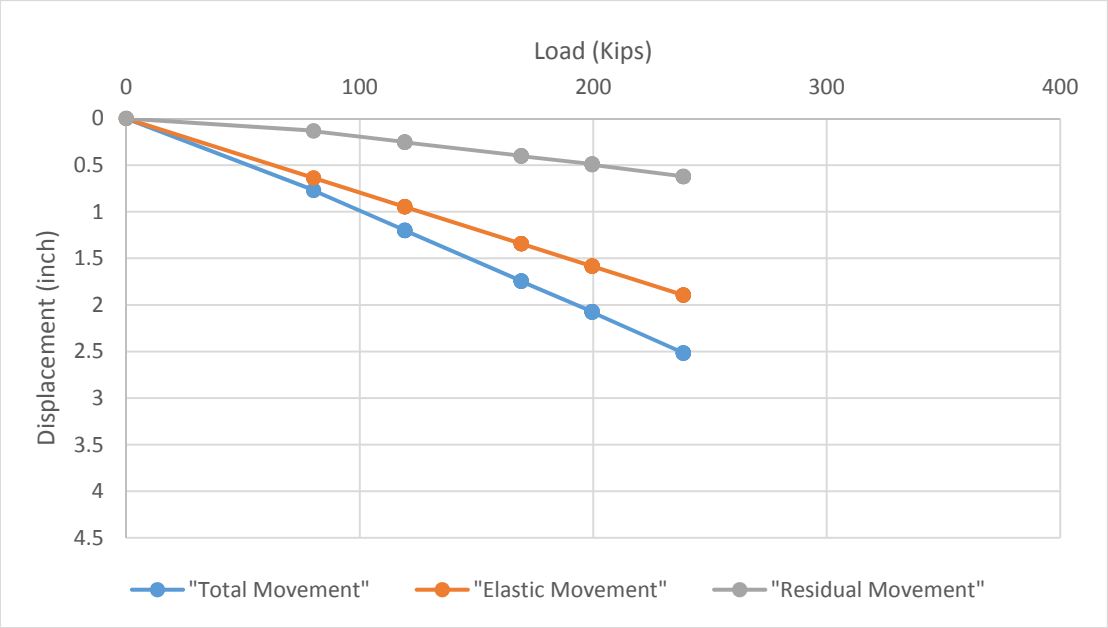

Figure 4-24. Load-Displacement for anchor 4

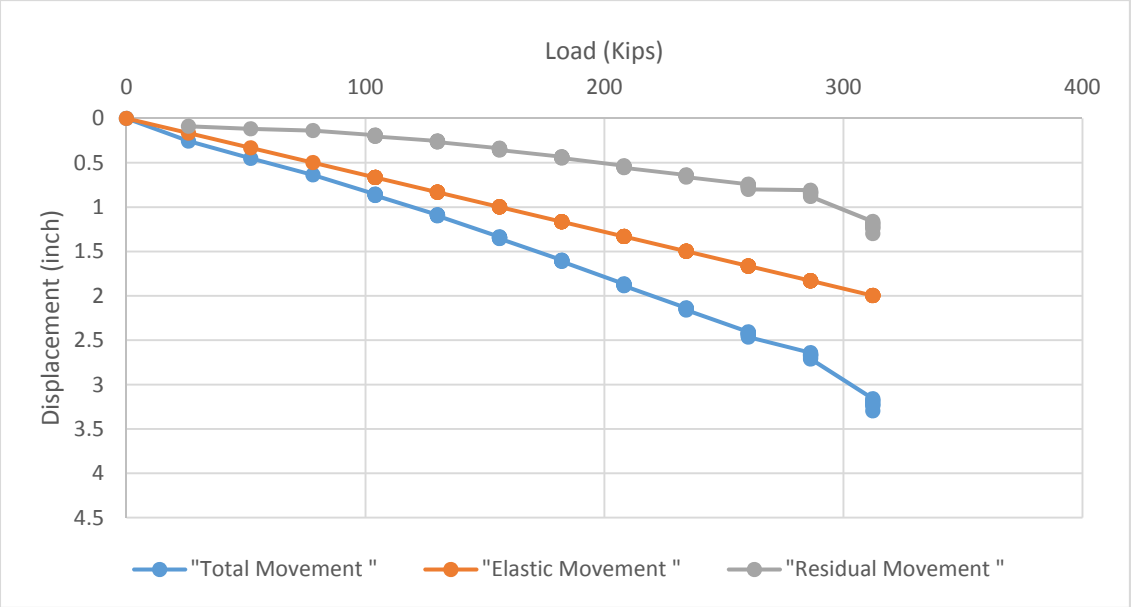

Figure 4-25. Load-Displacement for anchor 7

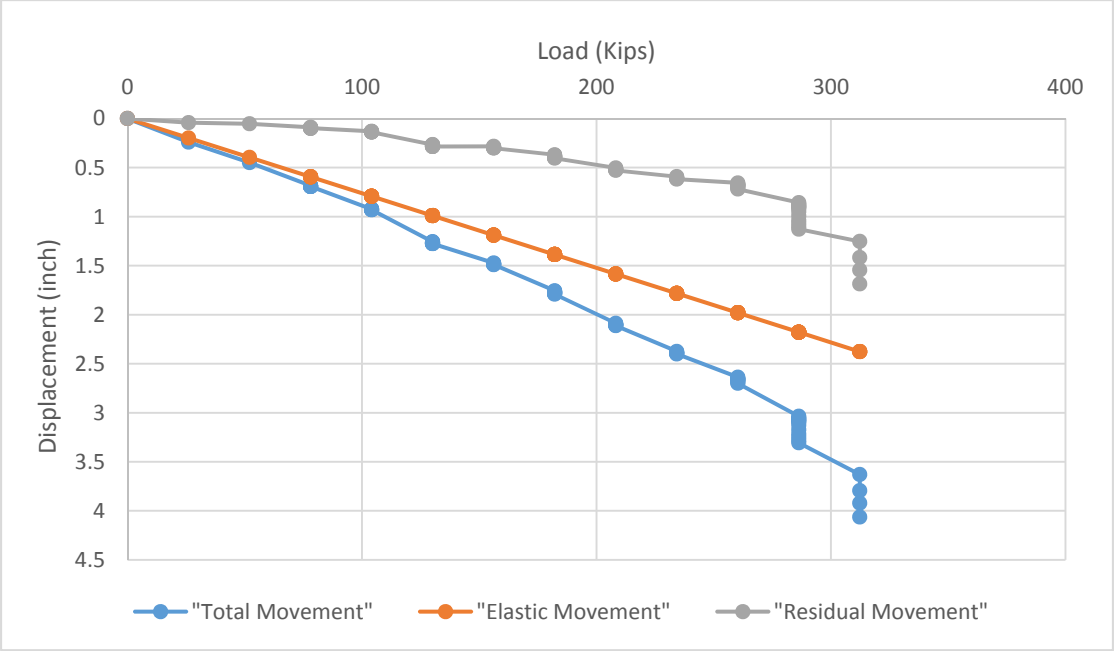

Figure 4-26. Load-Displacement for anchor 8

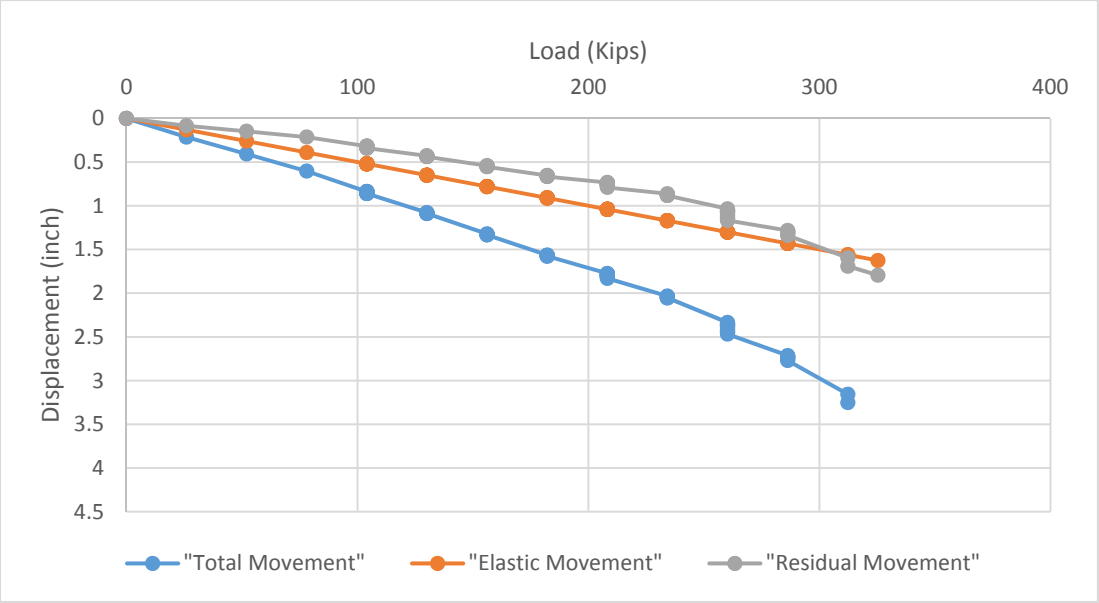

Figure 4-27. Load-Displacement for anchor 9

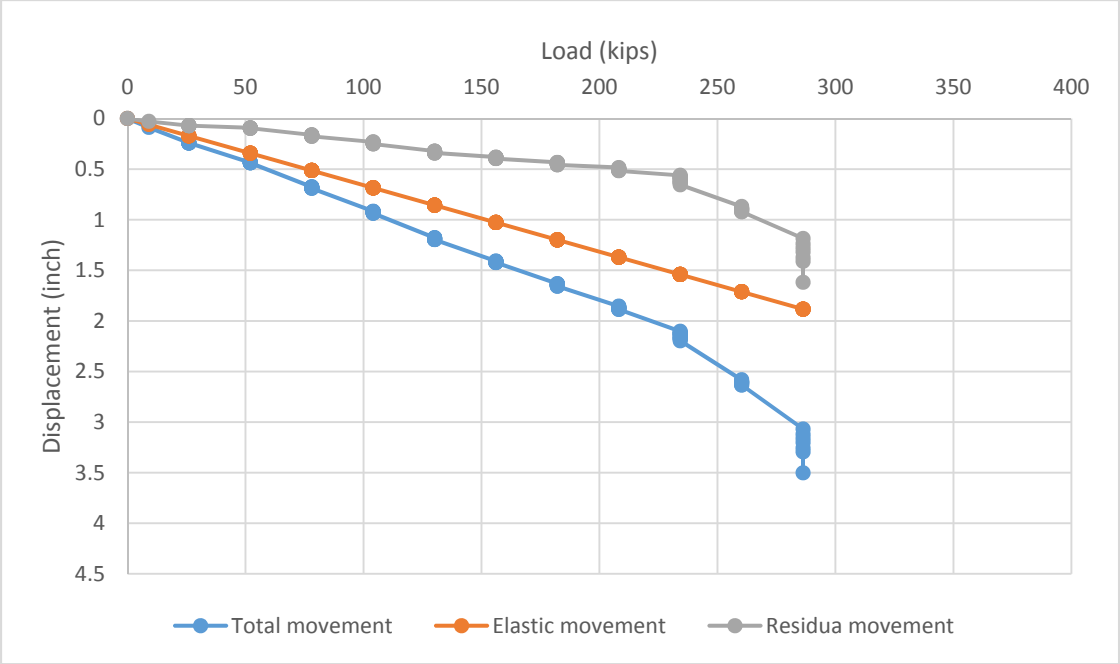

Figure 4-28. Load-Displacement for anchor 10

The lengths of the tested anchores are presented in Table 4-5. The drilled depths were 45 ft. Anchors 1 to 4 has 15 ft. bond length and 36 ft. unbonded length, while anchors 7 to 10 has 30 ft. bond length and 21 unbonded length.

Table 4-5. Length for tested anchors (after FHWA, 1998)

Anchor No.	Total Tendon Length (ft.)	Drilled Length (ft.)	Tendon Bond Length (ft.)	Unbonded Length (ft.)
1-4	51	45	15	36
7-10	51	45	30	21

Figure 4-29 and Figure 4-30 show the residual movement for the tested loads for anchors 1,2,3,4 and 7, 8,9,10 respectively.

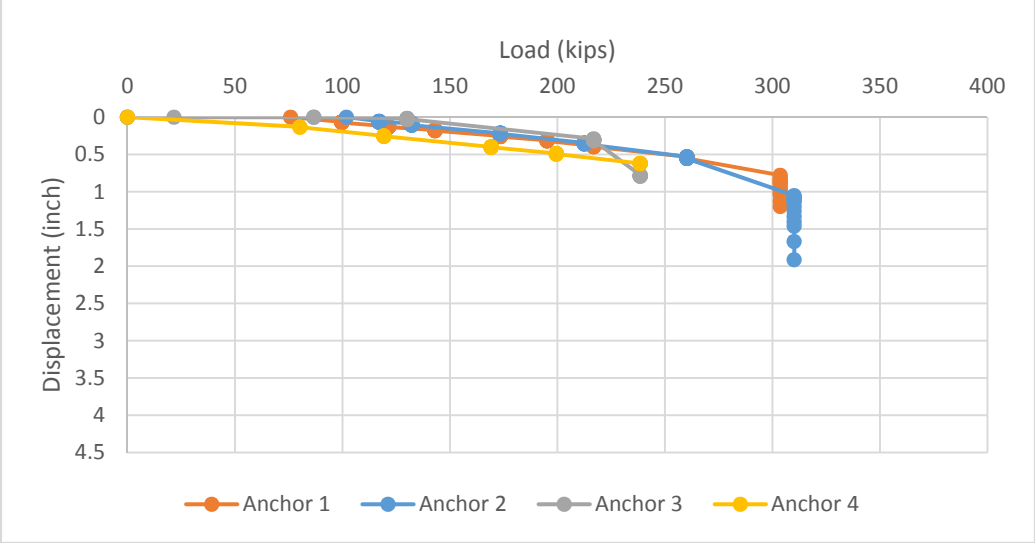

Figure 4-29. Residual displacement versus load for anchors 1 to 4

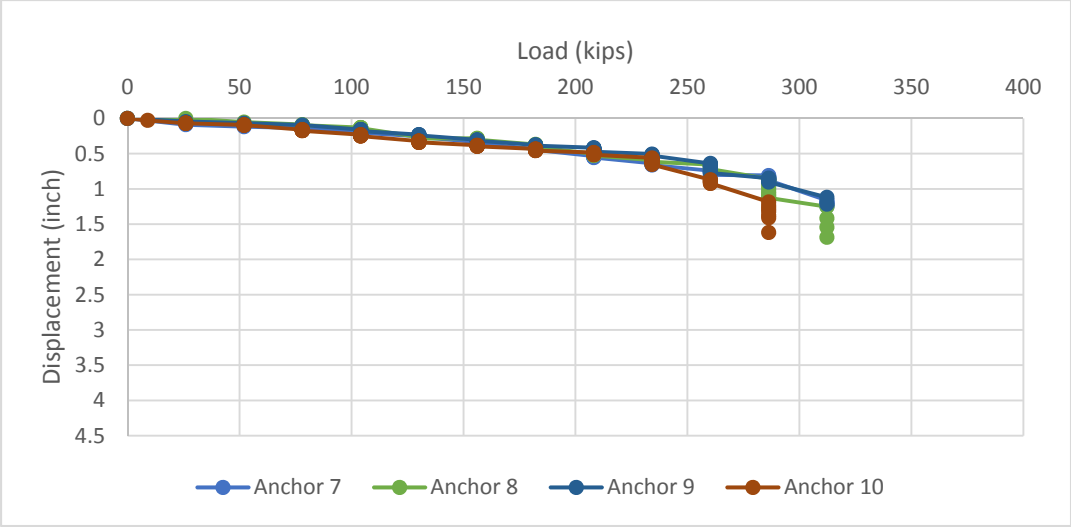

Figure 4-30. Residual displacement versus load for anchors 7-10

The ultimate load for each anchor was defined as the load obtained for a residual movement of the anchor equal to one-tenth of the anchor diameter (B/10) or for a total displacement of B/10 plus the elastic elongation of the anchor unbonded length (Briaud, 1998).

$$\frac{B}{10} = \frac{12in}{10} = 1.2\ inch \tag{4.1}$$

Therefore the ultimate load capacity of the anchors is defined as the load for the residual movement of 1.2 inch.

Ultimate load capacity is the load that mobilizes the maximum friction between grout and the soil. The ultimate pullout capacity of the anchors Q_u is defined as:

$$Q_u = \pi D L_a f_{max} = F_{max} L_a \text{ (Briaud, 1998)} \tag{4.2}$$

Where F_{max} is the maximum friction load per unit length of anchors; L_a is anchor bond length; D is diameter of drilling hole; f_{max} is the maximum shear strength of the interface between the soil and grout.

f_{max} is correlated to the undrained shear strength (S_u) of the soil and it is defined as:

$$f_{max} = \propto S_u \text{ (Briaud, 1998)} \quad (4.3)$$

As it is shown in Figure 4-31, the α value was measured and recommended by many researchers. The α value measured from the tests in 1991 and 1997 was 0.51. Whereas back-calculated α value from the tests in 2013 is 0.80.

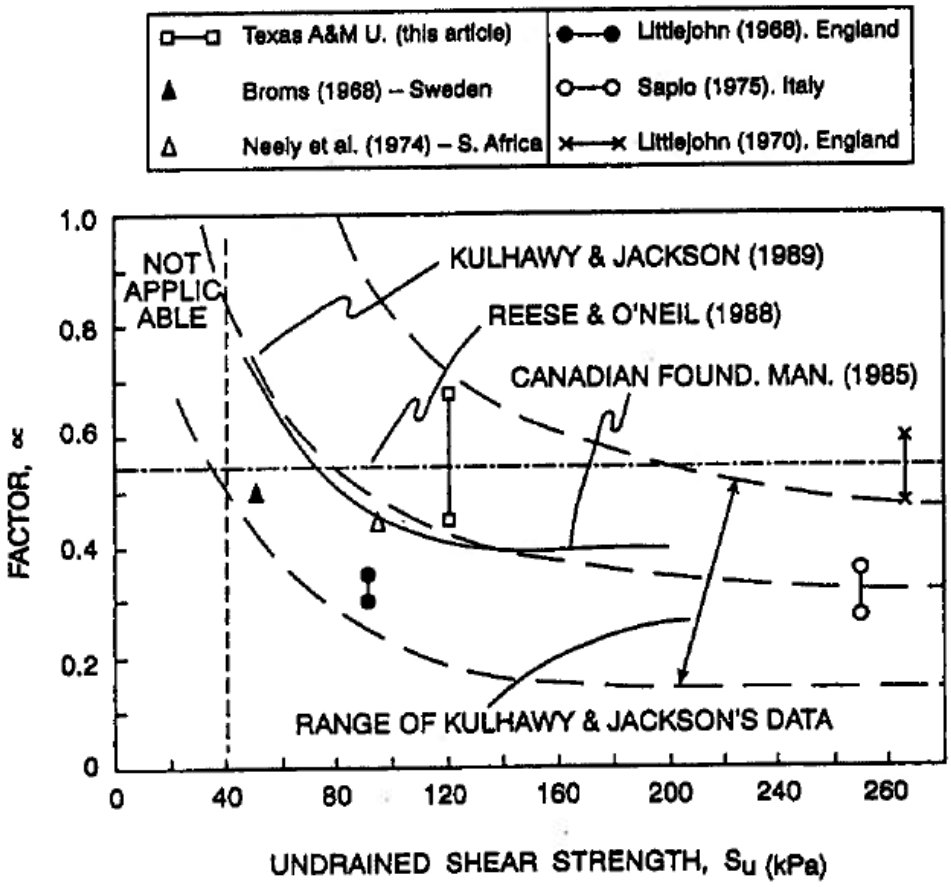

Figure 4-31. The α value for low pressure grouted anchors in clay (after Briaud, 1998)

The maximum shear strength of the interface between the soil and grout (f_{max}) obtained from the tests in 1997 is shown in Table 4-6. Back-calculated f_{max} from the tests in 2013 shows the maximum shear strength of the interface between grout and the soil has been increased 30% - 80 % since 1997. This means that the ultimate pullout capacity of the anchors in 2013 has been increased by almost 60% compared to the corresponding value measured in 1997. The comparison of tests results on anchors in 1991 and in 1997

shows that there is gain of 20% on strength (Briaud et al., 1998), and in 1997 and in 2013 there is gain of 60% on strength. This gain in strength could be due to long term aging effects and past loading history. The detailed comparison between the tests on anchors in 2013 and 1997 are presented in Table 4-6.

Table 4-6. Comparison of the tests on anchors on 1997 and 2013

Anchor No.	Predicted failure load for the anchors on 1997 (kips)	Friction stress at failure (psf)	Average undrained shear strength (psf)	α value (1991)	Actual Failure load on 2013 (kips) (not predicated)	Friction stress at failure (psf)	average undrained shear strength (psf)	α value (2013)
1	195	1380.04	2700	0.51	303	2144.37	2700	0.79
2	243	1719.75	2700	0.64	310	2193.91	2700	0.81
7	180	1273.89	2700	0.47	325	2300.07	2700	0.85
8	168	1188.96	2700	0.44	286	2024.06	2700	0.75
9	-	-	-	-	312	2208.07	2700	0.82
10	180	1273.89	2700	0.47	286	2024.06	2700	0.75
			avg	0.51			avg	0.80

Creep Test

During the pullout test, each load increment was held constant for 60 minutes and creep movements were recorded. Since anchors 3 and 4 failed during the test, no creep data was recorded for these two anchors. Creep movements at different load steps versus time are shown in Figure 4-32 to Figure 4-37.

Acceptance criteria typically requires that the creep movement must be less than 0.04 inch (1 mm) for the readings between 1 to 10 minutes, or it must be less than 0.08 inch (2mm) for the readings between 6 to 60 minutes (FHWA, 2003).

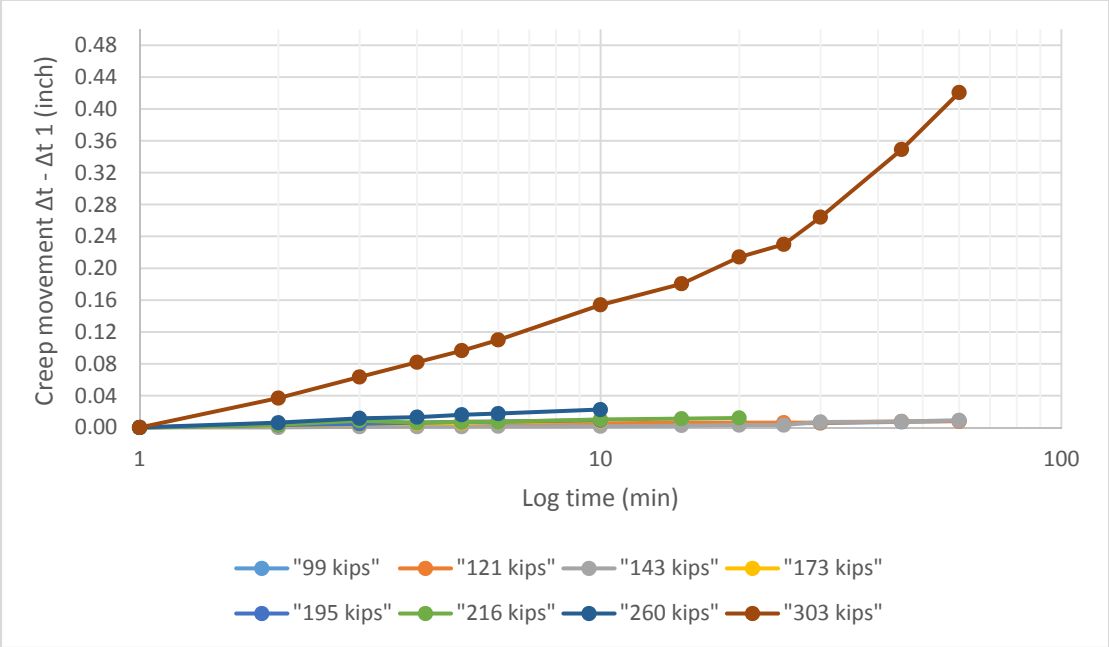

Figure 4-32. Creep movement versus time for anchor 1 at different load step

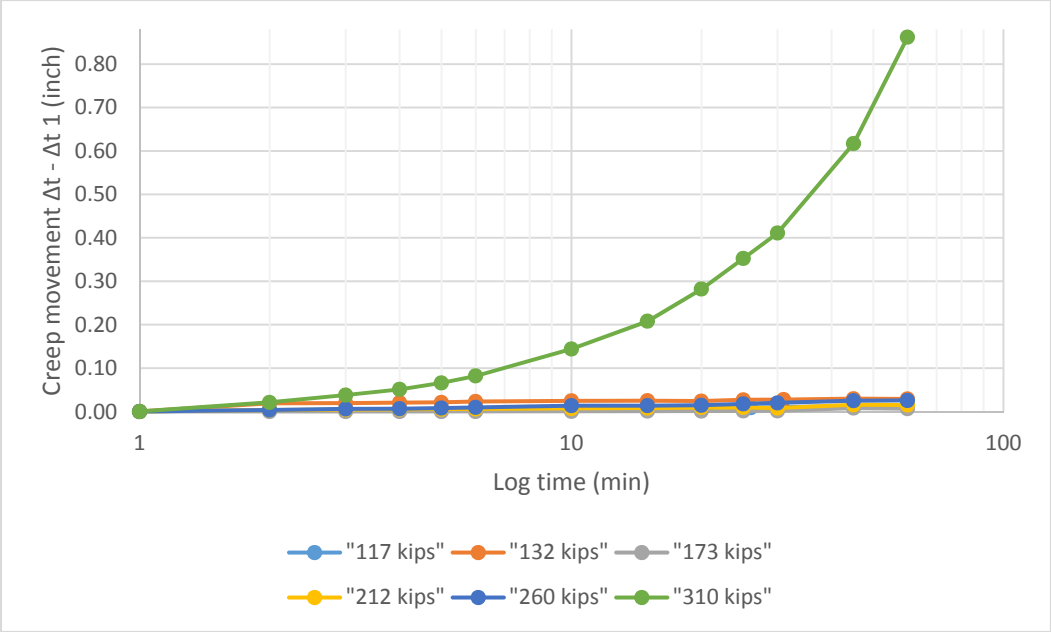

Figure 4-33. Creep movement versus time for anchor 2 at different load step

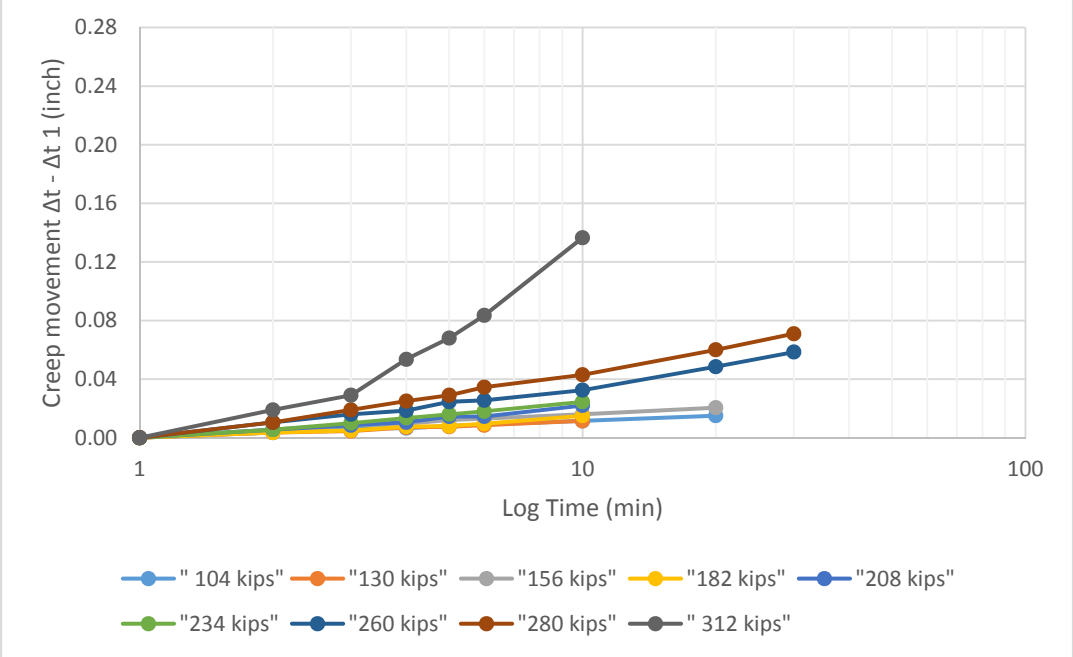

Figure 4-34. Creep movement versus time for anchor 7 at different load step

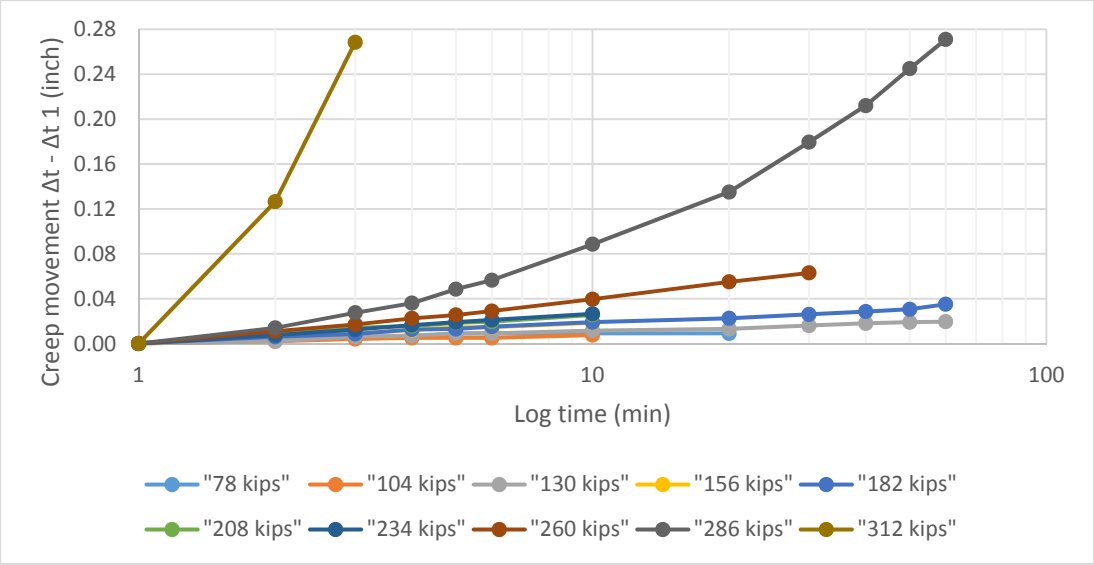

Figure 4-35. Creep movement versus time for anchor 8 at different load step

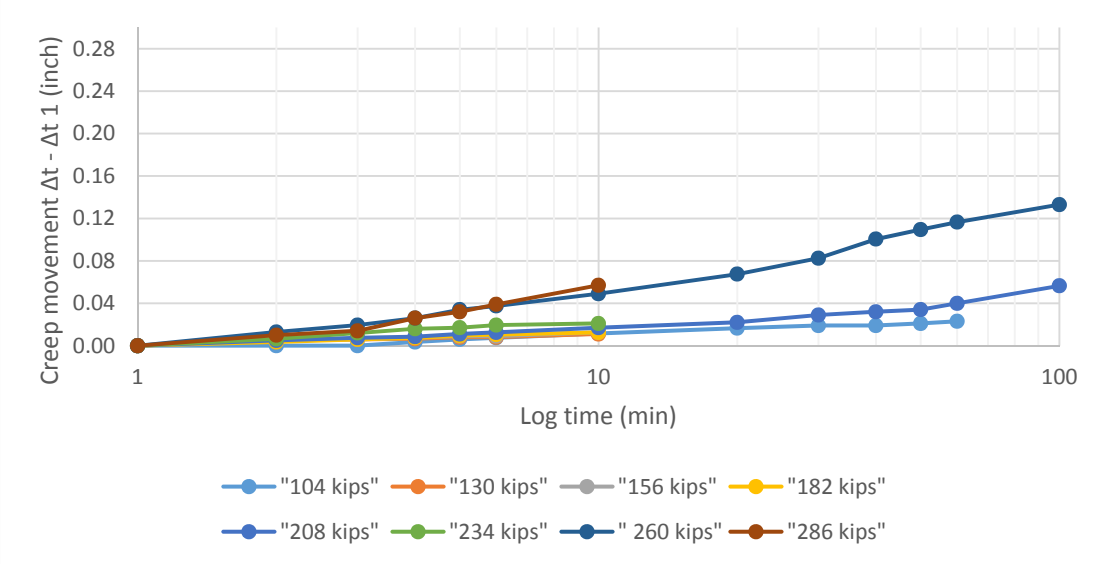

Figure 4-36. Creep movement versus time for anchor 9 at different load step

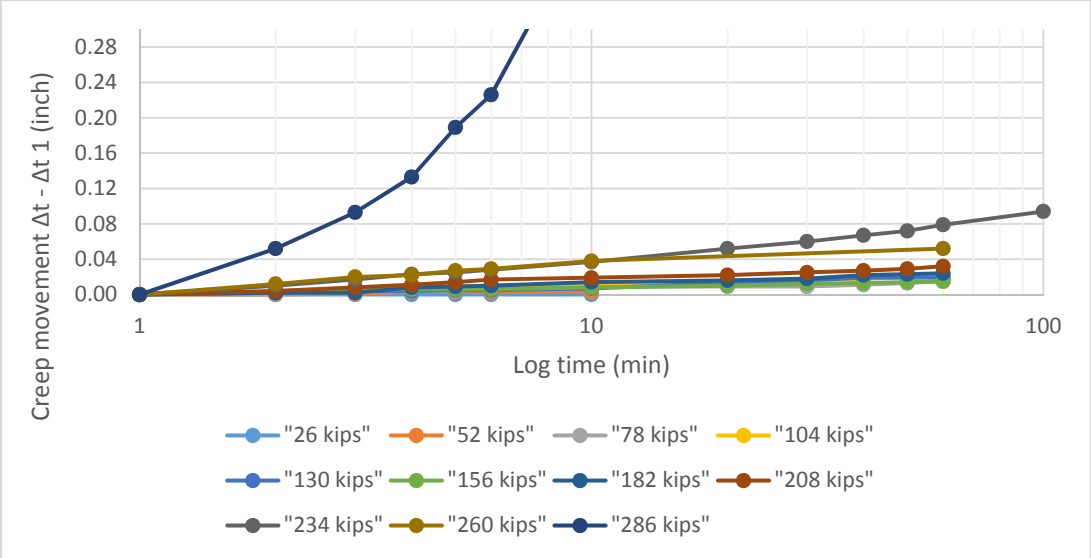

Figure 4-37. Creep movement versus time for anchor 10 at different load step

For anchors 1 and 2, no creep failure occurred until the ultimate pullout capacity of the anchors. These two anchors showed the creep failure at the %100 of failure load. Anchor 7 showed creep movement more than 0.04 inch for readings between 1 to 10 minutes at 280 kips load, while the ultimate pullout capacity for this anchor was 312 kips. Anchors 8, 9 and 10 showed creep movements at 100% of the pullout capacity which was 286 kips. Table 4-7 shows the load which creep failure occurred. It is concluded from Table 4-7 that load threshold for creep failure is about 90% of the ultimate pullout capacity of the anchors.

Table 4-7. Percentage of pullout capacity that creep occurred

Anchor No.	Pullout capacity (kips) (Failure load)	Creep failure load (kips)	Percentage of pullout capacity that creep occurred
1	303	303	100%
2	310	310	100%
7	312	280	89.7%
8	286	260	90.9%
9	286	260	90.9%
10	286	260	90.9%

The creep rate in unit of inch per log cycle of time at different load steps for anchors 1 and 2 are presented in Figure 4-38. The same parameter for anchors 7, 8, 9 and 10 are presented in Figure 4-39. The creep rate increases with low rate until the load approaches to almost 90% of the ultimate pullout capacity. At this point, the slope of creep rate changes rapidly and the creep rate increases significantly until failure occurs.

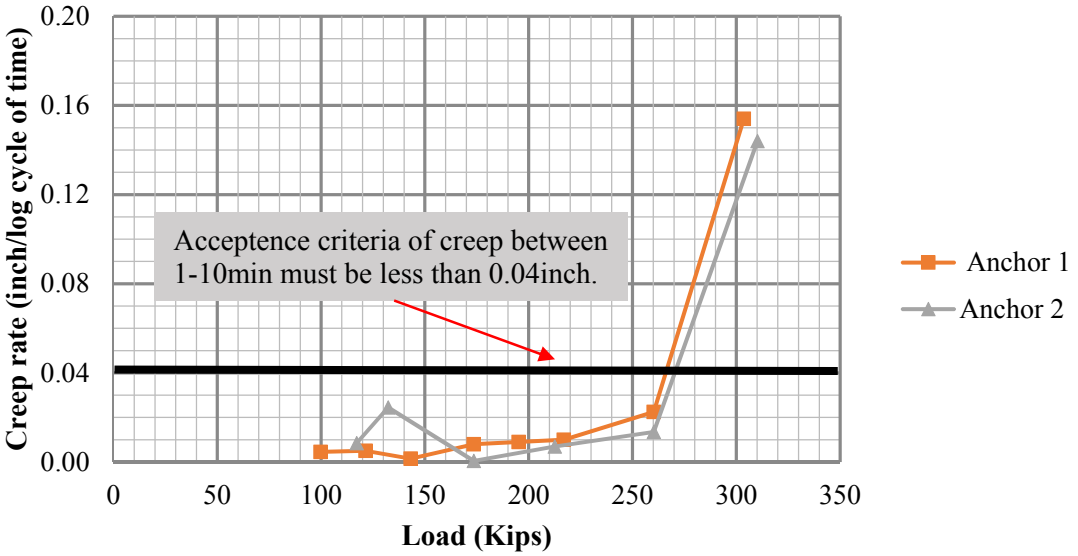

Figure 4-38. Creep rate at different load for anchors 1 and 2 (1 to 10 minutes reading)

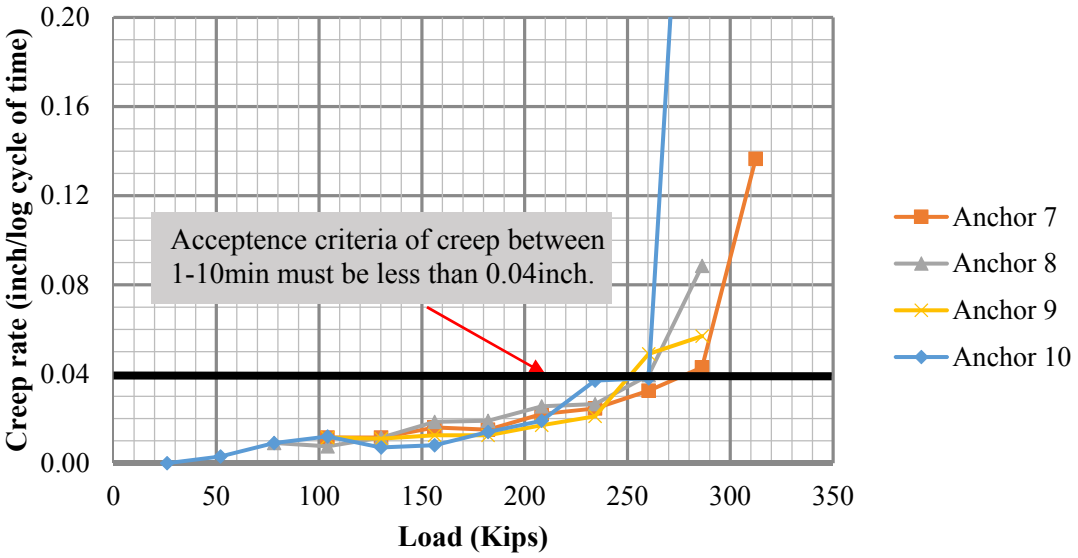

Figure 4-39. Creep rate at different load for anchors 7, 8, 9 and 10(1 to 10 minutes reading)

n Value

To estimate the creep movement of the anchors in each load step, the log of movement is plotted versus log of time (Figure 4-41 to Figure 4-46). The movement s(t) is normalized by the movement at 1 minute after beginning the load step s(t_1). Also the time (t) is normalized by time (t_1) equal to 1 minute. The model is a power model with an exponent "n" equal to the slope of the line in the log space.

$$\frac{s(t)}{s(t_1)} = (\frac{t}{t_1})^n \tag{4.4}$$

The viscous exponent "n" from pullout test on the anchors are presented in Figure 4-40. The "n" value varies between 0.001 and 0.01 for the load less than %90 of the ultimate pullout capacity of the anchors. At the load more than %90 of the ultimate pullout capacity, the "n" values are increased up to 0.04.

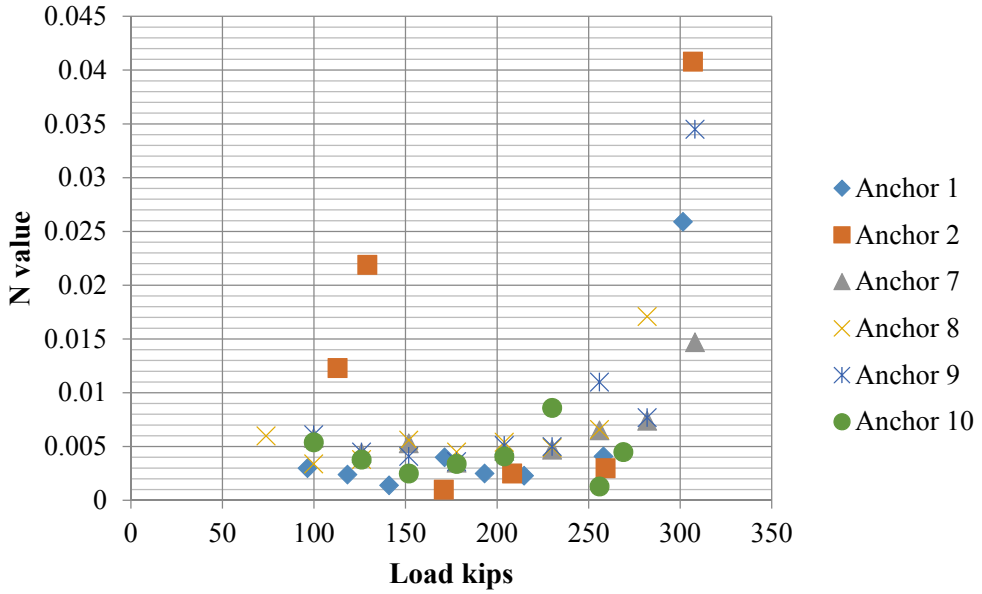

Figure 4-40. Viscous exponent "N" for the tested anchors

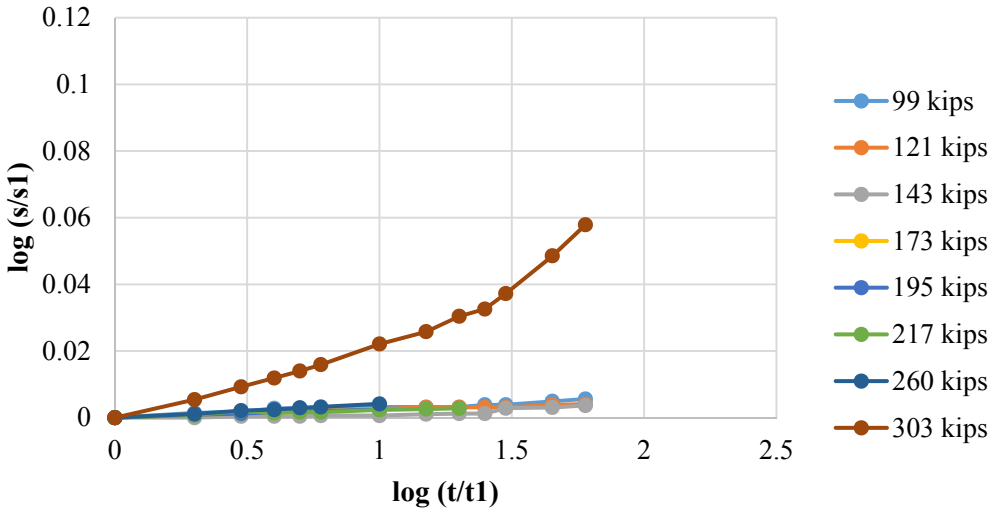

Figure 4-41. Normalized creep movement vs. normalized time, Anchor 1

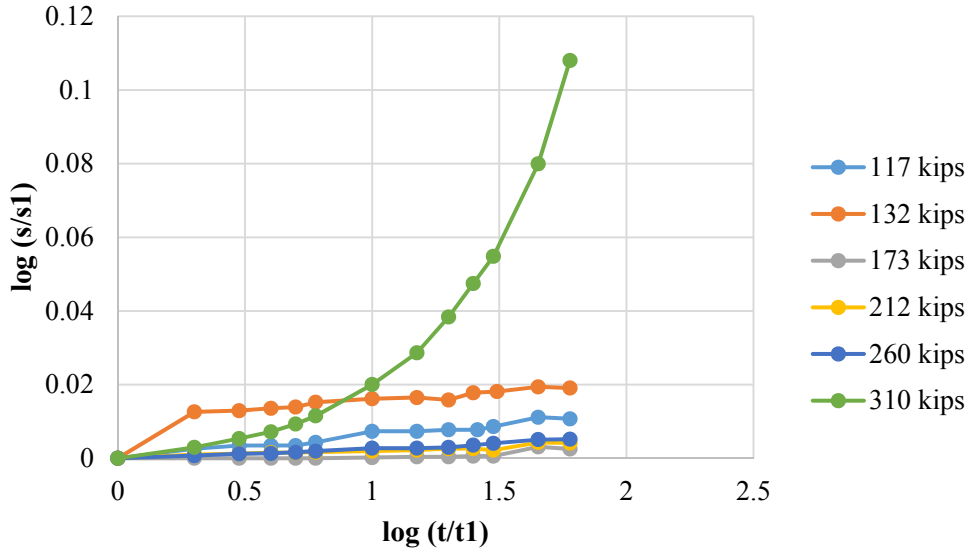

Figure 4-42. Normalized creep movement vs. normalized time, Anchor 2

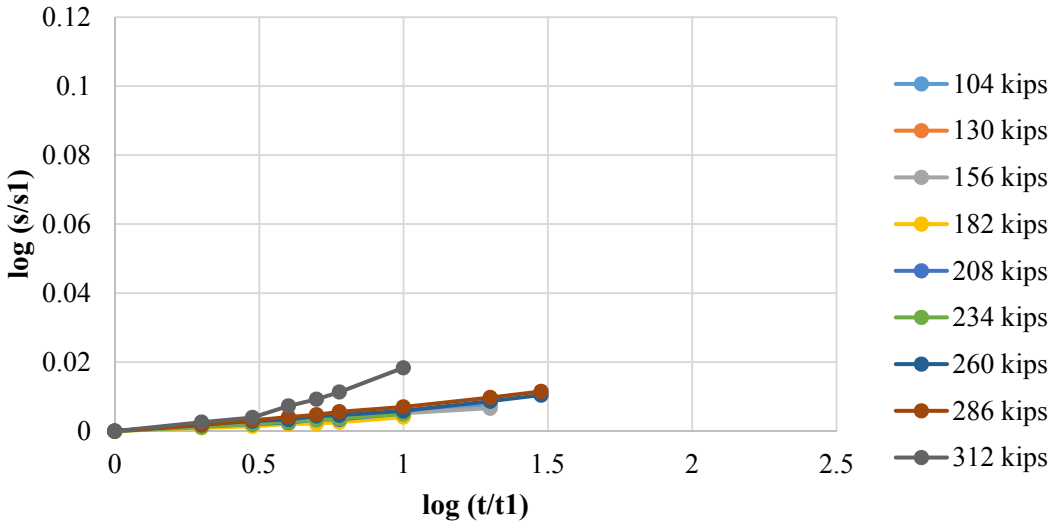

Figure 4-43. Normalized creep movement vs. normalized time, Anchor 7

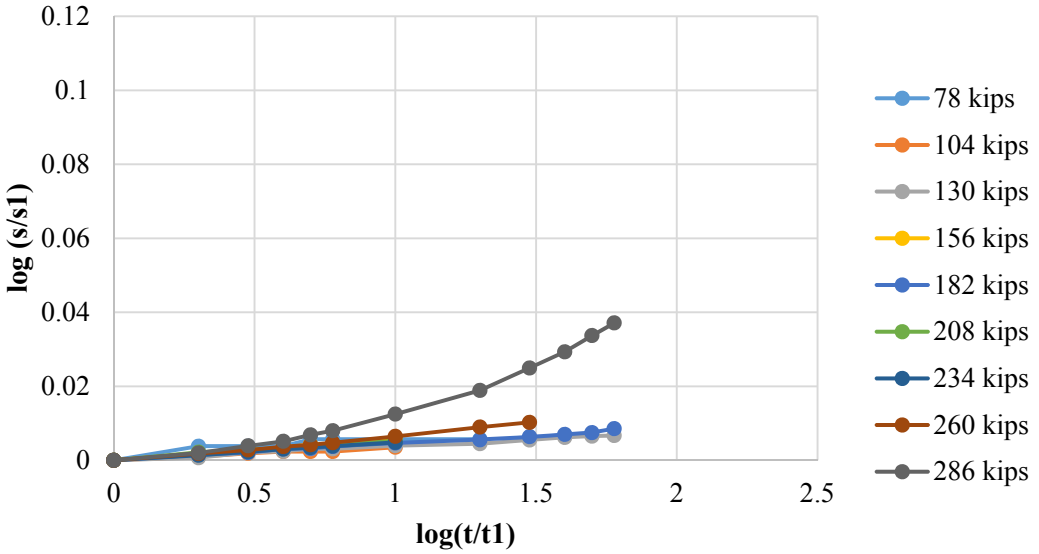

Figure 4-44. Normalized creep movement vs. normalized time, Anchor 8

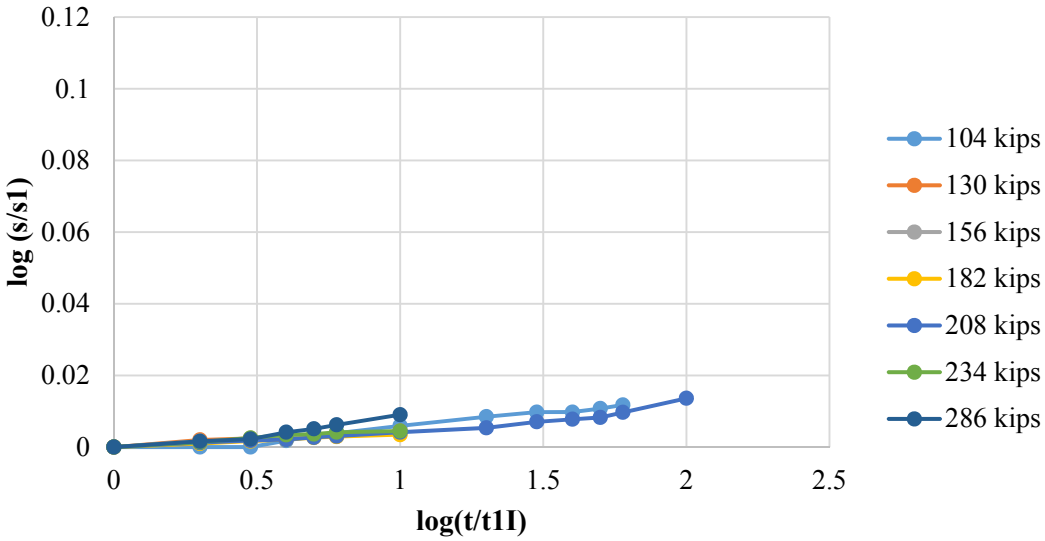

Figure 4-45. Normalized creep movement vs. normalized time, Anchor 9

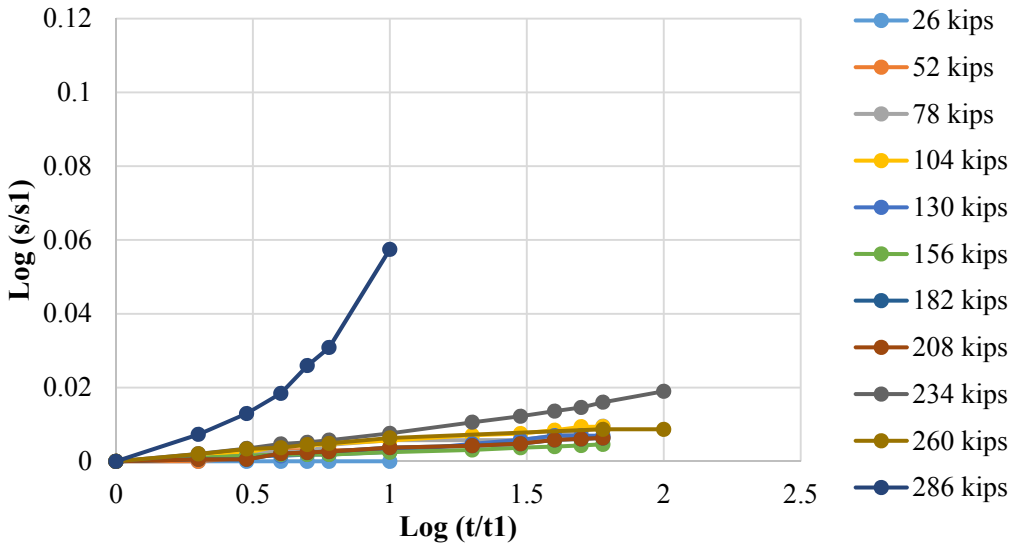

Figure 4-46. Normalized creep movement vs. normalized time, Anchor 10

4.4. New Nails at NGES-TAMU Clay Site

4.4.1. Introduction

To gain a better understanding of the creep phenomenon involving soil nails in high Plasticity Index (i.e. according to GEC#7, 2003, clays with Plasticity index IP>15), new nails installed and testes at NGES-TAMU clay site. Vertical nails are used in this research study. This is appropriate because the objectives of this research are:

- To study the basic mechanism of load transfer between the nail and the surrounding soils;
- To learn how creep develops under these conditions;
- To study the effect of stress level on creep.

These basics phenomena should not be affected by the nail orientation. Furthermore, to study the factors listed above, vertical nails have a number of advantages with respect to horizontal/inclined nails, for instance:

- The stress state around a vertical nail is easier to determine;
- Other factors that may affect the creep behavior, such as, excavation stages or rapid fluctuation of water level;
- They are much less expensive (because the excavation is not needed).

In Addition, to monitor changing in water content of the soil at NGES-TAMU clay site, four water content probes were installed at different depth of the soil. Soil nail layout installed at NGES-TAMU clay site is shown in Figure 4-3.

Instrumentations design, soil nails installation at NGES-TAMU clay site, and test details consists of load test protocol, load tests set-up and results of the tests will be presented in this section sections.

4.4.2. Design of Test Toad and Soil Nail Length

Some basic requirements regarding designing the tested nails in the GEC#7 are:

- The size of nail bar should be at least No. 8 (1 inch). This recommendation is to prevent bending effects.
- The unbounded length should at least 3 ft. (GEC#7, 2003).

Ultimate Bond Strength for New Soil Nails

The ultimate bond strength may be estimated in the field during the site investigation stage of the project from results of Pressuremeter Test (PMT), using the following correlation (GEC#7, 2003):

$$q_u(kPa) = 14P_L(MPa)[6 - P_L(MPa)] \text{ (SI Units)} \quad (4.5)$$

$$q_u(psi) = \frac{1}{214}P_L(ksf)[125 - P_L(ksf)] \quad \text{(imperial units)} \quad (4.6)$$

Where PL is the limit pressure (i.e. as measured with the pressuremeter), and qu is the ultimate bond strength calculated. With the above equation, the ultimate bond strength at NGES-TAMU clay site is shown in Table 4-8.

Table 4-8. Data of q_u two layers clay

Depth of Clay (ft.)	PI	S_u (psf)	P_L (psf)	q_u (psf)
0 to 18	32.8	2297 (110 kN/m^2)	16708 (0.8 MPa)	1216 (58.24 kPa)
21 to 41	43.5	2924 (140 kN/m^2)	45948 (2.2 MPa)	2444 (117.04 kPa)

Note:

1) q_u means ultimate bond strength per unit length,

2) pressuremeter data is from Briaud et al. (1998).

Therefore, for this preliminary design, the bond strength was found to be 1216 psf.

Bonded Length

Bonded length for verification testing, at least 3m (GEC#7, 2003),

$$L_{BVT} = \frac{C_{RT} \times A_t \times f_Y}{Q_{ALL} \times FS_{Tver}} \tag{4.7}$$

Where,

CRT reduction coefficient (CRT = 0.9);

At Nail bar cross-sectional area;

fY Nail bar yield tensile strength;

Q_{ALL} allowable pullout resistance per unit length, $Q_{ALL} = \frac{Q_u}{FS_P}$

FSTver Factor of safety against tensile failure during verification test, it is recommendable to use 2.5, or preferably 3.

With the above information and using the equations quoted above, the bonded length for design new nails is shown in Table 4-9.

Table 4-9. Bonded length

Test type	C_{RT}	A_t (inch^2)	f_Y (psi)	Q_u (lb/ft.)	FS_P	FS_{Tver}	L_{BVT} (ft.)
verification	0.9	0.79	75000	2216	2	3	16

Note: the nail used in the table above is No 8 and the Grade is 75.

Therefore, the bonded length should be between 10 and 16 ft., while the unbounded length is at least 3 ft. (GEC#7, 2003). In fact, nails have been purchased are 20 ft. long, while 3.3 ft. is for pullout test device (above ground), 16.7 ft. below ground (3.3 ft. unbounded length and 13.4 ft. bonded length).

Design Test Load (DTL) and Maximum Load

The design test load and maximum load for new nails are shown in Table 4-10.

Table 4-10. Design test load and maximum load

L_{BVT} (ft.)	Q_{ALL} (lb/ft.)	Bonded length (ft.)	Design test load (kips)	Maximum load (kips)	
16	1114	14 (4.26 m)	15.6 (69.3 kN)	3.0 DTL	16

Notes: Design test load = Q_{ALL} * bonded length

4.4.3. Instrumentation Design

As mentioned in the previous section, the estimated maximum load is 46.8 kips, so a 110 kips jack was used for the pull out tests. To measure the strains and load distribution on nails during the pullout tests the strain gauges type UFCA-5-11 (manufactured by Tokyo Sokki Kenkyujo Co. Ltd., TML) had been selected. The gauges were installed on nails at six different depths, as follows: 3.3, 3.9, 4.6, 7.8, 11.2, and 14.5 ft. The positions of strain gauges are illustrated in Figure 4-47.

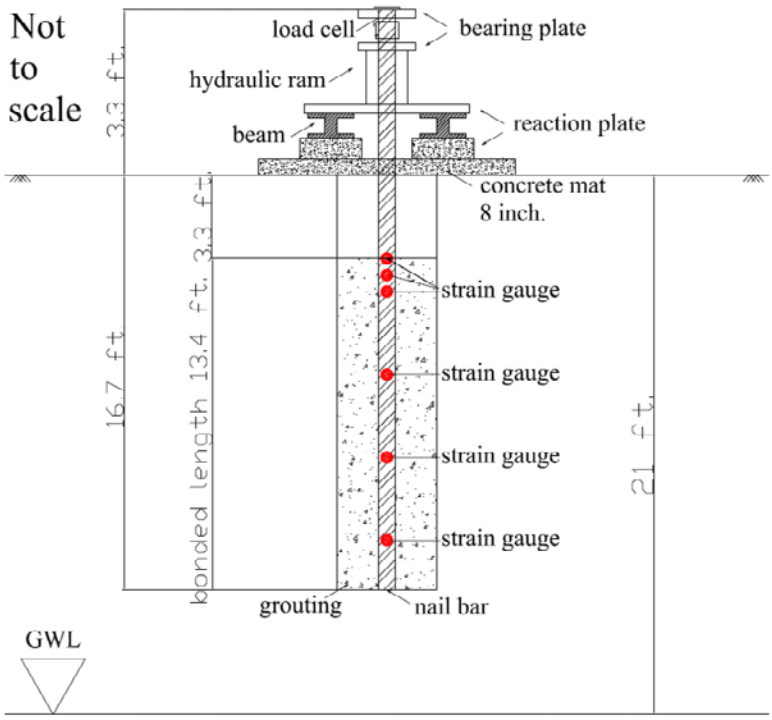

Figure 4-47. Drawing of positions of strain gauges along the soil nail

The step by step procedure necessary to properly attach the strain gauges to the metallic nails is briefly described below. The main steps contemplated in this procedure are as follows:

a) The positions at which the strain gauges will be attached to the nails are firstly marked (Figure 4-47).

b) At each position the nails have to be grounded down with an electric grinder.

c) Then the nails positions have to be carefully sanded with 200-grit sandpaper. The aim is to create a 4-inch long smooth surface to mount the strain gauge.

d) Afterwards ‘Vishay CSM-2’ degreaser has to be used to clean the smoothed surface.

e) A 400-grit extra-fine sandpaper has to be used then along with ‘Vishay M-Prep Conditioner A’ to further smooth and clean the surface areas.

f) It follows the application of ‘Vishay M-Prep Neutralizer 5A’ to neutralize the residual acid content in Vishay M-Prep Conditioner A on the surface areas.

g) After the surface areas at the designated locations are cleaned, the strain gauges are glued to the nail bar using ‘Vishay M-Bond GA-2’ adhesive. Teflon wires were used to create two half-bridge connections and ‘Vishay TEC-1 Tetra Etch’ was applied on the end of the wires, serving as the treatment agent for Teflon surface (Figure 4-48).

h) Each wired strain gauge (Figure 4-49) is then checked using ‘Vishay P3 Strain Indicator’ to ensure that the gauge is functional.

i) To extend the durability of the strain gauges, two layers of protective coatings (Figure 4-49) are applied to cover the wired gauges. That is, ‘Vishay M-Bond GA-2’ and ‘Vishay M-Coat J’ are applied as the first and second coatings, respectively, covering around the perimeter of each 4-inch long spot.

Figure 4-48. Gluing the Strain Gauges to the Threadbar

Figure 4-49. Testing the strain gauges with Vishay P3 Strain Indicator prior shipping to the NGES-TAMU clay site

4.4.4. Installation of Nails and Load Test Set-Up

Nails N1 to N6 were installed at NGES-TAMU clay site in July 2013. As it is shown in Figure 4-47, concrete slab was constructed and used as a reaction beam for these nails. Shorter nails (i.e. NS1 and NS2) were installed in south side of the concrete in September 2013. Eight additional nails were installed in north side of the concrete slab in

November 2014. In the following sections, concrete slab construction and nails installation will be fully describe.

Constructing Concrete Slab as a Reaction Beam for N1 to N6

In order to perform pullout test on new nails (i.e. N1 to N6), concrete slab was selected to use as a reaction beam (i.e. to simulate the same behavior of actual soil nail with permanent concrete facing). Step by step procedure to construct the concrete slab at NGES-TAMU clay site is briefly describe below and illustrate in Figure 4-50 to Figure 4-56.

1) Mowing the site (Figure 4-50);

2) Laying plastic membrane (Figure 4-51 a);

3) Marking nails location (Figure 4-51 b);

4) Placing the bottom reinforcement (Figure 4-52);

5) Placing the top reinforcement (Figure 4-53);

6) Placing surrounding wood frame support (Figure 4-54);

7) Pouring concrete (Figure 4-55);

8) Curing concrete (Figure 4-56).

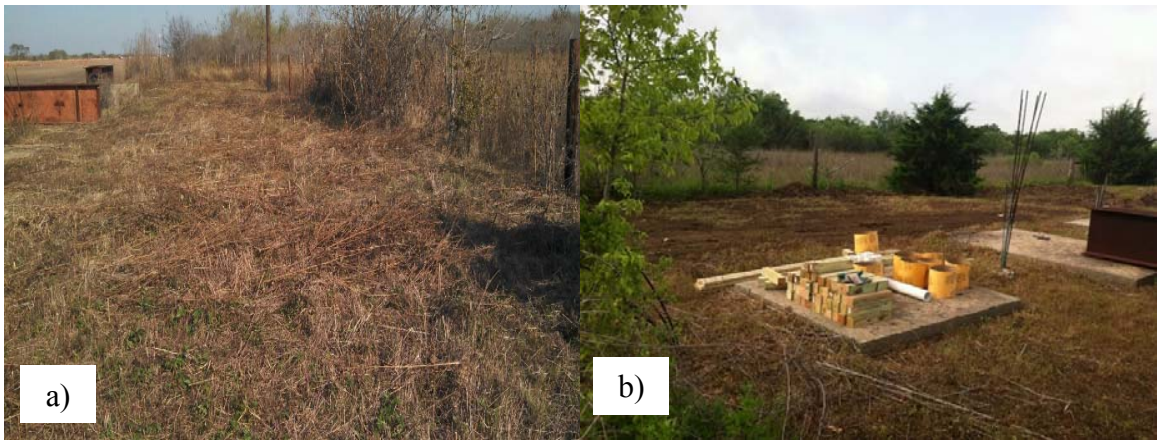

Figure 4-50. NGES- TAMU clay site: a) before mowing, b) after mowing

Figure 4-51. a) Laying plastic membrane, b) marking nails location

Figure 4-52. Placing the bottom layer reinforcement

Figure 4-53. Placing the top layer reinforcement

Figure 4-54. Surrounding support wood frame

Figure 4-55. Pouring concrete

Figure 4-56. Curing concrete

Installation Nails at NGES-TAMU Clay Site

N1 to N6 were installed in July 2013 in collaborating with Schnabel Foundation Company and Terracon consultant, Inc. NS1 and NS2 were installed in September 2013. In November 2014, eight more soil nails (i.e. NW1 to NW2) were installed at NGES-TAMU clay site. During the installation soil nails, soil samples were collected in order to conduct the laboratory tests by Terracon consultant, Inc. Step by step procedure to install soil nails at NGES-TAMU clay site is briefly describe below and presented in Figure 4-57 to Figure 4-61.

1) Drilling holes with 7in diameter (i.e. N1 to N6 18 ft., NS1 and NS1 10 ft., NW1 to NW8 15 ft.) (Figure 4-57);

2) Collecting the soil samples (Figure 4-58);

3) Grout preparation (Figure 4-59);

4) Nails installation (Figure 4-60);

5) Final view of the installed nails on the concrete slab (Figure 4-61)

Figure 4-57. Drilling the holes

Figure 4-58.Collecting the soil samples

Figure 4-59. Grout preparation

Figure 4-60. Groutings and nails installation

Figure 4-61. Final view of the installed soil nails on concrete slab

Load Test Set-Up

A center-hole jack is used to apply the load to the nails. For N1 to N6, the concrete slab is used as a reaction beam to simulate the behavior of actual soil nail with permanent shotcrete facing. For the nails out of concrete slab (NS1, NS2 and NW1 to NW8), eight wood post (i.e. 8 × 8 × 9 in.) is used as a reaction beams. Movement of the nail head is measured with two dial gauges mounted on a tripod independent of jacking set-up. These dial gauges are measured the movement the plate at top of the nail. A center-hole load cell (i.e. Geokon model 3000) is used to during the tests to monitor a constant applied load

during the tests. Over extended periods of time, any load loss in the jack will not be reflected with sufficient accuracy using a pressure gauge (GEC#7, 2003). Figure 4-64 shows the load test set-up for the nails on concrete slab, while Figure 4-65 shows the set-up for the nails out of concrete slab.

Figure 4-62. Load test set-up for the nails on concrete slab (N1 to N6)

Figure 4-63. Details of load test set-up for the nails out of the concrete slab (NS1, NS2 and NW1 to NW8)

4.4.5. Load Test Protocol

In this section the load test protocol for the tested nails at NGES-TAMU clay site is presented. Also in this section, prediction of the ultimate pullout capacity of the nails prior to the installation is described.

Ultimate Pullout Capacity Prediction

In 1991, based on the pullout test on the existing anchors, Briaud found that the α value for the anchors at NGES-TAMU clay site is equal to 0.52 (for Su=2297 psf)

(FHWA, 1998). Therefore, maximum shear strength of the interface between the soil and grout is f_{max} = 1194 psf.

Based on the site investigation performed in 1991, the limit pressure of the soil for the depth 0 to 18 ft. was 0.8. Therefore, the maximum shear strength of the interface between the soil and grout is equal to f_{max} =1216 psf (58.24 kPa). f_{max} =1216 psf was taken as the maximum shear strength of the interface between the soil and grout.Table 4-11 presents the expected ultimate pullout capacity for the nails installed on the concrete slab.

Table 4-11. Specifications of the nails installed on the concrete slab in July 2013

Nail No.	Drilled Length (ft.)	Nail Bonded Length (ft.)	Nail Unbonded Length (ft.)	Diameter of the hole (in.)	Su (psf)	f_{max} (psf)	Q_u (kips)
1	17.3	14.3	6	7	2297	1216	38
2	19.16	16.16	6	7	2297	1216	42
3	19	16	6	7	2297	1216	42
4	19.33	16.33	6	7	2297	1216	43
5	19.25	16.25	6	7	2297	1216	43
6	19.5	16.5	6	7	2297	1216	43

Load Tests Protocol

Verification tests were performed on N1, N2, N3 and N4 in July 2013. For each load steps during the verification test, load was held constant and the creep movements were recorded. These nails were incrementally loaded until failure. Total movement was recorded during the test.

Bonded length and unbonded length of the nails are presented in Table 4-11. Loading sequence for the tests on N1, N2, N3 and N4 are shown in Figure 4-64 to Figure 4-69.

For the pullout test on N1, the test load was held constant at 24.5 kips (65% of the predicted failure load) for 30 minutes. The load increment for the loads less than 24.5 kips was 4.3 kips, while for the loads greater than 24.5 kips was 5 kips until failure.

N2 was loaded with load increment of 5 kips until 57 kips. Each load was held constant for 10 minutes and creep movements were recorded. To study the effect of cyclic loading N2 unloaded to contact load and was loaded again to 57 kips for several times. In each cycle, the load was held constant at 57 kips for 10 minutes and creep movements were recorded.

N3 was loaded with load increment of 5 kips until the load reached to the predicted failure load at 37.5 kips. Then the nail was unloaded and reloaded to 37.5 kips. Loading with increment of 5 kips was continued until 61 kips. Each load step was held constant for 10 minutes and creep movements were recorded. At the loads 52 kips, 57.8 kips and 61.4 kips, the loads were held constant for 60 min, 100 min and 100 min, respectively. The creep movements were recorded during these steps.

The load sequence on N4 was almost the same as N3. For N4, loads 56, 60 and 65 kips were held constant for 60 minutes and creep movements were recorded during these steps.

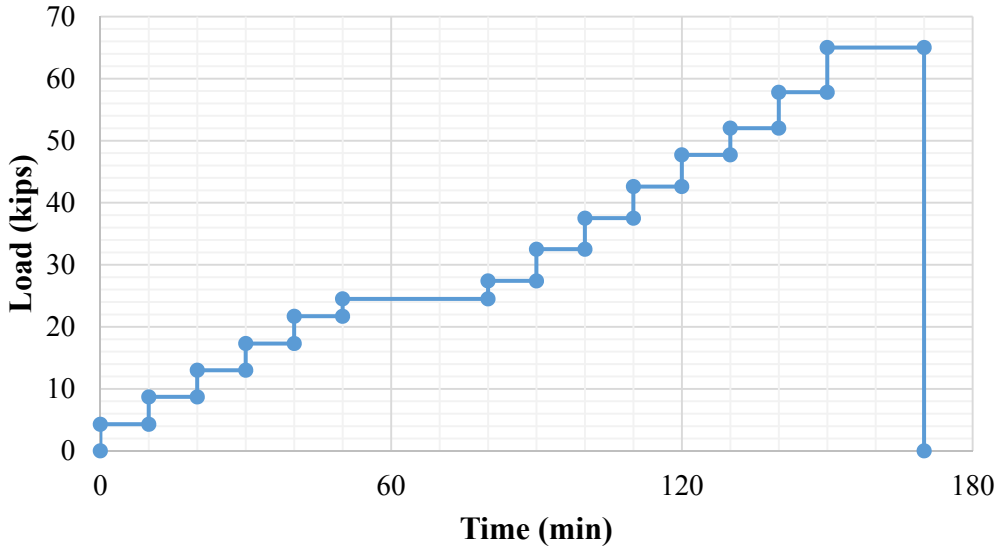

Figure 4-64. Loading sequence for pullout test on N1

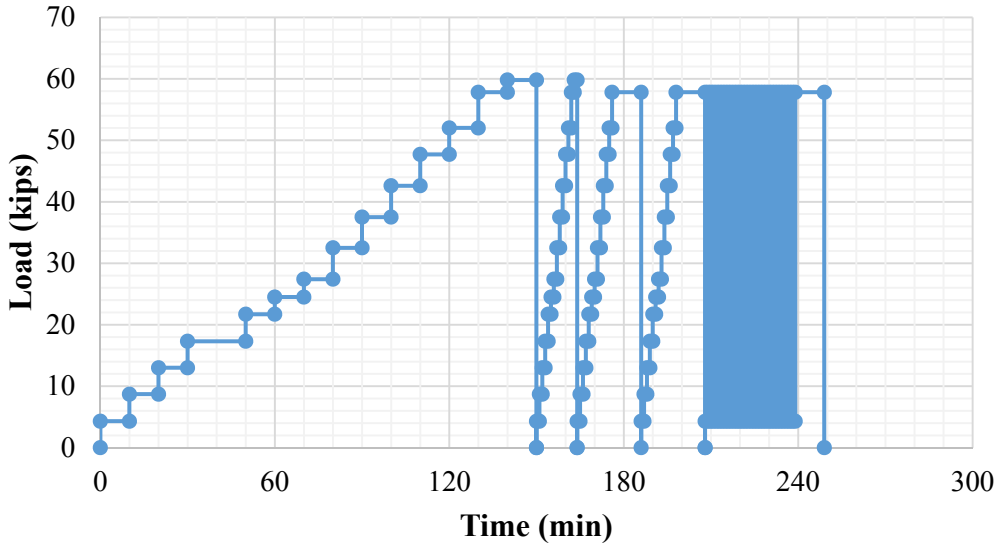

Figure 4-65. Loading sequence for pullout test on N2

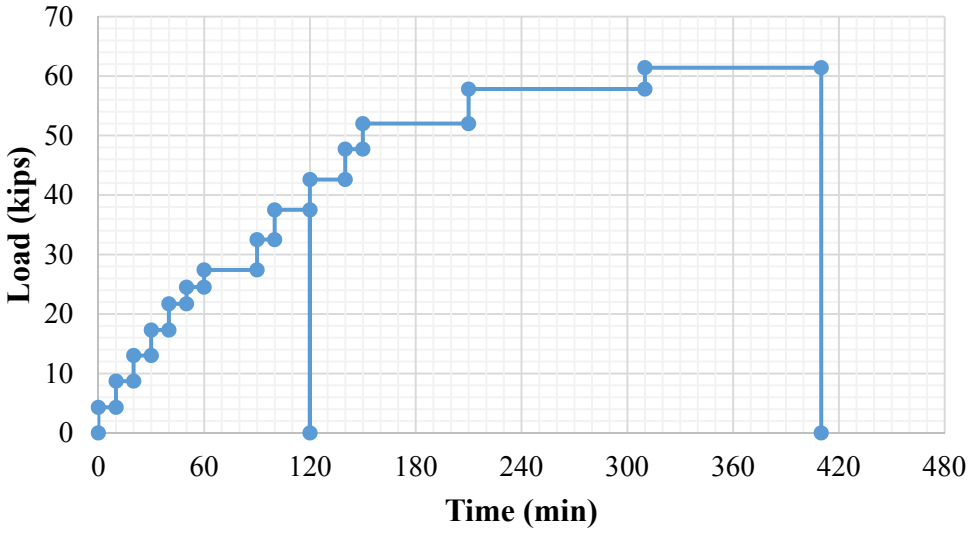

Figure 4-66. Loading sequence for pullout test on N3

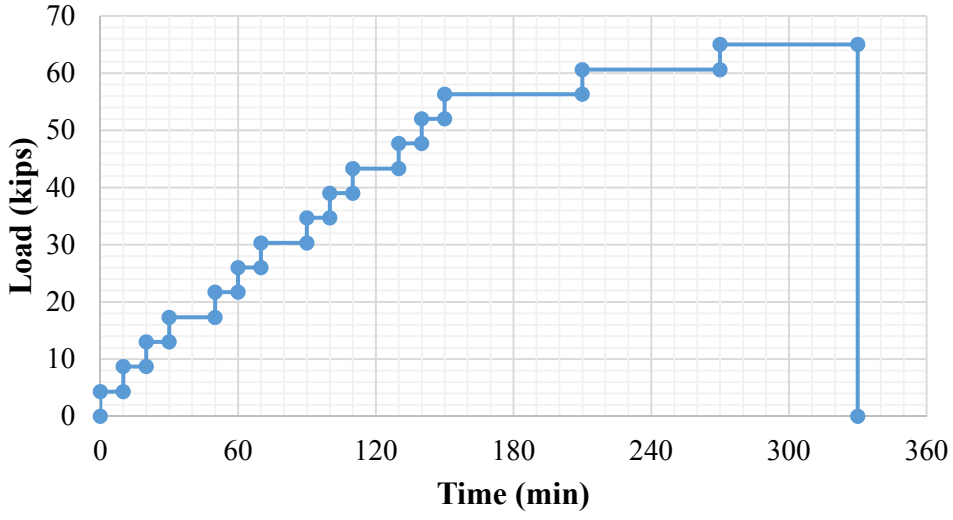

Figure 4-67. Loading sequence for pullout test on N4

N1 and N4 were retested in November 2013 and February 2014, respectively. Aim of this retests was gain a better underestanding of preloading (load history) on creep behavior and also determine the ultimate pullout capacity of these nails. Load test protocol for retesting the N1 and N4 are presented in Figure 4-68 and Figure 4-69, repectively. N1 was loaded up to 55 kips. Each load step was held for 10 minutes and creep movements were recorded. N4 was first loaded up to 33 kips. Each load step was held for 10 minutes and creep movements were recorded. Load of 33 kips was held for 240 minutes and creep movements were recorded. After 240 minutes, the nail was unloaded to contact load (2 kips) and then was loaded up to 48 kips with load increment of 4 kips. Each load step was held for 10 minutes and creep movements were recorded.

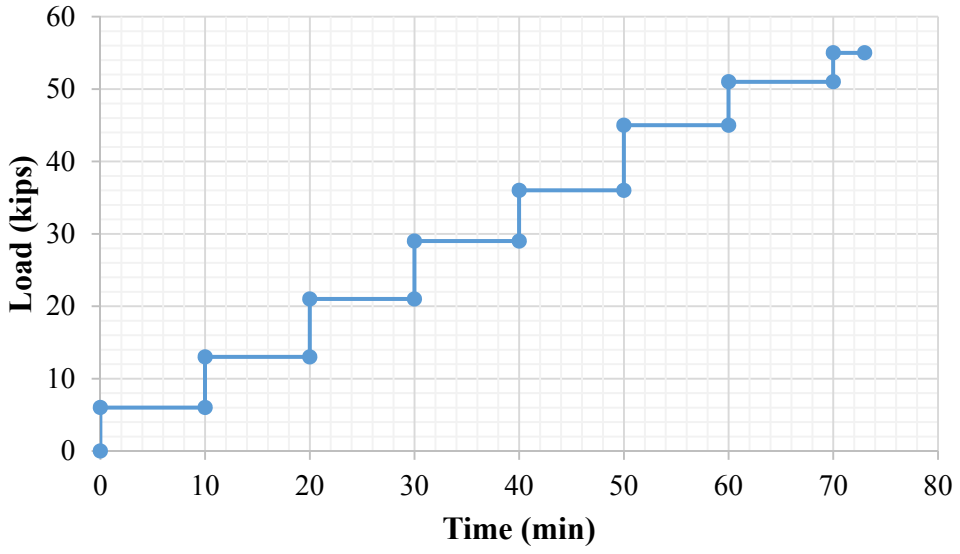

Figure 4-68. Loading sequence for retest on N1 on November 2013

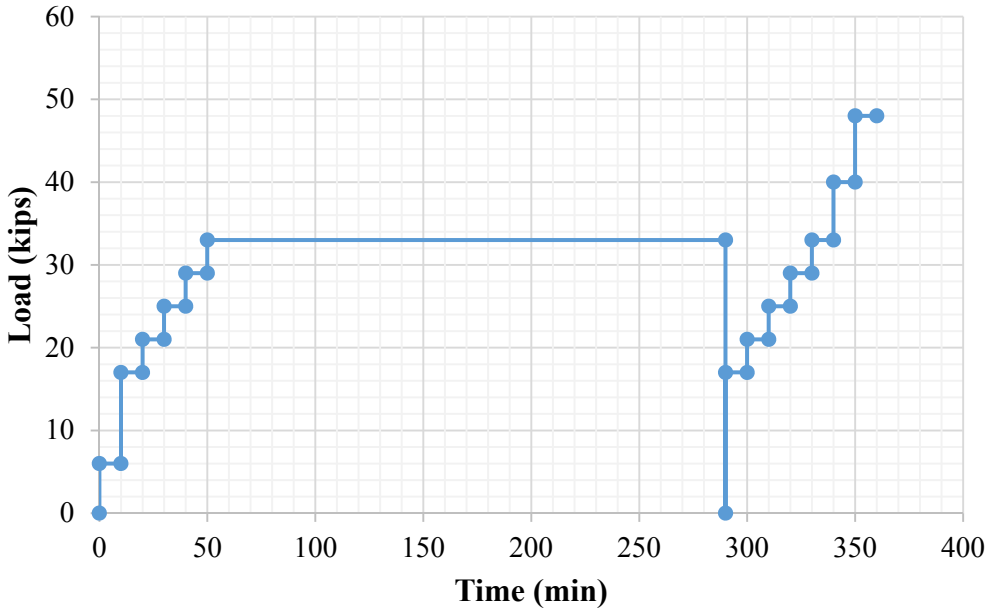

Figure 4-69. Loading sequence for retest on N4 on February 2014

Poullout test was performed on NS3 in September 2013. NS3 was loaded with increment of 5 kips untill failure. Each load was held for 10 minuets.

4.4.6. Test Results on New Nails

In this section, results of the pullout test will be presented. The results include total, elastic and residual movement of the nail head. Furthermore, the results of the creep tests and corresponding "n" value for power model will be presented.

Total, Elastic and Residual Movement

Total movement consisting of elastic and residual movement is the measured displacement of nail head during the test. Elastic movements are the recoverable

movements when the nail is unloaded (i.e. the nail load is reduced from a test load to an alignment load). Residual movements are non-recoverable movements measured when the nail is unloaded (FHWA, 1998). Results of the tests on all the nails are presented as follows:

a) Test on N1 to N6 in July 2013

Figure 4-70 to Figure 4-73 include the plots for total, elastic and residual movements for N1 to N4 from the tests in July 2013.

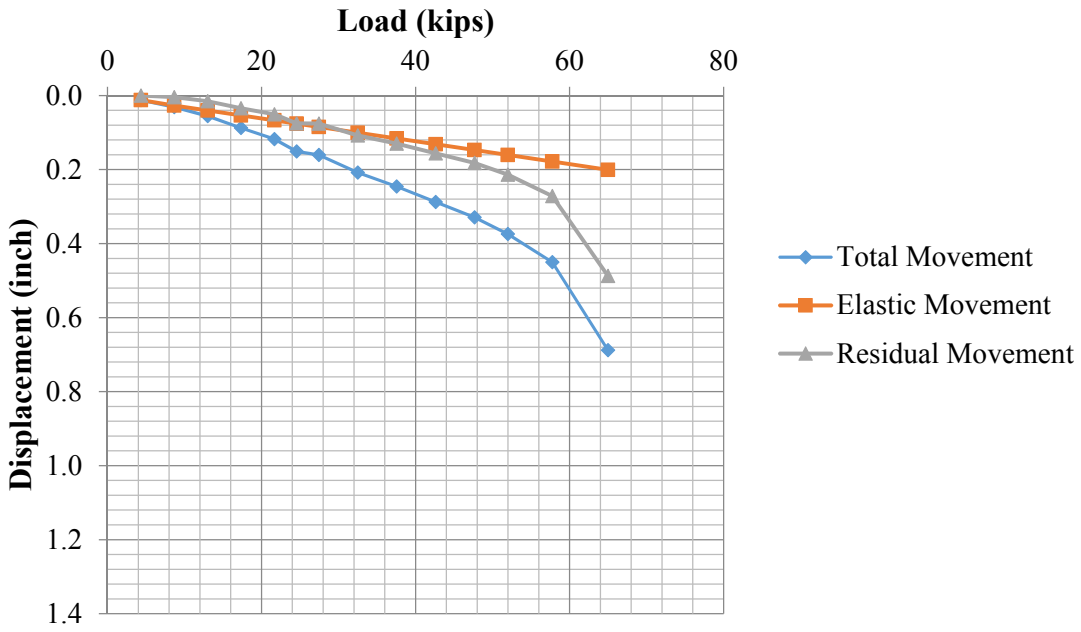

Figure 4-70. Load-Displacement curve for N1

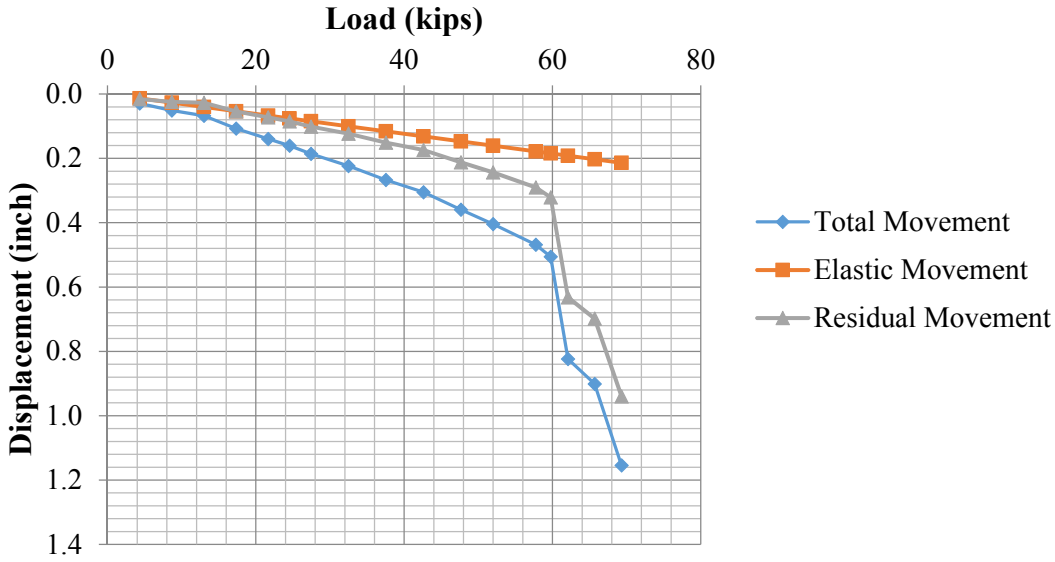

Figure 4-71. Load-Displacement curve for N2

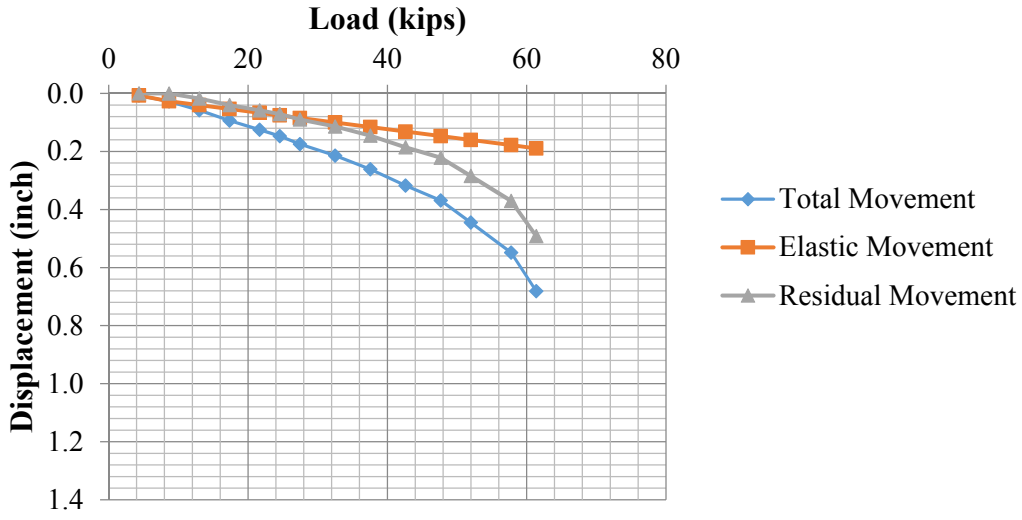

Figure 4-72. Load-Displacement curve for N3

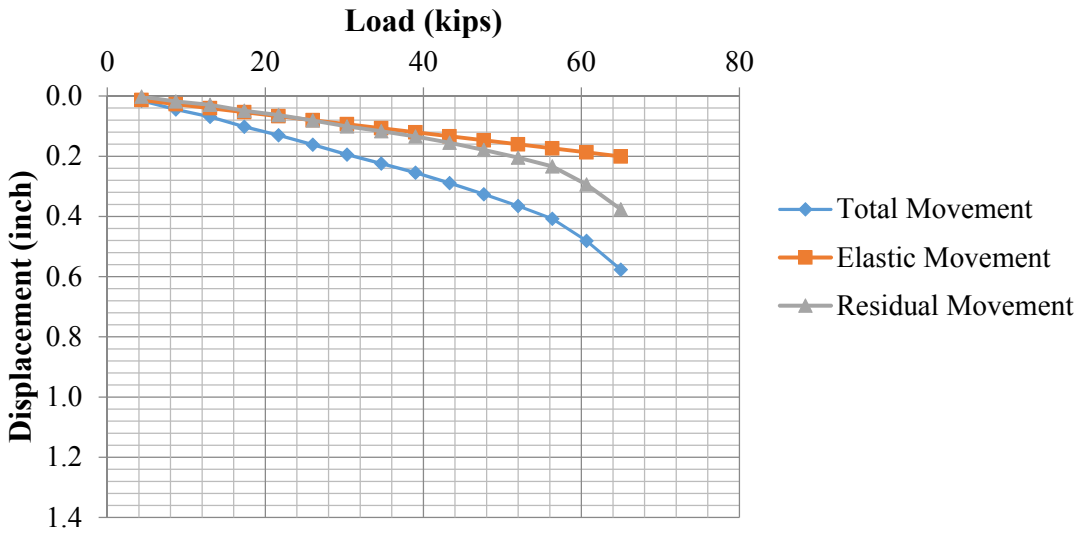

Figure 4-73. Load-Displacement curve for N4

Yield strength for the thread bar used for the nails at NGES (i.e. grade 75 size #8), is 59.3 kips. Therefore, the measured movements of the nail-head for the loads greater than 59.3 kips include the plastic movement of the thread bar. Figure 4-74 shows the residual movement of the nail for the load less than the yield capacity of the thread bar.

The nails did not fail during the tests in July 2013. However, by extending the load-displacement curve to the failure criteria, the failure load could be estimated to be in the range of 70 to 80 kips. This means that the assumed value for maximum shear strength of the interface between the soil and grout ($f_{max}=\alpha*S_u$) was significantly under-predicted. The results of the laboratory tests for the soil samples taken in July 2013 show that the undrained shear strength (S_u) of the soil for the top 15 ft. has noticeably increased. Also, change in f_{max} could be due to the assumed α value. Table 4-12 presents the α values

obtained from the tests performed in July 2013 for the undrained shear strength equal to 2880 psf (138 kPa). Even considering that the friction of the interface between the soil and grout (f_{max}) was equal to 80% of the undrained shear strength of the soil ($\alpha=0.8$), the nails did not reach the ultimate failure load.

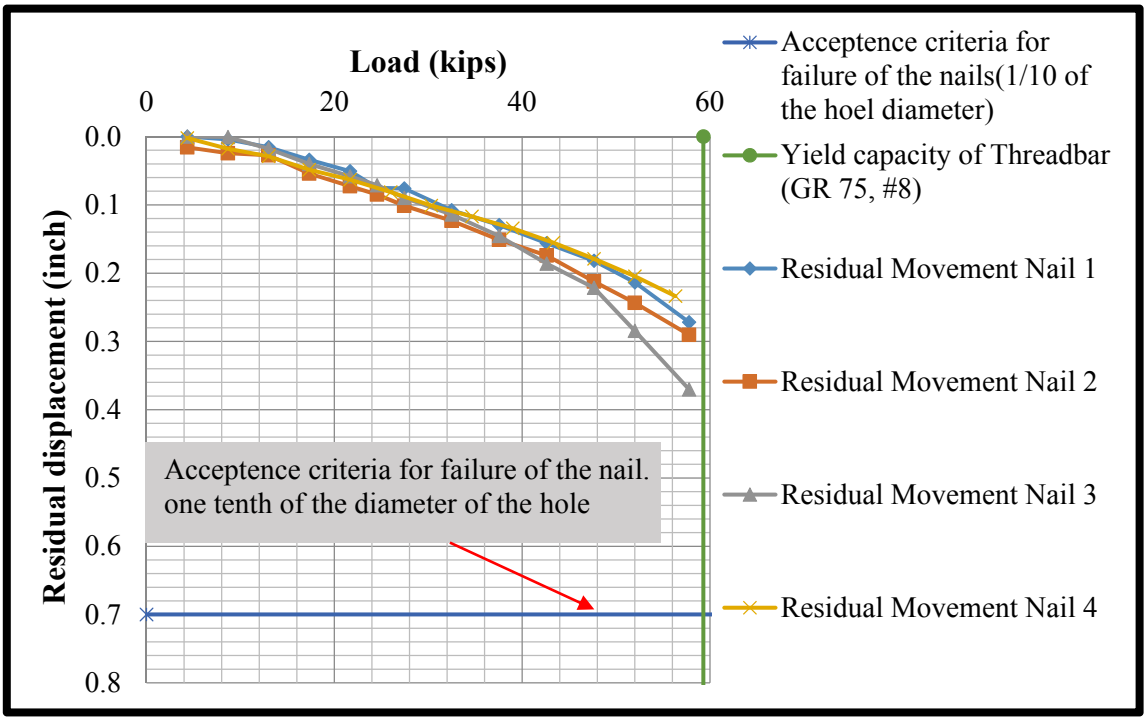

Figure 4-74. Residual movement vs. load for N1 to N4

Table 4-12. The α value obtained from the pullout tests on N1 to N4

Nail No.	Bond length(ft.)	Hole Diameter (inch)	Undrained shear strength S_u psf (This research study, Task#5)	Maximum load applied (kips)	α value
1	14.3	7	2880	65	0.86
2	16.16	7	2880	69	0.81
3	16	7	2880	61	0.72
4	16.33	7	2880	65	0.75

To address this issue, two more nails with shorter lengths (i.e. nails NS1 and NS2) were installed in September 2013, next to the concrete slab, with the aim to find out the actual maximum shear strength of the interface between the soil and grout at failure (f_{max}). In addition, nails N1 and N4 were retested in November 2013 and February 2014. The location of nails NS1 and NS2 is shown in Figure 4-3.

b) Test on NS1 in September 2013

Total, elastic and residual movement of the NS3 are presented in Figure 4-75.

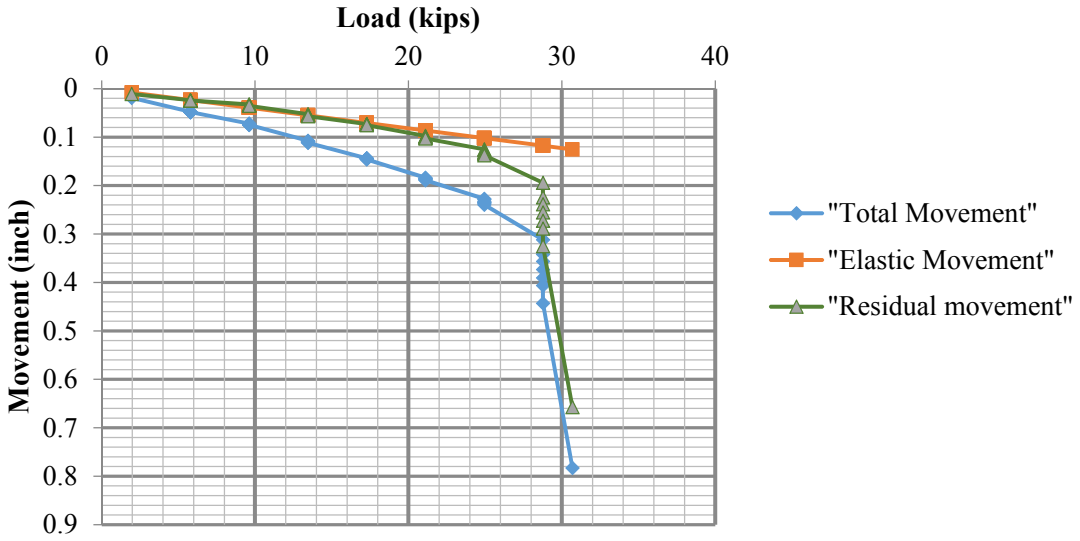

Figure 4-75. Load-Displacement curve for NS1 testes in Sep 2013

The ultimate pullout capacity for nail NS1 was 29 kips. With the known ultimate pullout capacity, a back-calculated α value equal to 0.78 was obtained ($\propto = Q_u/\pi D L_a S_u$) (Table 4-13). With α equal to 0.78 and S_u equal to 2880 psf (138 kpa), the ultimate pullout capacity of the nails on the concrete slab (i.e. nails N1 to N6) were recalculated (Table 4-14). Since the nails on the concrete slab did not fail, it was valuable to retest the nails in concrete slab. From retest, ultimate pullout capacity of the nails could be obtained.

Table 4-13. The α value back-calculated from the pullout test on NS4

Nail No.	Drilled Length (ft.)	Nail bonded Length (ft.)	Diameter of the hole (in.)	Su (psf)	Q_u (kips)	f_{max} (psf)	α
NS4	10	7	7	2880	29	2262	0.78

Table 4-14. Back calculating the ultimate pullout capacity of the nails on the concrete slab (N1 to N6) based on the test performed on shorter nail (NS1) in Sep 2013

Nail No.	Nail Bond Length (ft.)	Nail Unbonded Length (ft.)	Diameter of the hole (in.)	Su (psf)	α	f_{max} (psf)	Q_u calculated from the test on shorter nail(kips)
1	14.3	6	7	2880	0.78	2262	59
2	16.16	6	7	2880	0.78	2262	67
3	16	6	7	2880	0.78	2262	66
4	16.33	6	7	2880	0.78	2262	68
5	16.25	6	7	2880	0.78	2262	67
6	16.5	6	7	2880	0.78	2262	68

c) Retest N1 and N4 on Concrete Slab

Total, Elsatic and Residual movement for retests on the N1 in November 2013 and N4 in Februray 2014 for different load steps are shown in Figure 4-76, Figure 4-77, and Figure 4-78, respectively.

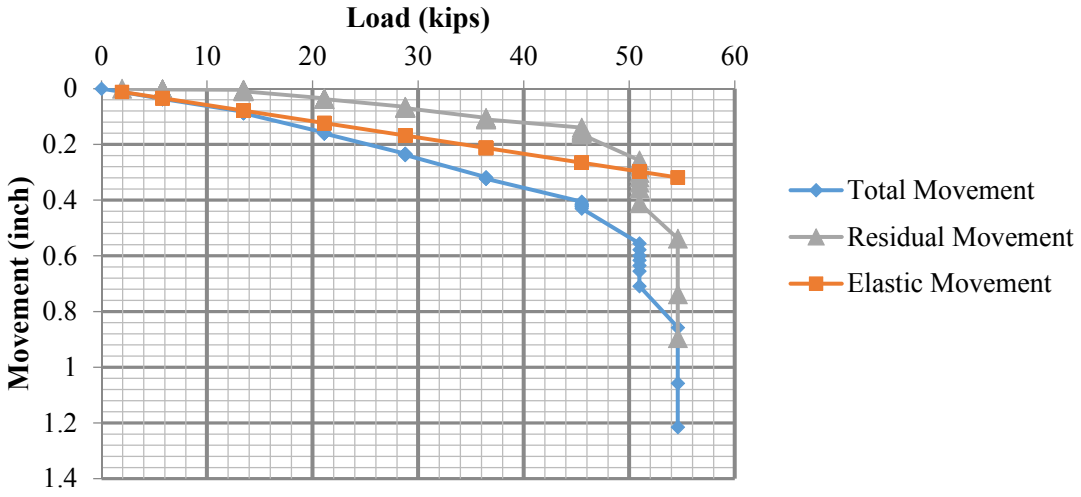

Figure 4-76. Total, elastic and residual movement for retest N1 in November 2013

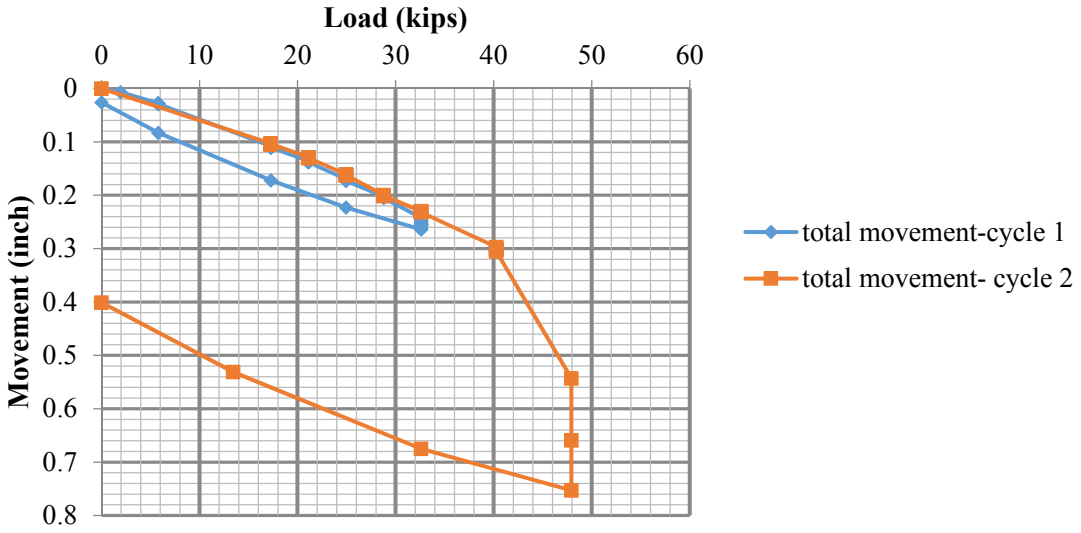

Figure 4-77. Total movement for two cycles retest N4 in February 2014

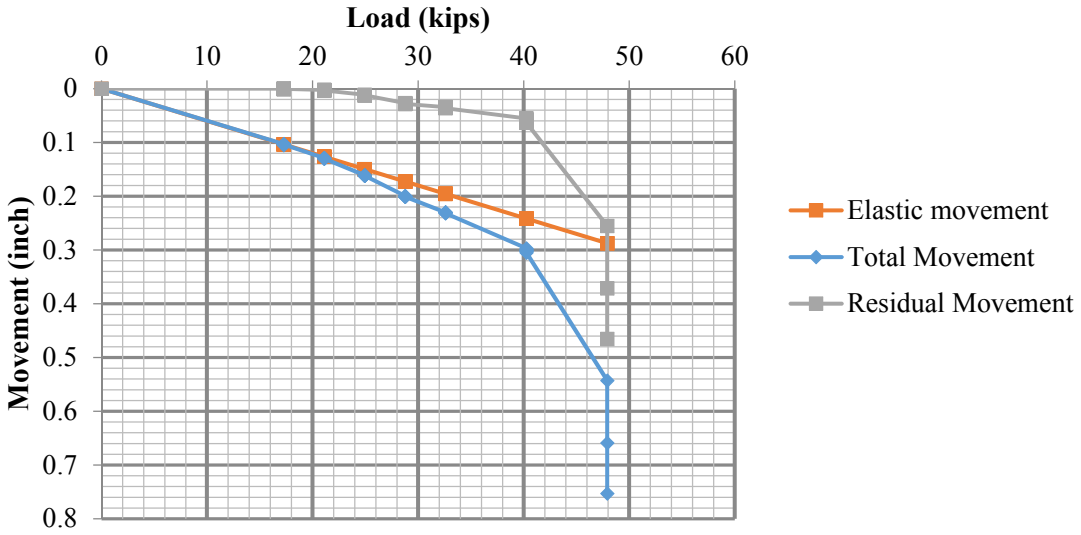

Figure 4-78. Total, elastic and residual movement for retest N4 in February 2014 (Second cycle)

In July 2013, soil N1 was loaded up to 65 kips, and it did not fail. However, in November 2013, nails N1 failed at 55 kips during the pullout test. As it was shown in Table 4-14, nail N1 was expected to fail at 59 kips. As nail N1, nail N4 failed during the pullout test at 48 kip in Feb 2014. It is worth to remember that this nail did not fail for the maximum load of 65 kips, applied in the previous test in July 2013. From back-calculating the ultimate pullout capacity, the nail N4 was expected to fail at 68 kips, but it failed at 48 kips. Therefore, it can be concluded that the ultimate pullout capacity of the nails depends on the soil moisture, associated with different season at which they were tested. This may be because, the undrained shear strength of the soil depends on the water content (or suction) of the soil, and it affects the ultimate pullout capacity of the nails. Details of the

comparison between the initial test in July 2013 and the retest performed in November 2013 and February 2014 on nails N1 and N4 are presented in Table 4-15.

Table 4-15. Comparison the test results on N1 and N4 on different seasons

Nail No.	Nail Bond Length (ft.)	Max load applied on July 2013 and the nail did not fail (kips)	α from the test on July 2013	Max load applied on Nov.2013 on N1 and Feb.2014 on N2, both nails failed (kips)	α from the test on Nov. and Feb.
1	14.3	65	0.86	55	0.73
4	16.33	65	0.75	48	0.56

Creep Tests

During the pullout test, each load increment was held constant and creep movements were recorded. Since some of the nails were loaded above yield strength of the thread bar (59 kips), the creep movements for those loads are not considered as the pure creep movement of the soil nails.

a) Test on N1 to N6 in July 2013

Figure 4-79 to Figure 4-83 present the creep rate for N1 to N2.

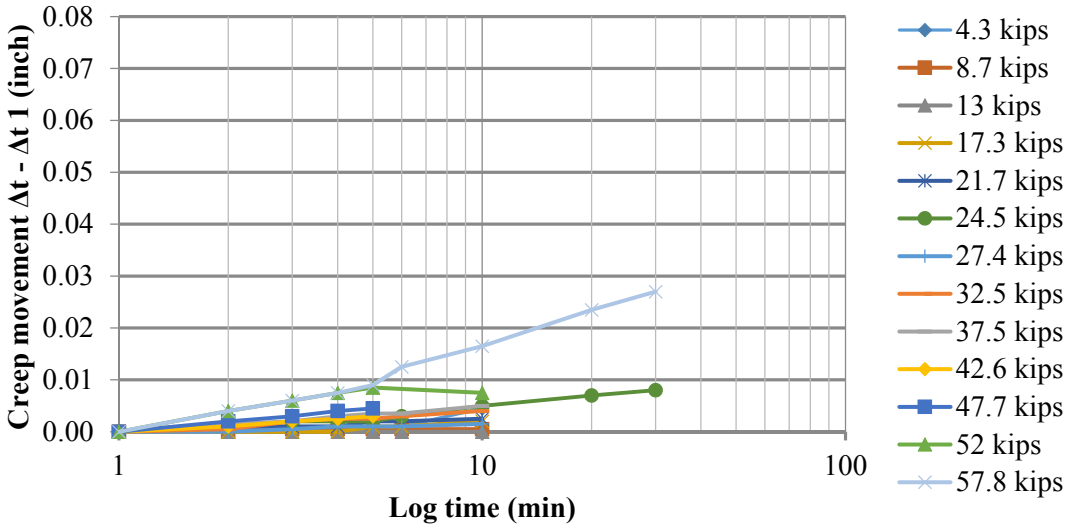

Figure 4-79. Creep movement versus time for N1 at different load step

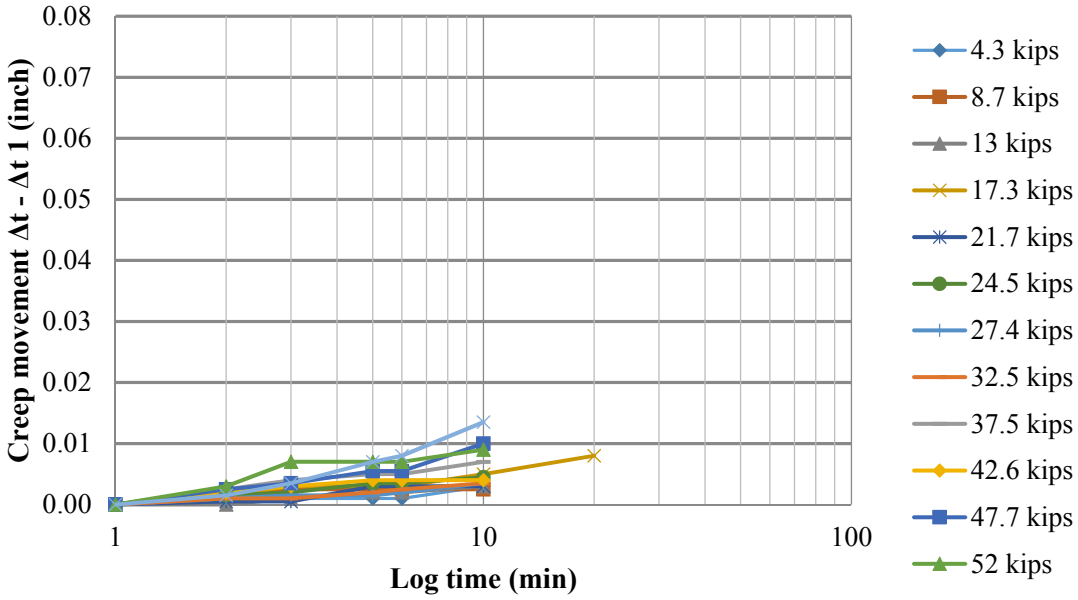

Figure 4-80. Creep movement versus time for N2 at different load step for the first cycle

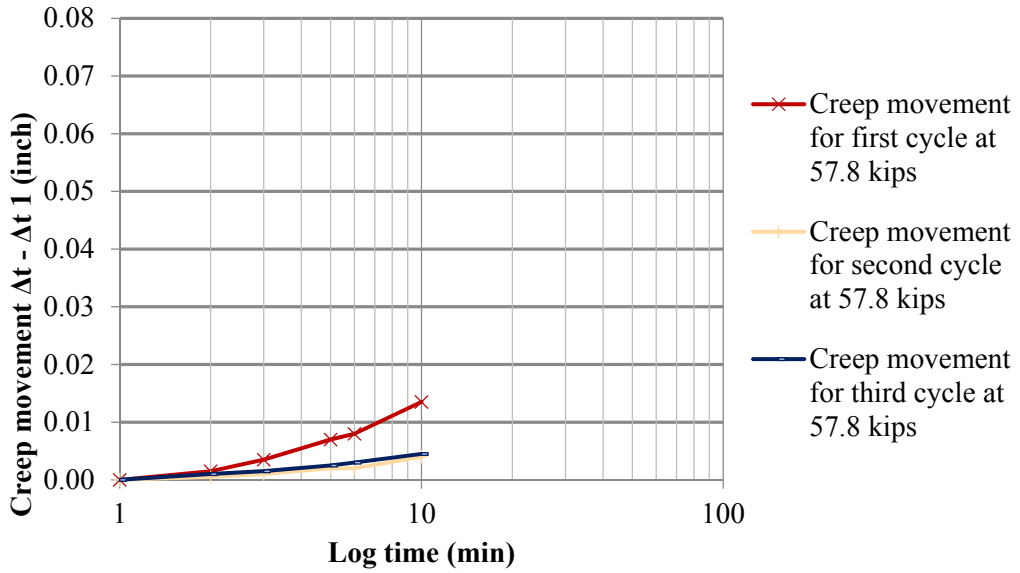

Figure 4-81. Creep movement versus time for N2 at different load step for first, second and third cycle

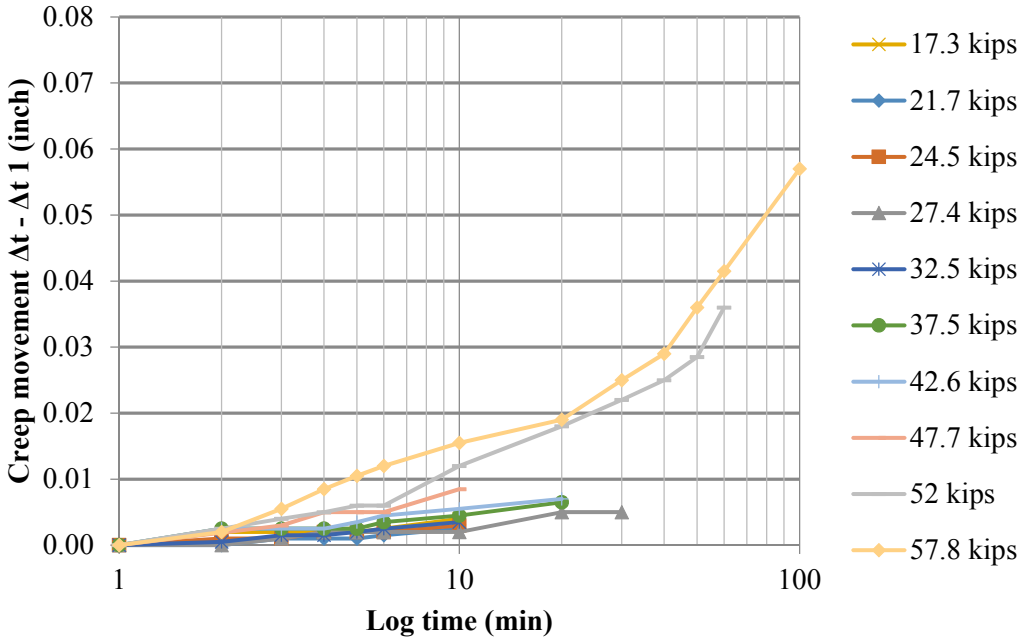

Figure 4-82. Creep movement versus time for N3 at different load step

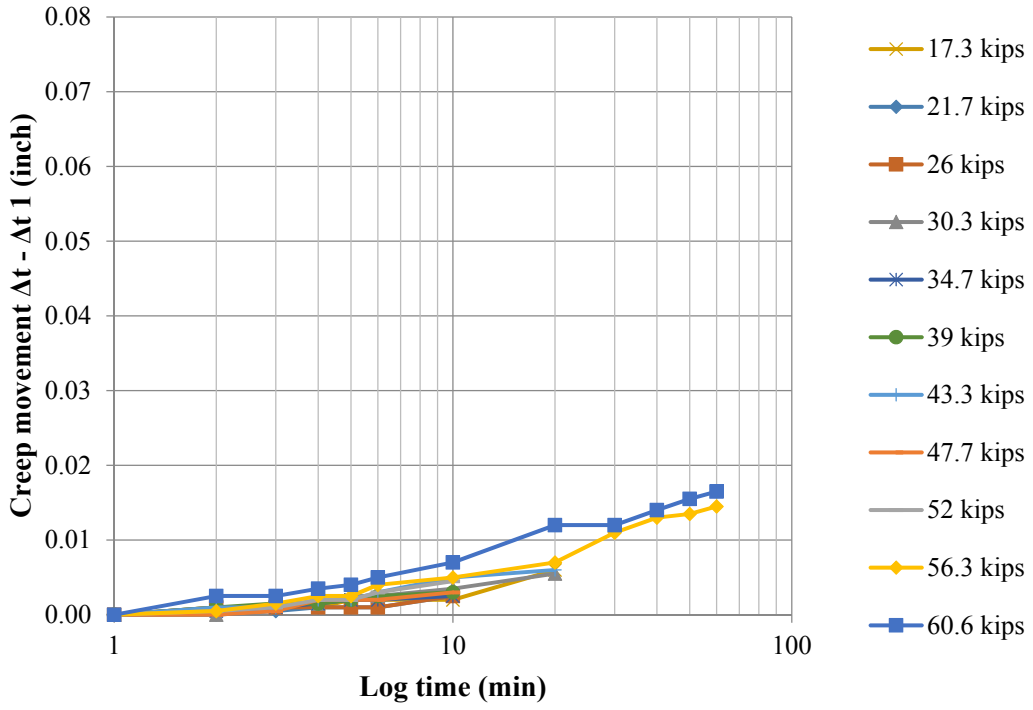

Figure 4-83. Creep movement versus time for N4 at different load step

The range of the creep movement for all the tested nails (N1, N2, N3 and N4) and all the load steps was less than the acceptance criteria (i.e. creep movement for the readings between 1 to 10 minutes was less than 0.04 inch).

As it is shown in Figure 4-81, the creep movement for the first cycle of loading is greater than the second and third cycle. This test clearly shows that preloading (load history) affects the creep behavior of the soil nails.

The creep rate in unit of inch per log cycle of time at different load steps for the nails N1, N2, N3 and N4 are presented in Figure 4-84. The creep rate for tested nails is well below the acceptance criteria.

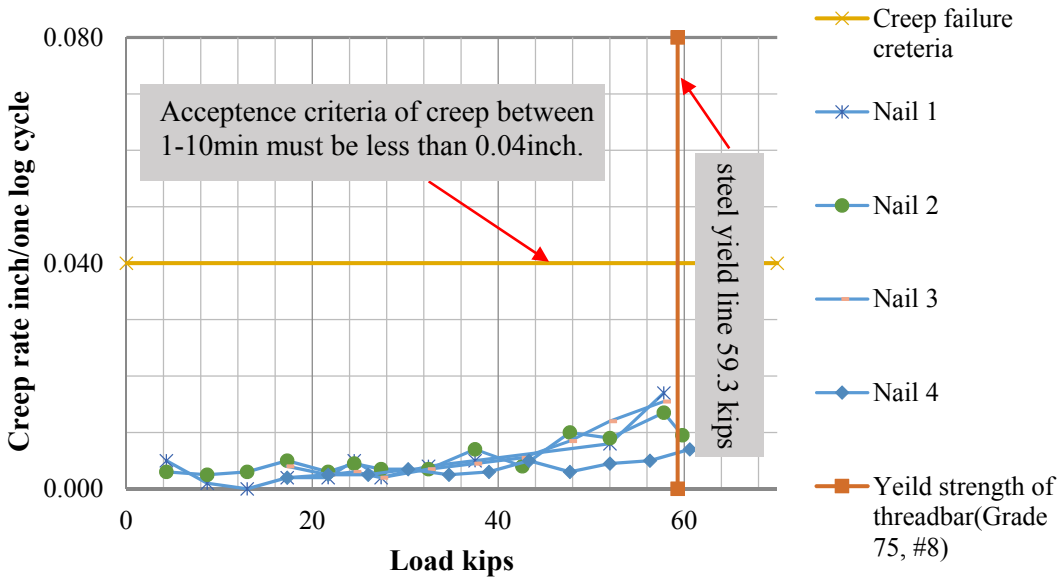

Figure 4-84. Creep rate at different loads for N1, N2, N3 and N4 (1 to 10 minutes reading)

b) Test on NS1 in September 2013

During the pullout test on nail NS3, each load step was held constant for 10 minutes and the creep movements were recorded. Figure 4-85 and Figure 4-86 show the creep movements and the creep rate (inch/log cycle of time) at different load steps for 1 to 10 minutes, respectively.

The creep movement recorded for the loads less than the failure load (29 kips) was significantly less than the acceptance criteria. For instance, at 86% of the failure load (i.e. one step before the failure load), the creep movement for 1 to 10 minutes was 0.012 in. At the failure load, the creep movement suddenly increased up to 0.131 in. This behavior is the same as the one observed during the tests on the existing anchors and the

new nails on the concrete slab. Creep movements more than acceptance criteria happened just at failure load or at the loads greater than 90% of the failure load.

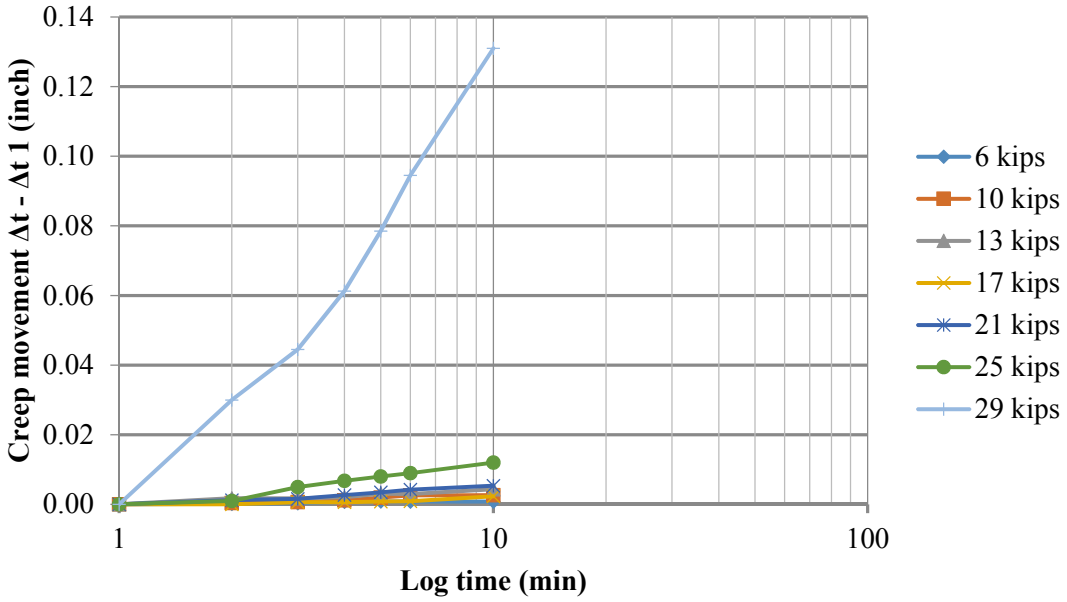

Figure 4-85. Creep movement versus time for NS3 at different load step

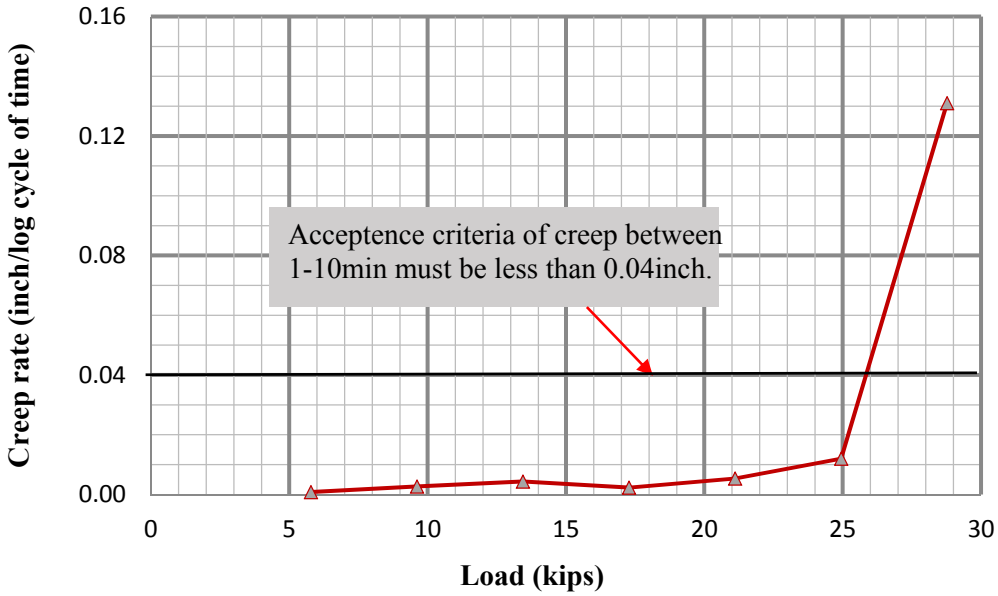

Figure 4-86. Creep rate at different load for NS3 (1 to 10 minutes reading)

c) Retest N1 and N4 on concrete slab

Creep movement for each load step versus time for N1 and N4 are illustarted in Figure 4-87 and Figure 4-88, respectively. Figure 4-89 and Figure 4-90 show the creep rate (inch/log of time) for N1 and N4, repectively.

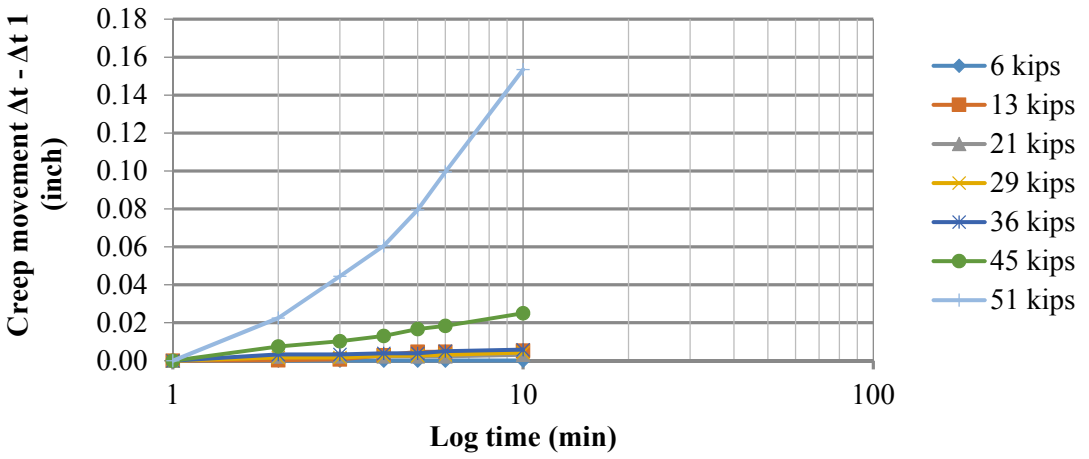

Figure 4-87. Creep movement versus time for retest on N1 at different load step (acceptance criteria for 1 to 10 min reading must less than 0.04 inch.)

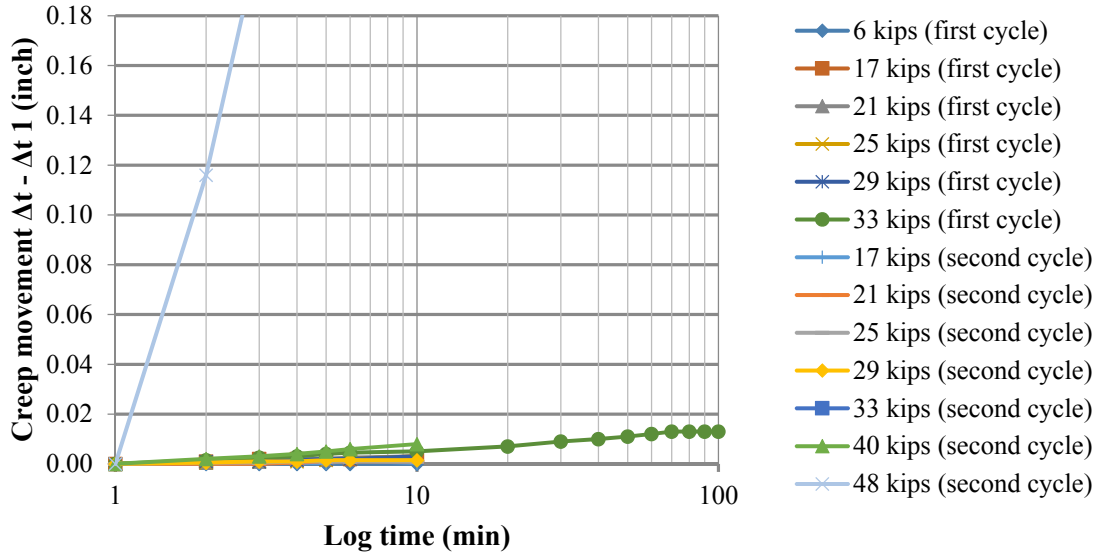

Figure 4-88. Creep movement versus time for retest on N4 at different load step at first and second load cycle (acceptance criteria for 1 to 10 min reading must less than 0.04 inch.)

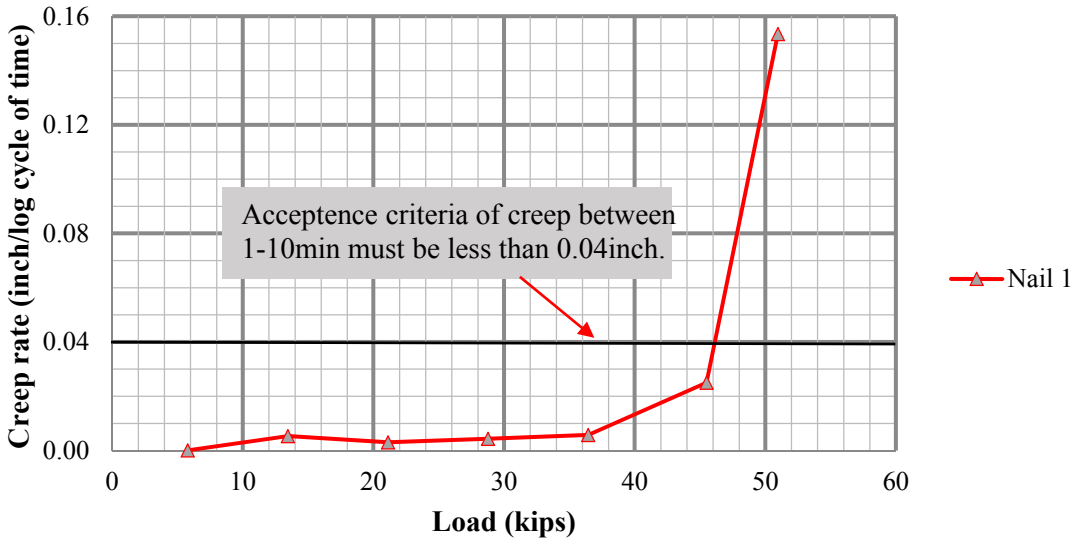

Figure 4-89. Creep rate at different load step for 1 to 10 minutes reading for retest on N1

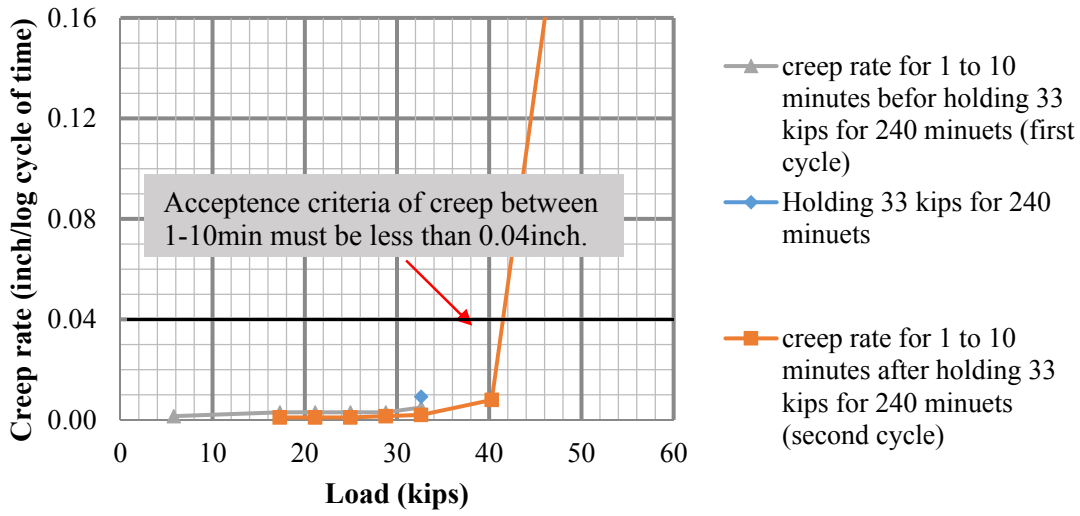

Figure 4-90. Creep rate at different load step for 1 to 10 minutes reading for retest on N4

The results of the creep tests show that the creep movement for the loads less than the failure load is much less than the acceptance criterion (i.e. creep movement for 1 to 10 minutes readings is less than 0.04 inch), and it suddenly becomes higher than the acceptance criterion at the failure load. The results of the cyclic loading test on nail 4 show that the creep movements are less in the second loading cycle when compared against the first cycle. Figure 4-91 shows the creep rate between for the first and second cycle, for the load in the range of 6 to 40 kips.

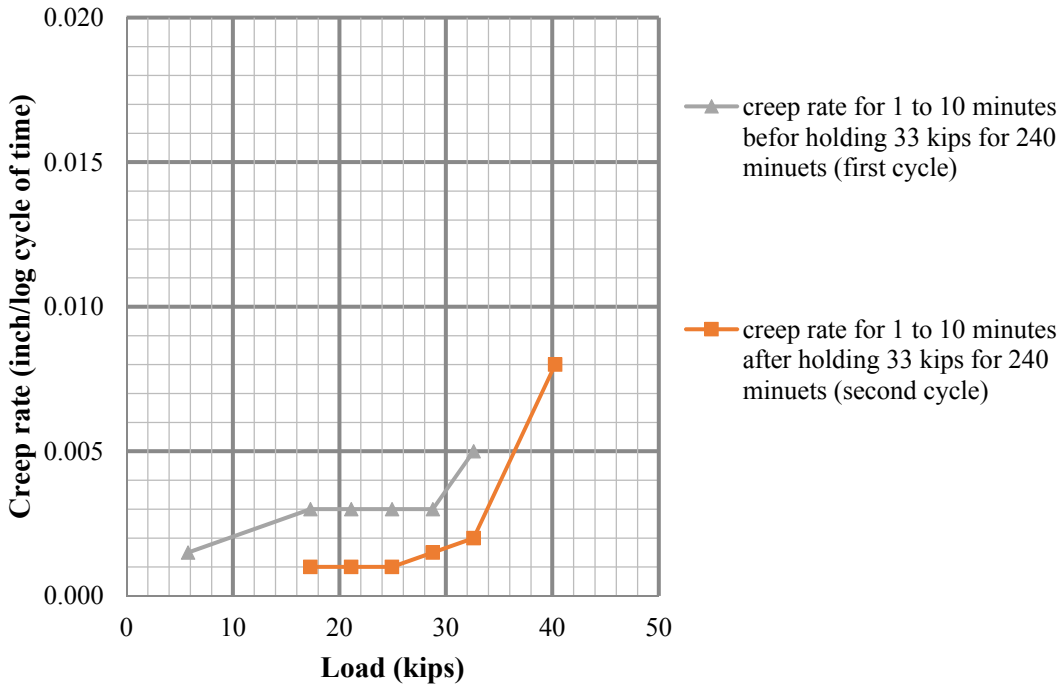

Figure 4-91. Compare the creep rate for first and second cycle of loading for retest on N4

n Value

The viscos exponent *n* obtained from the results of the pullout test on the new nails at NGES-TAMU clay site, for both original test (i.e. test on N1, N2, N3, and N4) and retest the nails (i.e. retest N1 and N4) are presented in Figure 4-92 and Figure 4-93, respectively.

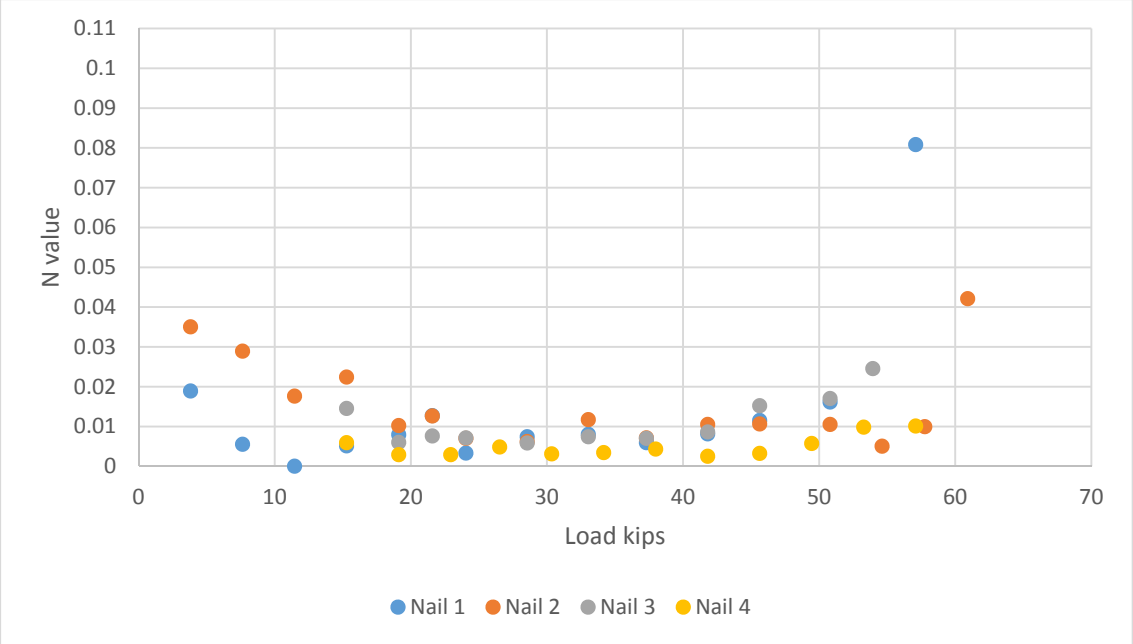

Figure 4-92. Viscous exponent "n" for N1, N2, N3 and N4

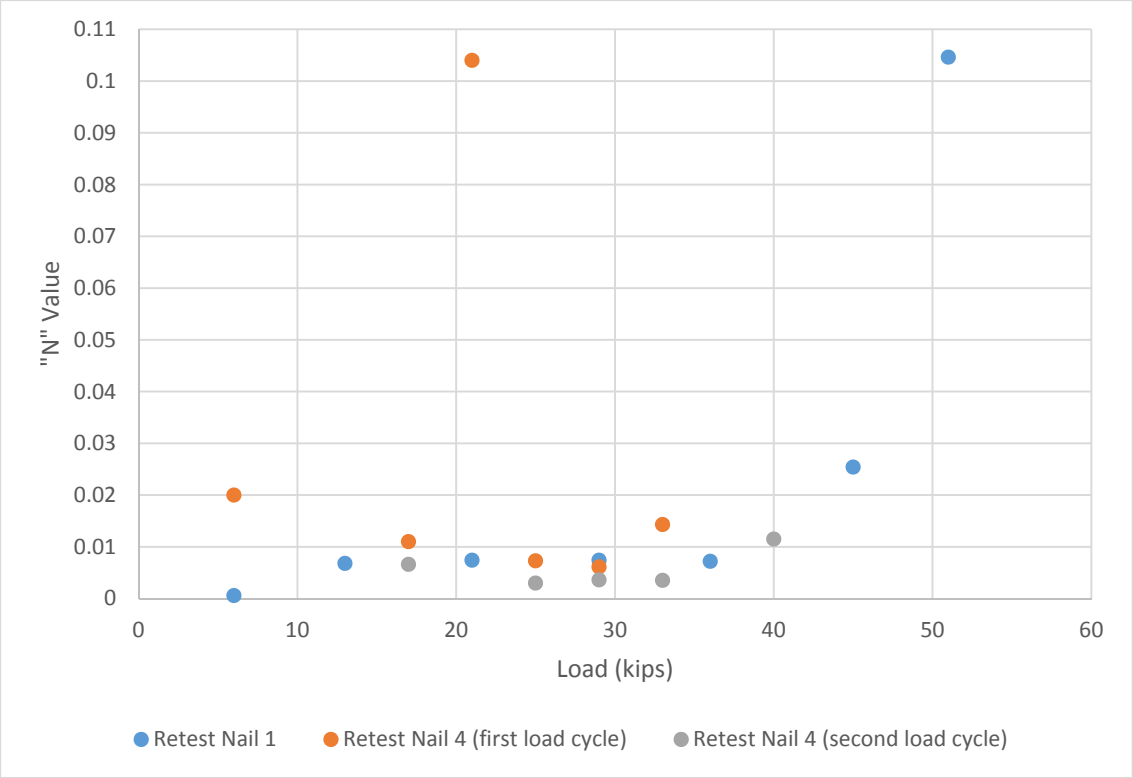

Figure 4-93. Viscous exponenet "n" for retested N1 to N4

Load Distribution in Nails During Pullout Test

Nails N3, N4, N5 and N6 were instrumented with strain gauges. The positions of the strain gauges along the nails are presented in Section 4.4.3. The cracking strain for the grout is assumed to be 100 με (100 x 10^{-6} in/in). The measured strains showed that most of the grout surrounding the threadbar was cracked. Since the measured strain exceeds the cracking strain in grout, load on the nails is related directly to the measured tensile strain of threadbar (FHWA, 1998).

The second strain gauge on nail 4 was broken during the nail installation. Figure 4-94 shows the load distribution on the nail 4 during the pullout test. During the pullout test, 60 kips load was held constant for 60 minutes. As it is shown in Figure 4-95, the load distribution on the nails for the constant load does not vary with the time.

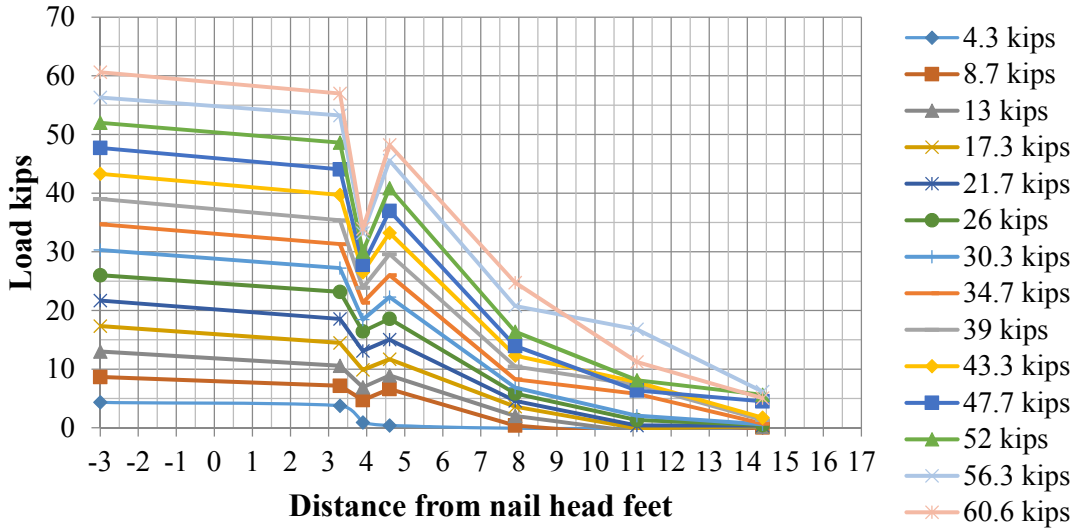

Figure 4-94. Load distribution on the N4 during the pullout test in July 2013

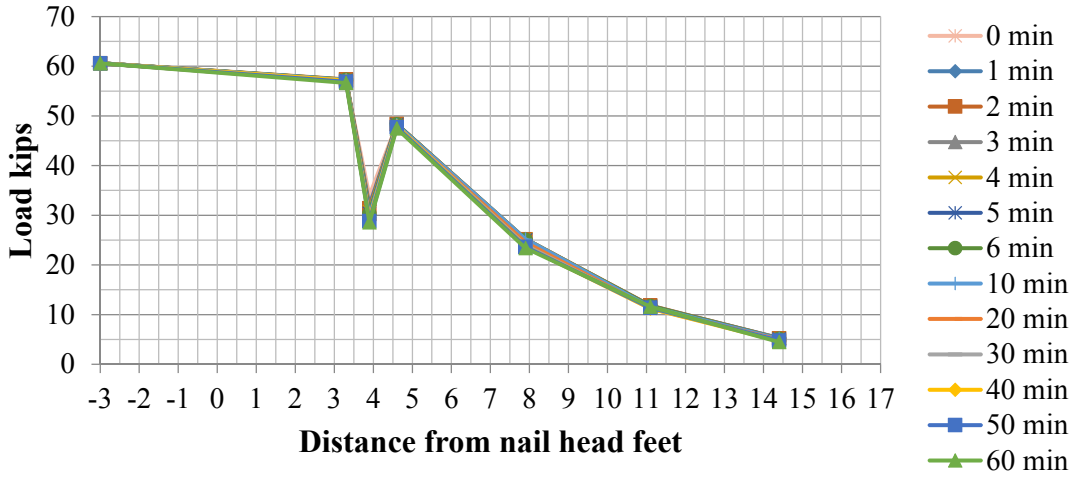

Figure 4-95. Load distribution during creep test for constant load of 60.6 kips for 60 minutes on N4

5. TESTING AND MONITORING A TTEXDOT SITE

5.1. Project Information

Emergency slope repair at the Beaumont district has been selected to study the time-dependent behavior of the soil nail wall in high plasticity clay. The site is located at the ramp below US 69 overpassing avenue A in the Beaumont district, Jefferson County. The coordinate of the project site is 30° 1'54.61"N 94° 5'22.77"W. Figure 5-1 and Figure 5-2 show the location of the project site.


Project Site
JEFFERSON COUNTY
Beaumont
Beaumont
Interstate 10
Washington
Fannett
Highland
Southern Pacific
Kcs Railroad
M L King Jr
Unnamed Street
Unnamed Street
P Railroad
FRA ADDED
Hillebrandt
Erie St
Bun St
Chambless Dr
Private Rd
W Florida St
W Cardinal Dr
W Virginia St
W Highland Dr
Basin St
Campus St
Shell St
Iowa St
Georgia St
E Virginia St
E Lavaca St
E Caston St
Woodrow St
Pipkin St
Edwin St
Lavaca St
Church St
Eigle St
Alma St
Euclid St
Rockwell St
Terrell St
Corley St
Lyle St
Fulton St
Porter St
Grant St
Schwarner St
Lamar St
Buford St
Finis St
Toltec St
Milam St
Irma St
Crockett St
Cedar St
Smart St
Hollywood St
Brenham St
Fannin St
Stagg Dr
Milam St
Bolivar St
Cartwright St
Roberts St
Elinor St
W Euclid St
Waverly St
Glenwood St
Charity Rd
Sarah St
Lela St
Nora St
Rena St
May St
Threadneedle St
Harriot St
Terrell St
Ohio St
Sulphur Dr
Spindletop Rd
Anco Rd
Highland Ave
Cochran St
Maddox St
Sunset St
Elsa St
Wyatt St
Ecta St
Park St
Reed St
Brandon St
Irving
Victoria St
Nichols St
Avenue A
Avenue B
Avenue D
Avenue E
Avenue G
Emilie St
Blanchette St
Gilbert St
Royal St
Craig St
Gray St
Neches St
Pennsylvania St
Sabine Pass Ave
Saint Anthony St
Carroll St
Burt St
Doucette St
Guill Stokes Rd
Ocean Dr
Rainbow
Executive Blvd
Blossom Dr
Ward St
Latin Dr
Booker St
Pradera St
Usan St
Marie St
Bob St
Ramming Ln
Edna St
Ogden Ave
Kenneth Ave
Reed St
Maddox St
University Dr
Iowa St
Shell St
Basin St
Avenue A
Private Rd
Bun St
Chambless Dr
Erie St
Unnamed Street
Unnamed Street
Highland Ave
Spindletop Rd
Sulphur Dr
Anco Rd
Ohio St
E Cardinal Dr
W Cardinal Dr
W Florida St

Figure 5-2. Top view of the project site

Figure 5-3 shows the condition of the embankment soil before the project was started. The soil was unstable and failed at the section next to the bridge. Soil nail technique was selected to stabilize the slope.

As it is shown in Figure 5-4, length of the soil nail wall is 453 ft. (i.e. starts from station 0+00 and ends at station 4+53). Maximum height of the soil nail is 25 ft. at station 0+76 (i.e. next to the bridge) and it is decreased to 3.75 ft. at station 4+53. Number of the soil nail rows and length of the soil nails are different at various sections. Table 5-1 shows the details of the soil nails at different sections.

Figure 5-3. Condition of the soil before the project was started

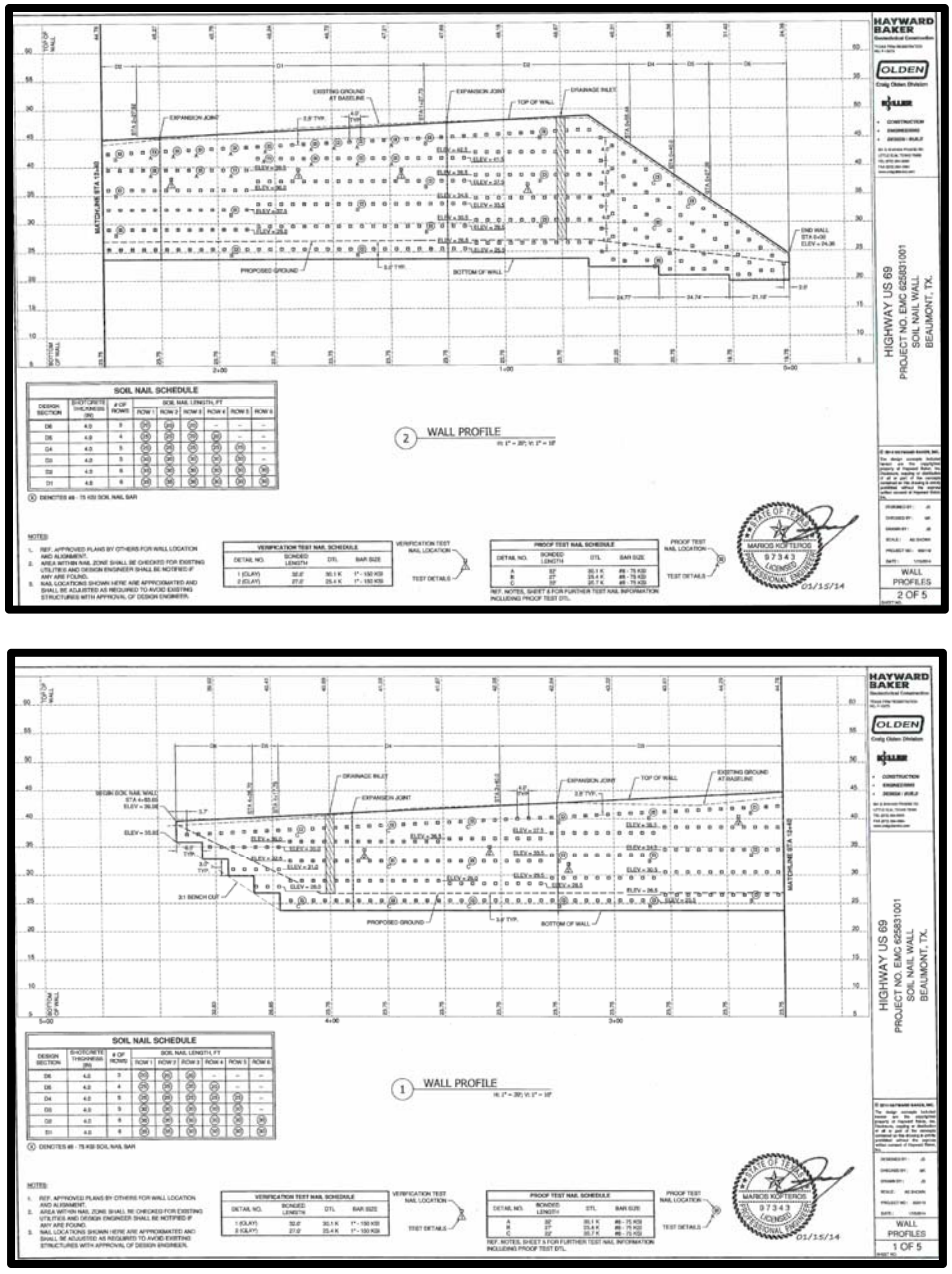

Figure 5-4. Soil nail wall profile

Table 5-1. Soil nail specifications

DESIGN SECTION	SHOTCRETE THICKNESS (IN.)	# OF ROWS	LOCATIONS OF THE SECTION	SOIL NAIL LENGTH FT.					
				ROW #					
				1	2	3	4	5	6
D6	4	3	ST 0+00 to ST 0+27 , ST 4+26 to ST 4+53	20	20	20	-	-	-
D5	4	4	ST 0+27 to ST 0+40 , ST 4+17 to ST 4+26	25	25	20	20	-	-
D4	4	5	ST 0+40 to ST 0+55 , ST 3+40 to ST 4+17	25	25	25	25	25	-
D3	4	5	ST 2+40 to ST 3+40	30	30	30	30	30	-
D2	4	6	ST 0+55 to ST 1+27 , ST 2+27 to ST 2+40	30	30	30	30	30	30
D1	4	6	ST 1+27 to ST 2+27	35	35	30	30	30	30

5.2. Load Tests on Sacrificial Nails

Since the actual load acting on the soil nail depends on the nail position, study the behavior of soil nail at different heights is considered very relevant. Therefore, to explore the behavior of the soil nails at different positions, a total of six sacrificial nails were installed at three different heights. At each height, two sacrificial nails, one with instrumentation and the other without instrumentation, with the horizontal spacing of 8 ft., were installed. Preparation, installation and test implementation are presented in the following.

5.2.1. Preparation of Instrumented Nails

Total of six sacrificial nails were installed at the emergency slope repair at Beaumont district. Three of them were instrumented at the Texas A&M University.

To study the load distribution on the soil nails during the load tests, the nail bars were instrumented with foil strain gauges (i.e. model EA-06-125VB-120). The strain gauges were glued to the nail bar in pairs, and were mounted to top and bottom of the prepared positions. First pair of strain gauges were attached at 6.5 ft. from top of the wall (i.e. 6.5 ft. of the nail bars were left for load test set-up and unbonded length of the sacrificial nail) and the rest were installed at 5 ft. intervals. Distribution of the strain gauges are shown in Figure 5-5.

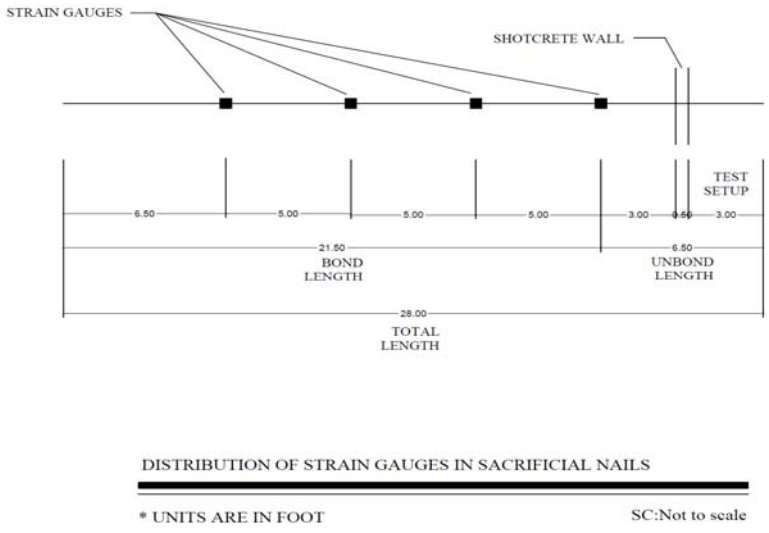

Figure 5-5. Positions of strain gauges for sacrificial nails

Procedure of attaching the strain gauges are presented in the following:

- The ribs of the nail bar at the designated locations were ground down with an electric grinder (Figure 5-6a.)
- Sanded with 200-grit and 400-grit sandpaper to create a 4-inch long smooth surface.
- The strain gauges were glued to the nail bar in pair (i.e. top and bottom of the designated position) (Figure 5-6b.).
- The strain gauges were wired (Figure 5-6c.).

To extend the persistence of the strain gauges, two layers of protective coating (i.e. Vishay M-Coat J) were applied to the strain gauges on the nail bar (Figure 5-6d).

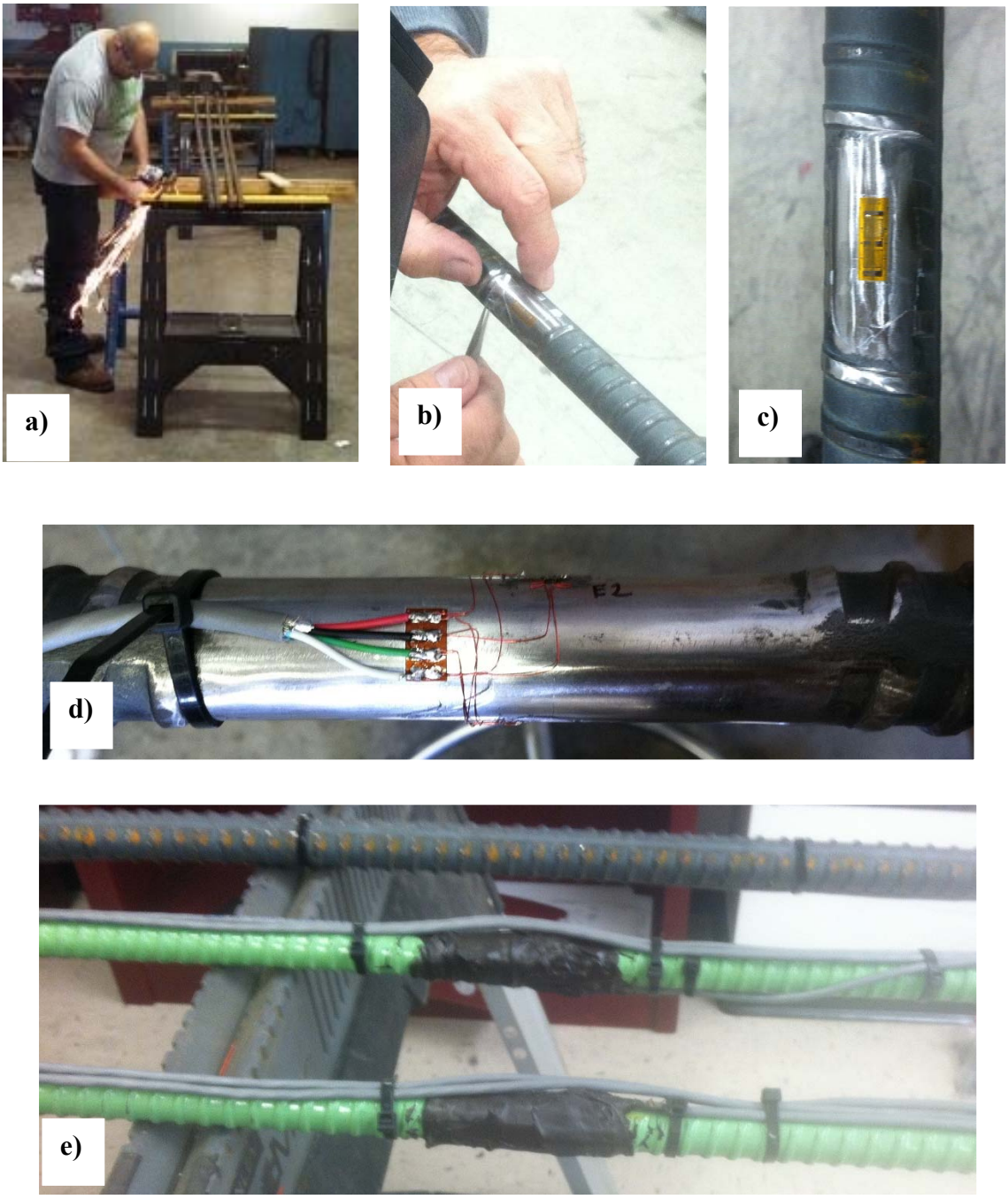

Figure 5-6. Procedure of attaching the strain gauges: a) grinding the nails bar, b and c) gluing the strain gauges to nails bar, d) wiring the strain gauges, and e) double coating

Prior to shipping the nail bars to the site, pullout test were performed on all the instrumented thread bars to make sure that all of them work properly. The nail bars were loaded up to 10 kips and the strain was recorded with data acquisition system during the tests. Figure 5-7 illustrates the set-up for the pullout test.

Figure 5-7. Set-up for pullout test at Texas A&M University prior to shipping the nail bars to the Beaumont site

5.2.2. Installation of Instrumented Nails

As it is shown in Figure 5-8, six soil nails were installed at three different heights (i.e. three different rows). Each row comprises one sacrificial nail with instrumentation and one without instrumentation. First row of sacrificial nail was installed between second and third row of the production nails at 7.4 ft. from top of the wall. Second row and third row of the sacrificial nails were installed between fourth and fifth, and fifth and sixth row of the production nails, respectively. The second row of sacrificial nail was installed at 14.4 ft. from top of the wall while the third row was installed at 17.9 ft. from top of the wall. Figure 5-9 shows the positions of the sacrificial nails at the soil nail wall profile.

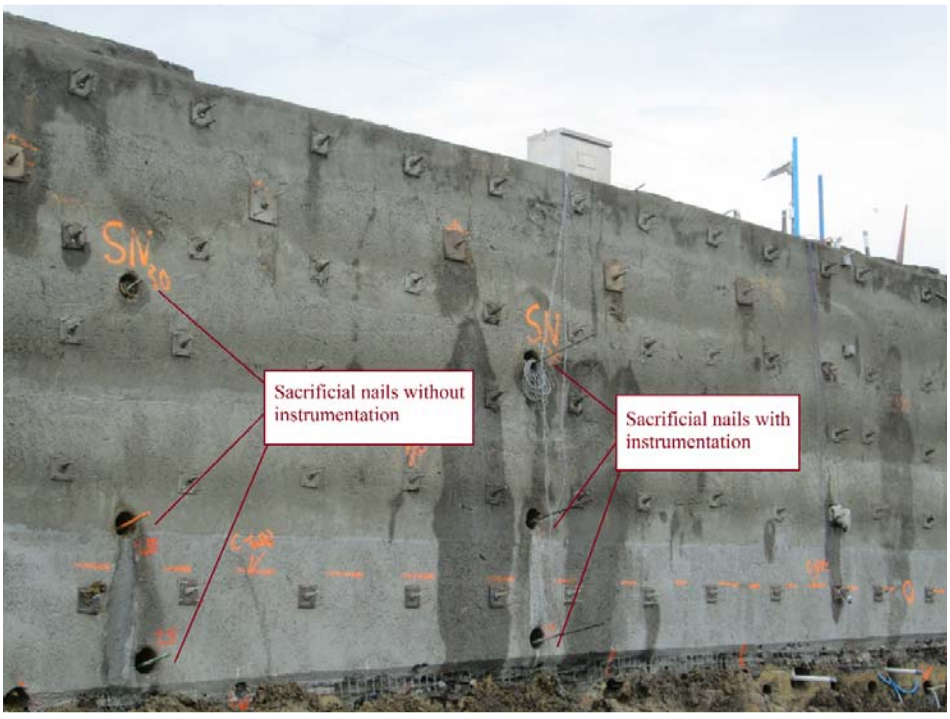

Figure 5-8. Sacrificial nails at different height

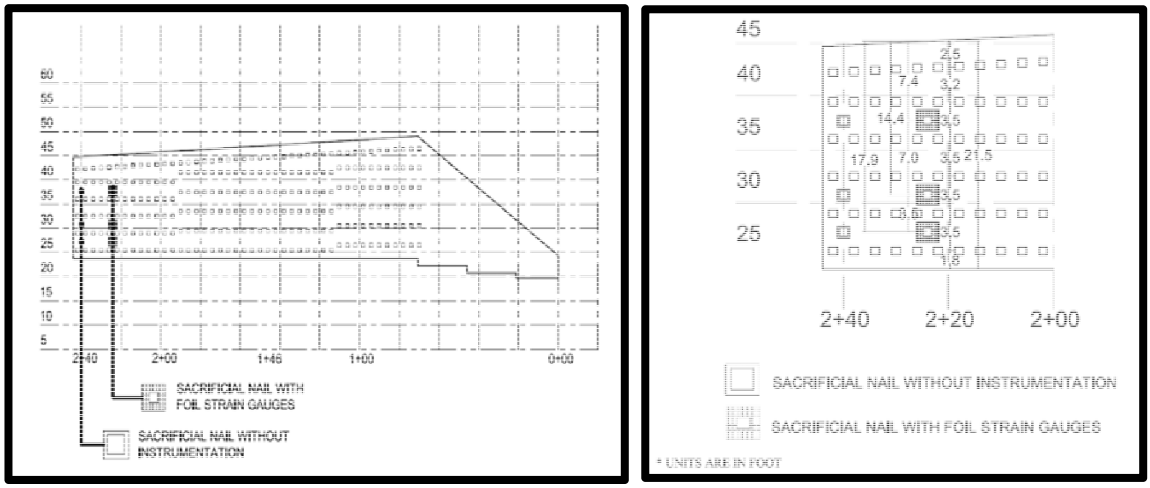

Figure 5-9. Positions of the sacrificial nails at the soil nail wall profile

5.2.3. Load Sequence

Verification tests and modified creep tests were carried out on the sacrificial nails. To evaluate the maximum shear strength between grout and soil (f_{max}) and the maximum pullout capacity of the nail in this row, verification test according to GEC#7, 2003 were performed on the sacrificial nail without instrumentation. Knowing the maximum pullout capacity, creep test with load increment of 4 kips was conducted on the instrumented nails. Figure 5-10 illustrates the load sequence on the sacrificial nails at the first row.

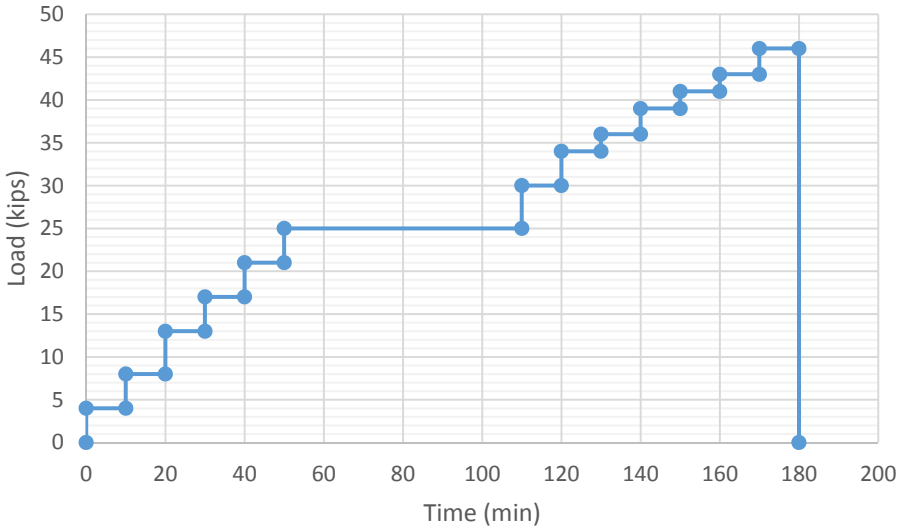

Figure 5-10. Pullout load sequence on first row of sacrificial nail (at 7.4 ft. from top of the wall)

Second row of sacrificial nails (i.e. at 14.4 ft. from top of the wall) were tested on May 22, 2014. Verification test according to GEC#7, 2003 with load increment of 4 kips was conducted on the sacrificial nail without instrumentation to evaluate the maximum pullout capacity of the nails at this row. After evaluating the pullout capacity, modified creep test was performed on the instrumented sacrificial nail. While keeping the load increment at 5 kips, each load step was held for 60 minutes and creep movement was recorded. As it is shown in Figure 5-11, the test lasted for 540 minutes.

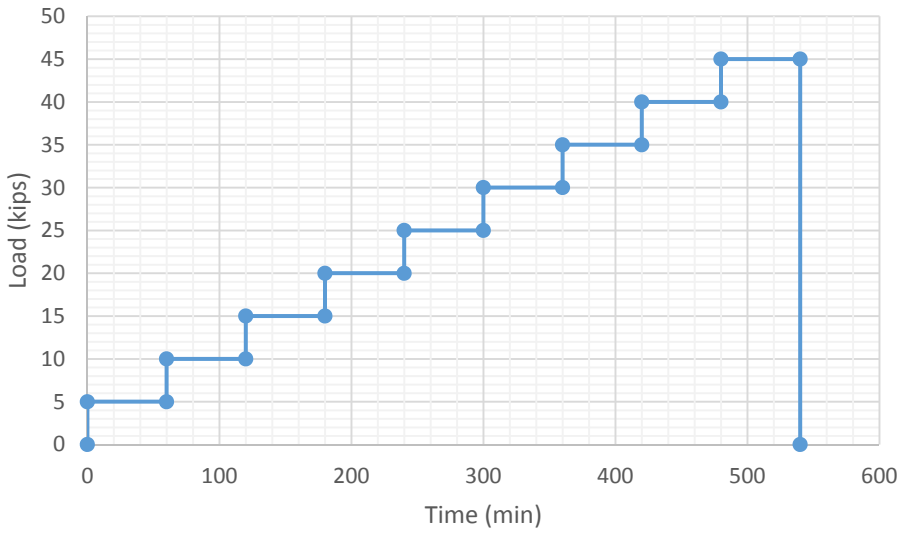

Figure 5-11. Pullout load sequence for the second row of sacrificial nail (at 14.4 ft. from top of the wall).

5.2.4. Load Test Set-Up

A center hole hydraulic jack and electrical hydraulic pump were used to apply load to the sacrificial nails. A reaction beam was placed between hydraulic jack and the shotcrete facing to align the axis of nail bar and axis of hydraulic jack. To monitor a constant load during creep test, a center hole load cell was placed at top of the nail. Figure 5-12 shows the load test set-up. As it is shown in Figure 5-13, wires of the strain gauges were connected to data acquisition system during the load test and data from strain gauges were recorded.

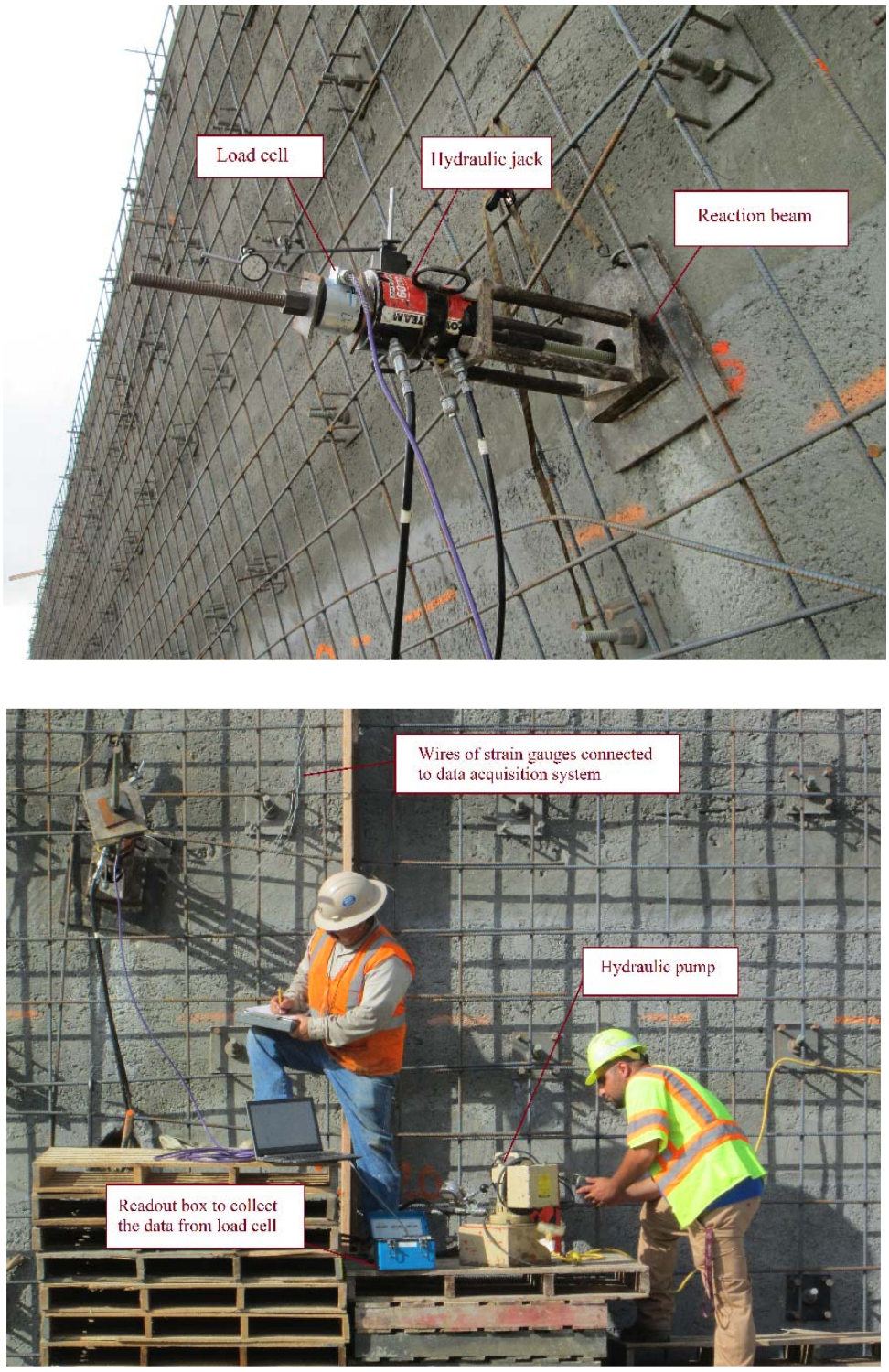

Figure 5-12. Load test set-up

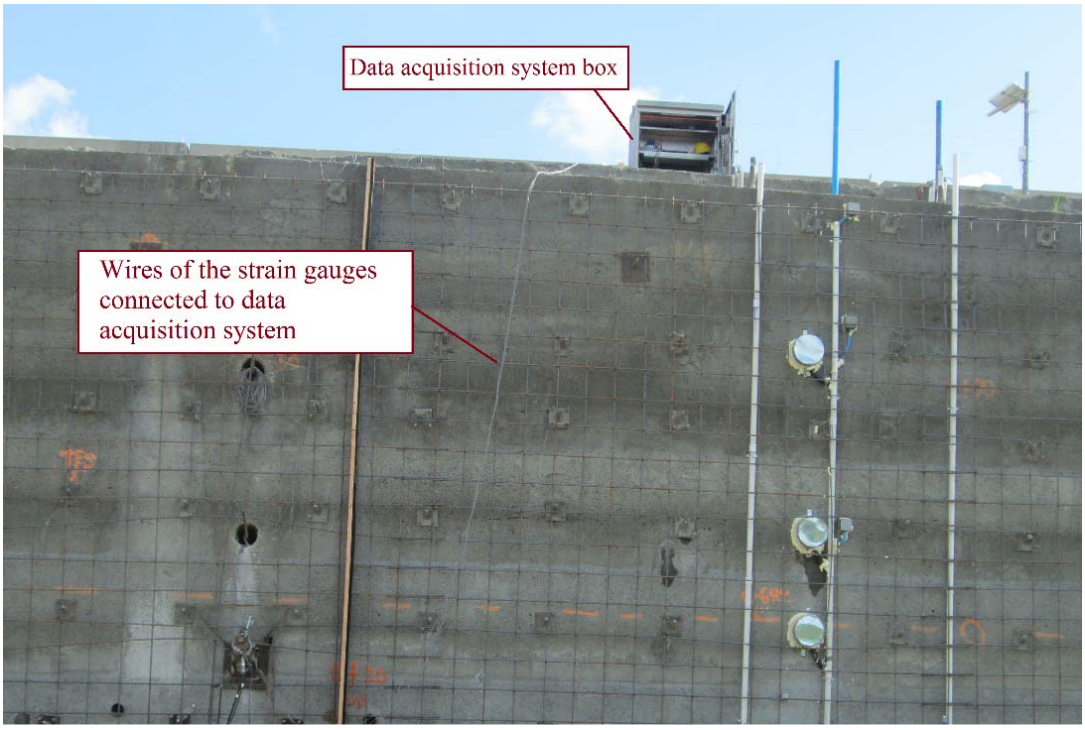

Figure 5-13. Connecting the wires to the data acquisition system during the test

5.2.5. Test Results: Total, Elastic and Residual Movement

During the test, sacrificial nails were incrementally loaded until failure occurred. Total movement is defined as the measured movement of the nail head during the test. Total movement consists of elastic movement and residual movement. Elastic movements are the recoverable movements when the tested nail is unloaded (i.e. the nail's load is reduced from a test load to an alignment load). Residual movements are non-recoverable movements measured when the nail is unloaded (FHWA, 1998). Results of the pullout tests on the sacrificial nails are presented as follows:

a) Tests on Sacrificial Nails 1 at Height = 7.4 ft.

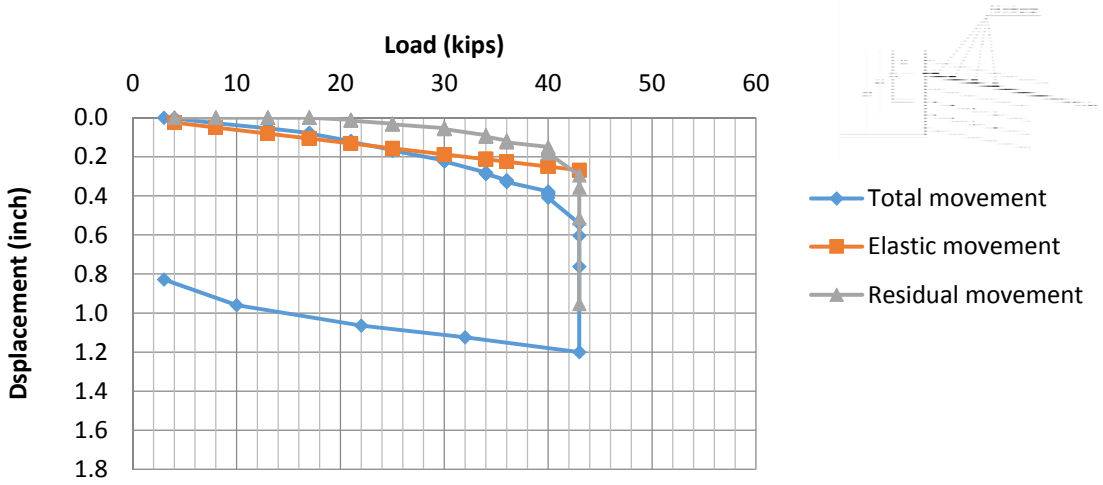

Figure 5-14. Total, elastic and residual movement vs load for non-instrumented sacrificial nail 1

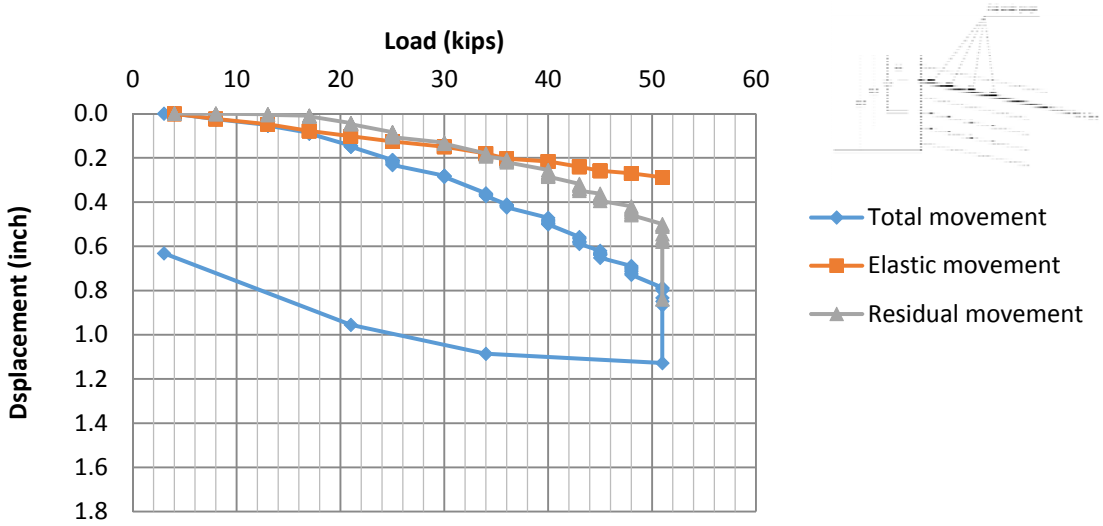

Figure 5-15. Total, elastic and residual movement vs load for instrumented sacrificial nail 1

b) Tests on Sacrificial Nails 2 at Height = 14.4 ft.

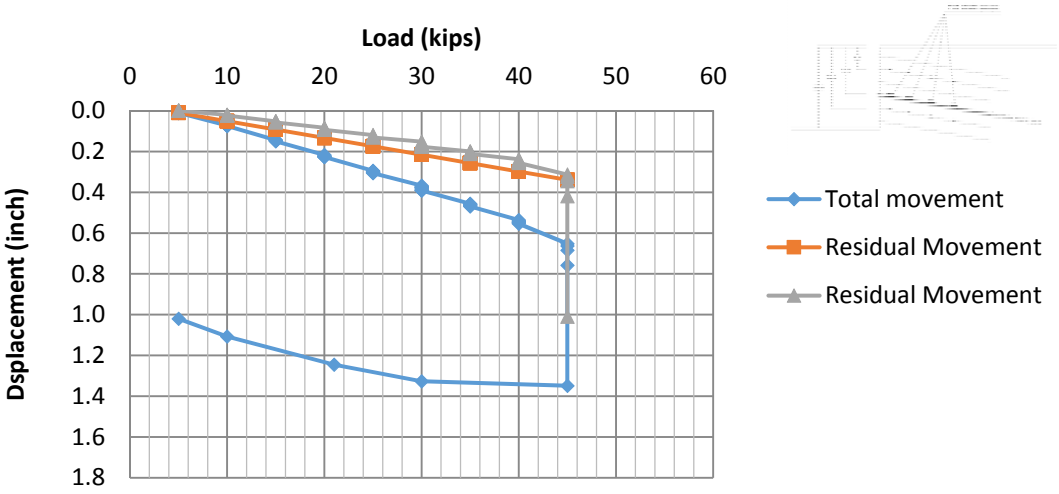

Figure 5-16. Total, elastic and residual movement vs load for non-instrumented sacrificial nail 2

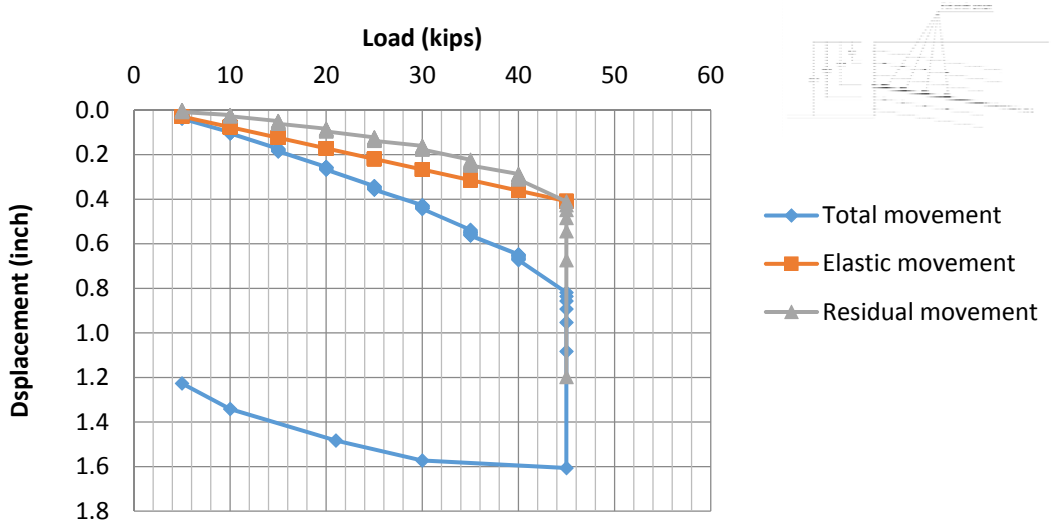

Figure 5-17. Total, elastic and residual movement vs load for instrumented sacrificial nail 2

c) Tests on Sacrificial Nails 3 at Height = 17.9 ft.

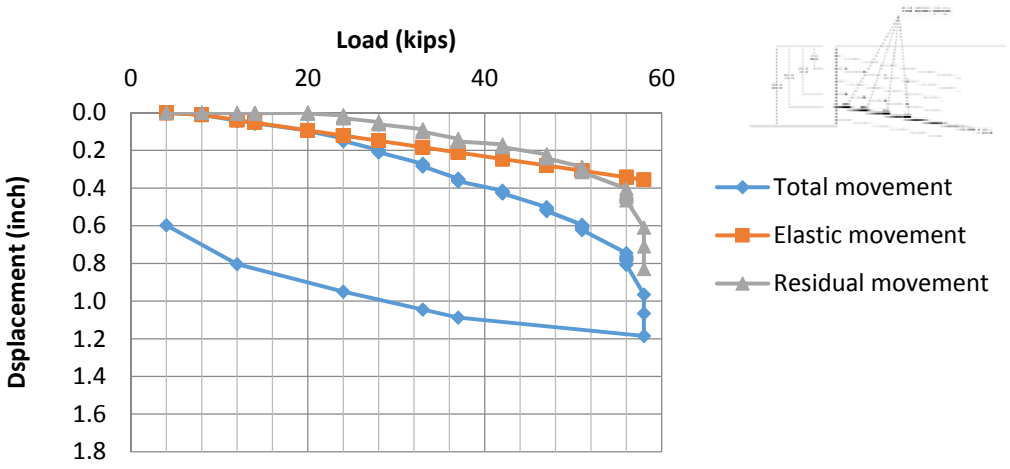

Figure 5-18. Total, elastic and residual movement vs load for non-instrumented sacrificial nail 3

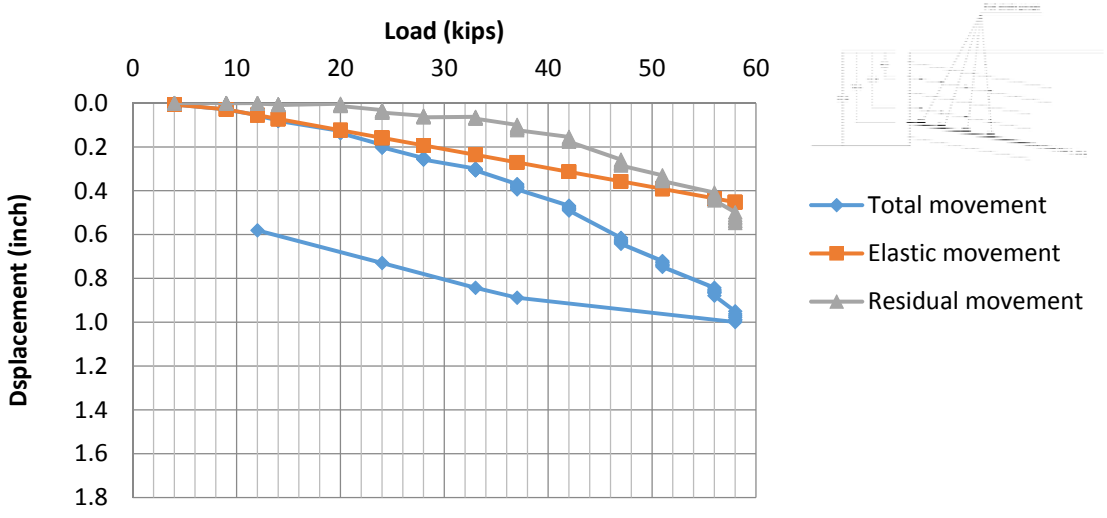

Figure 5-19. Total, elastic and residual movement vs load for instrumented sacrificial nail 3

Summary of the tests results and sacrificial nails specification is presented in Table 5-2. Bond length for sacrificial nails 1 (h=7.4) are 27 ft. bond length, while sacrificial nails 2 and 3 (h=14.4 and 17.9, respectively) have 23 ft. bond length.

Table 5-2. Test summary on sacrificial nails

Nail No.	Bond Length (ft.)	Hole diameter (inch)	Failure load (kips)	Maximum bond stress at failure (psf.)	Design bond stress (psf.)
Non-instrumented 1 (H=7.4 ft.)	27	8	43	760	300
Instrumented 1 (H=7.4 ft.)	27	8	51	902	300
Non-instrumented 2 (H=14.4 ft.)	23	8	45	935	300
Instrumented 2 (H=14.4 ft.)	23	8	45	935	300
Non-instrumented 3 (H=17.9 ft.)	23	8	58	1204	300
Instrumented 3 (H=17.9 ft.)	23	8	58	1204	300

As it is shown in Table 5-2, factor of safety for design bond stress at top of the soil nail wall is 2.5, while for the nails at bottom of the wall is 4.

5.2.6. Creep Test on Non-Instrumented Sacrificial Nails

During the verification tests on nun-instrumented nails, each load increment was held for 10 minutes and creep movement of the nail head was recorded. At 150% of the design load (i.e. Design bond stress 300 psf.), load was held for 60 minutes and creep movement was recorded. By relating the increment of nail head displacement over a

certain time, a creep rate can be obtained. Acceptance criteria typically requires that creep movement between the 1- and 10-minute readings, must be less than 0.04 in. (1 mm), or that the creep movement between the 6- and 60-minute readings must be less than 0.08 in. (2 mm) (GEC#7, 2003). Results of the creep tests on non-instrumented nails are presented as follows:

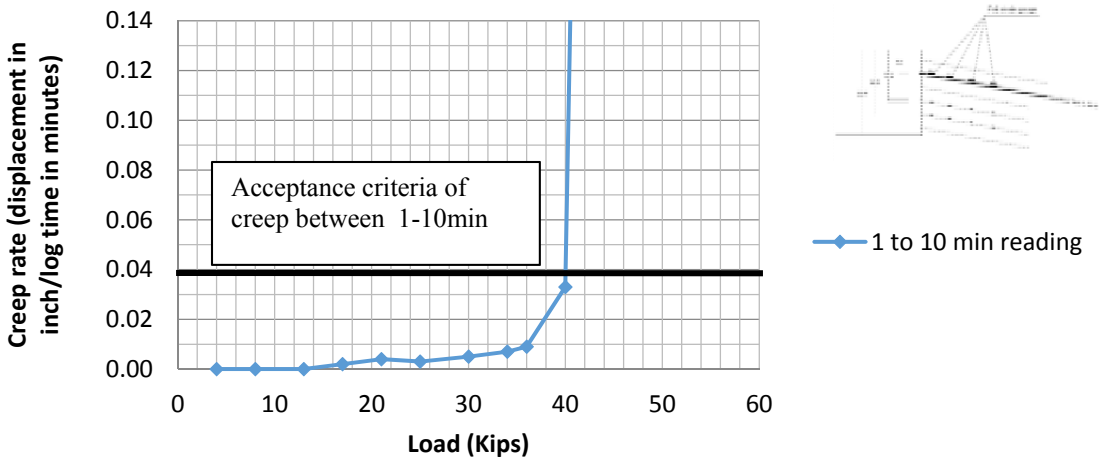

Figure 5-20. Creep rate for 1 to 10 min readings a different load during verification test on non-instrumented sacrificial nail 1

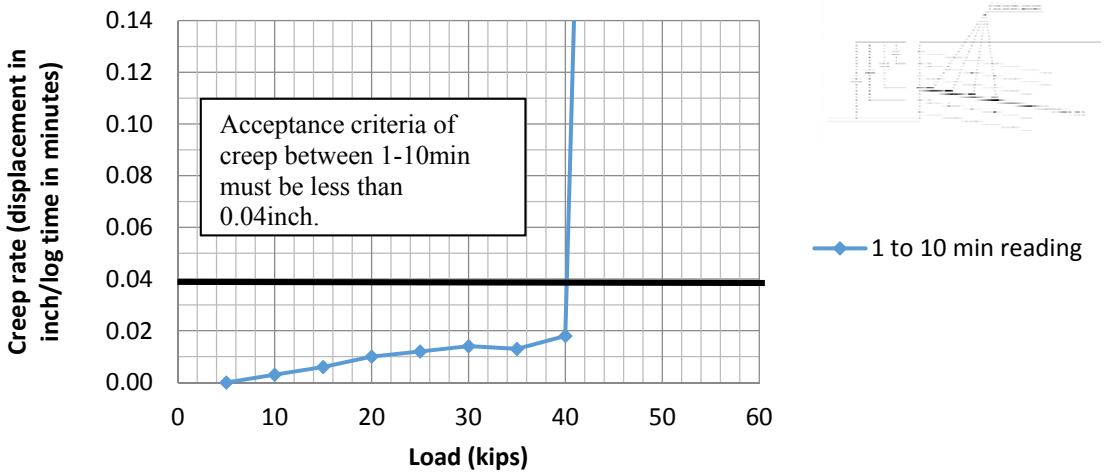

Figure 5-21. Creep rate for 1 to 10 min readings a different load during verification test on non-instrumented sacrificial nail 2

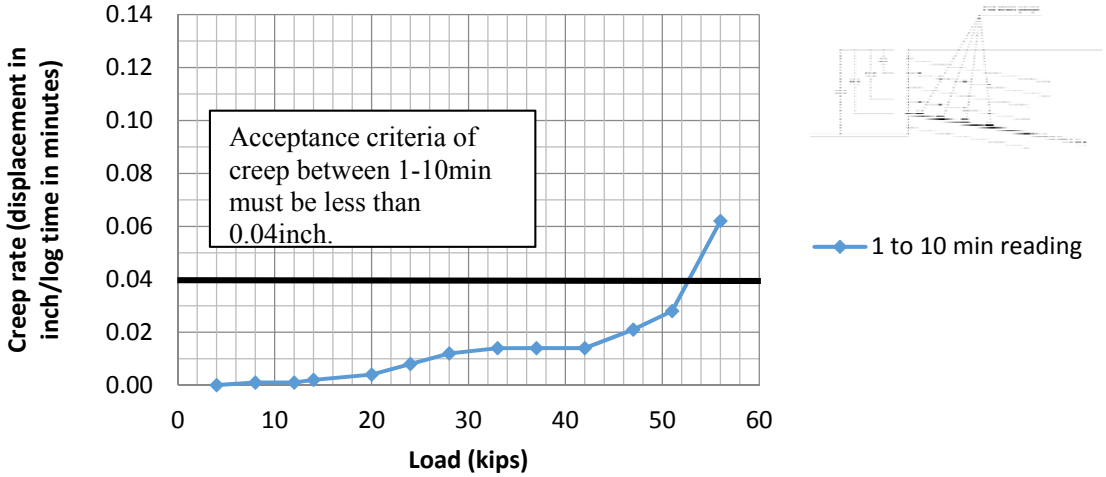

Figure 5-22. Creep rate for 1 to 10 min readings a different load during verification test on non-instrumented sacrificial nail 3

Figure 5-20 to Figure 5-22 clearly illustrate that the creep rate of the soil nails depends on the load level. By increasing the test load in non-instrumented nail 1, creep rate also increases but creep rate is significantly less than the acceptance criteria (i.e. creep rate 0.04 inch. For 1 to 10 min readings). At the failure load, 43 kips, creep rate notably increases. Same behavior observed in the non-instrumented nail 2 and 3. Creep rate for the loads less than the failure are less the acceptance criteria and the failure load it is increased significantly.

5.2.7. Creep Test on Instrumented Sacrificial Nails

Modified creep tests were performed on instrumented nails. By knowing the maximum pullout capacity of these nails from the verification tests results on the non-instrumented nails in the same height, load incremented of 5 kips was selected. Each load was held for 60 minutes and creep movement of the nail head was recorded. Creep rate for 1 to 10 minutes readings are illustrated in Figure 5-23 to Figure 5-25, while Figure 5-26 is presenting the creep rate for 6 to 60 min readings on instrumented sacrificial nail 2.

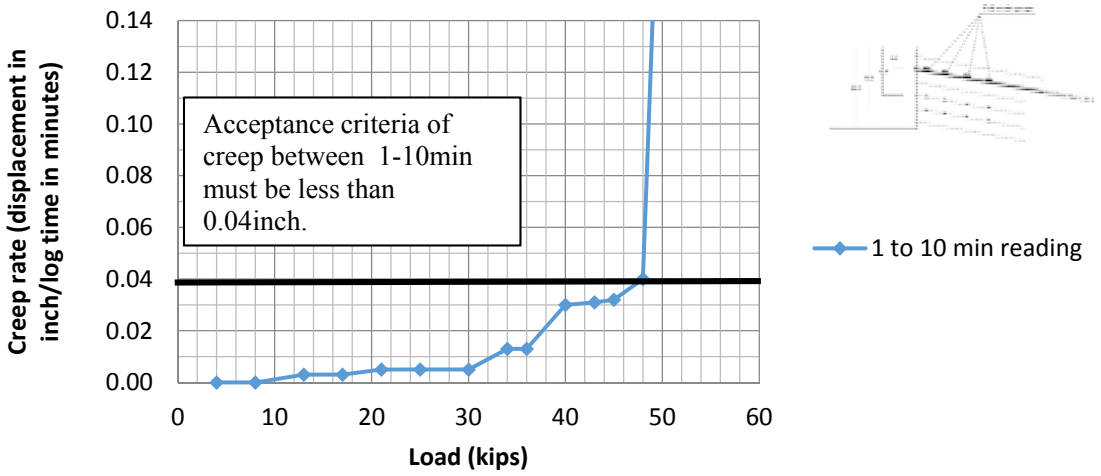

Figure 5-23. Creep rate for 1 to 10 min readings a different load during the modified creep test on instrumented sacrificial nail 1.

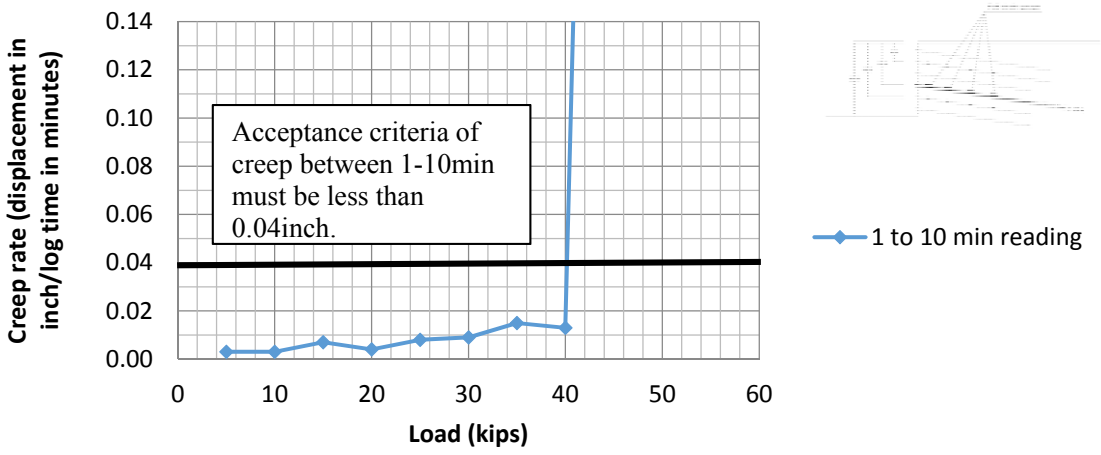

Figure 5-24. Creep rate for 1 to 10 min readings a different load during the modified creep test on instrumented sacrificial nail 2.

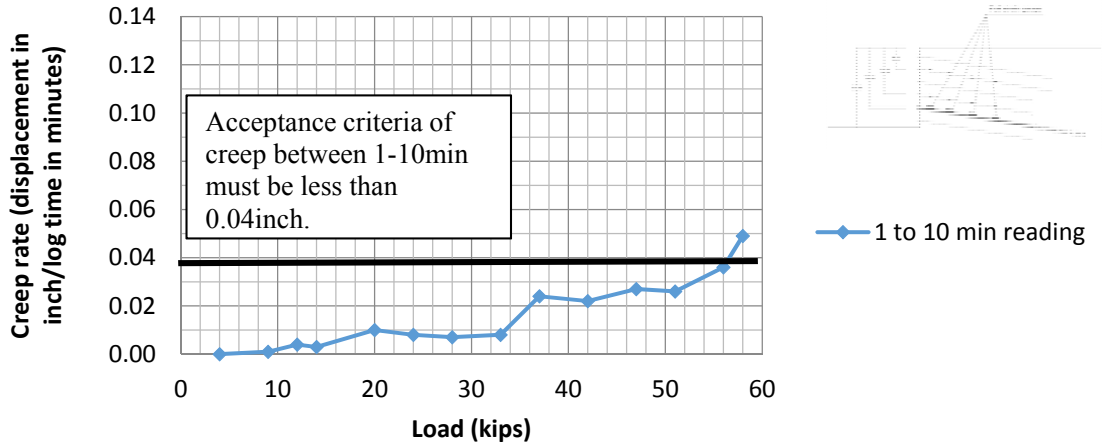

Figure 5-25. Creep rate for 1 to 10 min readings a different load during the modified creep test on instrumented sacrificial nail 3.

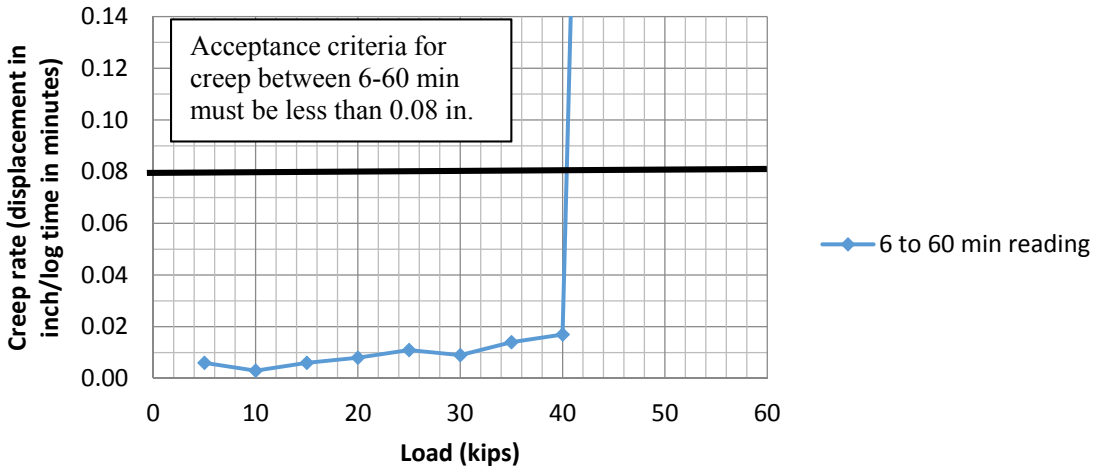

Figure 5-26. Creep rate for 6 to 60 min readings a different load during the modified creep test on instrumented sacrificial nail 2.

Same creep behavior was observed from the creep tests on the instrumented sacrificial nails. Creep rate is increased with increasing the load level. The creep rate is significantly below the acceptance criteria for the load less than failure load. At the failure load, creep rate is increased and the tested nail fails. Summary of the creep tests on instrumented sacrificial nails is presented in table 3. Creep failure is occurred at the load more than 94% of the pullout capacity.

Table 5-3. Summary of the creep tests on instrumented nails

Nail No.	Failure load (kips)	creep failure threshold (kips)	Maximum bond stress at failure (psf.)	Design bond stress (psf.)	Bond stress creep threshold (psf.)	Creep load threshold % of pullout capacity
Instrumented 1	51	48	902	300	849	94%
Instrumented 2	45	45	935	300	935	100%
Instrumented 3	58	56	1204	300	1162	96%

5.2.8. Load Distribution Along Instrumented Nail During Test

The cracking strain for the grout is assumed to be 100 με (100 x 10-6 in/in). The measured strains showed that most of the grout surrounding the threadbar was cracked. Since the measured strain exceeds the cracking strain in grout, load on the nails is related directly to the measured tensile strain of threadbar (FHWA, 1998). During the pullout tests on these nails, strain gauges were attached to the data acquisition system, figure 13, to

record the load distribution along the nails. Figures 27 to 29 illustrate the load distribution along the nails.

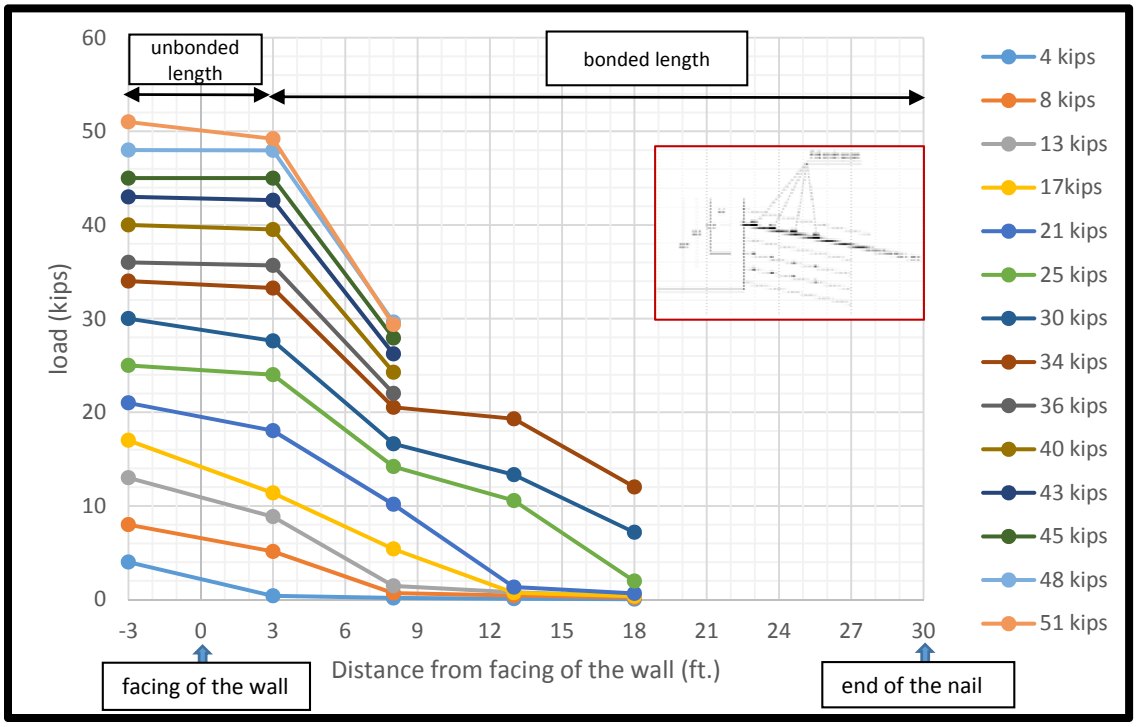

Figure 5-27. Load distribution along the instrumented sacrificial nail 1 (Height = 7.4 ft.)

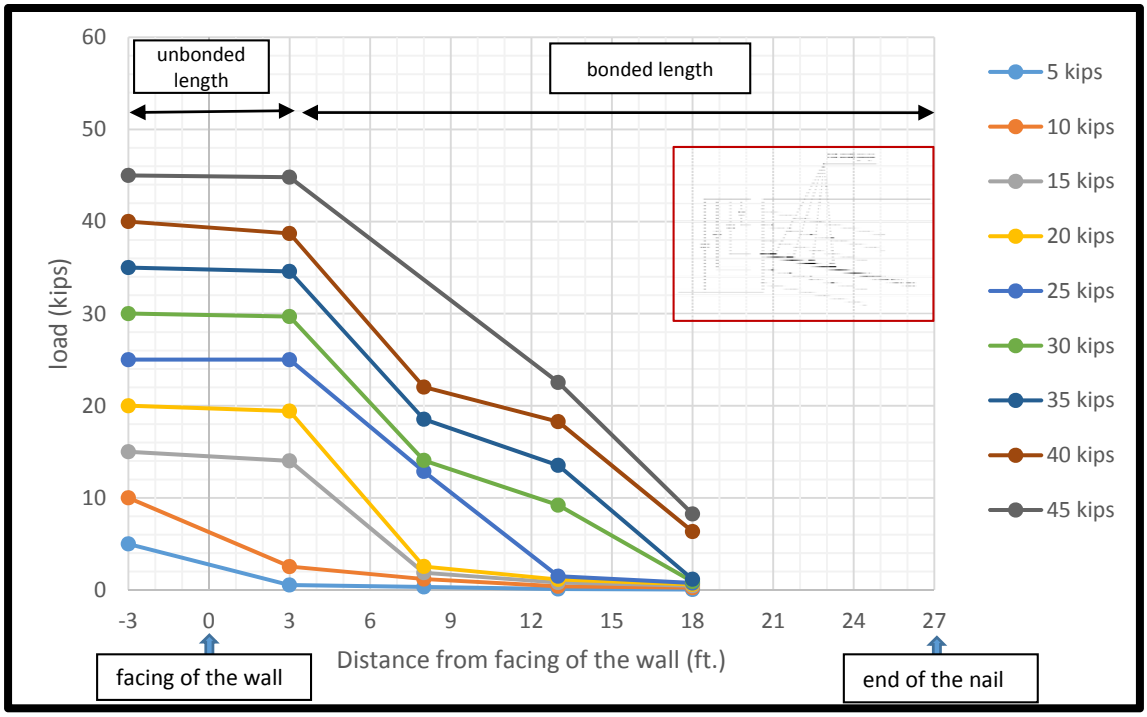

Figure 5-28. Load distribution along the instrumented sacrificial nail 2 (Height = 14.4 ft.)

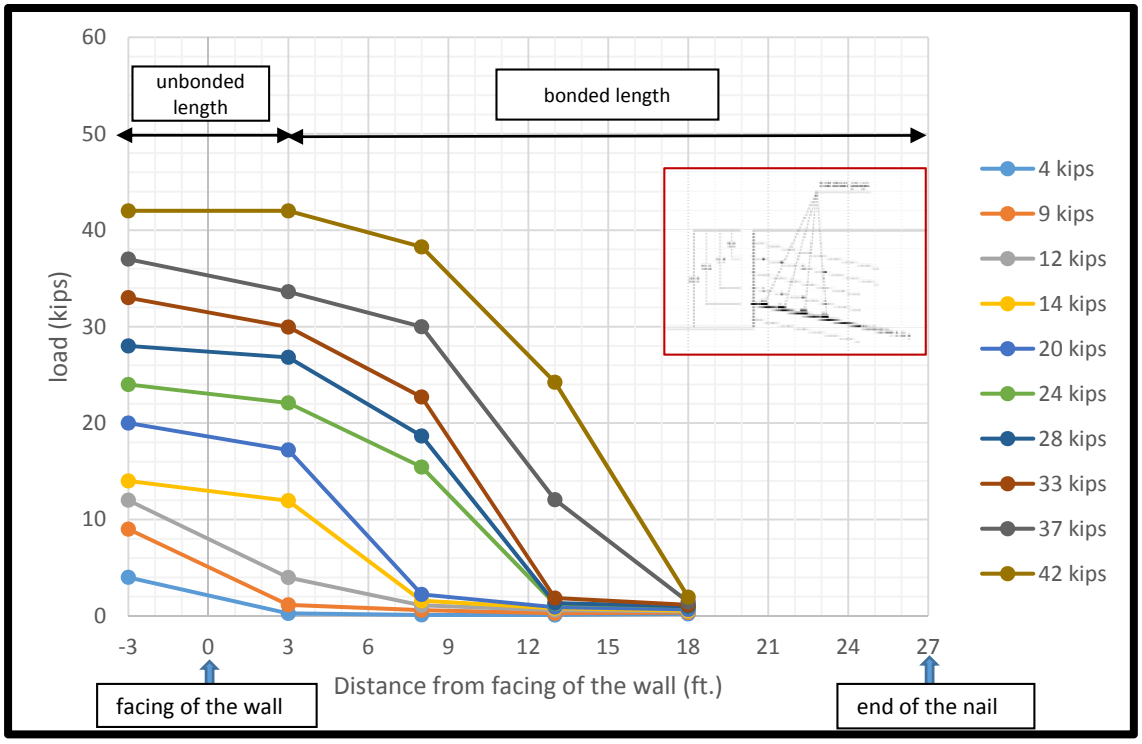

Figure 5-29. Load distribution along the instrumented sacrificial nail 3 (Height = 17.9 ft.)

During the test on instrumented sacrificial nail 1, third and fourth strain gauges (i.e. 13 and 19.5 ft. behind the shotcrete, respectively) were broken for the loads greater than 34 kips. As it is shown in Figure 5-27, the loads correspond to this strain gauges for the load greater than 34 kips are not shown. For the instrumented sacrificial nail 3, all the four strain gauges were broken for the load greater than 42 kips, there is no data shown in the Figure 5-29 correspond to the loads 47, 51, 59 and 58 kips.

5.3. Long Term Monitoring

The main objective of the long-term monitoring of the actual soil nail wall is to study its performance on a site with high plasticity clays. Data collection from the field experiment and monitoring the soil nail wall behavior is a critical component of this research study. The study will provide useful information of the soil nails behavior under real operational conditions. Information obtained from actual site will be used to calibrate the numerical modeling. The parameters to be monitored during long term monitoring are (GEC#7, 2003):

- Horizontal movements of the wall due to the construction ;
- Horizontal movement of the wall due to the creep of the soil mass;
- Service load of the nails at different depths;
- Load distribution in the nails;
- Load change in the nails as a function of time (due to the creep);
- Load at nail head;
- Change in temperature in the soil mass;
- Change in water content of the soil mass;

In order to perform the above investigations, the following instrumentations were installed at the site project.

- Inclinometers;
- Tiltmeters;
- Load cell at the nail head;
- Strain gauges;

5.3.1. Slope Inclinometers

Slope inclinometers provide significant quantitative data associated with the deflection or inclination along a borehole. This device is perhaps the more common one use to measure lateral movement of earthworks or structures. It also provides the pattern of deformation and the zone of potential failure. The inclinometer allows recording the deflection of the entire profile (in depth) at given times. This technique requires the installation of the inclinometer casing in a borehole behind the shotcrete facing.

On March 26, 2014 the first inclinometer casing was installed at station 2+00 (Figure 5-30). The casing was installed 4 ft. behind facing of the wall. To obtain a good soil movement profile, the inclinometer casing was installed 23 ft. below the embankment soil (to make sure that the soil deformation is zero at this depth). The length of the inclinometer casing is 46 ft.

Figure 5-30. First inclinometer casing at station 2+00

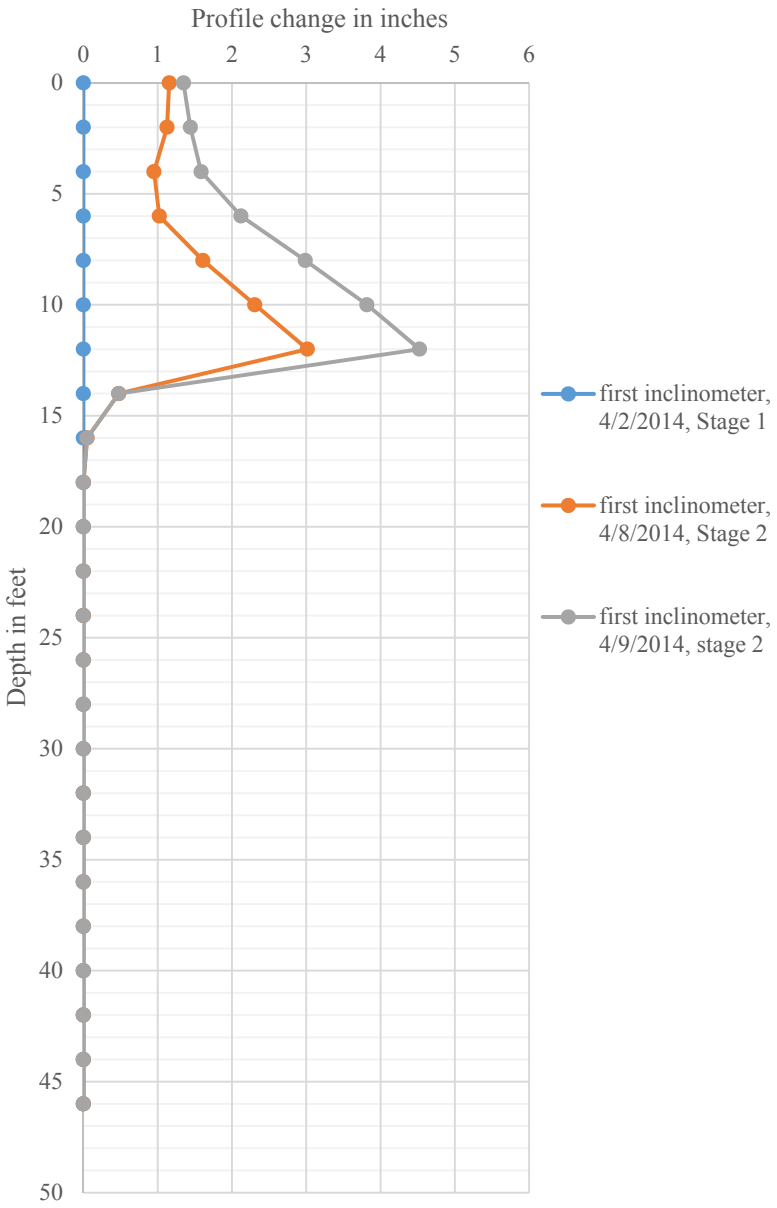

Figure 5-31. Soil profile for inclinometer casing

Figure 5-31 shows the soil profile obtained from inclinometers reading on April 2, April 8 and April 9 (i.e. the construction stage was at stage 2 and the height of the excavation was 7 ft.).

Due to the movement of the soil at the depth of 12 ft. from top of the ground, the inclinometer casing was bended at this depth and the inclinometer probe could not go further inside the casing.

On April 14, two more inclinometer casings were installed at stations 1+46 and 2+00. The length of these casings are 46 ft. (Figure 5-32 to Figure 5-35).

Figure 5-32. Installation of second inclinometer casing at station 2+00 on April 14.

Figure 5-33. Installation of second inclinometer casing at station 1+46 on April 14

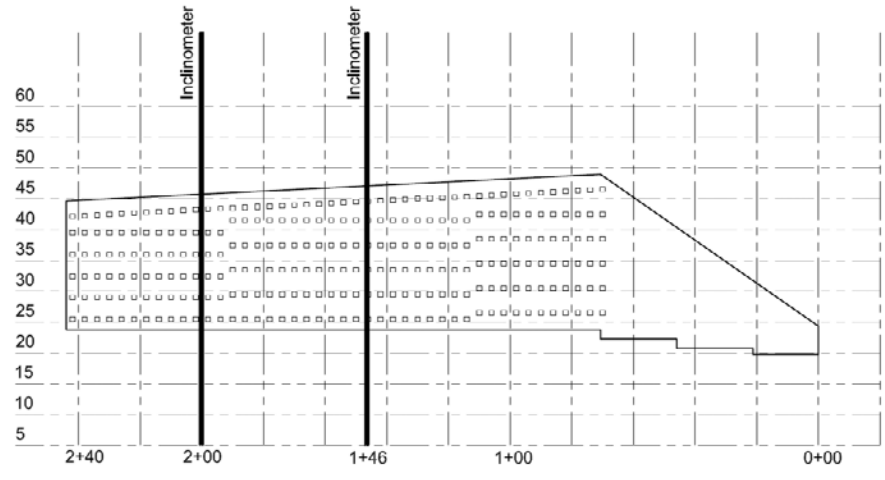

Figure 5-34. Location of the second set of inclinometers casing (at stations 2+00 and 1+46).

Figure 5-35. Inclinometer probe and casing

In each stage of construction, inclinometer readings for station 2+00 and 1+46 have taken. Figure 5-36 and Figure 5-37 present the lateral deformation of the wall during the construction at station 2+00 and 1+46, respectively.

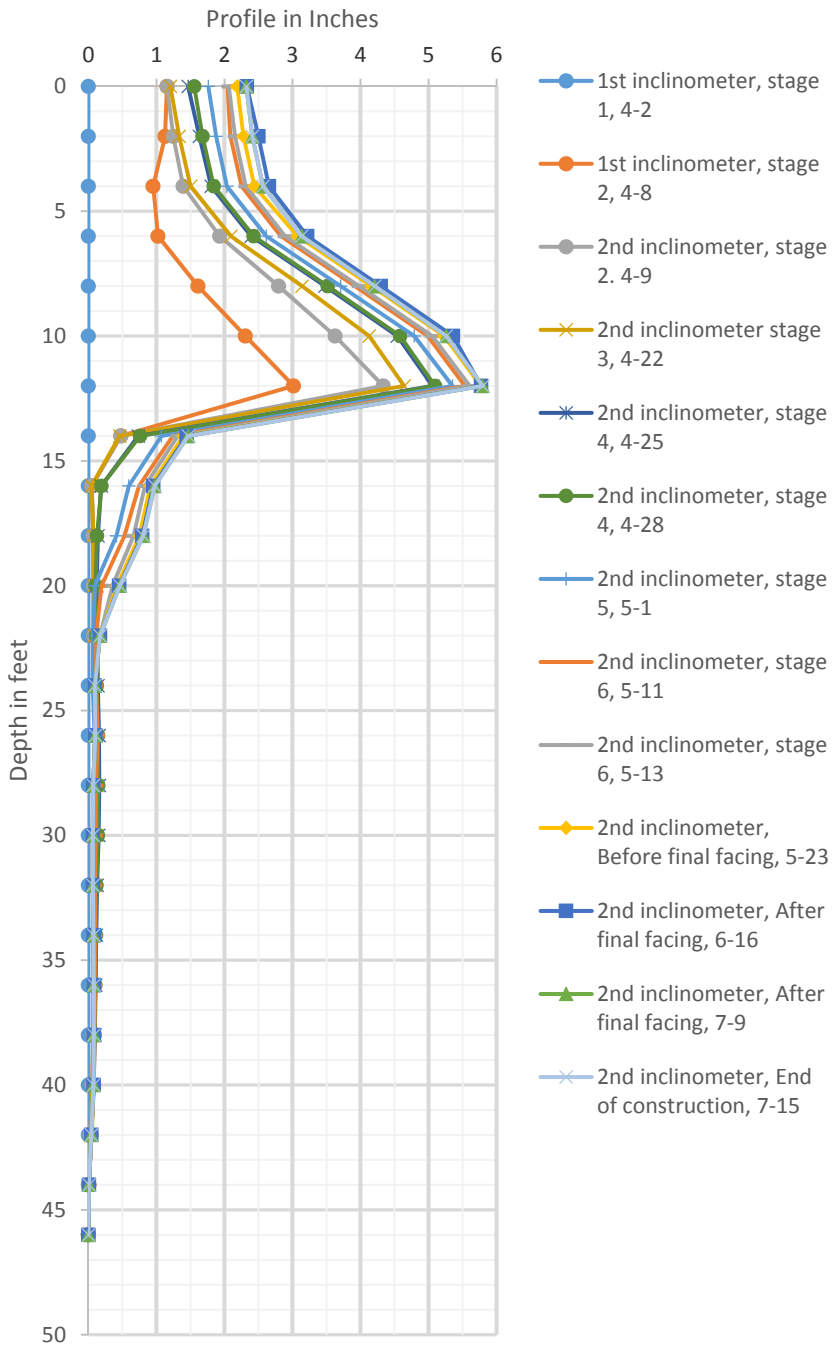

Figure 5-36. Lateral displacement of the soil profile 3 ft. behind the facing of the wall at station 2+00 during the construction (each line presents the lateral displacement in different stage of construction)

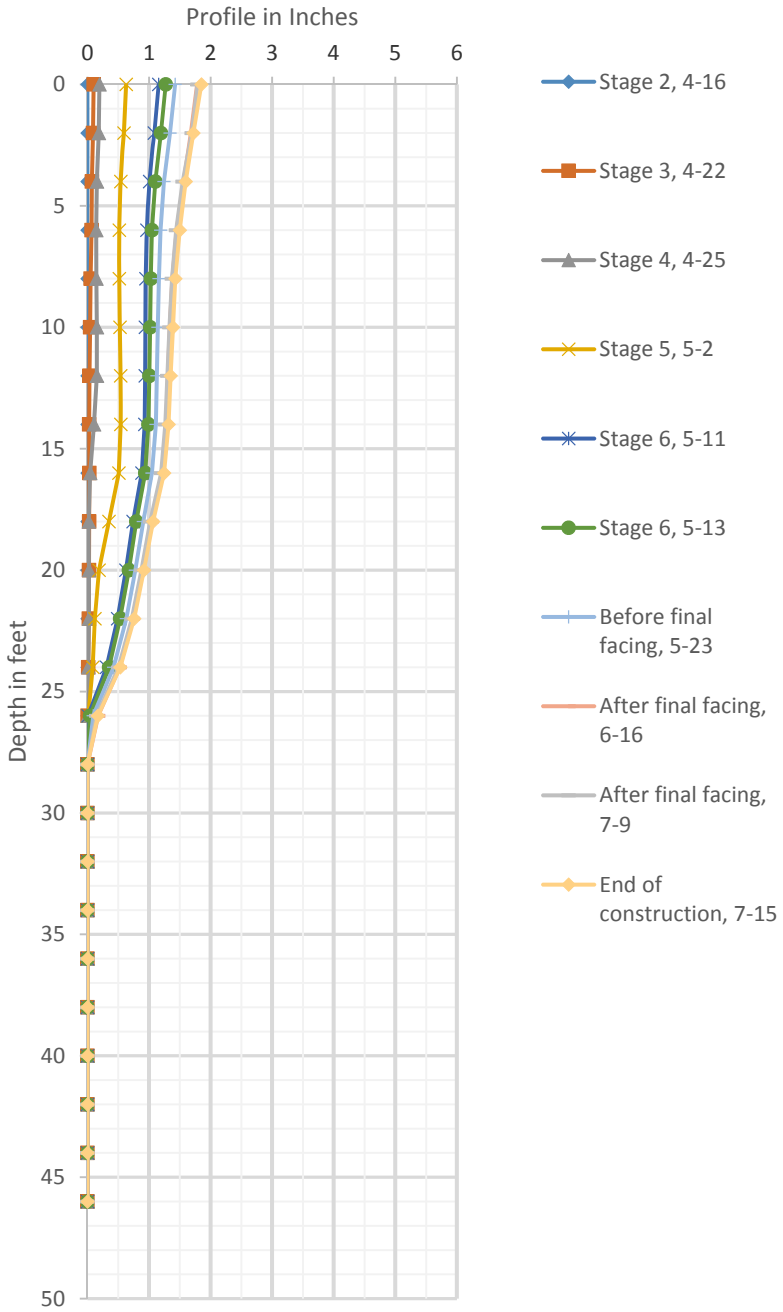

Figure 5-37. Lateral displacement of the soil profile 3 ft. behind the facing of the wall at station 1+46 during the construction (each line presents the lateral displacement in different stage of construction)

The soil profile at station 2+00 showed the excessive deformation at depth of 12 ft. in second stage of construction. Some modification to the original design such as reducing the height of the excavation in each stage, increasing the diameter of the holes (i.e. from 6 in. to 8 in.), and adding more pre-tension soil nails between the current soil nails in stage two was considered. Therefore, as it is illustrated in Figure 5-36, the excessive lateral deformation was reduced for the remaining stages. At station 1+46 the maximum lateral displacement took place at top of the wall and decrease towards the toe of the wall. Maximum horizontal displacement at top of the wall is 1.85 in. at sixth stage of construction which is 0.006 times of the height of the wall (i.e. 25 ft.).

In order to monitor the horizontal displacement of the wall after the construction, inclinometer readings were taken every month for period of 13 month after the construction. As it is shown in Figure 5-38 and Figure 5-39, the deformation of the wall at station 2+00 for the post-construction monitoring is less than 0.08 inch, while the deformation of the wall at station 1+46 is less than 0.2 in. which is 10% of the deformation observed soon after construction. Typically, the post construction deformation increases up to 15 percent of the deformations observed soon after construction (GEC#7, 2003).

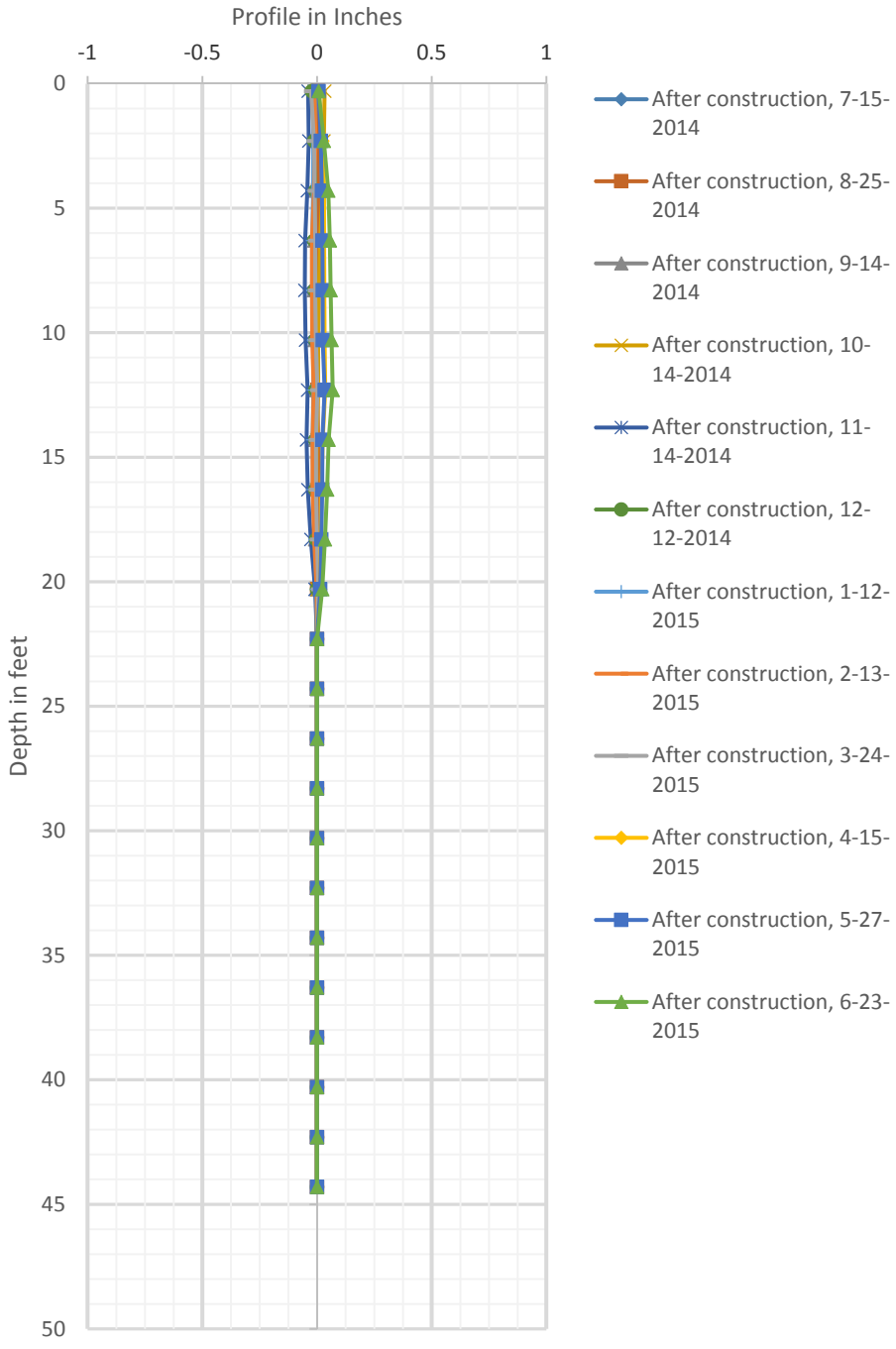

Figure 5-38. Lateral displacement of the soil profile 3 ft. behind the facing of the wall at station 2+00 after construction (each line presents the lateral displacement at different month of post-construction monitoring)

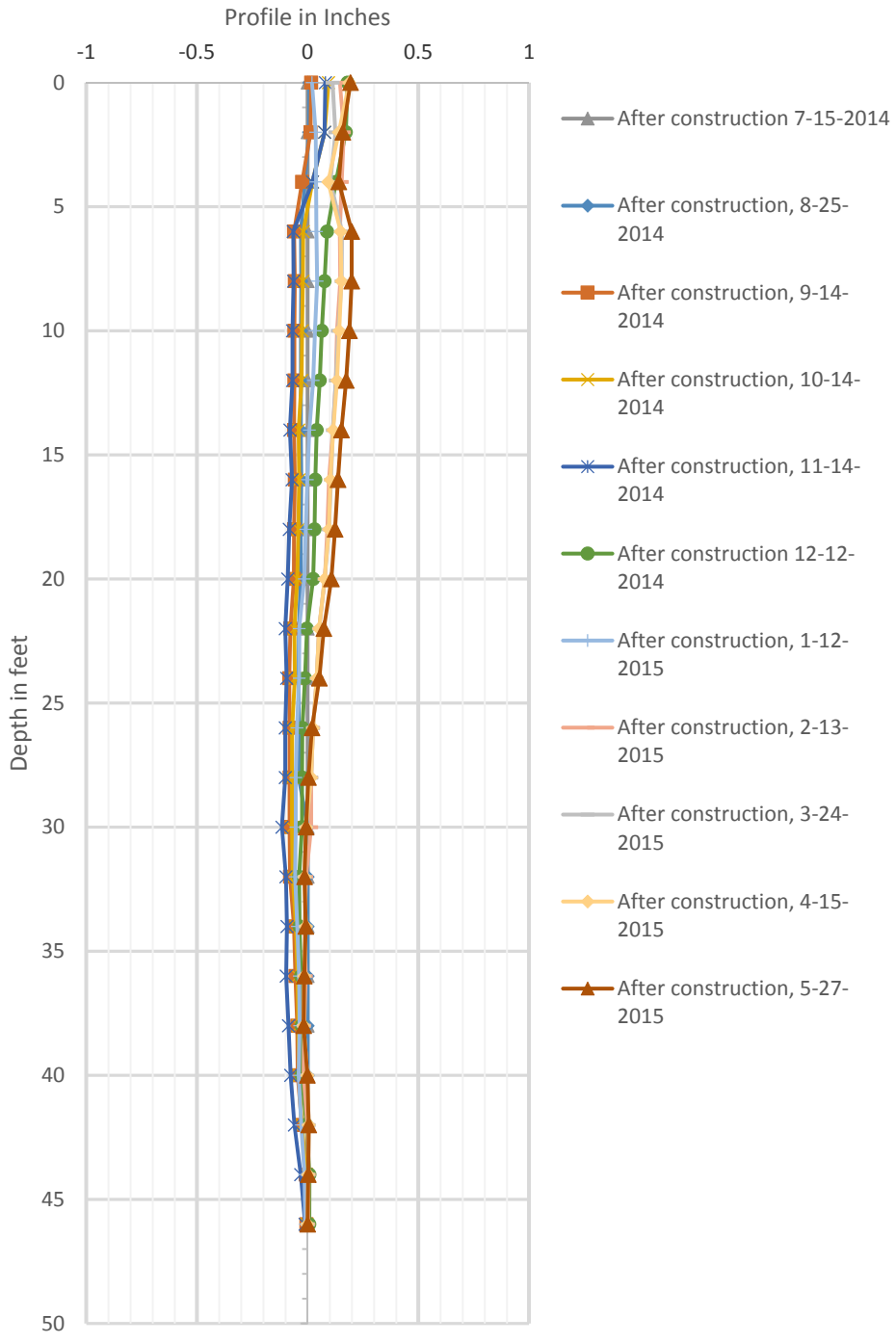

Figure 5-39. Lateral displacement of the soil profile 3 ft. behind the facing of the wall at station 1+46 after construction (each line presents the lateral displacement at different month of post-construction monitoring)

Figure 5-40 shows the maximum movement of the wall at station 2+00 in 12 ft. height versus time during the construction. 78 % (i.e. 4.4 in.) of the movement was occurred at the second stage of construction, and 22% (i.e. 1.2 in.) of the movement was occurred during third stage of construction toward the end of construction. In Figure 5-41, the lateral displacements of top of the wall at station 2+00 and 1+46 are illustrated.

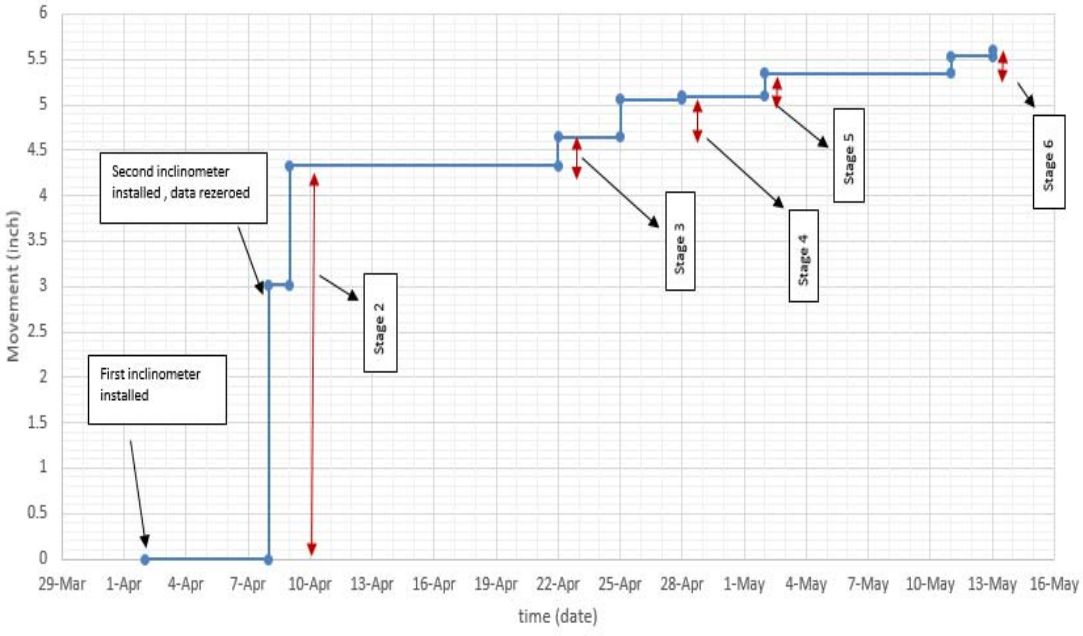

Figure 5-40. Movement of the wall at station 2+00 in 12 ft. height during the construction

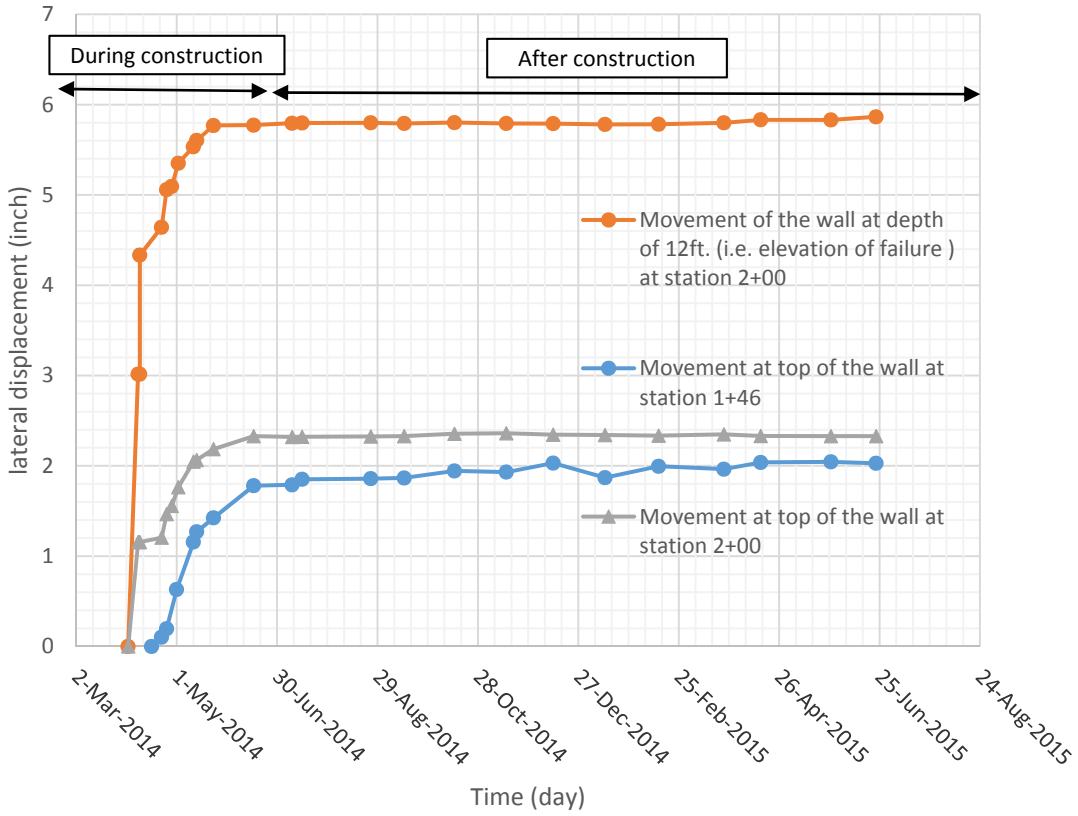

Figure 5-41. Movement of top of the wall at station 2+00 and 1+46 from starting the project to 13 moth post-construction monitoring.

5.3.2. Tiltmeters

The tiltmeter is an instrument that allows for the measurement of the inclination of an object. It responds to the local acceleration of gravity 'g'. Tiltmeter output is determined by the mass distribution of the earth. This instrument allows tracking the (continuous) variation of the inclination in time at fixed positions. To protect tiltmeters, they were put in aluminum boxes as shown in Figure 5-42.

Figure 5-42. Aluminum box used to protect tiltmeter

Figure 5-43. Three tiltmeters were installed at different depths of the wall

In total, three tiltmeters were installed to the facing of the wall at station 2+00 (Figure 5-43) at depth of 1, 5, and 13 ft. from top of the wall. These tiltmeters were connected to the data acquisition system to record the change of the inclination of the wall during and after the construction. During the final facing of the soil nail wall, third tiltmeter was broken (i.e. due to the pressure of shooting the shotcrete). Figure 5-44 and Figure 5-45 present the angel of inclination for the first (i.e. 1 ft. from top of the wall) and second (i.e. 5 ft. from top of the wall) tiltmeter, respectively. After the construction, first tiltmeter shows a lot of variation along the time and second inclinometer shows a big jump and then stay almost constant. Big jump can be due to shooting the final facing concrete. Unfortunately valuable information regarding the inclination of the wall versus time cannot be retrieved from the tiltmeters.

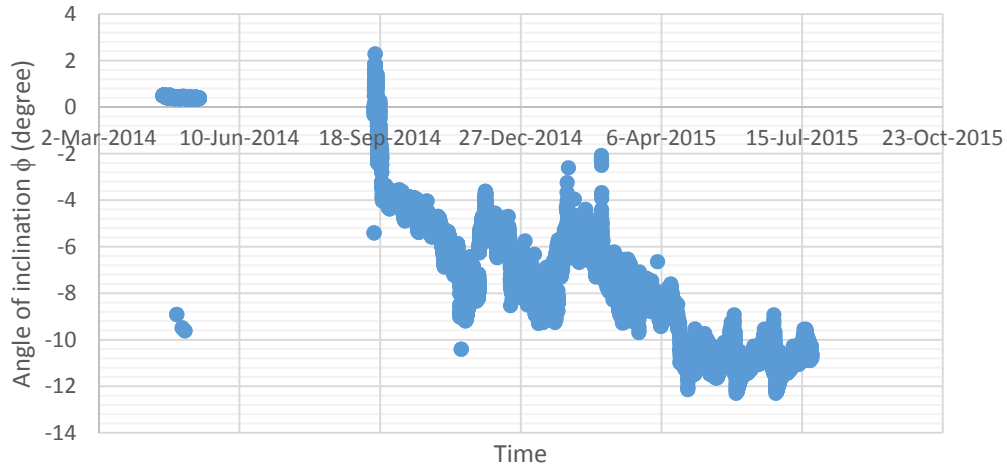

Figure 5-44. Inclination of the wall versus time for the first tiltmeter at 1 ft. from top of the wall. Tiltmeter was installed with initial inclination of 0.49007°

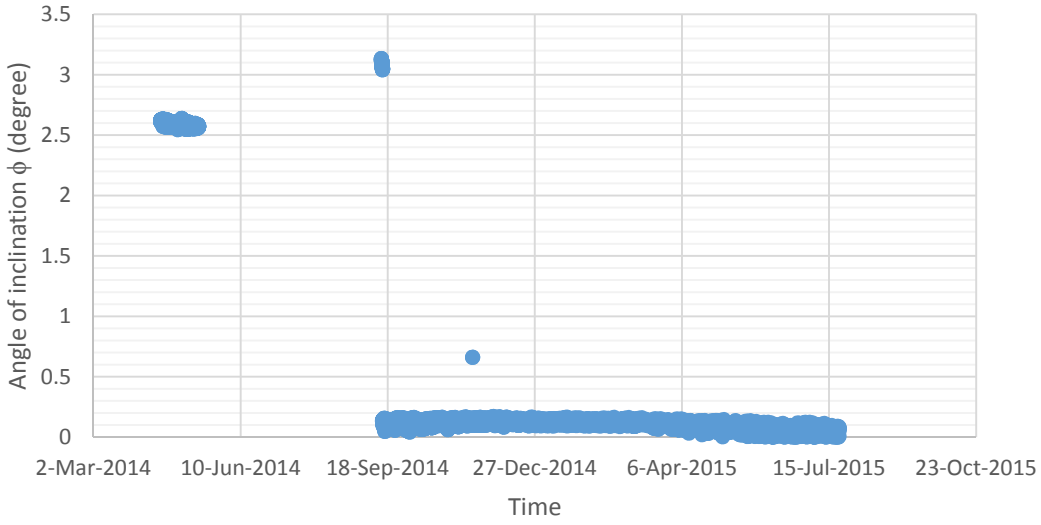

Figure 5-45. Inclination of the wall versus time for the second tiltmeter at 5 ft. from top of the wall. Tiltmeter was installed with initial inclination of 2.614968°

5.3.3. Strain Gauges

The instrumented soil nails with strain gauges are used to assess the load distribution along the nails during (i.e. as the excavation progresses) and after the construction. In addition, the strain gauges can provide useful information about the service load of the soil nails.

Six instrumented production nails were instrumented with Vibrating Wire (VW) strain gauges (i.e. model 4150 Geokon) while three production soil nails were instrumented with micro-measurements foil strain gauges (i.e. model EA-06-125VB-120).

In total, 9 instrumented production nails were installed at two sections of the wall (i.e. stations 1+98 and 2+06). Preparation process, installation and related instruments for VW and foil strain gauges are presented next.

5.3.4. Preparation of Instrumented Production Nails with Foil Strain Gauges

The procedure of instrumentation is the same as the procedure of instrumentation for the sacrificial nails mentioned in section 5.2.1.

First strain gauges were attached 2 ft. behind the wall facing. Second strain gauges were attached with 5 ft. distance from the first one. Third and fourth strain gauges were attached with 6 ft. intervals from the second strain gauges. Figure 5-46 illustrates the distribution of the strain gauges along the nail bars.

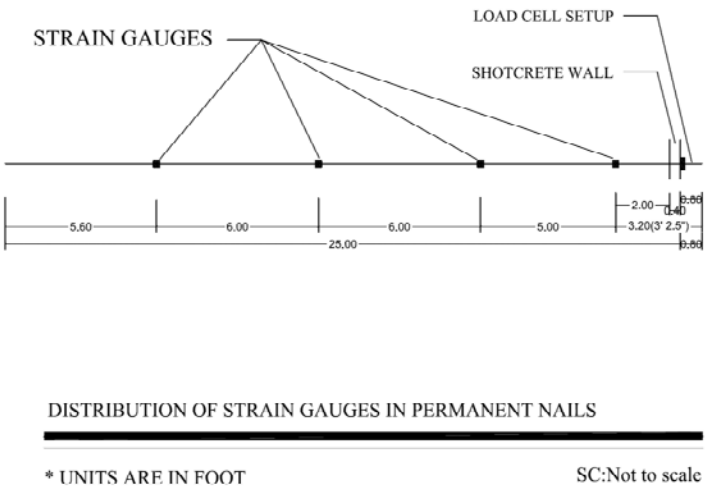

Figure 5-46. Distribution of the foil strain gauges along the production nails

5.3.5. Data Acquisition System

The data acquisition system is used to read and storage the data from the instruments. In order to collect the data from the strain gauges during the construction, data acquisition system was set-up at the temporary location at top of the wall (Figure 5-47) prior to construction. After finishing the construction, the data acquisition system box was moved to bottom of the wall on the ground surface. Solar panel was used to provide the power for data acquisition system (Figure 5-48).

Figure 5-47. Temporary location of the data acquisition system and solar panel

Figure 5-48. Solar panel for providing the power for data acquisition system

5.3.6. Installation of Instrumented Nails with Foil Strain Gauges

The instrumented nails were installed at second (6 ft. from top of the wall), fourth (13 ft. from top of the wall) and fifth (16.5 ft. from top of the wall) row of the soil nails at

station 2+06. Figure 5-49 and Figure 5-50 show the position of these instrumented nails on the wall profile. The height of the wall at this station is 22 ft.

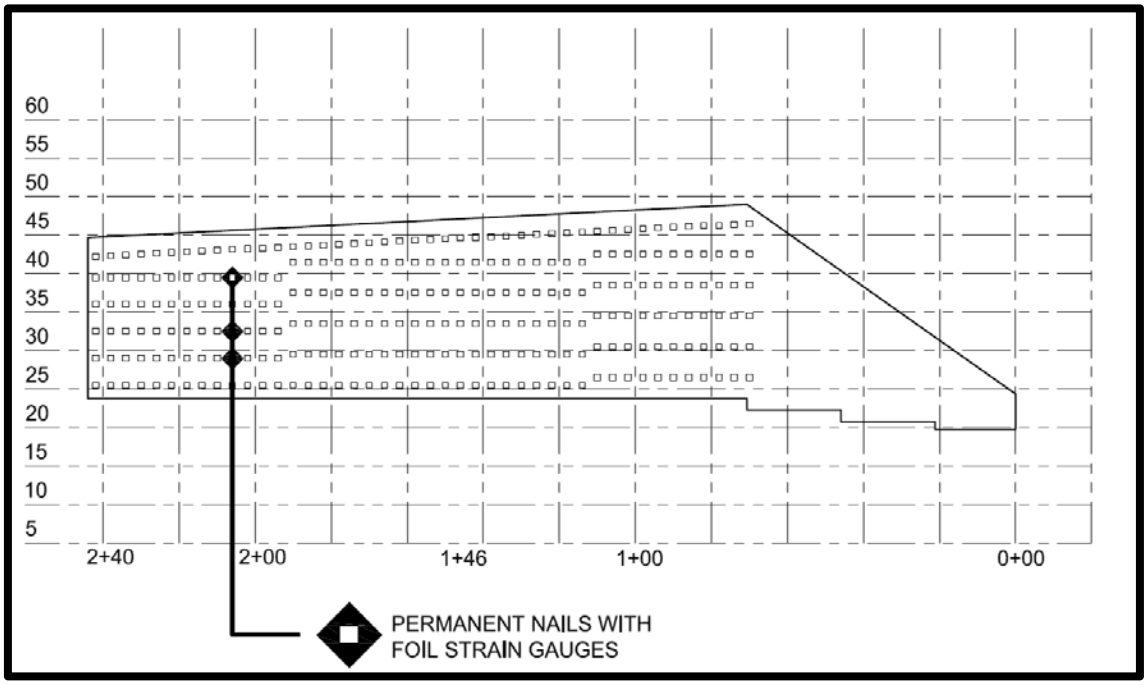

Figure 5-49. Positions of the instrumented production nails with foil strain gauges at station 2+06

Figure 5-50. Instrumented production nails with foil strain gauges at station 2+06

Reading the strain gauges during the construction is the significant part of this research. Following parameters can be obtained by reading the strain gauges during the construction:

- Zero reading of the strain gauges (i.e. forthwith after installation while the grout is still liquid);

- Service load of the nails at different stages of construction;
- Load change in the nails due to the excavation at each stage of construction;
- Load change in the nails due to the creep at each stage of construction;
- Magnitude and location of the maximum load;

In order to take the reading during the construction, the wires of the strain gauges need to be connected to the data acquisition system during the construction. The only way is to conduct the wires to the temporary location by passing them from behind the shotcrete facing. After the nails were installed and prior to shooting the shotcrete, PVC tubes were placed in front of the excavated facing. The wires of the strain gauges were passed through the PVC pipe. Since there were three instrumented nails, at the first stage of excavation, four PVC pipes were placed. The fourth PVC pipe was placed to bring all the wires from the temporary location of the data acquisition system (i.e. at top of the wall) to the permanent location (i.e. at bottom of the wall on the ground surface). Figure 5-51 to Figure 5-53 show the PVC pipes to conduct the wires to the data acquisition system.

Figure 5-51. Placing the PVC pipes to conduct the wires to the data acquisition system at the first stage of construction

Figure 5-52. Extending the PVC pipes to conduct the wires to the data acquisition system at the second stage of construction

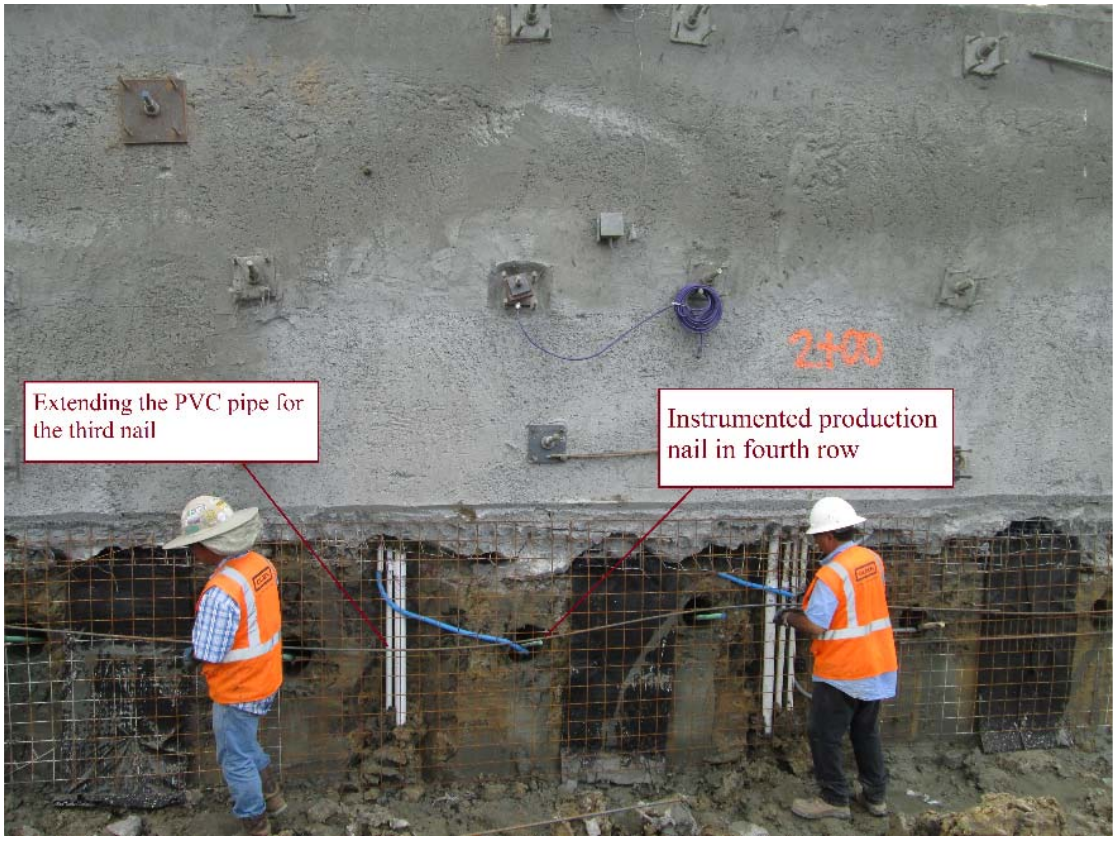

Figure 5-53. Extending the PVC pipes to conduct the wires to the data acquisition system at the fourth stage of construction

5.3.7. Monitoring the Instrumented Nails with Foil Strain Gauges

Readings of the strain gauges during and after the construction have been recorded continuously every 30 minutes. Figure 5-54 to Figure 5-56 illustrate the service load in the nails during the construction. Foil strain gauges would normally expected to last over a period of long time, but the foil strain gauges at three production nails did not last long.

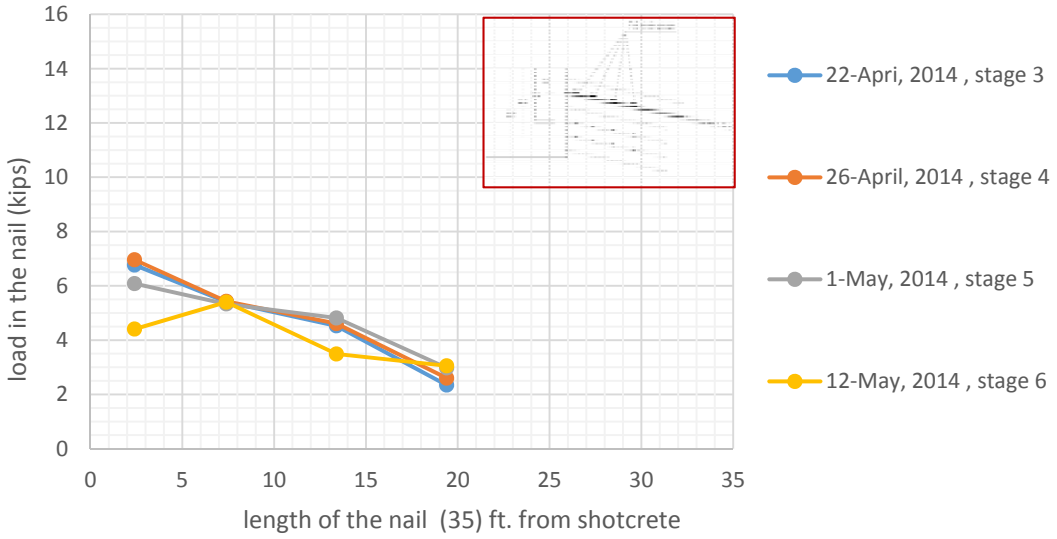

Figure 5-54. Load distribution along the instrumented production nail in second row of the soil nails

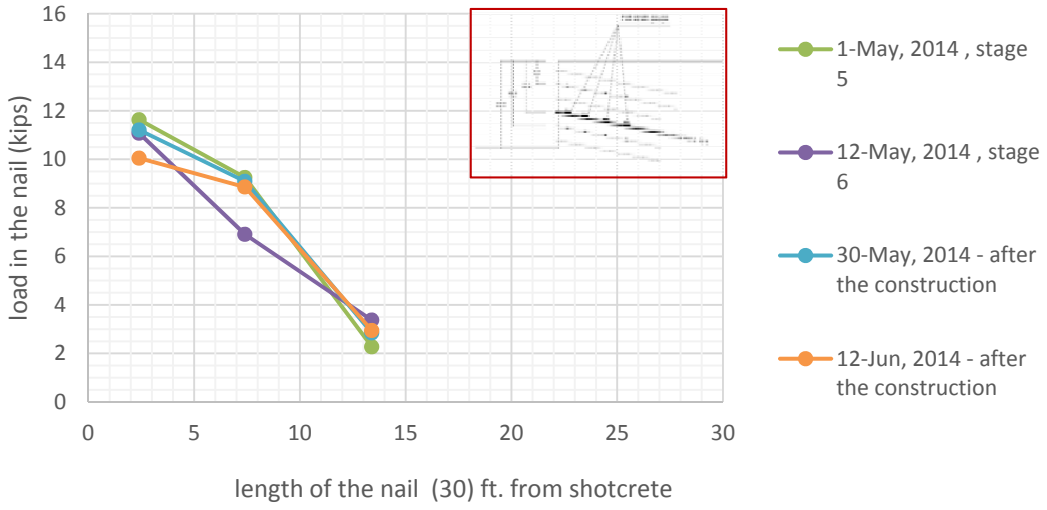

Figure 5-55. Load distribution along the instrumented production nail in fourth row of the soil nails

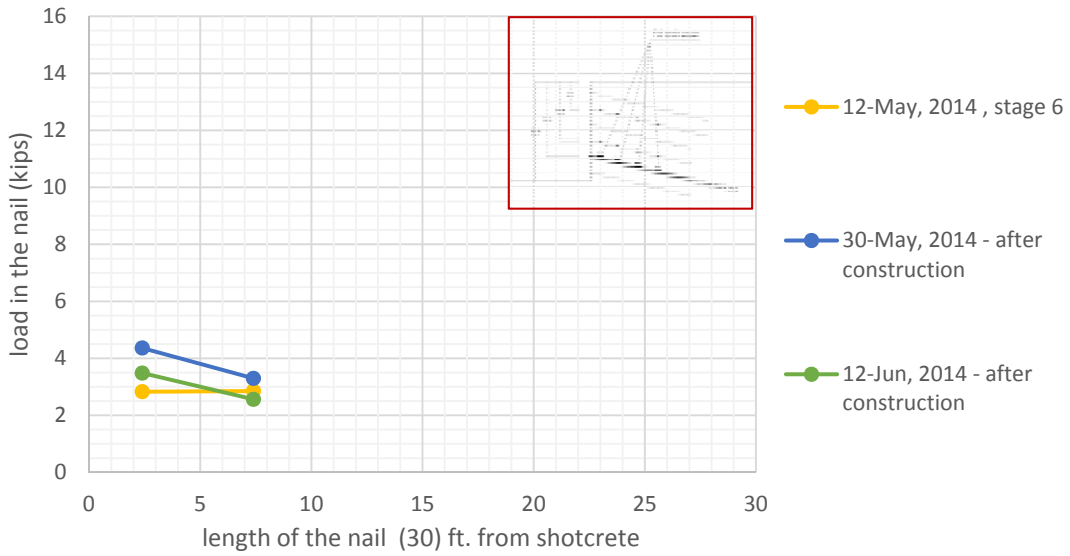

Figure 5-56. Load distribution along the instrumented production nail in fifth row of the soil nails

As it is shown in Figure 5-54, first instrumented production nail was installed at second stage of construction. Third and fourth strain gauges in instrumented nail at fifth row were broken during the installation of the nail. It is clear in Figure 5-54 to Figure 5-56 that significant portion of the service load took place at the next excavation after the installation of the nails.

These instrumented production nails were installed at the same height of the sacrificial nails. Table 5-4 presents the result of the pullout tests on the sacrificial nails along with the service load on the nails. It is concluded that the service load in the nails is maximum 60% of the design load and maximum 22% of the maximum pullout capacity of the nails.

Table 5-4. Comparison of the service load, design load and the maximum pullout capacity

Nail No.	Length of the nail (ft.)	Maximum Pullout capacity from load test (kips)	Design load (kips)	Maximum service load in the nail (kips)
Nails in second row	35	63	21	7
Nails in fourth row	30	56	18	12
Nails in fifth row	30	72	18	5

The service load obtained from the strain gauges data are used in numerical modeling to validate the numerical modeling.

5.3.8. Preparation of Instrumented Production Nails with VW Strain Gauges

Figure 5-57 shows the distribution of the VW strain gauges along the nail bars. The first and second strain gauges were welded at 2.5 ft. and 15 ft. from top of the nail bar, respectively.

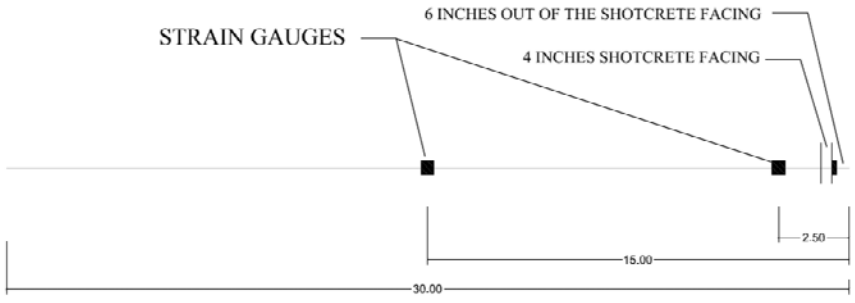

Figure 5-57. Distribution of the VW strain gauges along the nail bar

Related instruments for six additional production nails are listed below:

- Vibrating wire strain gauge with plucking coil and cover plate (model 4150 Geokon);
- MICRO-800 Data logger with integral multiplexer (16 VW + 16 Thermistors);
- LoggerNet software and starter data logger program;
- Solar panel 20W;
- Rental spot welder;
- Rental VW readout (i.e. GK-404);

Procedure of attaching the strain gauges are listed as follows:

- The ribs of the nail bar at the designated locations were ground down with an electric grinder (Figure 5-58);
- Welding the gauges to the nail bars with spot welder (Figure 5-59);
- Testing the gauges before installing the aluminum cover (Figure 5-60);
- Installing the aluminum cover (Figure 5-61);

Figure 5-58. grinding the nail bars at the designated position with electric grinder

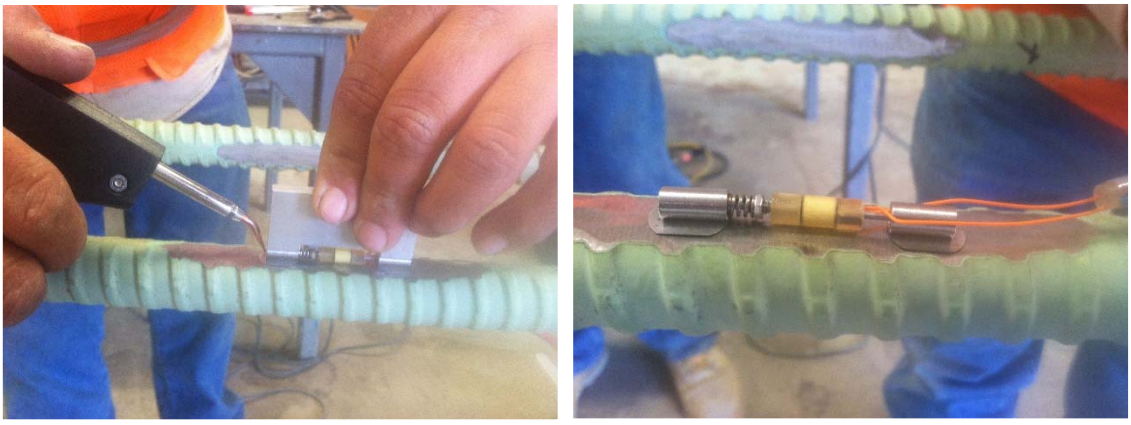

Figure 5-59. Welding the gauges to the nail bars with spot welder

Figure 5-60. Testing the gauges before installing the aluminum cover

Figure 5-61. Installing the aluminum cover

Prior to shipping the instrumented nails to the site, and to make sure none of the strain gauges fail due to the transportation or installation at the site, plastic tube was placed around the bar and the gap between tube and bar was filled with grout. Cross section and final view of the instrumented nails are shown in Figure 5-62 and Figure 5-63, respectively.

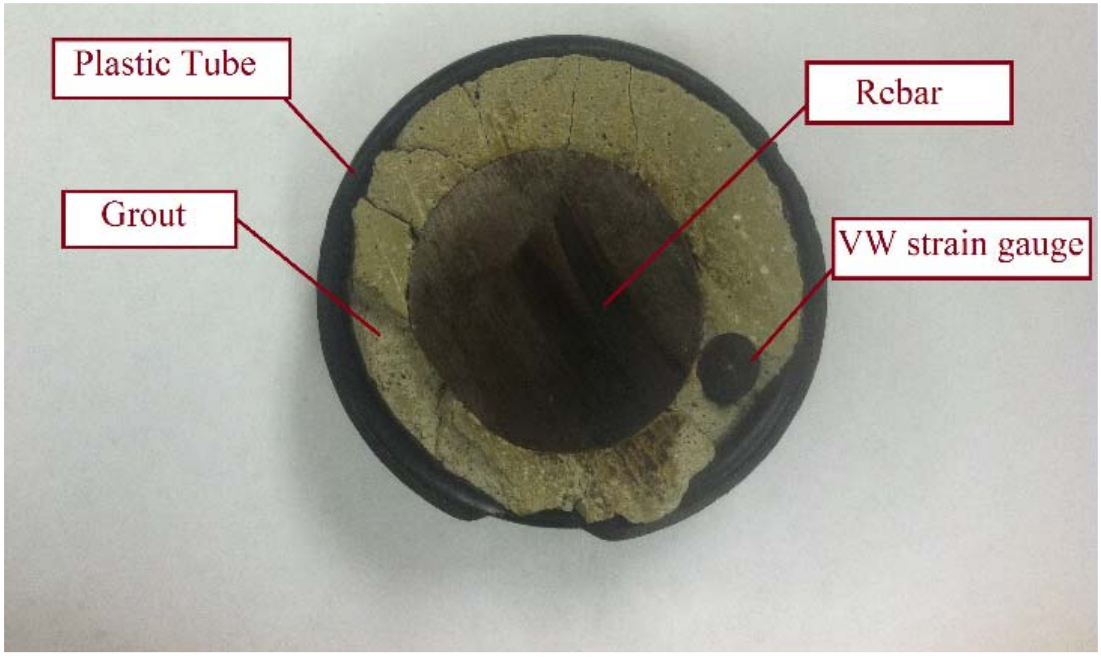

Figure 5-62. Cross section of the instrumented nail

Figure 5-63. Final view of the instrumented nails

5.3.9. Data Logger

MICRO-800 Data logger was used to read the data form the instrumented nails with VW strain gauges. After construction of the wall, data logger was moved to the permanent location at bottom of the wall at station 2+00. Figure 5-64 shows the temporary location of the data logger. To provide the power for data logger, 20W Solar panel was installed next to the data logger (Figure 5-65).

Figure 5-64. Data logger box at temporary location at top of the wall at station 2+00

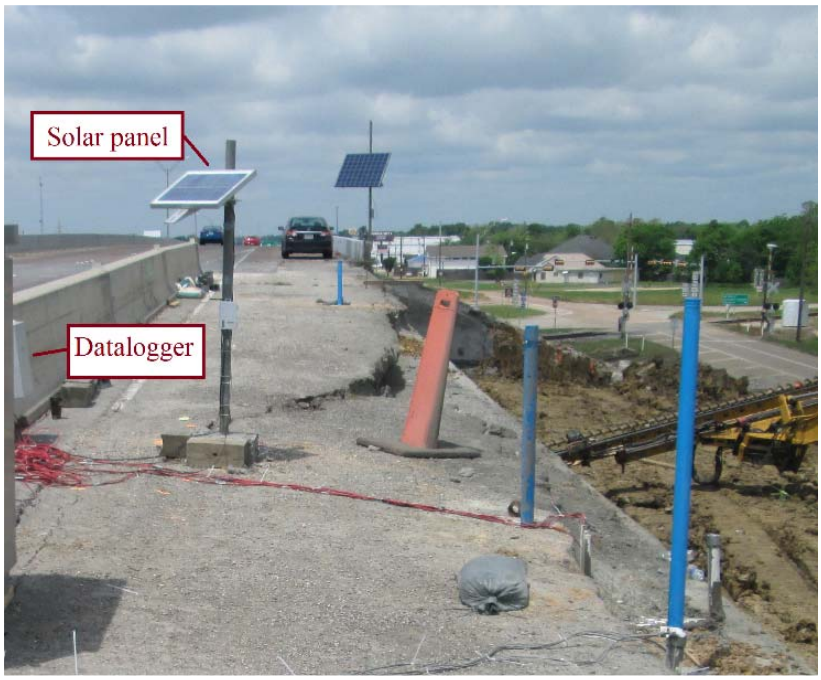

Figure 5-65. Solar panel installed next to the data logger at the temporary location at station 2+00

5.3.10. Installation of Instrumented Nails with VW Strain Gauges

Instrumented nails with VW strain gauges were installed at all the rows (i.e. row 1, 2, 3, 4, 5 and 6) at station 1+98. Figure 5-66 and Figure 5-67 show the locations of these nails on the wall profile. The height of the wall at this station is 22 ft.

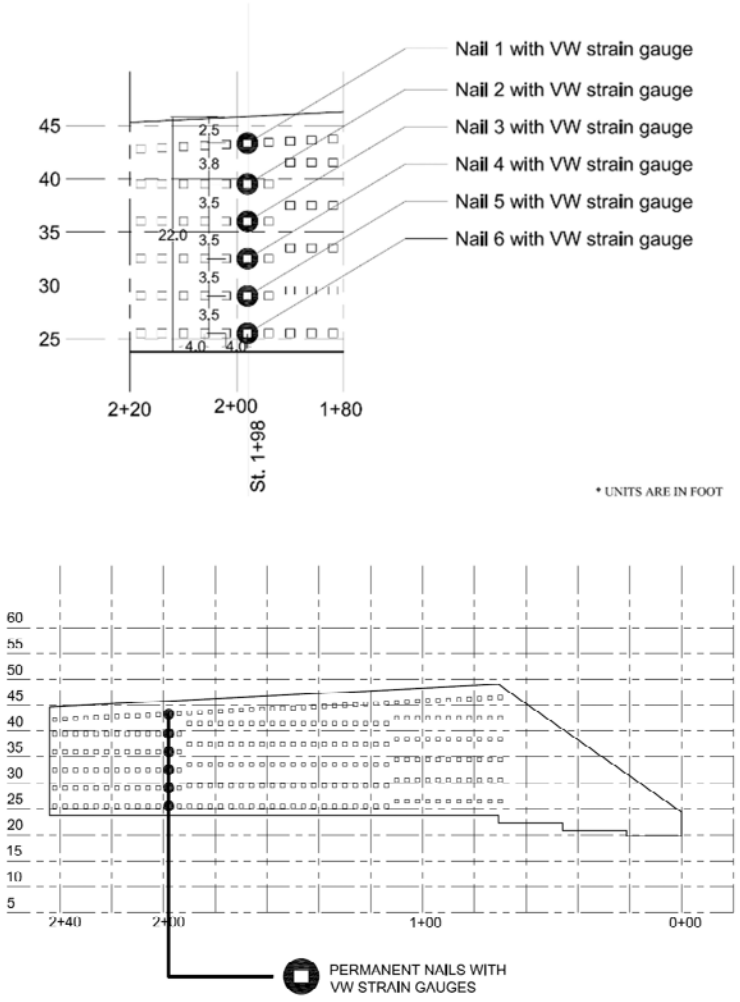

Figure 5-66. Location of the instrumented nails with VW strain gauges on wall profile at station 1+98

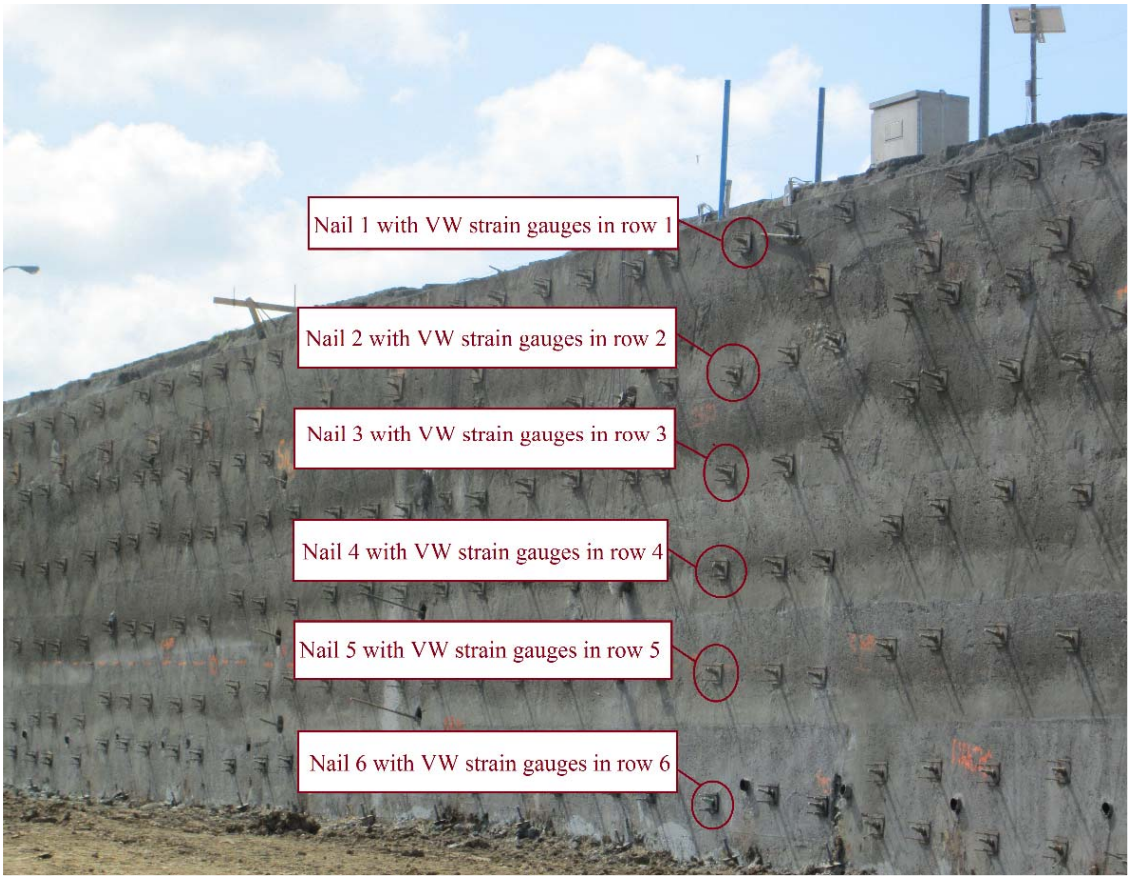

Figure 5-67. Location of the instrumented nails with VW strain gauges on wall profile at station 1+98

During the construction wires of each instrumented nail were connected to data logger. Wires were passed through the PVC pipes behind the shotcrete facing in the same way as performed for the instrumented nails with foil strain gauges. Since there are six instrumented nails with VW strain gauges, seven PVC pipes were placed in front of the excavation facing at the first stage of the construction (Figure 5-68 and Figure 5-69). Six PVC pipes were used to conduct the wires of six instrumented nails to the temporary

location of the Data logger, while the seventh PVC pipe was used to conduct all the wires (i.e. wires of six instrumented nails) from the temporary location of the data logger (i.e. top of the wall at station 2+00) to the permanent location of the data logger (i.e. bottom of the wall at station 2+00).

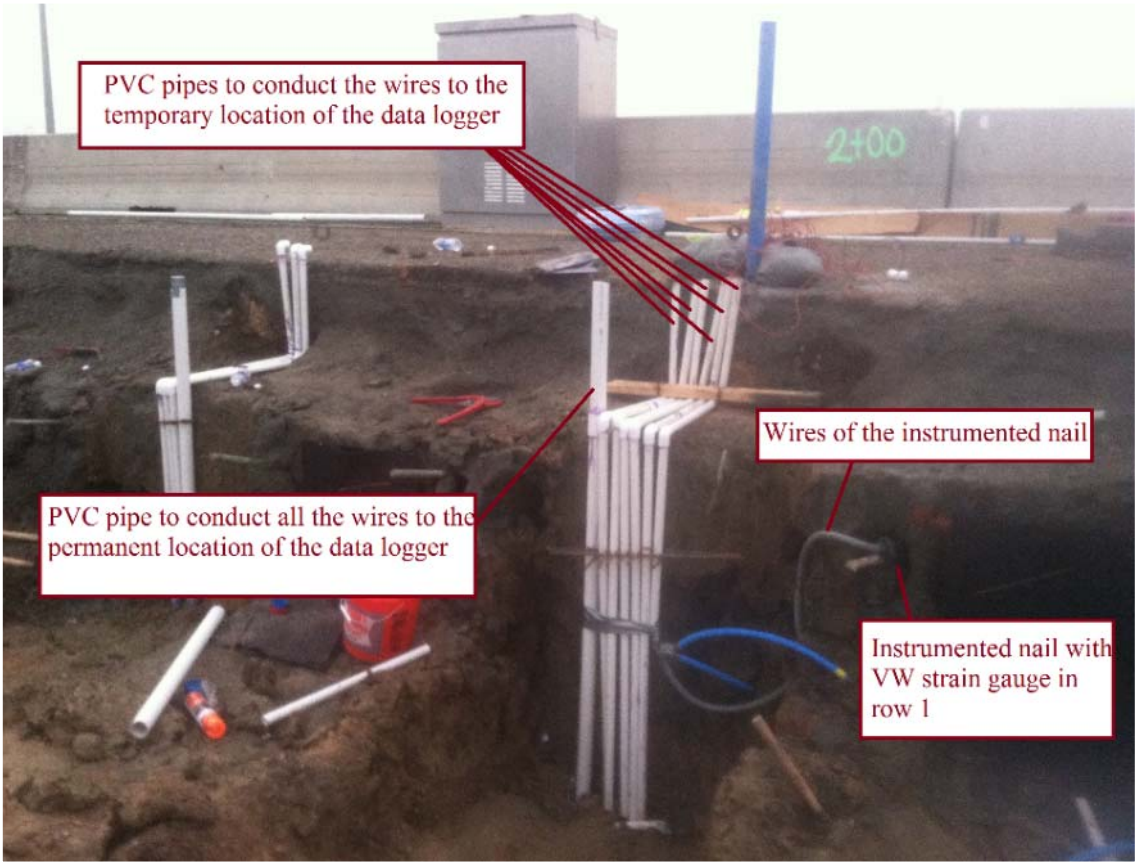

Figure 5-68. PVC pipes to conduct the wires to the data logger at first stage of construction at station 2+00

Figure 5-69. PVC pipes to conduct the wires to the data logger at fourth stage of construction at station 2+00

5.3.11. Monitoring the Instrumented Nails with VW Strain Gauges

Reading intervals for VW strain gauges are the same as foil strain gauges. During the construction, readings were recorded every 30 minutes. In order to have the zero readings, the readings were taken immediately after the installation of the nails. Load distribution along the nails in each stage of construction are shown in figures 67 to 72.

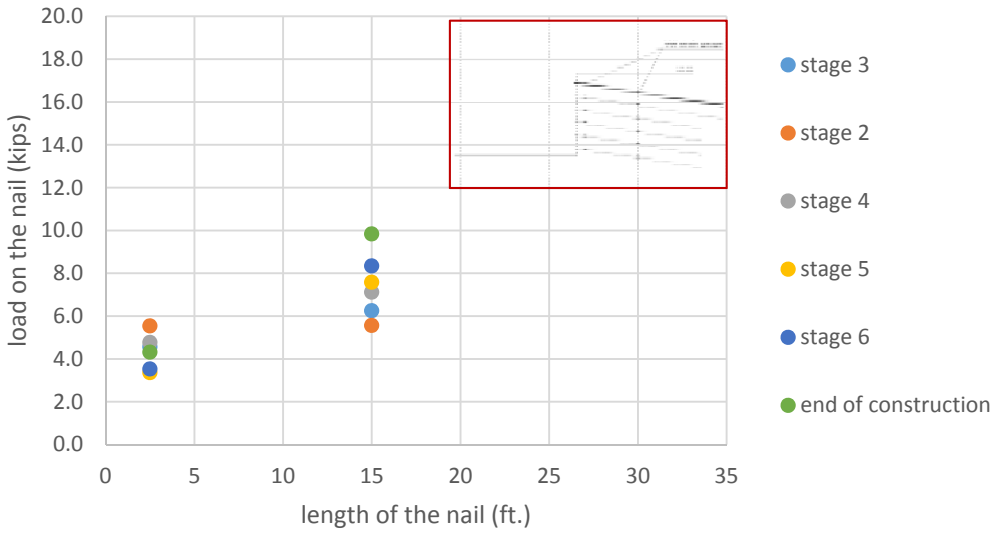

Figure 5-70. Load distribution along the instrumented nail at first row of soil nails from top.

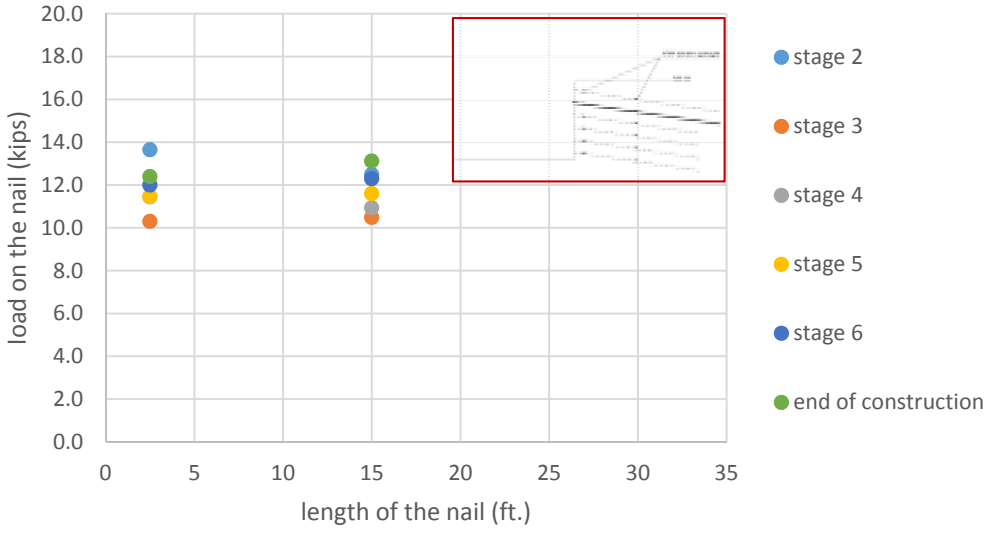

Figure 5-71. Load distribution along the instrumented nail at second row of soil nails from top.

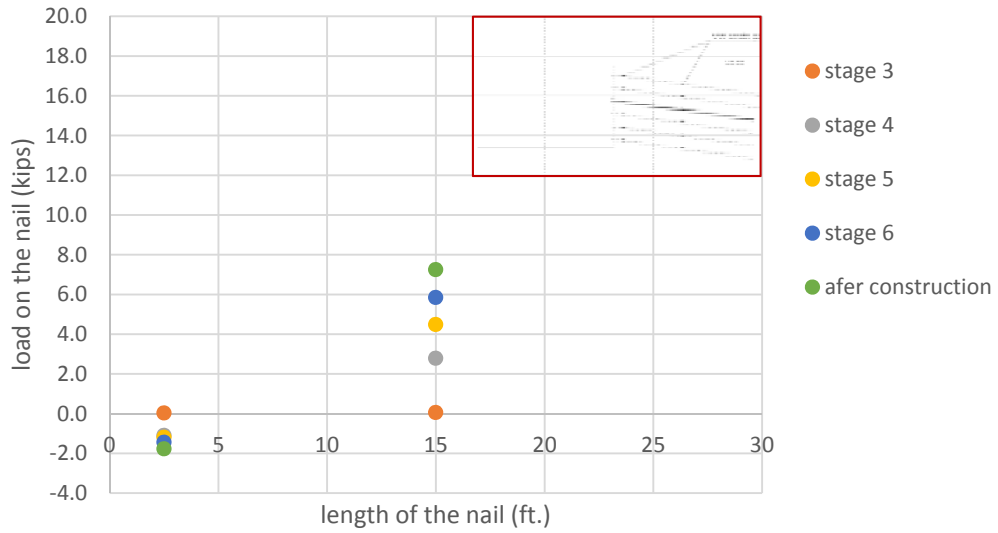

Figure 5-72. Load distribution along the instrumented nail at third row of soil nails from top.

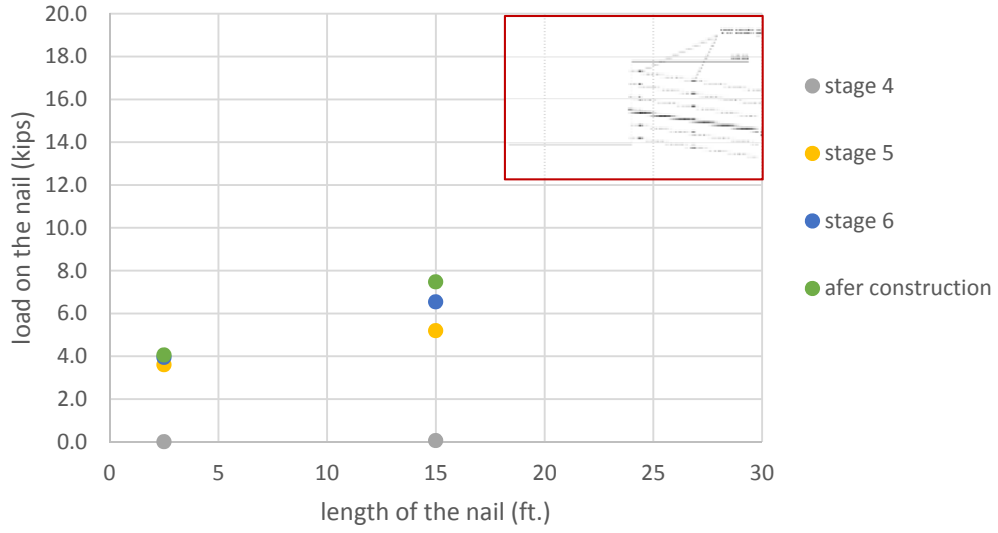

Figure 5-73. Load distribution along the instrumented nail at fourth row of soil nails from top.

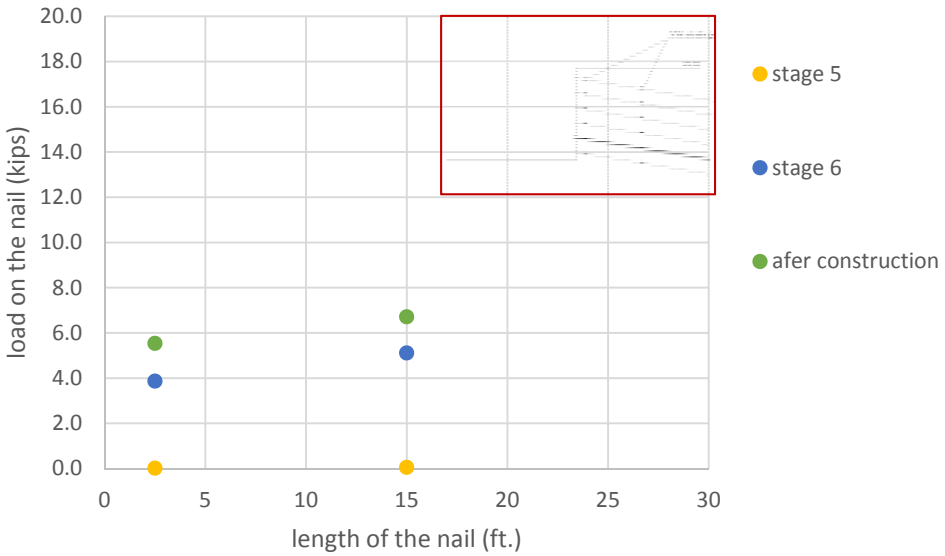

Figure 5-74. Load distribution along the instrumented nail at fifth row of soil nails from top.

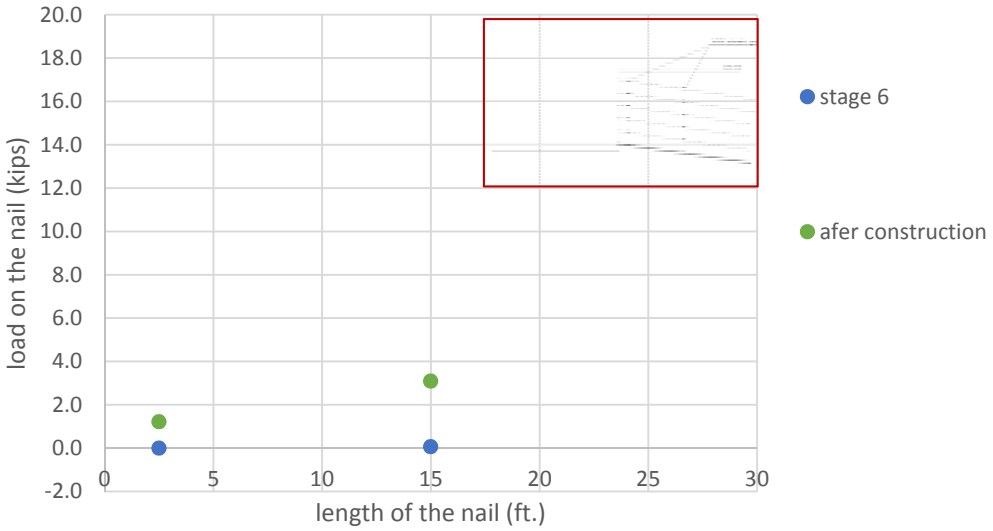

Figure 5-75. Load distribution along the instrumented nail at sixth row of soil nails from top.

During the construction only the first strain gauges (i.e. at 2.5 ft. from head of the nail) in third row was broken. In each nail, significant portion of the service load took place in the subsequent excavation. Since after the second stage of construction, one row of pre-tension nails were installed in the middle of the first and second row, load in the first strain gauges (i.e. at 2.5 ft. from head of the nail) in the first and second production nail was decreased in each stage. For instance, in the first position of the nail 1 (i.e. first row of the soil nails), at stage 2 the load was 5.5 kips, while after the installation of the pre-tension nails the service load was drop to 4.6 kips.

As same as the readings during the construction, for post construction monitoring readings were taken every 30 minutes. After the construction, only second strain gauges in sixth nail was broken. Figure 5-76 to Figure 5-81 illustrate the one year post construction monitoring the service load along the nails.

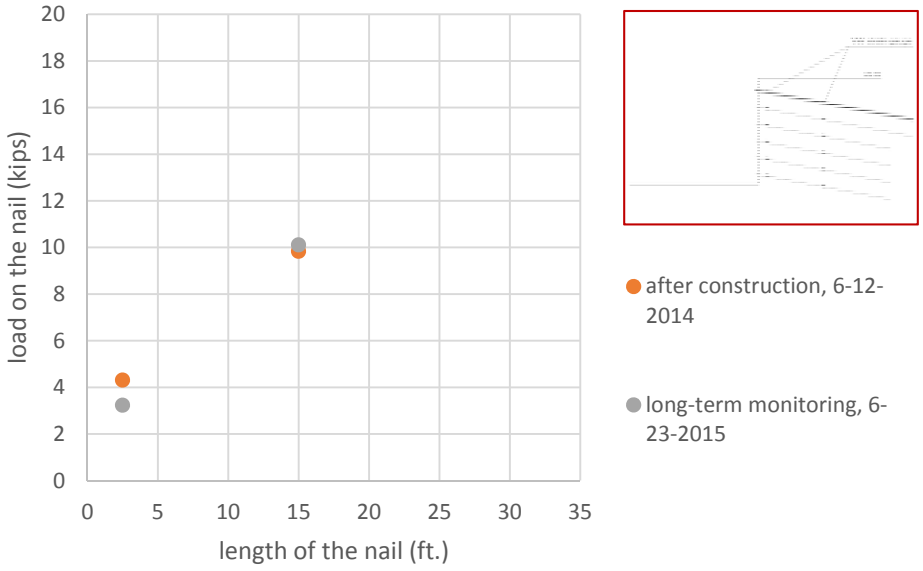

Figure 5-76. One year post construction long term monitoring, load distribution along the instrumented nail at first row of soil nails from top.

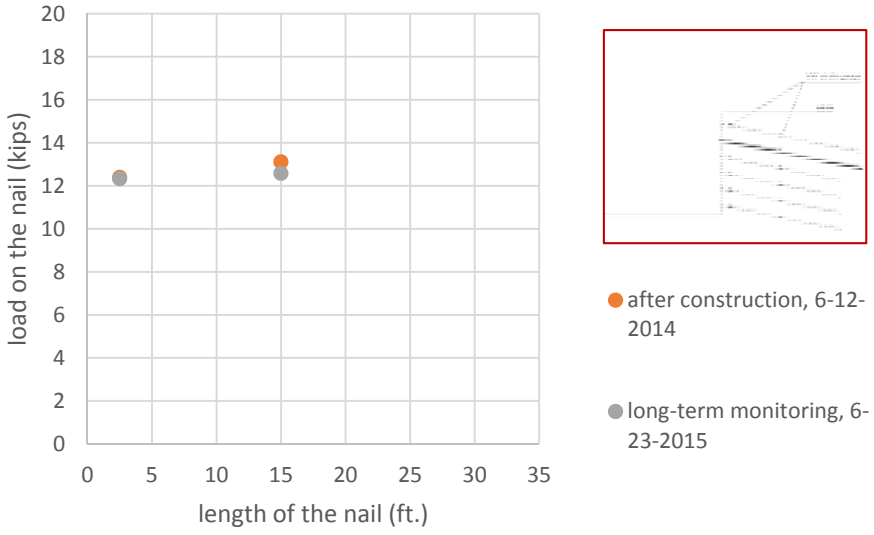

Figure 5-77. One year post construction long term monitoring, load distribution along the instrumented nail at second row of soil nails from top.

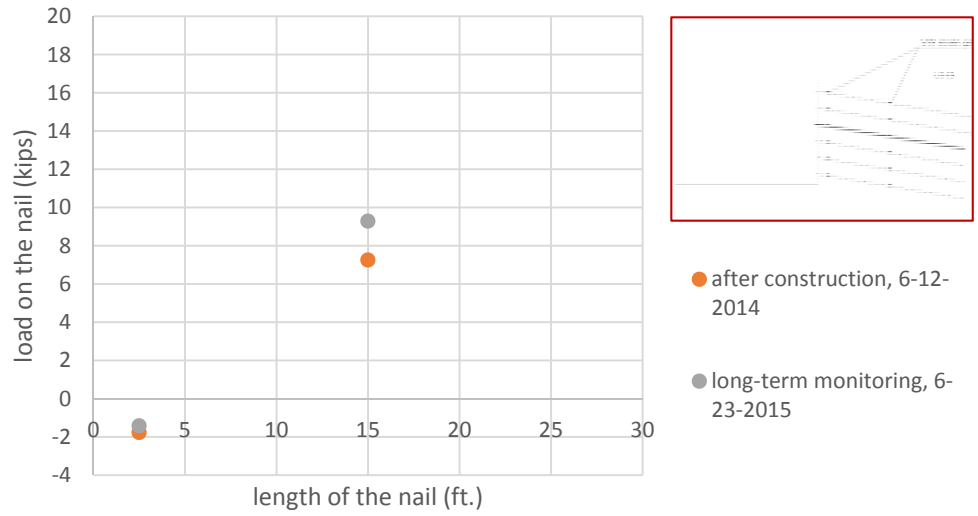

Figure 5-78. One year post construction long term monitoring, load distribution along the instrumented nail at third row of soil nails from top.

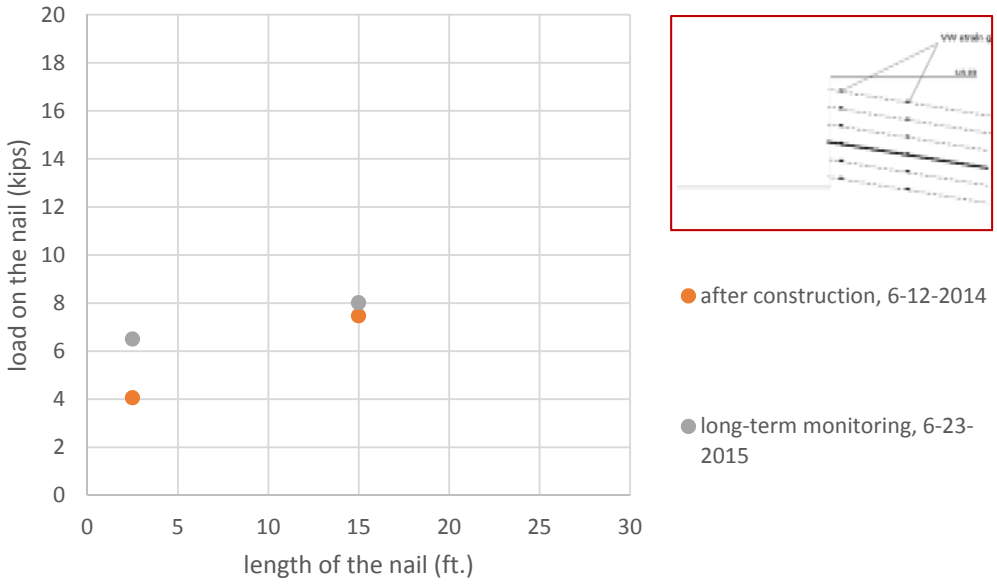

Figure 5-79. One year post construction long term monitoring, load distribution along the instrumented nail at fourth row of soil nails from top.

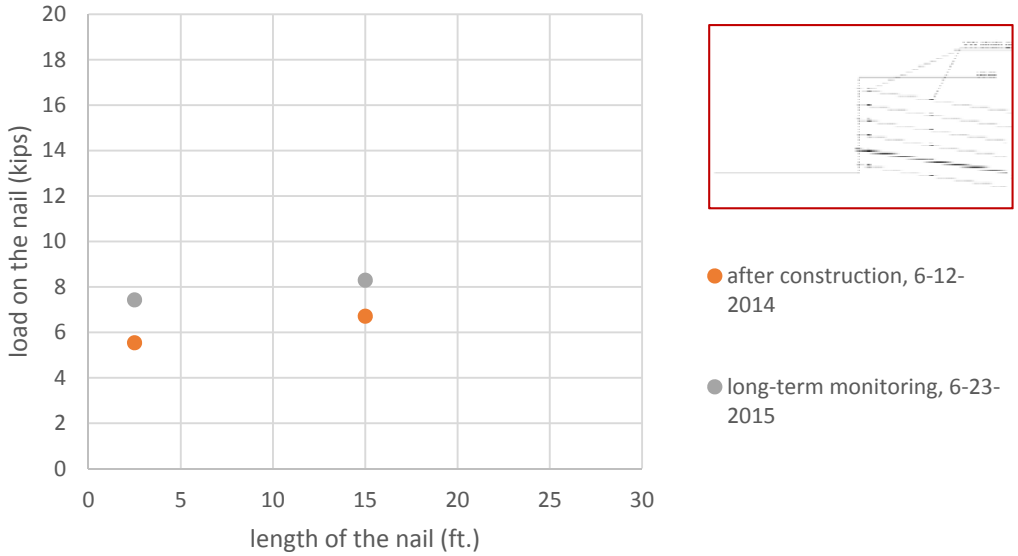

Figure 5-80. One year post construction long term monitoring, load distribution along the instrumented nail at fifth row of soil nails from top.

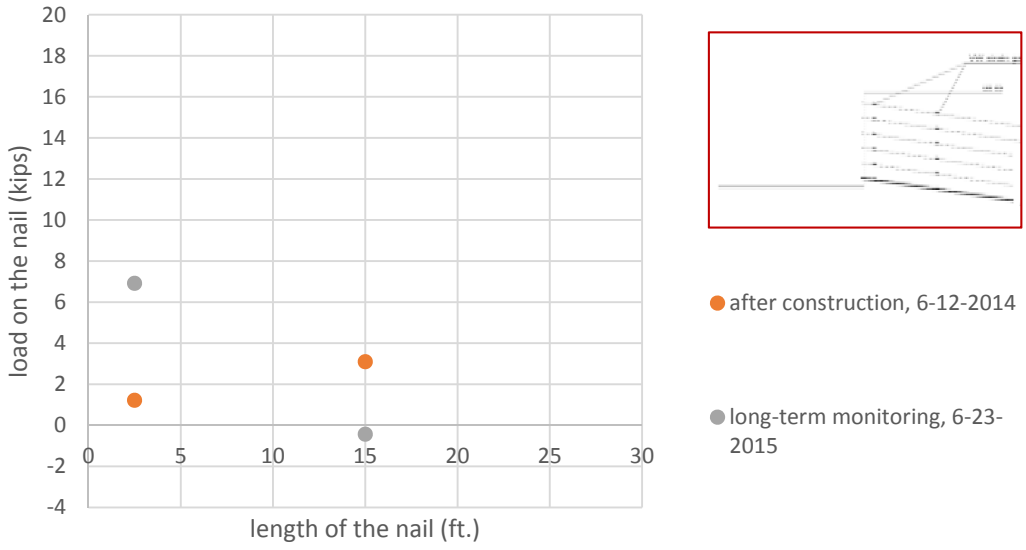

Figure 5-81. One year post construction long term monitoring, load distribution along the instrumented nail at sixth row of soil nails from top.

The soil nail wall showed the extra lateral displacement after the construction (i.e. due to the creep). As a results of this movement, additional tension is developed in the nails (GEC#7, 2003). Since after the second stage of construction pretensions nails were installed and the service load in the first two row dropped by minimum 12%, these nails do not show additional load after one year of monitoring. In the other word, these nails were loaded to the higher load (i.e. due to the excessive deformation at second stage of construction) and then reloaded (i.e. due to the installation of the pre-tension nails in between row 1 and 2). In addition, the pre-tension nails take the additional load due to the post construction movement of the wall. In the other nails (i.e. rows 3 to 6) it is clear that the service load in the nails is increased due to the creep movement of the wall after the construction. Table 5-5 is summarized the additional load in the nails due to the post construction movement of the wall.

Table 5-5. Service load in the nails at end of construction and one year after the end of construction.

Nail No.	Design load (kips.)	Max. service load by the end of the construction (kips)	Max. service load one year after the construction (kips)	Percentage of the additional load in the nails due to the creep (%)
Nail in first row	21	9.8	10.11	3
Nail in second row	18	13.11	12.57	-
Nail in third row	18	7.25	9.28	28
Nail in fourth row	18	7.47	8.01	7
Nail in fifth row	18	6.7	8.3	24
Nail in sixth row	18	1.2	6.9	-

Since in the last stage of the construction (i.e. stage 6) there is no further excavation; therefore, the service load of these nail were almost zero at the end of the construction. Tension load will be mobilized in these nails soon after the construction due to the any movement of the wall. The maximum additional load in the nails due to the creep movement of the soil nail wall is maximum 30% of the service load. But even with the additional load in the nail due to the creep behavior of the soil nail wall, the service load of the nails for a period of one year after the construction is maximum 80% of the design load of the nails, and less than 22% of the maximum pullout capacity.

5.3.12. Load Cell Set-Up at Nail Head

Load cell was used to measure the load directly at the nail head during the monitoring period. Three load cells were installed at top of the three instrumented nails with foil strain gauges. Set-up of the load cell at nail head is shown in Figure 5-82 (FHWA, 1998).

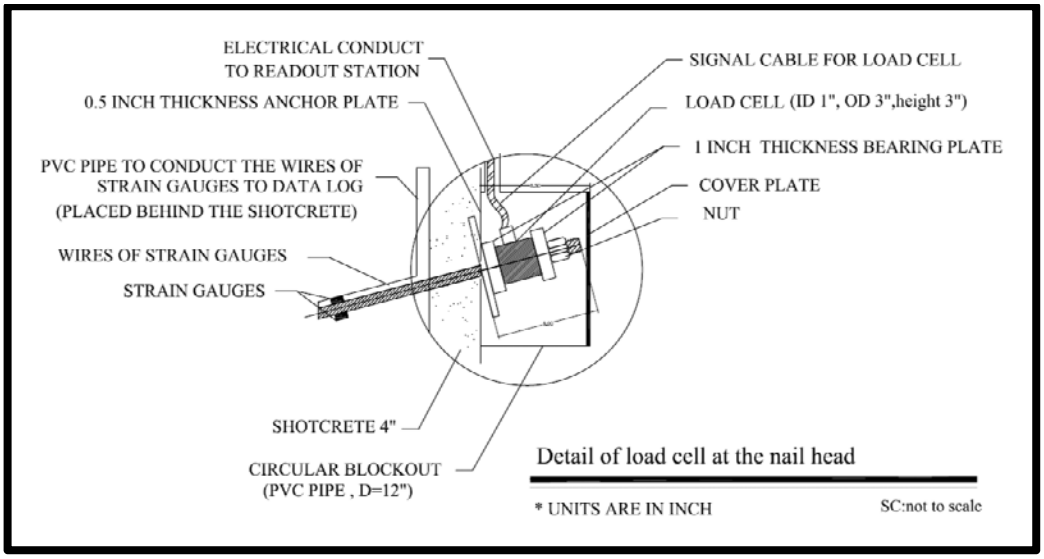

Figure 5-82. Details of the load cell at the nail head

The procedure of the load cell set-up at the nail head is as follows:

- Eight inches of the designated nail bar (instrumented nails with foil strain gauges) was left out of the shotcrete facing;
- Anchor plate, 1 in. bearing plate, load cell, and 1 in. bearing plate were placed at the nail head, respectively (Figure 5-83);
- 12 in. diameter PVC pipe was cut and was placed at top of the nail in a way that the load cell would be in the middle of the PVC pipe (Figure 5-84);
- A hole is drilled at bottom surface of the PVC pipe to pass the load cell cable;
- Cover plate was placed at top of the PVC pipe (Figure 5-85);
- Gap between the PVC pipe and the shotcrete facing was sealed (Figure 5-85);

- PVC pipe was installed at the instrumented section (i.e. station 2+06) to conduct the wires to the bottom of the wall (Figure 5-86);

Figure 5-83. Anchore plate, load cell and bearing plates

Figure 5-84. 12 in. diameter PVC tube around the load cell set-up

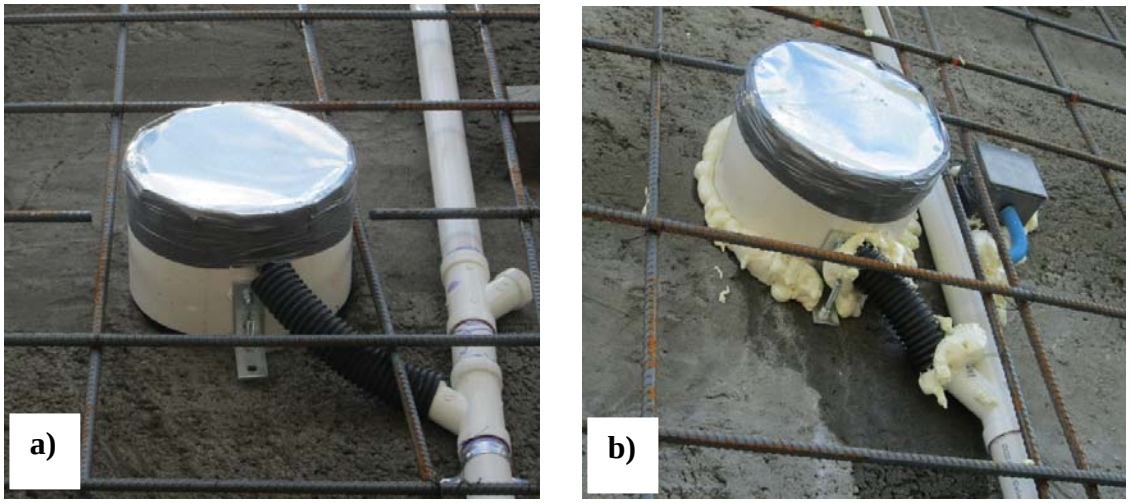

Figure 5-85. a) Cover plate at top of the wall, b) seal the PVC pipe

Figure 5-86. Conducting the load cells's cable to the ground

Since the load cell is placed in front of the shotcrete (i.e. at top of the nail), it was not possible to connect the load cells to the data acquisition system during the construction. Upon after the installation, the zero readings for each load cell was taken, and after the construction load cells were connected to the data acquisition system and the data was recorded every 30 minutes. Service load at the nail head obtained from the load cells for the period of one year post monitoring of the wall is illustrated in Figure 5-87. It is concluded from the results of the load cells that the load at the nail head remains constant even though the service load along the nail is increased.

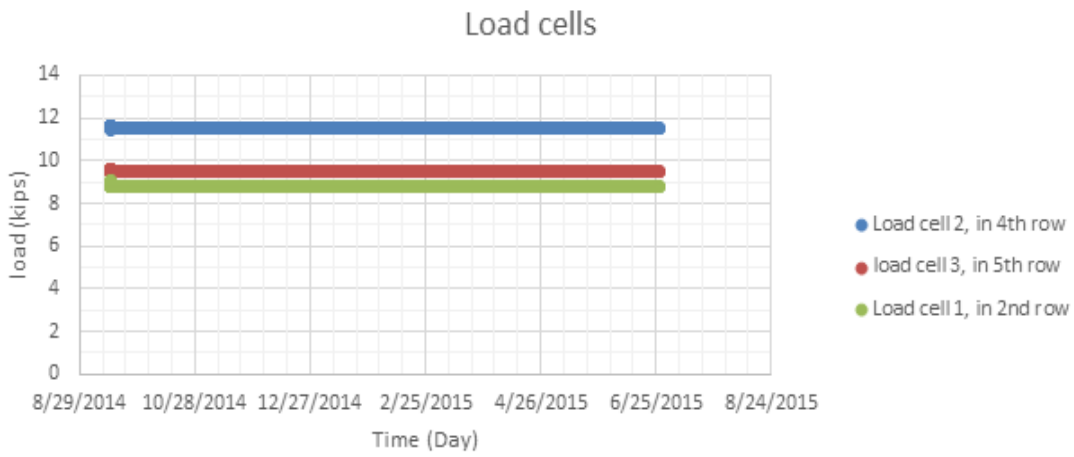

Figure 5-87. Service load at the nail head for three instrumented nails in second, fourth and fifth row of the soil nails

5.4. Water Content Probe

To monitor the seasonal variation of water content of the embankment soil, five water content probes (i.e. Decagon 5TE VWC+Temp+EC) were installed at different height of the wall at station 2+00. Figure 5-88 shows the distribution of the probes at station 2+00.

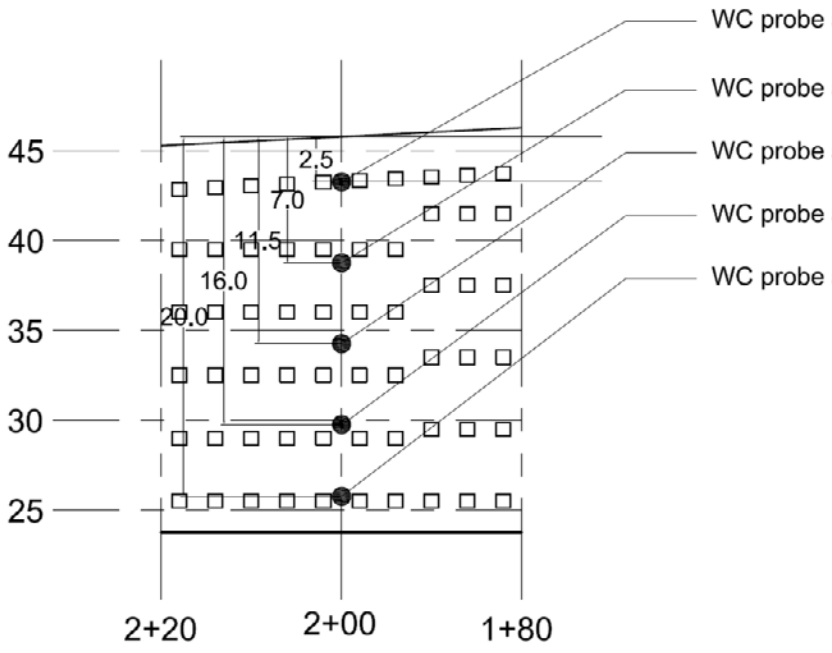

Figure 5-88. Distribution of the water content probes on the wall at station 2+00

Water content probes were installed at different stage of construction. The wires of these probes were passed through the PVC pipe along with the wires of VW strain in each stage of construction. The wires of water probes were connected to the data logger,

and the data were recorded every 30 minutes during and after construction. Water content probe and the data logger (i.e. EM50 ECH$_2$O logger) are shown in Figure 5-89.

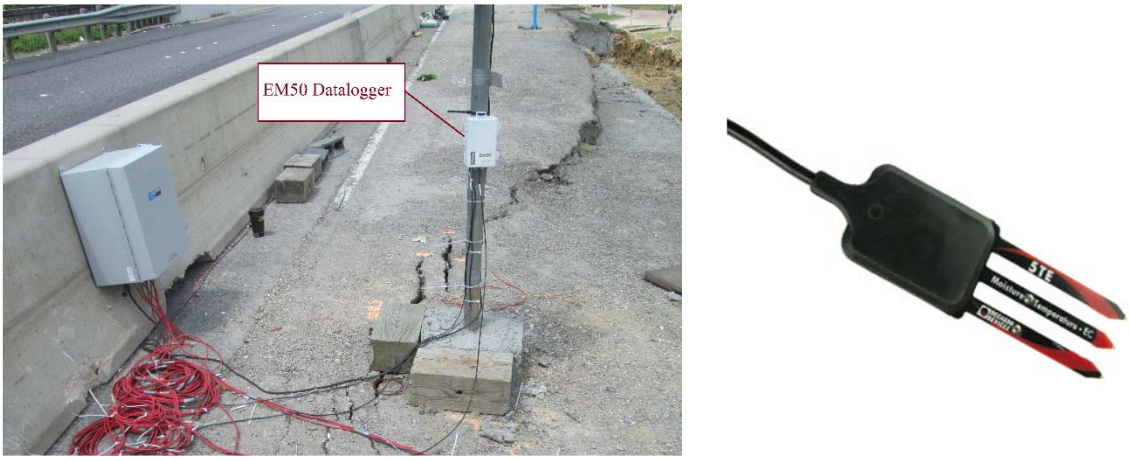

Figure 5-89. EM50 Data logger and water content probe

Variation of the water content of the embankment during and for a period of one year after the construction is shown in Figure 5-90 . During the construction (i.e. from April to June), water content of the embankment was increased at depth of 4 and 12 ft. by 5% and at the depth of 8 ft. by almost 6%. For the period of July and August, 2014, the probes did not record any data, but with interpolation the data it seems that the embankment soil started to dry out and the water content was decreased by almost the 4%. Again the probes did not record any data for the January, 2015, but it is clear that the water content started to increase. It is concluded from the results of the water content probes that

the variation of the moisture content of the embankment soil is almost 4% to 5% during the wet season and dry season.

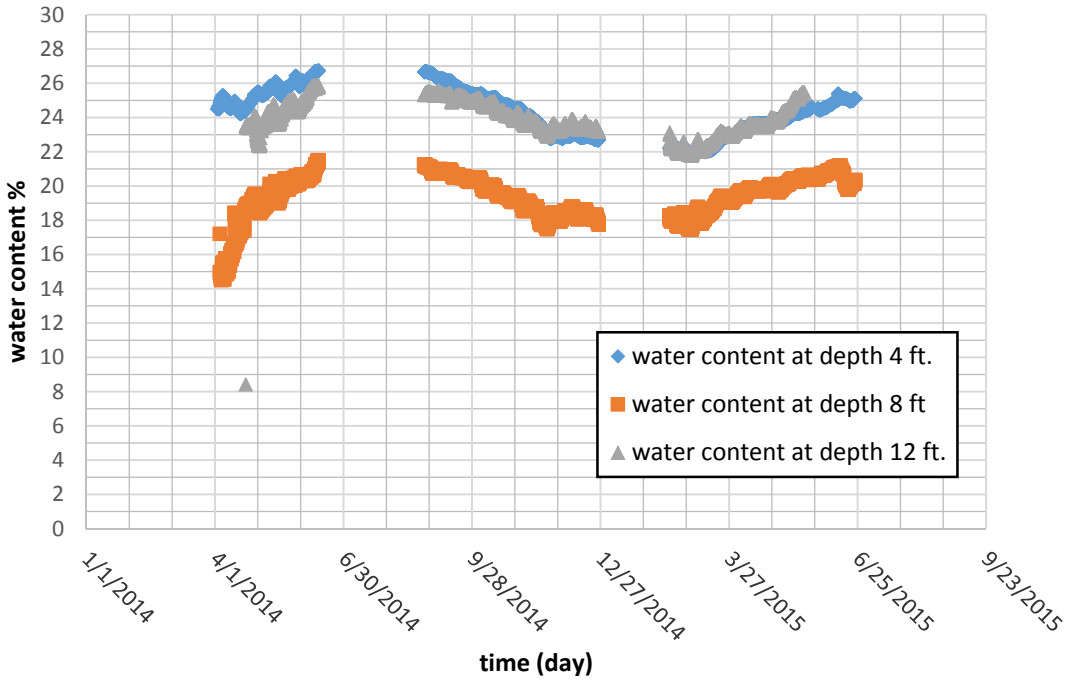

Figure 5-90. Variation of the water content of the embankment during and one year after the construction

6. NUMERICAL MODELING

6.1. Introduction

This section discusses results of simulation of the pullout tests on the sacrificial nails installed at the Beaumont project. Results of this simulation are used to verify the nail-grout interface parameter adopted in the numerical modeling of the soil nail wall. Model calibration and results of the numerical simulation of the soil nail wall at the end, and after the construction are presented in this section. In contexts of this research, UU triaxial creep tests were carried out on the soil samples from NGES-TAMU clay site and the Beaumont project. Results of simulation of the UU creep tests and model calibration are covers in section 6.6. Once the numerical model is validated, it was used to study the behavior of soil nails walls exploring other scenarios, for example: different geometries, and ground condition. Sections 6.8 and 6.9 present the results of the parametric study on the typical Texas turn around soil nail wall. FLAC 3D (version 4.0) was adopted to perform the numerical modeling.

6.2. Simulation of Pullout Tests

6.2.1. Introduction

Six sacrificial nails were installed at three different heights (i.e. 7.4, 14.4, and 17.9 ft. from top of the wall) at the emergency slope repair at Beaumont district. At each height, two sacrificial nails, one with instrumentation (i.e. strain gauges) and the other without instrumentation, with the horizontal spacing of 8 ft., were installed (section 5). These sacrificial nails are shown in Figure 6-1.

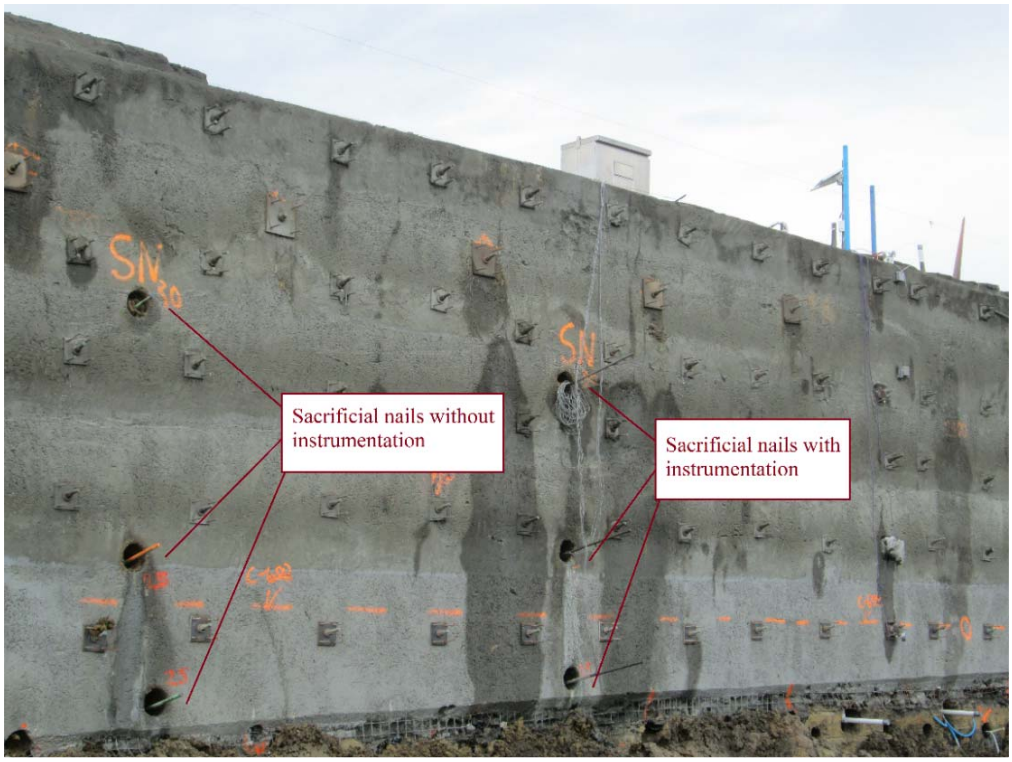

Figure 6-1. Sacrificial nails installed at Beaumont project at three different height

Summary of the tests results, and sacrificial nails specification is presented in Table 6-1. Bond length for sacrificial nails 1 (h=7.4) are 27 ft. bond length, while sacrificial nails 2 and 3 (h=14.4 and 17.9, respectively) have 23 ft. bond length.

Table 6-1. Summary of the results of the pullout tests on sacrificial nails at Beaumont project

Nail No.	Bond Length (ft.)	Hole diameter (inch)	Failure load (kips)	Maximum bond stress at failure (psf.)
Non-instrumented 1 (H=7.4 ft.)	27	8	43	760
Instrumented 1 (H=7.4 ft.)	27	8	51	902
Non-instrumented 2 (H=14.4 ft.)	23	8	45	935
Instrumented 2 (H=14.4 ft.)	23	8	45	935
Non-instrumented 3 (H=17.9 ft.)	23	8	58	1204
Instrumented 3 (H=17.9 ft.)	23	8	58	1204

6.2.2. Simulation of Pullout Test

The main goal of the modeling is to calibrate the constitutive model using the information gathered from the pullout tests on sacrificial nails at the Beaumont project.

FLAC 3D is a numerical code for advanced geotechnical analysis (Itasca, 2006) that can be used to simulate the creep behavior of soil nail walls in high plasticity clays. The cable structural elements are used to model the soil nail in FLAC 3D. These elements provide a shearing resistance (by means of grout properties) along their length (Itasca, 2006). For the cable elements, effects of bending are not important. To consider the effect of bending, pile structural elements should be used. The grout behaves as an elastic, perfectly plastic material, with its peak strength being confining stress dependent.

The shear behavior of cable-soil interface is cohesive and frictional. The idealized system of grout-soil interface is shown in Figure 6-2a. This system numerically is represented as a spring (the grout shear stiffness Kg) and a slider (the grout cohesive stiffness Cg) located at the nodal points along the cable axis (Figure 6-2b).

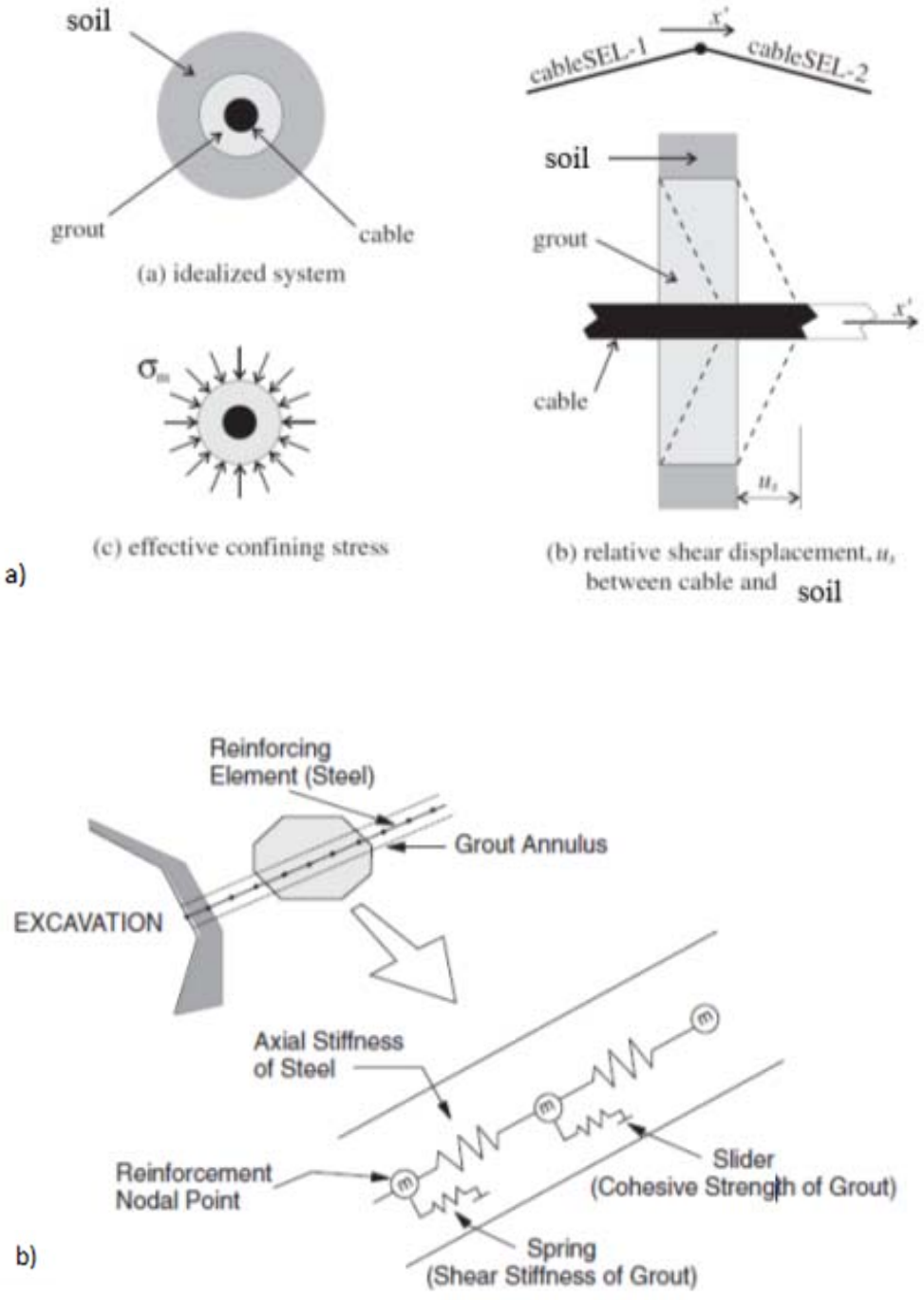

Figure 6-2. Cable structural elements a) Idealization of grouted-cable system b) mechanical representation of fully bonded reinforcement (after Itasca, 2006)

In order to obtain the soil – grout interface behavior (i.e. grout cohesive strength, Cg, and grout shear stiffness, Kg), pullout tests on the sacrificial nails at Beaumont project (task#4) are modeled in FLAC3D. Figure 6-3 illustrates the geometry and mesh generation of the model. Cable element is located at the middle of the geometry. In order to simulate the pullout test, vertical velocity is applied to top of the cable element and the axial force in the cable element is measured. The parameters adopted in the modeling is presented in Table 6-2.

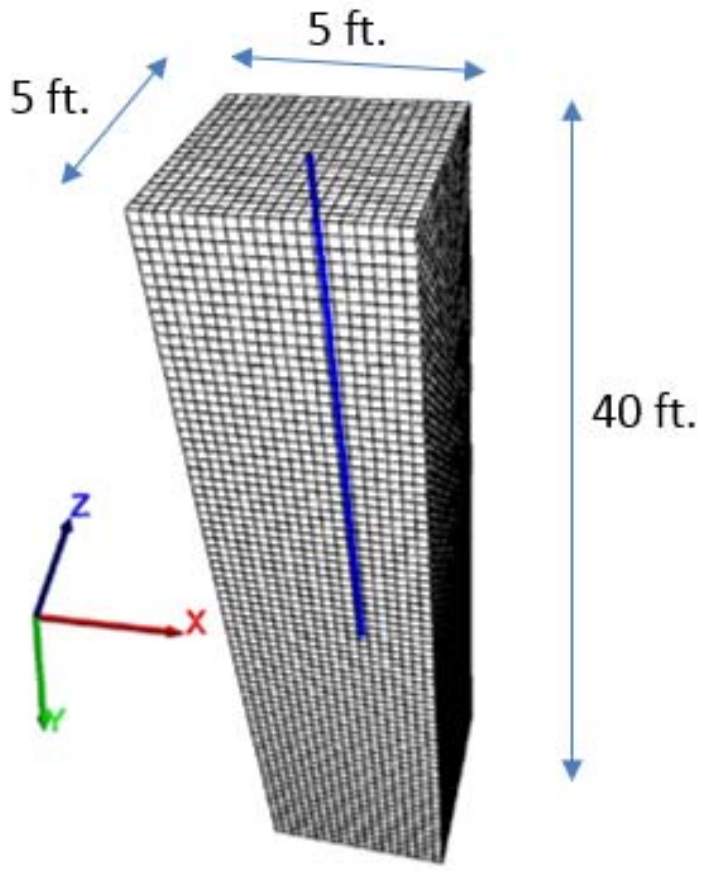

Figure 6-3. Geometry of the pullout test

Table 6-2. Parameters used in simulation of the pullout test

Pullout test		
Material	**Constitutive model**	**properties**
soil	Mohr-Coulomb	E=2.9e5 psf (14 MPa), v=0.3, γ=125 pcf, c=0, Φ=26 degree
Nail (cable element)	Elastic-perfectly plastic	E steel=4.17e9 psf (200 GPa), c_grout=1e3 psf , Φ_grout=20 degree

Results of the numerical modeling for three different heights of the sacrificial nails are shown in Figure 6-4 to Figure 6-6.

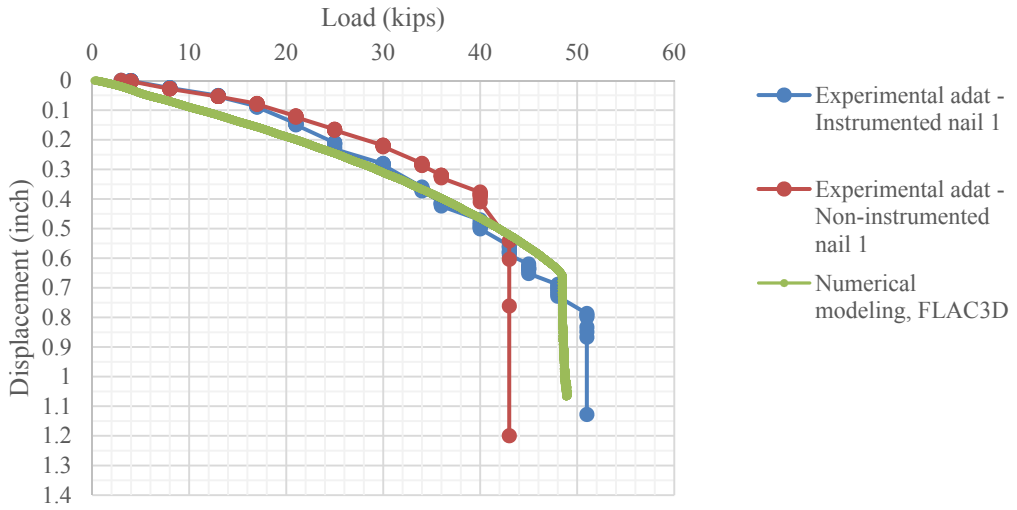

Figure 6-4. Comparison of the experimental results with numerical modeling for the sacrificial nail installed at depth of 7.4 ft. from top of the wall

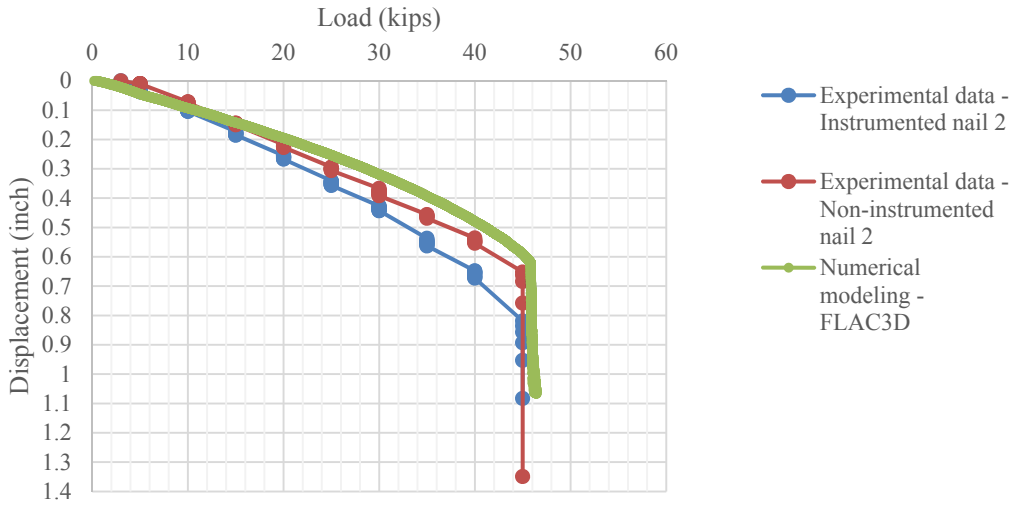

Figure 6-5. Comparison of the experimental results with numerical modeling for the sacrificial nail installed at depth of 14.4 ft. from top of the wall

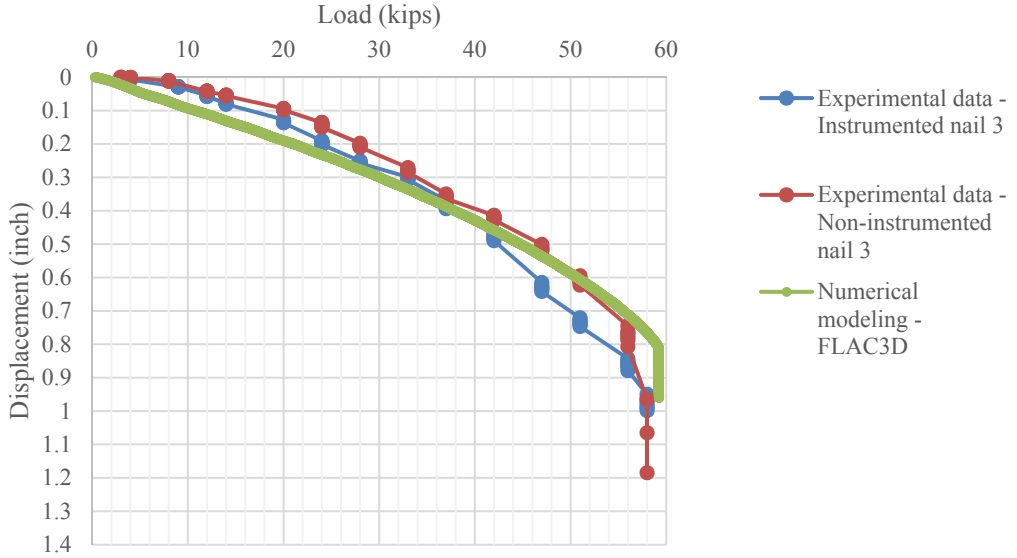

Figure 6-6. Comparison of the experimental results with numerical modeling for the sacrificial nail installed at depth of 17.4 ft. from top of the wall

Shear stress at the interface of soil-grout is shown in Figure 6-7 to Figure 6-9. As observed from the results of modeling the pullout test, a very good agreement between experimental and model results was obtained. The soil – grout interface parameters (i.e. grout cohesive strength, Cg, and grout shear stiffness, Kg) obtained from the modeling will be used to simulate the nails element in the soil nail wall modeling.

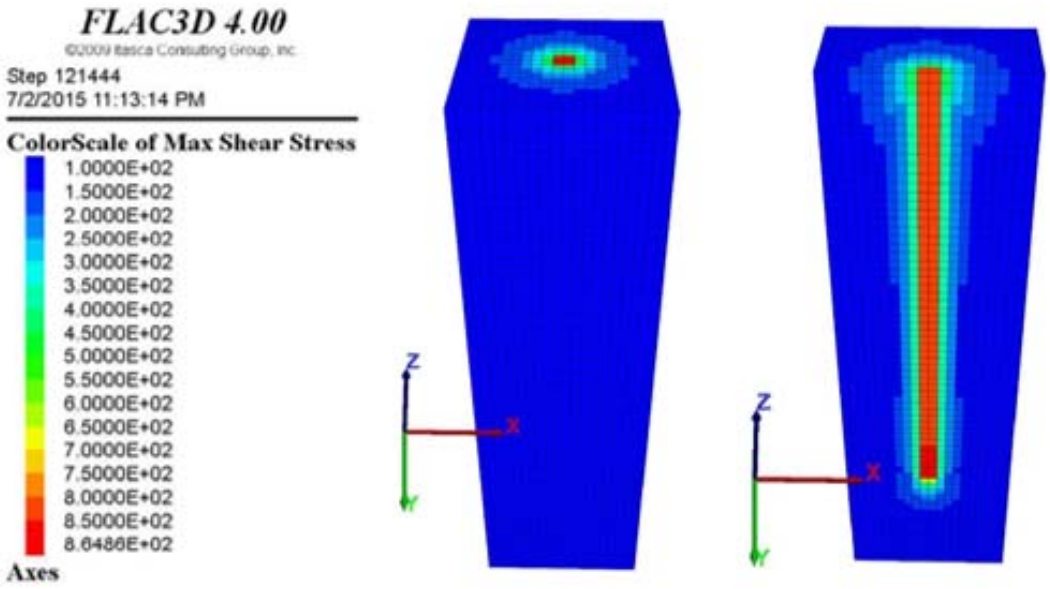

Figure 6-7. Shear stress at the interface of the soil – grout for the modeling of the sacrificial nail at 7.4 ft. from top of the wall (shear stress obtained from numerical is 864 psf).

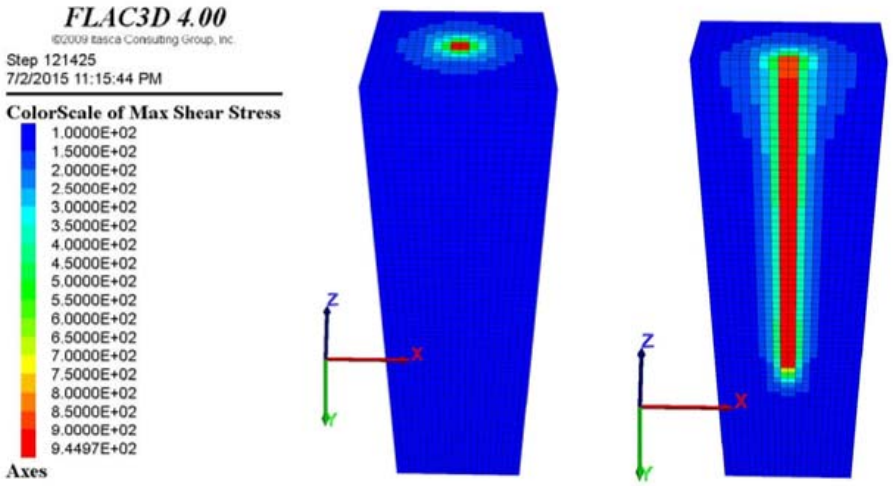

Figure 6-8. Shear stress at the interface of the soil – grout for the modeling of the sacrificial nail at 14.4 ft. from top of the wall (shear stress obtained from numerical is 950 psf).

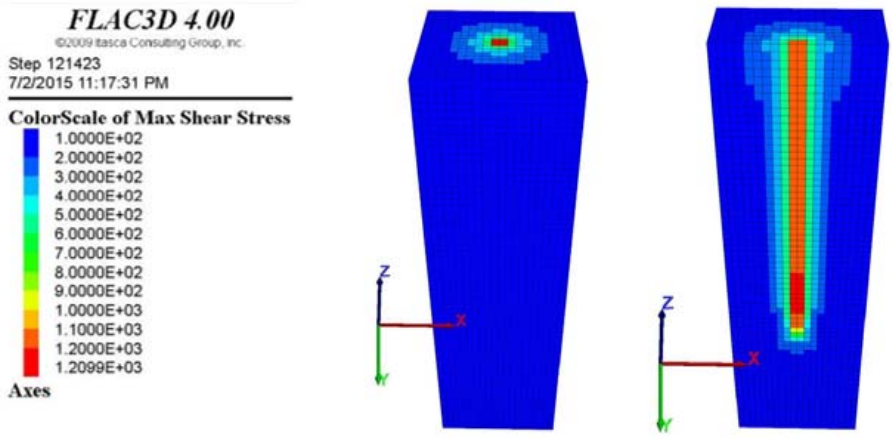

Figure 6-9. Shear stress at the interface of the soil – grout for the modeling of the sacrificial nail at 17.9 ft. from top of the wall (shear stress obtained from numerical is 1200 psf).

6.3. Simulation of Soil Nail Wall at End of Construction

6.3.1. Introduction

Numerical modeling of the soil nail wall is carried out for two phases; end of the construction and after the construction. The numerical modeling for the end of the construction is validated with the lateral displacement of the wall, and load distribution along the nails (i.e. service load) at the end of the construction. Modeling procedure for end of the construction is presented as follows, while results of the modeling of the wall and model calibration for after the construction will be discussed in section four.

6.3.2. FLAC3D Model – End of Construction

The main components of the soil nail walls are embankment soil, nails element (reinforcement element), soil-grout interaction and facing of the wall. Modeling of these components are presented as follow.

Mohr-Coulomb constitutive model is adopted to simulate the soil behavior during the construction. In fine-grained soils for the soil nail walls, the drained strength should be considered when analyzing the long-term stability of the soil nail wall under a steady, static loading condition (GEC#7, 2003). The drained shear strength of the soil is defined as effective friction angle. Mitchel 1993, proposed the correlation between drained angle of friction of fine-grained soils and plasticity index (Figure 6-10). This correlation can be used to estimate the drained shear strength.

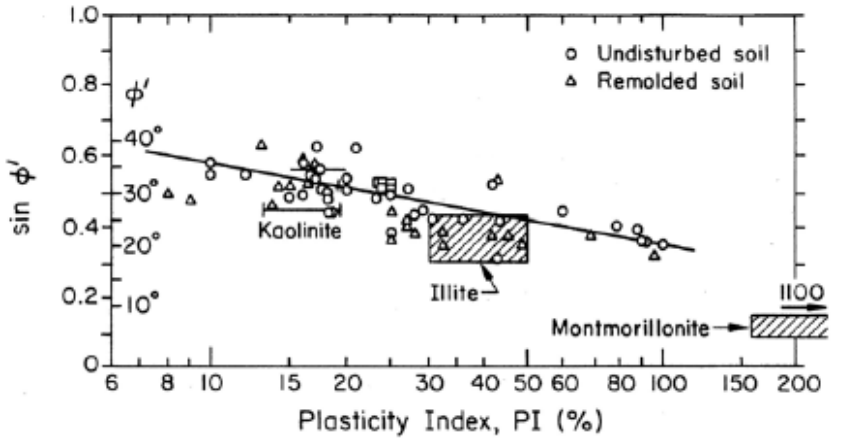

Figure 6-10. Correlation between drained angle of friction of fine-grained soils and plasticity index (after Mitchell, 1993)

The reinforcement elements (nails) were modeled as cable element. The shear behavior of grout-soil interface is cohesive and frictional. The idealized system of grout-soil interface is shown in Figure 6-2a. This system were modeled as a spring (the grout shear stiffness Kg) and a slider (the grout cohesive stiffness Cg) located at the nodal points along the cable axis (Figure 6-2b). These parameters were obtained from the modeling of the pullout test on sacrificial nails.

Geometry of the model for the soil nail wall at the Beaumont is shown in Figure 6-11. Coarse mesh density is adopted globally, which is refined to fine density in the vicinity of the soil nail wall (Singh and Babu, 2010). Mesh boundaries are taken far enough to minimize the effect of the boundaries on the results of numerical modeling (Briaud, 1997).

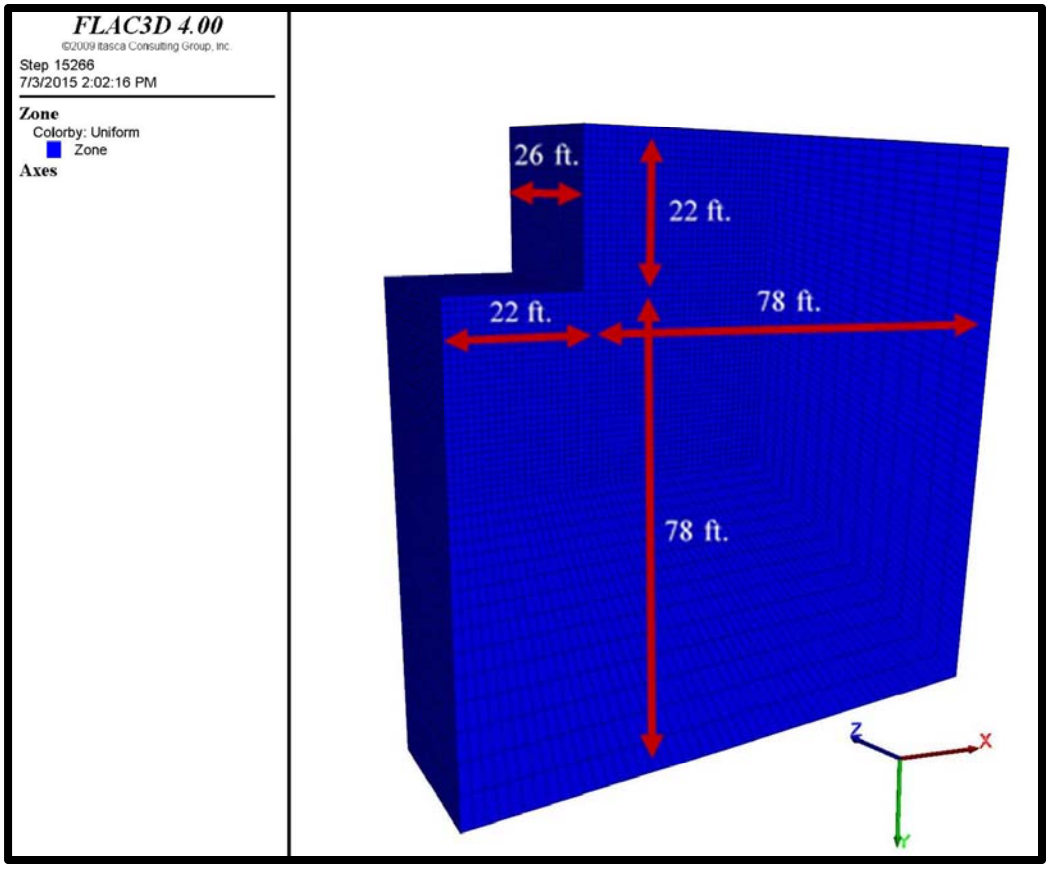

Figure 6-11. Geometry of the soil nail wall model

The modeling of the wall was performed in sequential steps. At first, the geometry of the embankment was generated. Soil properties which obtained in the laboratory were applied to the model. This step is followed by specifying the boundary condition. In order to reach to the initial condition (i.e. in-situ stresses), FLAC3D is run until an equilibrium state is obtained (Itasca, 2006). After the equilibrium state, stage construction is used to simulate the construction of the soil nail wall (Singh and Babu, 2010). In each stage of construction, excavation depth of 4 ft. is simulated by assigning the null model to the zone

of excavation. This step is followed by installing the soil nails and shotcrete. The simulation is continued until an equilibrium state is obtained at each stage of construction. Six stages of construction are carried out to simulate the soil nail wall (i.e. reach to the bottom of the excavation). For each stage, lateral displacement of the wall and service load in the nails are calibrated using the data obtained from the field data. Figure 6-12 illustrates the six stages of the construction defined in modeling.

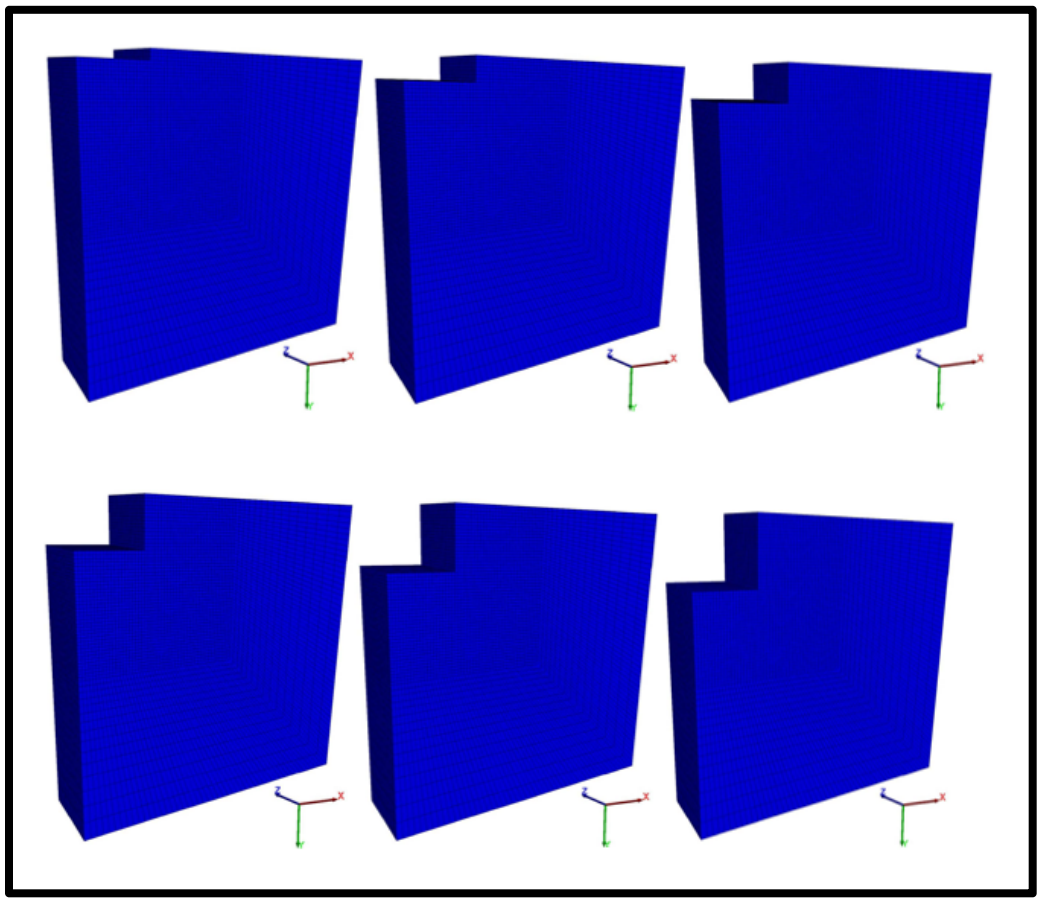

Figure 6-12. Simulation of the soil nail wall at the Beaumont project in 6 stages of construction

Table 6-3 summarizes the parameters adopted for numerical simulation of the soil nail wall at the Beaumont project using FLAC3D. Figure 6-13 presents the contours of the horizontal deformation of the model at the end of construction (stage 6). Horizontal movement obtained from the simulation is compared to the results of the inclinometer readings at station 1+46 in Figure 6-14. The model under predicts the horizontal movement of the wall for the first 5 ft., but for the remaining height of the wall, the numerical results are comparable with the actual data obtained from wall monitoring.

Table 6-3. Parameters adopted for numerical simulation of the soil nail wall at Beaumont project

Material	Constitutive model	Properties
Embankment soil	Mohr-Coulomb	Φ'=26, C'=0, Y=125 pcf, E=2.9e5 psf. , υ=0.3
Soil nails (cable element)	Elastic-perfectly plastic	E steel=4.17e9 psf (200 GPa), c_grout=1e3 psf , Φ_grout=20 degree
Shotcrete (shell element)	Elastic (isotropic)	E shot = 2.2e8 psf, υ=0.25, thickness=4 in.

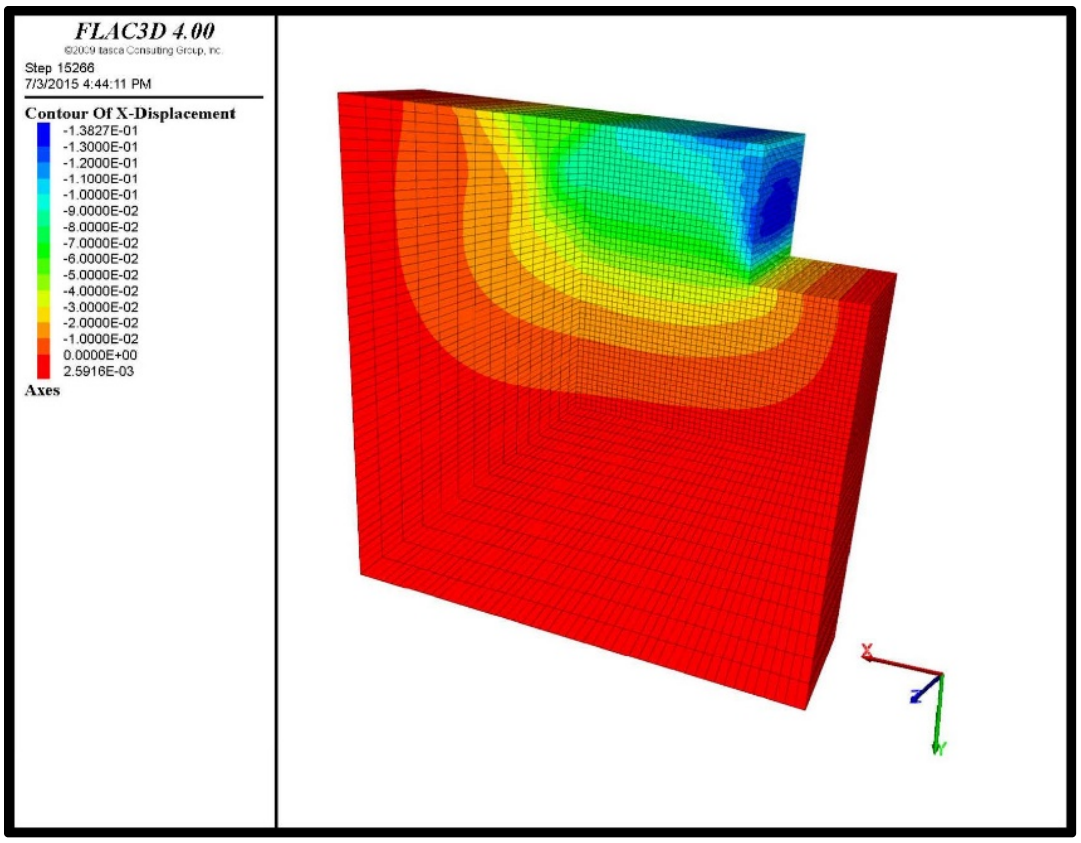

Figure 6-13. Contours of the lateral displacement of the soil nail wall model at the end of the construction

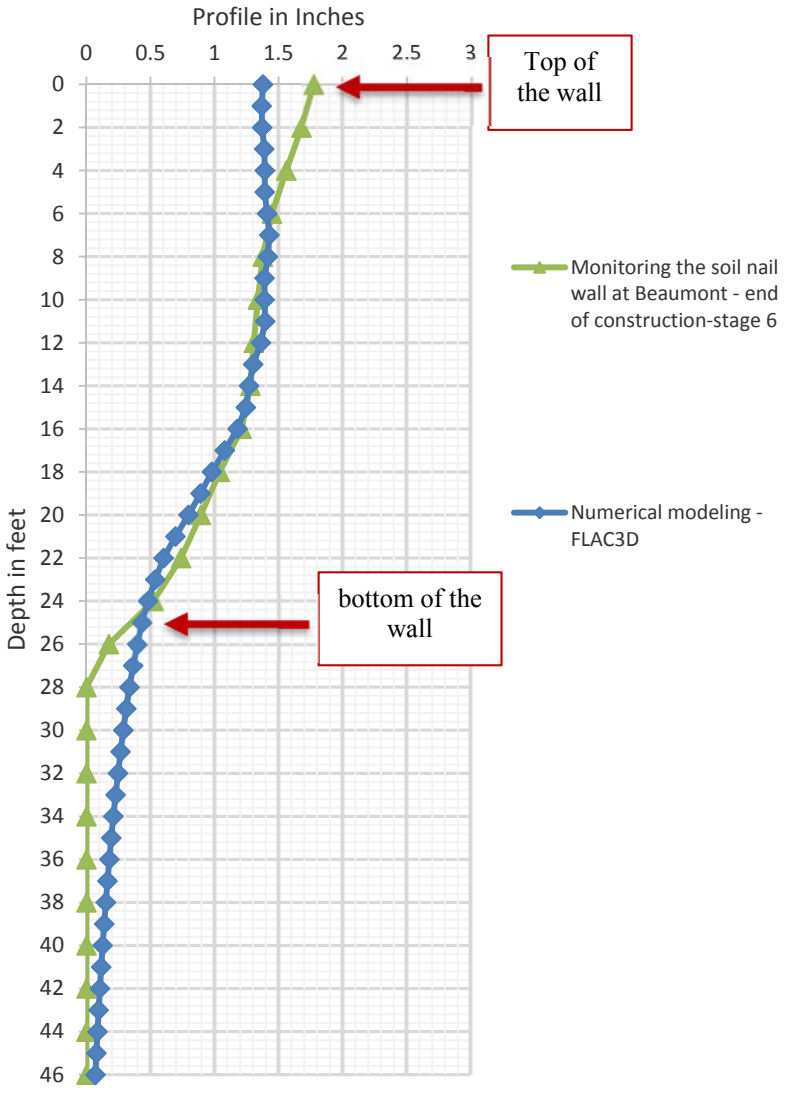

Figure 6-14. Comparison of the results of the lateral displacement of the soil nails obtained from numerical modeling with the actual lateral displacement of the wall obtained from inclinometer readings at station 1+46.

Service load in the nails obtained from the numerical modeling at the end of the construction is compared to the service load obtained from instrumentation of the soil nail

wall at Beaumont in Figure 6-15 to Figure 6-20. Since the numerical model under predicts the horizontal deformation of the wall for the first 5 ft., service load developed in these two rows of soil nails are also less than the actual service load in the nails for this two rows. But for the other row of soil nails, results of modeling are comparable with the field data.

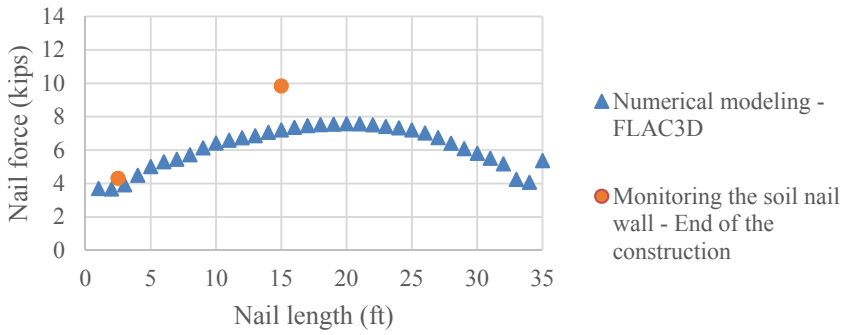

Figure 6-15. Comparison of the service load in the nails in first row of the soil nails obtained from numerical modeling with the service load obtained from instrumentation of the soil nail wall at Beaumont

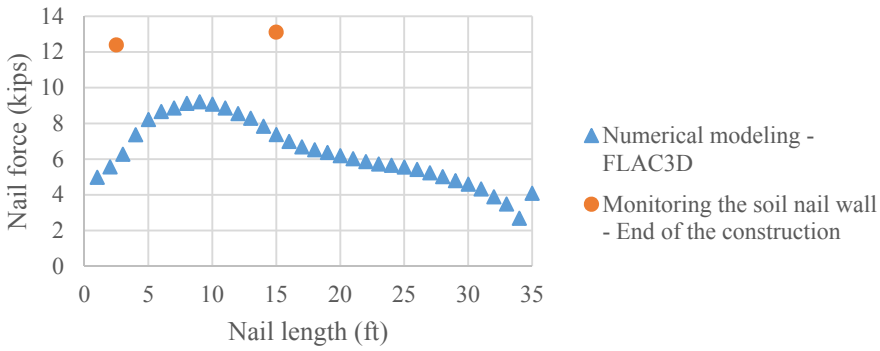

Figure 6-16. Comparison of the service load in the nails in second row of the soil nails obtained from numerical modeling with the service load obtained from instrumentation of the soil nail wall at Beaumont

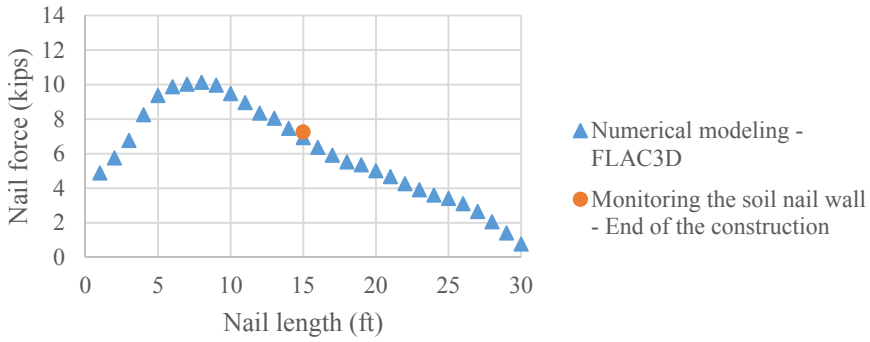

Figure 6-17. Comparison of the service load in the nails in third row of the soil nails obtained from numerical modeling with the service load obtained from instrumentation of the soil nail wall at Beaumont

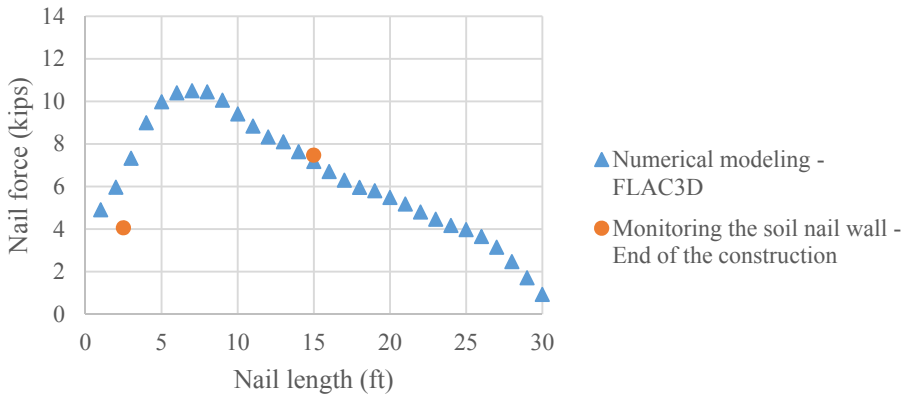

Figure 6-18. Comparison of the service load in the nails in fourth row of the soil nails obtained from numerical modeling with the service load obtained from instrumentation of the soil nail wall at Beaumont

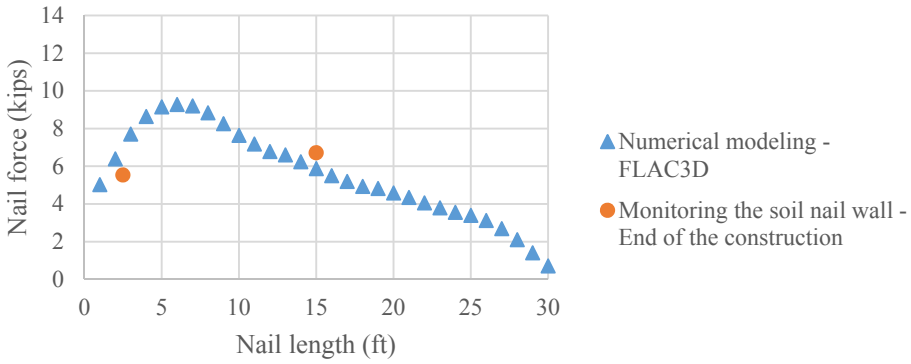

Figure 6-19. Comparison of the service load in the nails in fifth row of the soil nails obtained from numerical modeling with the service load obtained from instrumentation of the soil nail wall at Beaumont

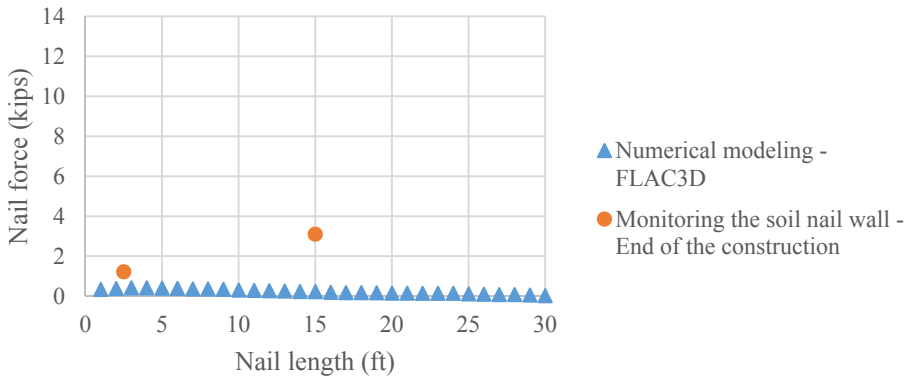

Figure 6-20. Comparison of the service load in the nails in sixth row of the soil nails obtained from numerical modeling with the service load obtained from instrumentation of the soil nail wall at Beaumont

6.4. Rheological Behavior of High Plasticity Clay

Any material is subjected to deformation in the course of time at a constant load. The magnitude of the time–dependent deformation depends on the strength of the material. Rheology investigates the relations between stress, strain and time (Feda, 1992). Creep is a long-term deformation of the material under the constant applied load. This section briefly presents the rheological behavior of the soil.

Furthermore, in this section, viscous behavior of the high plasticity clay and available models to present this behavior are discussed. In addition, in order to gain a better understanding of the long-term behavior of the soil, the UU creep tests were carried out on the soil samples. These tests were modeled with FLAC3D. Results of this simulation are used to verify that behavior of the constitutive model used in the modeling, and also to obtain the viscos parameters of the soil for modeling the soil nail wall.

6.4.1. Rheological Behavior of Soil

Rheological behavior or time-dependent behavior of the soil can be defined like viscous fluid (Whitman, 1957). In 1687, Newton studied the flow behavior of the liquids, and he observed that the fluid has the constant viscosity (flow). Non-Newtonian fluids change their viscosity under the applied force or change in the stress. Bingham, 1917, stated that the viscoplastic material behaves as a rigid body at low stresses and flows as a viscous fluid at high stress (Bingham, 1917). In Bingham model, a material is considered as a rigid body for the shear stresses less than the critical value,τ_0, and once the shear stresses exceed the critical value (i.e. yield stress), material flows with a constant viscosity. Figure 6-21 presents different fluid models.

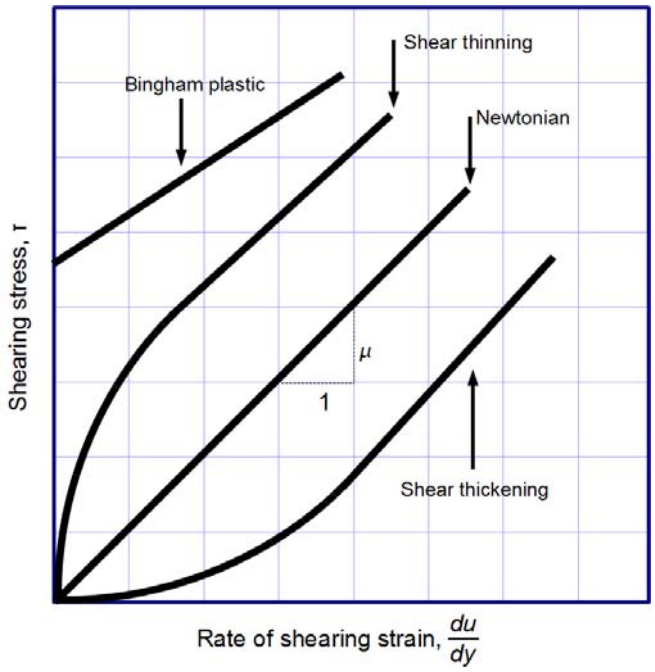

Figure 6-21. Fluid models (viscosity is the slope of each line)

O'donovan and Tanner (1984) proposed the bi-viscosity model to represent the behavior of the materials which exhibit the higher viscosity for the shear stresses less than the yield shear stress. For the shear stresses more than the yield shear stress, viscosity is 1000 times less than the viscosity for the shear stresses below the yield stress (O'donovan and Tanner, 1984; Mitsoulis, 2007). The general form of bi-viscosity model (modified Bingham model) is presented as:

$$\tau = \eta_{pN}\dot{\gamma} \qquad for\ \dot{\gamma} \leq \dot{\gamma}_c \tag{6.1}$$

$$\tau = [\eta_p + \frac{\tau_y}{\dot{\gamma}}]\dot{\gamma} \qquad for\ \dot{\gamma} > \dot{\gamma}_c \tag{6.2}$$

Where, η_{pN} is the pseudo-Newtonian viscosity in the unyielded zone, η_p is the Bingham viscosity, and $\dot{\gamma}_c$ is the critical shear rate in the model (Jeong, 2013). Shear stress vs shear strain rate for the modified Bingham model is illustrated in Figure 6-22.

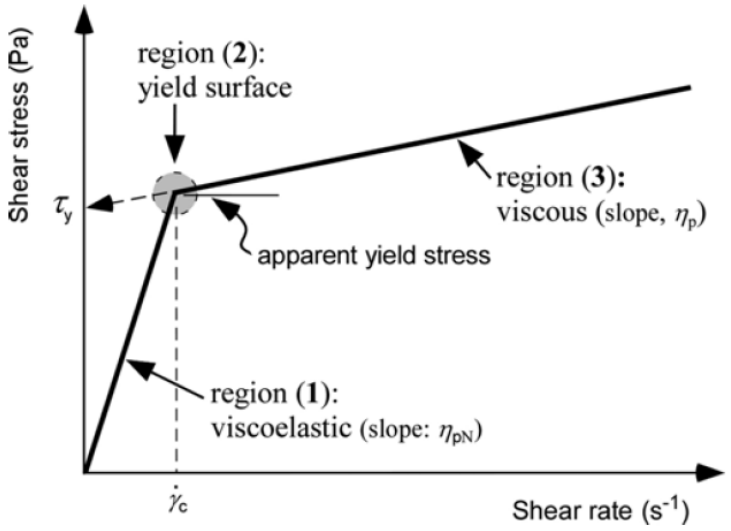

Figure 6-22. Schematic view of a bi-viscosity model, shear stress vs. shear strain rate for modified Bingham fluids model $\dot{\gamma}$= critical shear strain rate, (after Jeong, 2013)

Viscoelastic materials exhibit both viscous and elastic behaviors (Itasca, 2006). Elastic behavior is defined by a spring with elastic constant "G". According with Hooke's law, the shear behavior is defined as:

$$\tau = G\gamma \tag{6.3}$$

Where, τ is the shear stress, G is the elastic constant (i.e. shear modulus) and γ is the shear strain.

Viscous behavior in rheological model is defined as dashpot. According to Newton's law, the viscous behavior is specified as:

$$\tau = \mu\dot{\gamma} \tag{6.4}$$

Where, μ is the shear viscosity of the material and $\dot{\gamma}$ is the shear strain rate. Figure 6-23 illustrates the viscoelastic elements in mechanical rheological models. Mechanical rheological models are different combination of these elements. Mechanical rheological models are used to study the time – dependent behavior of the soil. Maxwell model is the combination of elastic spring and dashpot in series (Figure 6-24a.), while Kelvin- Voigt model consists of dashpot and elastic spring in parallel. Burger model consists of Maxwell and Kelvin model in series (Figure 6-24b.)

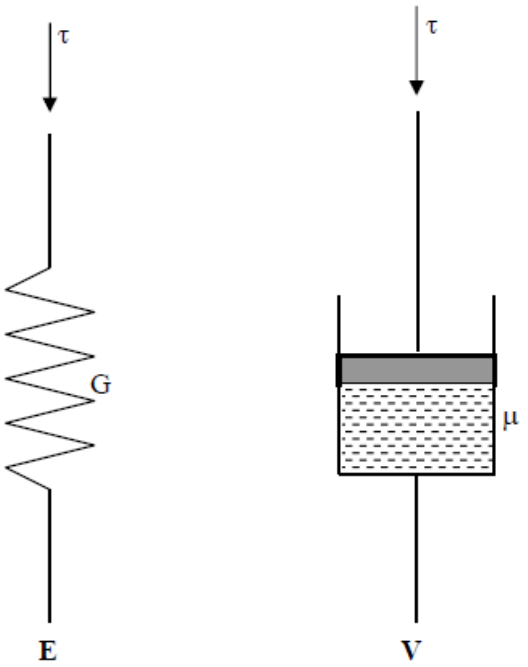

Figure 6-23. Elastic (E) and Viscous (V) element in mechanical rheological models (after Mahajan and Budhu, 2006)

There are eight optional rheological mechanical models in FLAC 3D available to simulate creep behavior of soil such as the classical viscoelastic (Maxwell) model, and the Burgers substance viscoelastic model. In these models, creep deformation is simulated by displacement of dashpot.

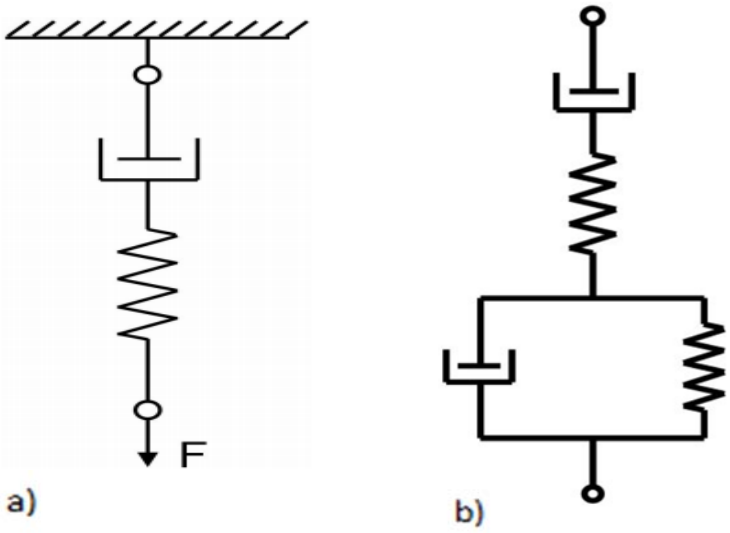

Figure 6-24. Rheological model a) Maxwell model b) Burger model

In Mechanical rheological models, total stain of the body can be written as:

$$\gamma = \gamma_0 + \gamma(t) \tag{6.5}$$

Where, γ_0 is the elastic deformation (developed immediately after loading) and $\gamma(t)$is the strain developed in time due to the viscous behavior of the material. Maxwell model (dashpot and spring in series), exhibits constant strain rate ($\dot{\gamma} = \frac{d\gamma}{dt}$) under an

applied constant shear (Figure 6-25a). The Burger model is composed of the Kelvin model (dashpot and spring in parallel) and the Maxwell model (dashpot and spring in series). In the Burger model, elastic deformation γ_0 is observed immediately after the loading, but in this model, rate of the strain is decreased with time under an applied constant shear unlike the Maxwell model (Figure 6-25b).

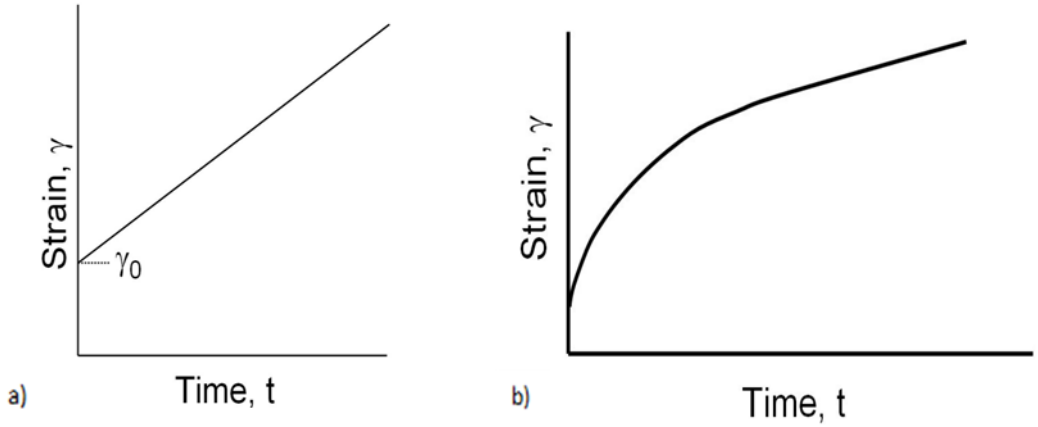

Figure 6-25. Strain vs time for a) Maxwell model, b) Burger model

Many researchers have studied the rheological (creep) behavior of the soil (e.g. Whitman, 1957; Keedwell, 1984; Vyalov, 1986; Feda, 1992). They generally agreed that the creep of the most soils is nonlinear, and therefore the linear mechanical rheological models (Maxwell) usually represent a simplified soil behavior.

In 2009, Segalini performed several UU triaxial tests with creep steps and did simulations with FLAC using the finite difference method to study the creep behavior of the landslide in Italy. In his research, the Burger model was adopted to study the creep behavior of the soil. Normalized stain with confining pressure versus time for laboratory test and numerical modeling is shown in Figure 6-26.

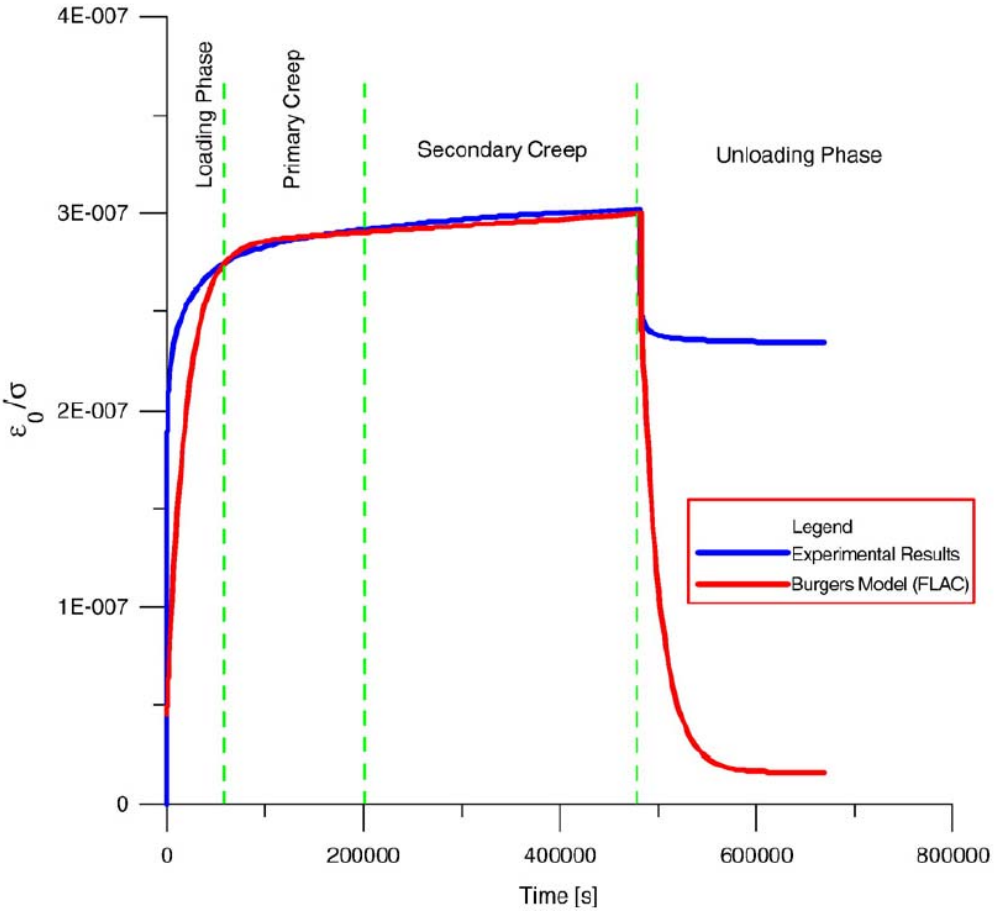

Figure 6-26. Results of the triaxial UU creep test along with numerical modeling using Burger model (after Segalini et al., 2009)

In 1986, Vyalov developed series of creep curves (i.e. Family of creep curves) (Figure 6-27). Each curve corresponds to certain loading. At the higher load, the soil exhibits the excess deformation and the creep rate is significantly increased.

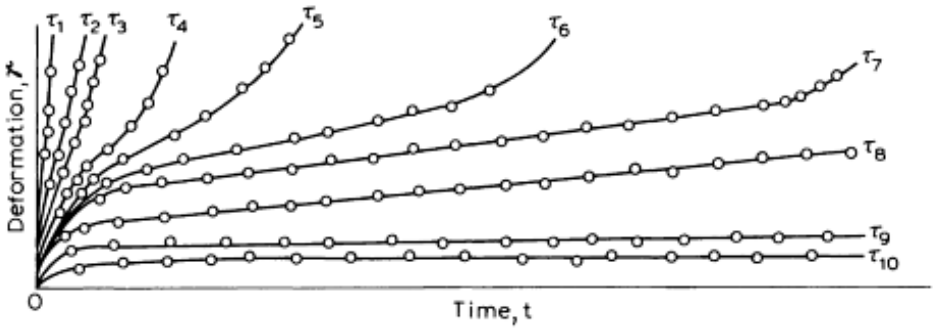

Figure 6-27. Curves of creep in soil for various constant loading (after Vyalov, 1986).

6.5. Shear Viscosity of High Plasticity Clay

The key parameter to determine the rheological behavior of the high plasticity clay is the soil's shear viscosity. The available literature on the viscosities of the soils relevant to the soil flow such as landslides, mudslides or earth flow. Many researchers have studied the viscos behavior of the soil in these conditions. Soil in such conditions has the water contents more than their liquid limits.

Liquidity Index (LI) is defined as:

$$LI = (w - w_p)/(w_l - w_p) \tag{6.6}$$

Where w is the natural moisture content, w_l is the liquid limit, and w_p is the plastic limit of the soil. The liquidity index indicates the consistency of the soil in its natural states (i.e. very soft when the liquidity index close to unity and very stiff when it is close to zero) (Keedwell, 1984). LI of the soil at NGES-TAMU CLAY and the Beaumont site are presented in Table 6-4 and Table 6-5, respectively.

Table 6-4. Liquidity Index of the samples from NGES-TAMU clay site

NGES-TAMU clay site						
Borehole	**Depth (ft.)**	**Plastic limit (PL)**	**Liquid Limit (LL)**	**Plasticity Index (PI)**	**Water content %**	**Liquid Index (LI)**
N2	13 to 15	23	71.4	48	22	<0
N1	8 to 10	20.5	55.6	35	24	0.10
N1	6 to 8	20	69.1	49	16	<0
N5	16 to 18	17.8	62.7	45	22	0.09

Table 6-5. Liquidity Index of the samples from the Beaumont site

Beaumont site						
Borehole	**Depth (ft.)**	**Plastic limit (PL)**	**Liquid Limit (LL)**	**Plasticity Index (PI)**	**Water content %**	**Liquid Index (LI)**
B1	3 to 5	23.7	77.8	54	33.8	0.19
B1	8 to 10	21.3	72.7	51	23.6	0.04
B1	13 to 15	24.3	91.9	68	25.5	0.02
B1	23 to 25	16.8	65.1	48	21.8	0.10
B1	33 to 35	14.8	63.2	48	15.2	0.01
B2	23 to 25	17.4	65.5	48	22.4	0.10

As it was shown in Table 6-4 and Table 6-5, the LI for the both site is less than 0.1, expect for the soil sample from Beaumont site at depth of 3-5 ft. At this depth since it is so close to the ground surface; therefore, the natural water content of the soil is higher than the other depth.

The viscos parameter for the soil with high water content is determined with viscometer. However, high plasticity clay exhibits viscous behavior for the water content less than liquid limit. The shear viscosity of the high plasticity clay cannot be measured using viscometer. There is no standard method to determine the viscous parameter of the clay with low water content (Mahajan and Budhu, 2006).

Locat and Demers (1988) investigated the viscosity of the sensitive clays with liquidity index between 1.5 and 6 with a rotational viscometer. They proposed based on field and experimental observation a relationship between viscosity and liquidity index which is shown in Figure 6-28.

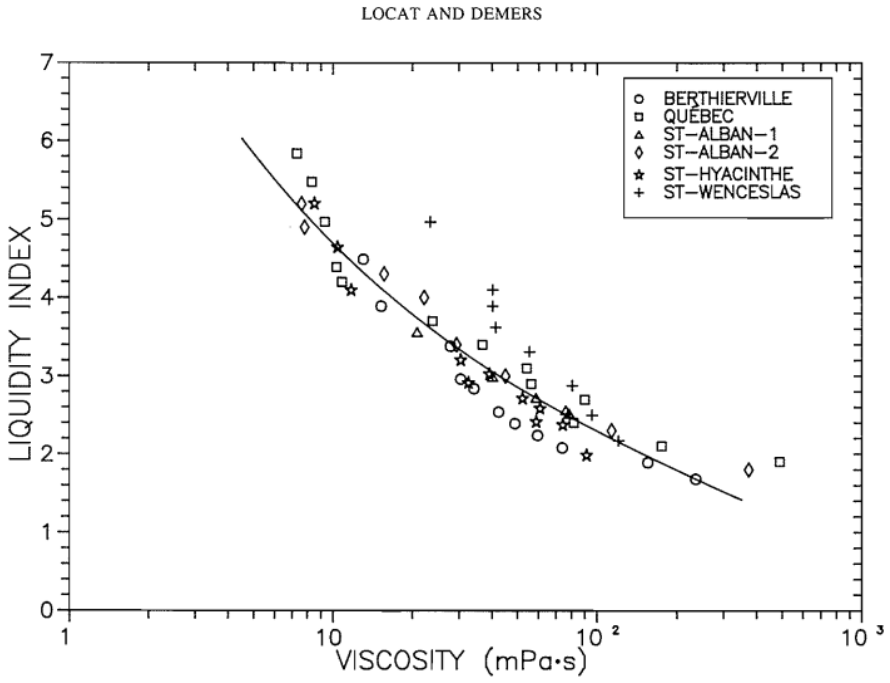

Figure 6-28. Relation between Liquidity Index and viscosity (after Locat and Demers, 1988)

For the soil with low water content (i.e. less than the liquid limit), rotary viscometer cannot be used to measure the viscosity (Fakher, 1999).

Mahajan and Budhu (2006) investigated the viscous behavior of the clay during penetration of a rigid shaft. He investigated the shear viscous behavior of the plasticity clay based on the results of the fall cone test. He proposed the experimental equation (Figure 6-29) to determine the viscosity of the clay with low water content (low liquidity index). No information was provided for the viscosity of the soil with liquidity limit less than 0.5.

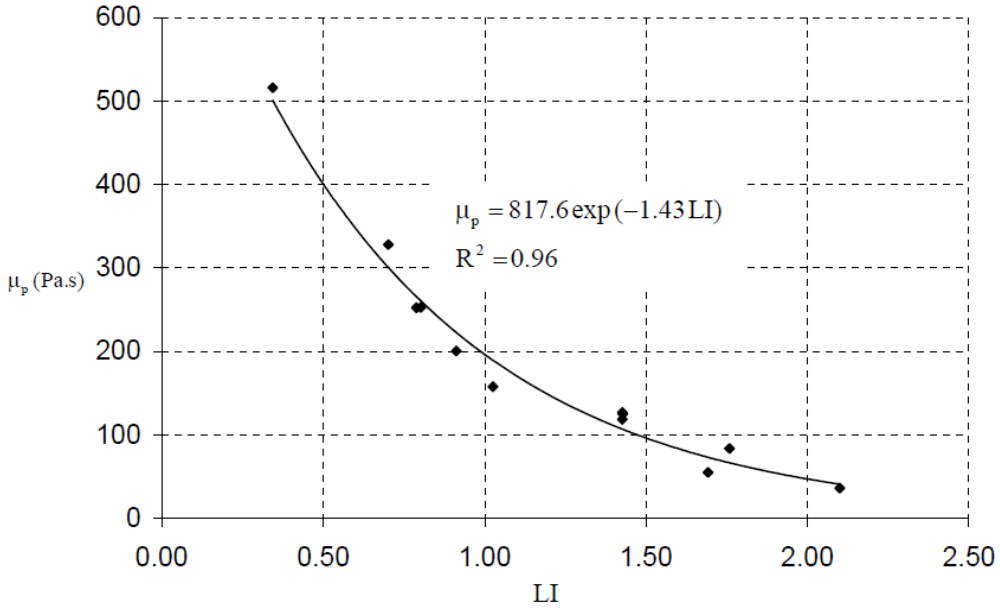

Figure 6-29. Relation between shear viscosity and liquidity index based on the results of the fall cone test on Kaolin (after Mahajan and Budhu, 2006)

Segalini (2008) investigated the rheological behavior of the clay under a constant active stress by performing the unconsolidated undrained (UU) triaxial test with creep steps. Viscose parameters of the soil was obtained from the results of the creep test; besides, the creep test was modeled by a finite different code (i.e. FLAC) for the calibration of the viscous parameters.

Briaud and Garland (1985) proposed the rate effect model to predict the time-dependent behavior of soils. The model can be expressed as follows:

$$\frac{s}{s_1} = (\frac{t}{t_1})^n \tag{6.7}$$

Where the settlement s_1 is the value of settlement "s" observed at a time = 1 minute (after the beginning of a load step); and "*n*" is the creep exponent which is considered a soil property. Typical n values range from 0.005 to 0.03 for sands and 0.02 to 0.08 for clays.

6.6. Unconsolidated Undrained (UU) Triaxial Creep Test

In contexts of this research, and in order to investigate the rheological behavior of the high plasticity clay and investigate the viscos parameters, the UU creep tests were carried out on the soil samples from National Geotechnical Experimental Site (NGES) at Texas A&M University and the Beaumont project. Furthermore, numerical modeling of these tests were performed in FLAC3D, and the viscos parameters were calibrated. Results of the UU creep test, and numerical modeling are briefly presented in this section.

6.6.1. Test Results

Test procedure to perform the UU creep tests is same as the standard triaxial UU test, except for the loading protocol. The loading part is strain control; after the test reaches to the first chosen load, the triaxial device is switched to stress control (or load control) to allow samples to creep for 24 hours. After the creep time, the triaxial device is switched back to strain control and it remains in this mode until reaching the next chosen load. These steps are continued until the sample fails.

For the sample at 8-10 ft, NGES-TAMU clay site, the axial loads equal to 30, 70, 110, 150, 190, 230, and 265 lbs. were kept constant for 24 hours and strain was recorded at constant load. Figure 6-30 presents the change in the strain vs time for each load. The test stopped at the failure load which is 265 lbs.

For the sample at 10-12 ft, NGES-TAMU clay site, the axial loads equal to 70, 110, and 140 lbs. were kept constant for 24 hours and strain was recorded at constant load, while for the sample at 16-18 ft, NGES-TAMU clay site, the holding loads were 150, 190, 230, and 255. Figure 6-31 and Figure 6-32 present the strain-time curve for each load.

For the sample at depth of 33-35 ft. from the Beaumont project, the axial loads at 30, 70, 110, 150, 190 and 230 lbs. were held for 24 hours. Results of the tests on the sample from the Beaumont project is presented in Figure 6-33. The sample failed at 11 psi.

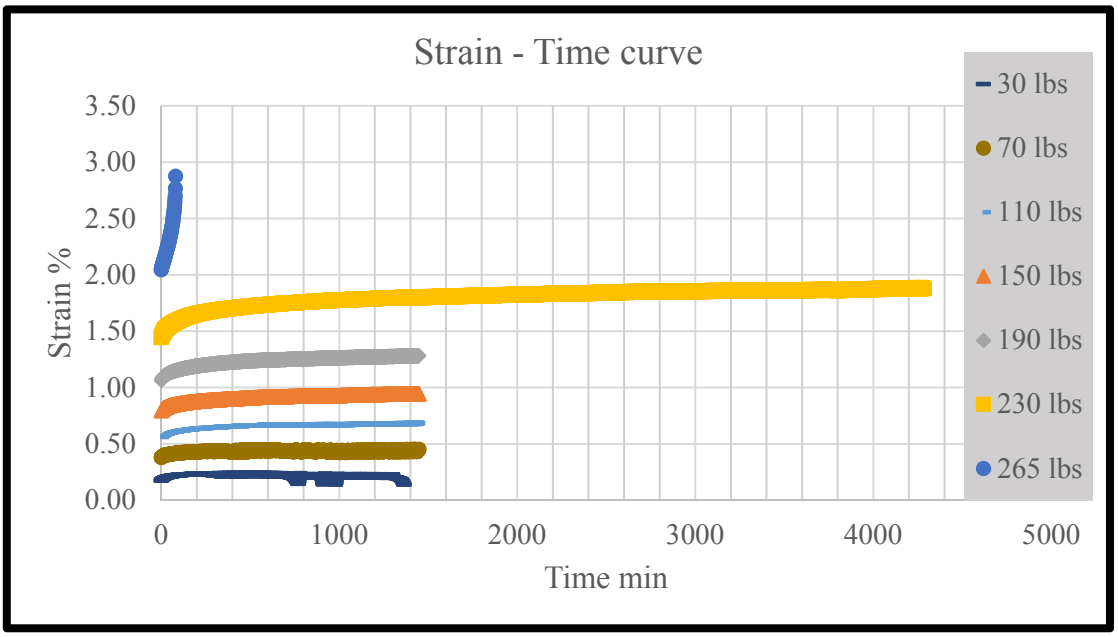

Figure 6-30. Strain time curves (linear scale) for the triaxial UU creep test performed on the sample from NGES-TAMU clay site at the depth of 8-10 ft. (during the tests, holding loads were 30, 70, 110, 150, 190, 230 and 265 lbs.)

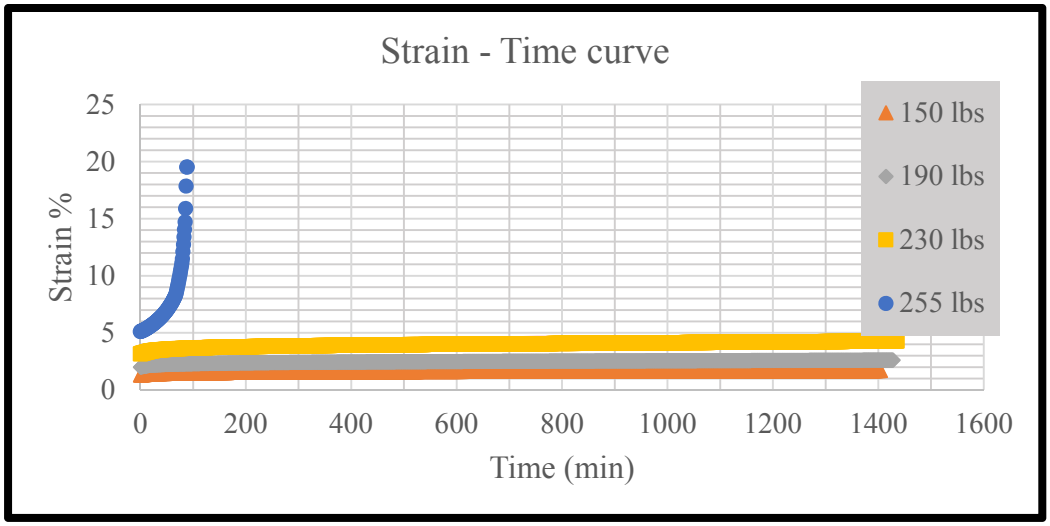

Figure 6-31. Strain time curves (linear scale) for the triaxial UU creep test performed on the sample from NGES-TAMU clay site at the depth of 10-12 ft. (during the tests, holding loads were 150, 190, 230, and 255 lbs.)

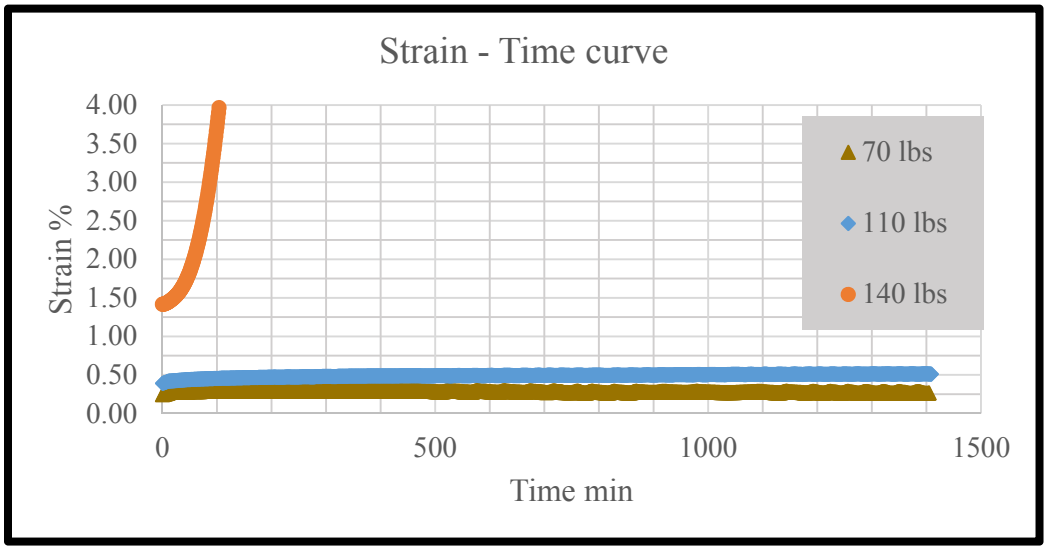

Figure 6-32. Strain time curves (linear scale) for the triaxial UU creep test performed on the sample from NGES-TAMU clay site at the depth of 16-18 ft. (during the tests, holding loads were 70, 110, and 140 lbs.)

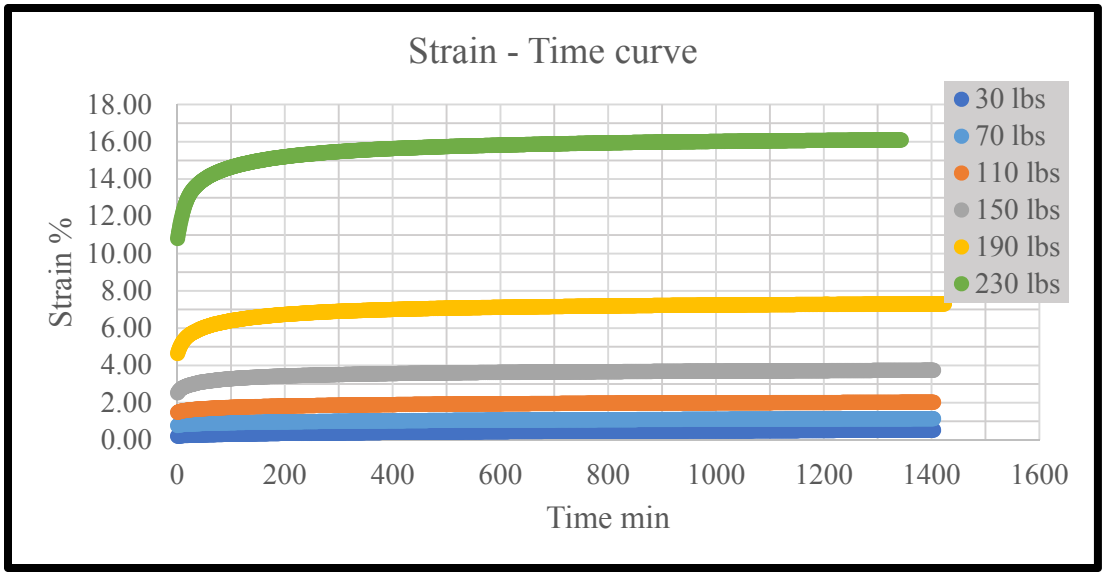

Figure 6-33. Strain time curves (linear scale) for the triaxial UU creep test performed on the sample from Beaumont project at the depth of 33-35 ft. (during the tests, holding loads were 30, 70, 110, 150, 190 and 230 lbs.)

The series of creep curves obtained from the UU triaxial creep test are shown in Figure 6-30 to Figure 6-33. Same behavior as Vyalov (1986) proposed was observed for all the tests. At the higher load, the soil exhibits the excess deformation and the creep rate is remarkably increased. For instance, for the sample from 10-12 ft., at the load 230 lbs. (i.e. one step before failure), soil shows the same behavior as τ_8 in Figure 6-27. In the next loading step, soil failed at 265 lbs. ($\tau_1$in Figure 6-27). No curves were obtained for the creep behavior of the soil in between (i.e. $\tau_7$to $\tau_2$in Figure 6-27). It is concluded that for the load less than 90% of the shear stress at failure creep behavior of the sample are same, and for the shear stress above the 90%, soil tends to fail. Viscous behavior of the soil for the shear stress less than 90% of the shear stress (i.e. yield shear stress) at failure is

different from the viscous behavior for the shear stress above the yield shear stress. Therefore, in the numerical modeling for the shear stress more than 90% of the shear stress at failure, different viscosity were be adopted.

As it was discussed, Briaud and Garland (1985) used the rate effect model to predict the time-dependent behavior of soils. In the UU triaxial creep tests, if the strain-time curve is normalized with s_1 and t_1 respectively, and plotted in log-log scale, the slope of the line is n value. Strain-time curves in log-log scale for the UU triaxial creep test performed at NGES-TAMU clay site are illustrates in Figure 6-34 to Figure 6-36.

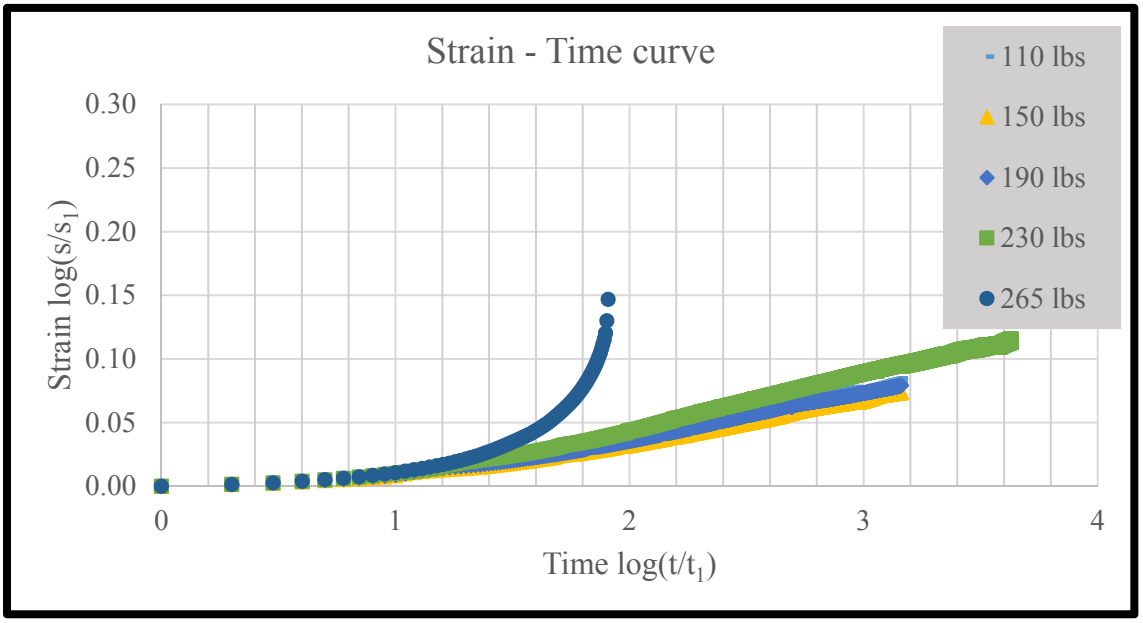

Figure 6-34. Strain – time curves for all the holding loads plotted in log-log scale on the samples from NGES-TAMU clay site depth 8-10 ft.

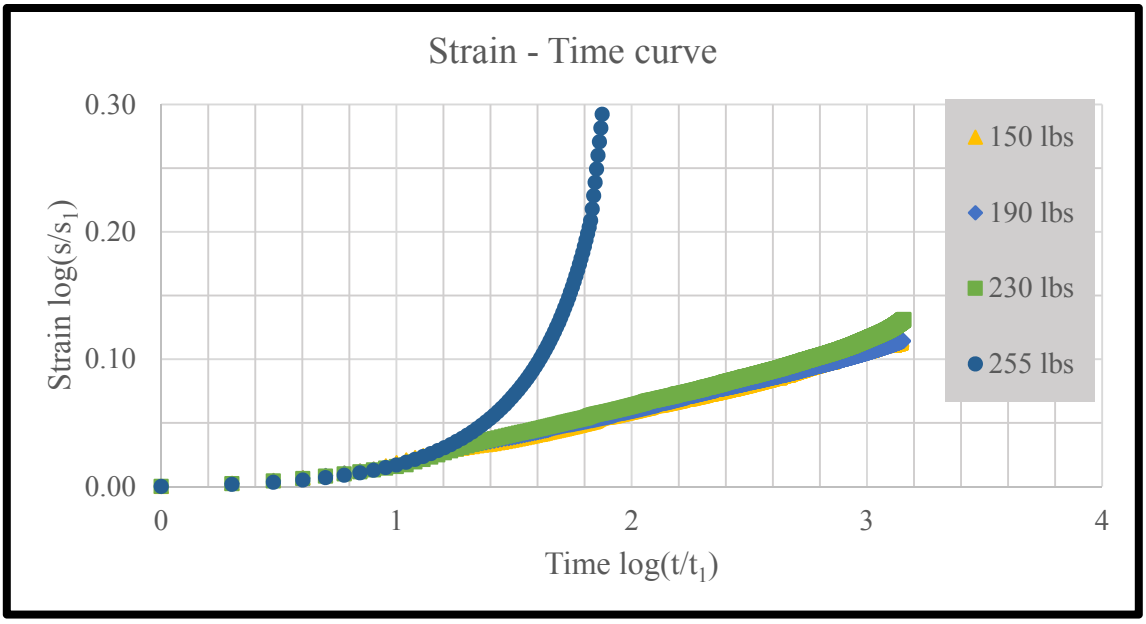

Figure 6-35. Strain – time curves for all the holding loads plotted in log-log scale on the samples from NGES-TAMU clay site depth 10-12 ft.

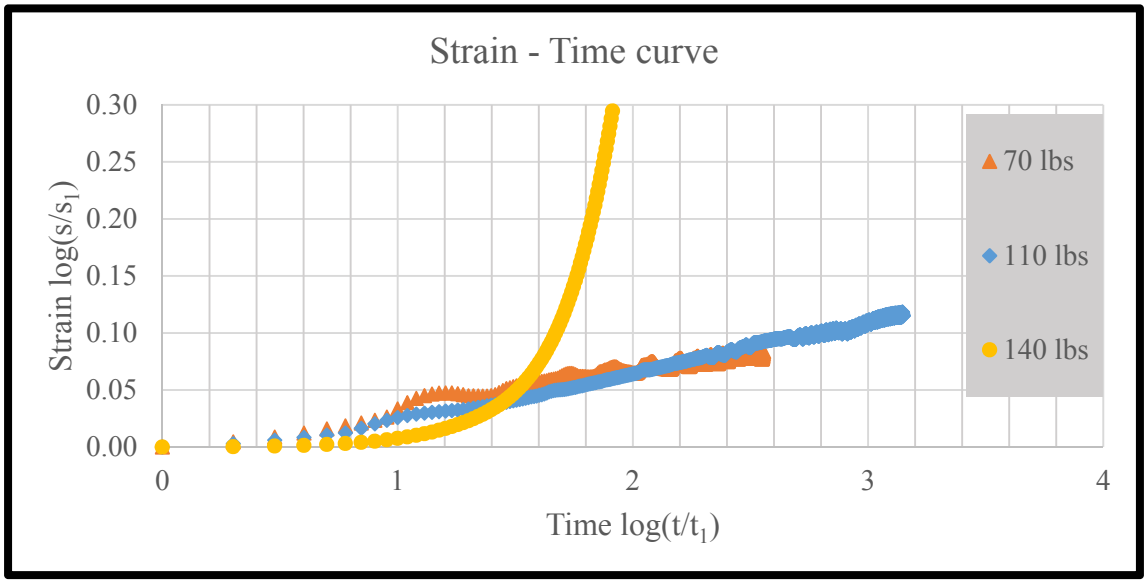

Figure 6-36. Strain – time curves for all the holding loads plotted in log-log scale on the samples from NGES-TAMU clay site depth 16-18 ft.

As it was shown in Figure 6-34 to Figure 6-36, the strain rate for the load less than 90% of the failure load is the same. Significant increase in the strain rate is observed for the loads more than 90% of the failure load. The n value obtained from UU triaxial creep on the soil samples from NGES-TAMU clay site at different depth is presented in Figure 6-37. The n value varies between 0.02 and 0.04.

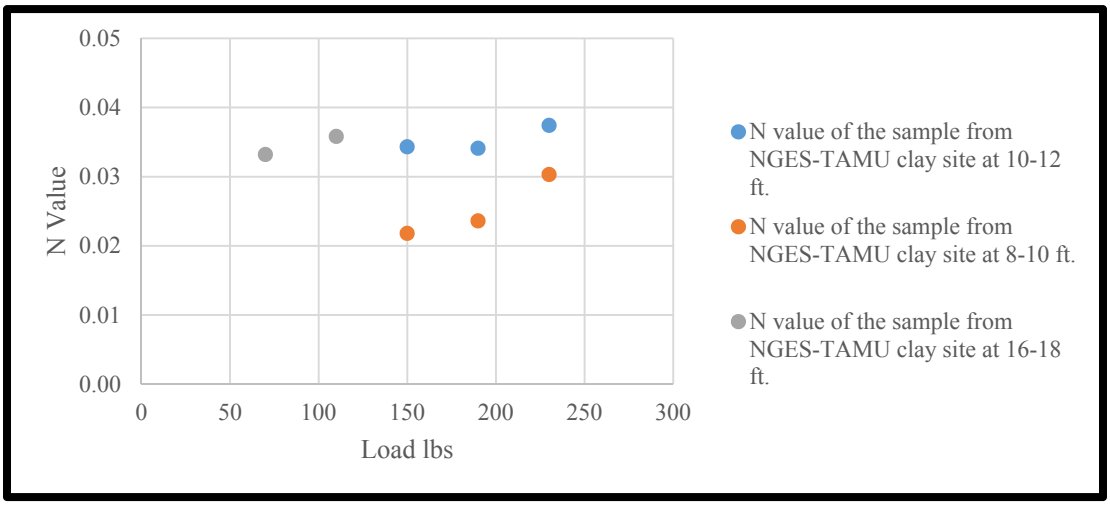

Figure 6-37. The n value obtained from the UU triaxial creep tests on the samples from NGES-TAMU clay site at different depth

Strain-time curve in the log-log scale at different holding loads, and the n value for the UU triaxial creep test performed at the Beaumont site are illustrated in Figure 6-38, and Figure 6-39, respectively. The n value varies between 0.04 and 0.065.

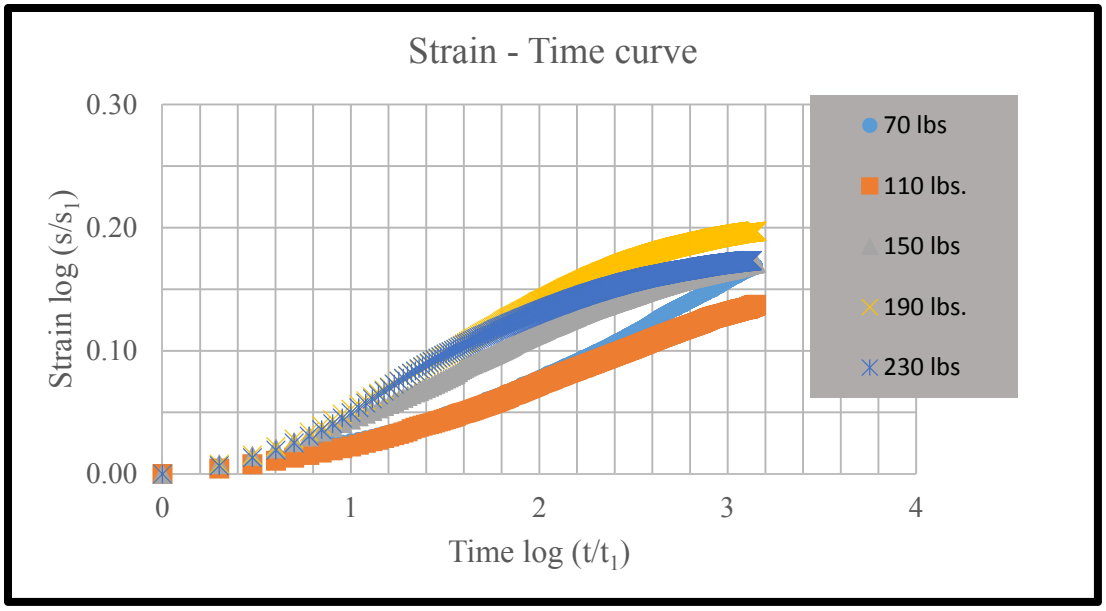

Figure 6-38. Strain – time curves for all the holding loads plotted in log-log scale on the samples from the Beaumont site.

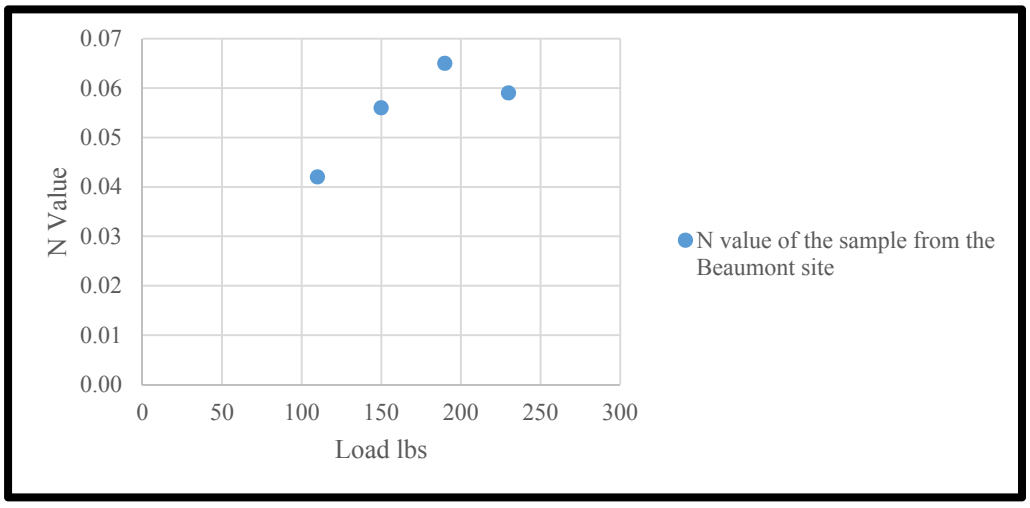

Figure 6-39. The *n* value obtained from the UU triaxial creep tests on the samples from the Beaumont site

The n values obtained from the tests on the sample from the Beaumont are higher than the soil from the NGES-TAMU clay site. The n value is the slope of the strain-time curve in log-log space. Higher the n value means the higher strain rate for the constant load. In other words, the soil samples from the Beaumont site exhibits more viscos behavior (i.e. lower viscosity parameter) than the samples from NGES-TAMU clay site.

It can be concluded that there is a unique curve (i.e. strain-time curve in log-log space) to describe the creep behavior of the clay on the triaxial UU test. By knowing the n value, the creep behavior can be predicted. In this next section, the UU triaxial creep test will be simulated with FLAC3D. The viscos parameters will be calibrated with n value.

6.6.2. Modeling UU Triaxial Creep Test

In order to investigate the relation between the n value and viscosity parameters, UU triaxial creep tests were simulated in FLAC3D. The viscoelastic model known as a Burger model was adopted to simulate the time-dependent behavior. The numerical modeling was calibrated with the laboratory UU creep tests. Table 6-6 summarizes the adopted viscous parameters at each test for different n values.

Table 6-6. Adopted viscosity in the modeling for the different n value

Soil sample	load (lbs)	n value	m vis (lb*s/ft2)	m shear (lb/ft2)	k shear (lb/ft2)	k vis (lb*s/ft2)
NGES-TAMU 8-10 ft.	150	0.021	9.00E+10	1.00E+06	6.00E+05	4.50E+09
NGES-TAMU 8-10 ft.	190	0.023	1.12E+11	1.00E+06	4.50E+05	4.50E+09
NGES-TAMU 8-10 ft.	230	0.033	1.45E+11	1.00E+06	3.10E+05	4.50E+09
NGES-TAMU 10-12 ft.	150	0.034	3.34E+10	1.00E+06	2.08E+05	1.15E+09
NGES-TAMU 10-12 ft.	190	0.0341	3.34E+10	1.00E+06	2.08E+05	1.15E+09
NGES-TAMU 10-12 ft.	230	0.0374	1.45E+10	1.00E+06	1.50E+05	1.15E+09
NGES-TAMU 16-18 ft.	110	0.035	6.80E+10	1.00E+06	5.00E+05	1.60E+09
Beaumont site 33-35 ft.	110	0.042	2.20E+10	1.00E+06	1.00E+05	7.00E+08
Beaumont site 33-35 ft.	150	0.056	2.00E+10	1.00E+06	5.50E+04	3.00E+08
Beaumont site 33-35 ft.	190	0.0658	2.00E+10	1.00E+06	2.80E+04	2.00E+08
Beaumont site 33-35 ft.	230	0.059	1.70E+10	1.00E+06	1.60E+04	8.00E+07

Relation between n value and different viscous parameters adopted in the numerical modeling are plotted in Figure 6-40 to Figure 6-42. It is noted that the viscous parameters in the Burger model include spring and dashpot for the Maxwell element, Mshear, and Mvis, respectively, and spring and dashpot for the Kelvin element, Kshear and Kvis, respectively.

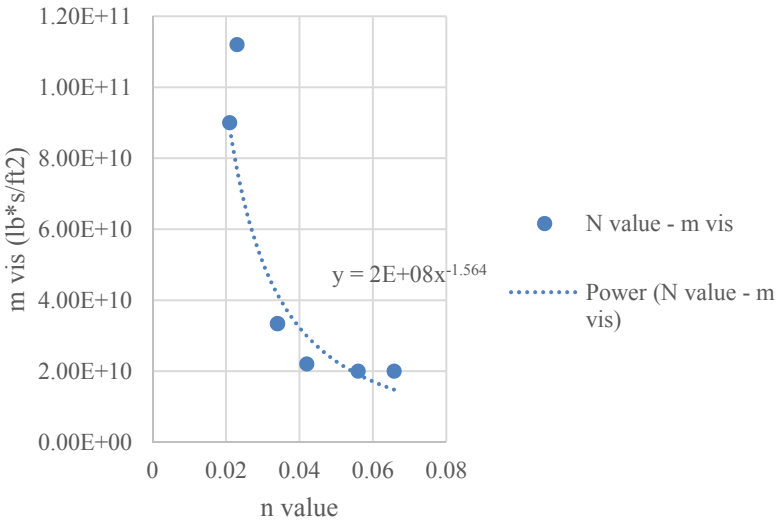

Figure 6-40. Relation between *n* value and mvis ($y = 2E+08x^{-1.564}$), (viscosity of the Maxwell element in the Burger model).

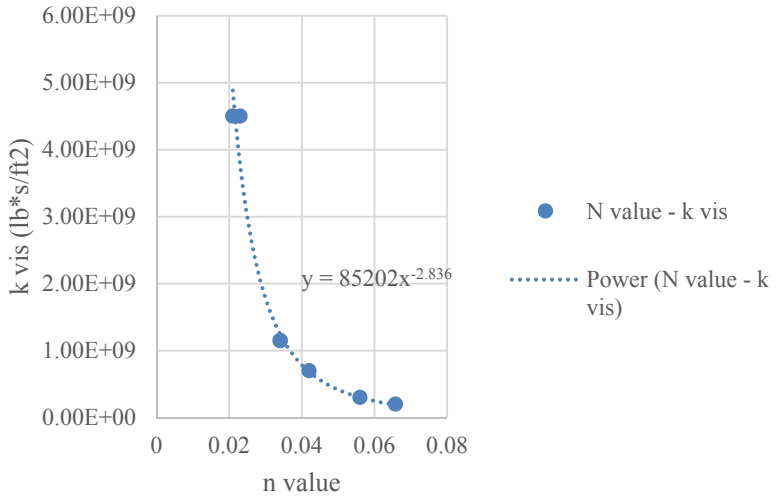

Figure 6-41. Relation between *n* value and kvis ($y = 85202x^{-2.836}$), (viscosity of the Kelvin element in the Burger model).

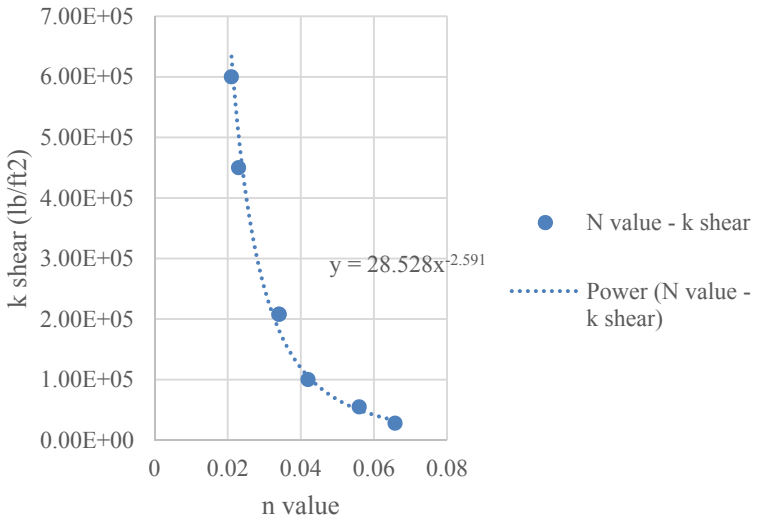

Figure 6-42. Relation between *n* value and kshear ($y = 28.528x^{-2.591}$), (stiffness of the Kelvin element in the Burger model).

Figure 6-43 to Figure 6-46 illustrate the strain-time curve obtained from the numerical modeling and compare to the results of the laboratory UU triaxial creep tests.

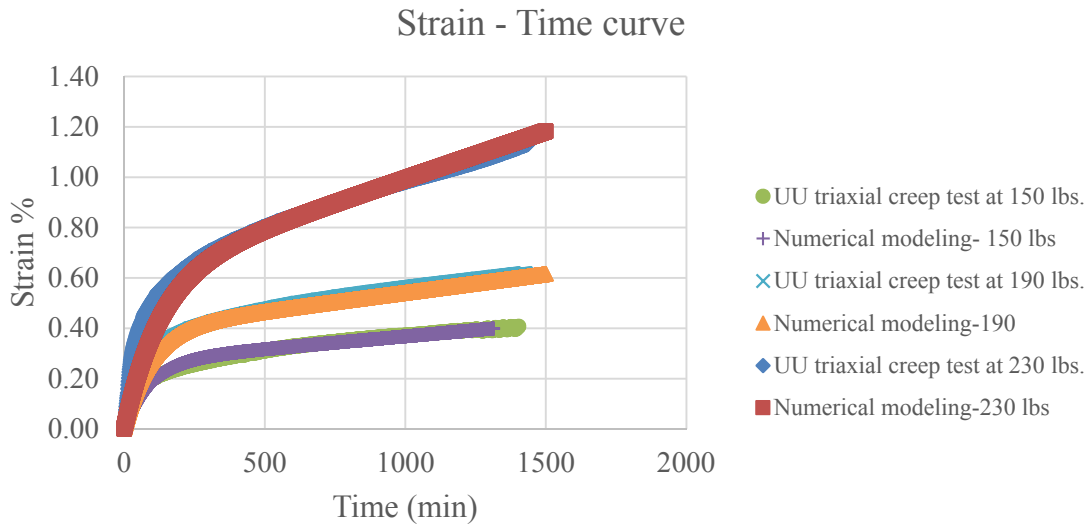

Figure 6-43. Strain-time curve for the both numerical modeling and UU triaxial creep test on the sample from the NGES-TAMU clay site at the depth of 10-12 ft.

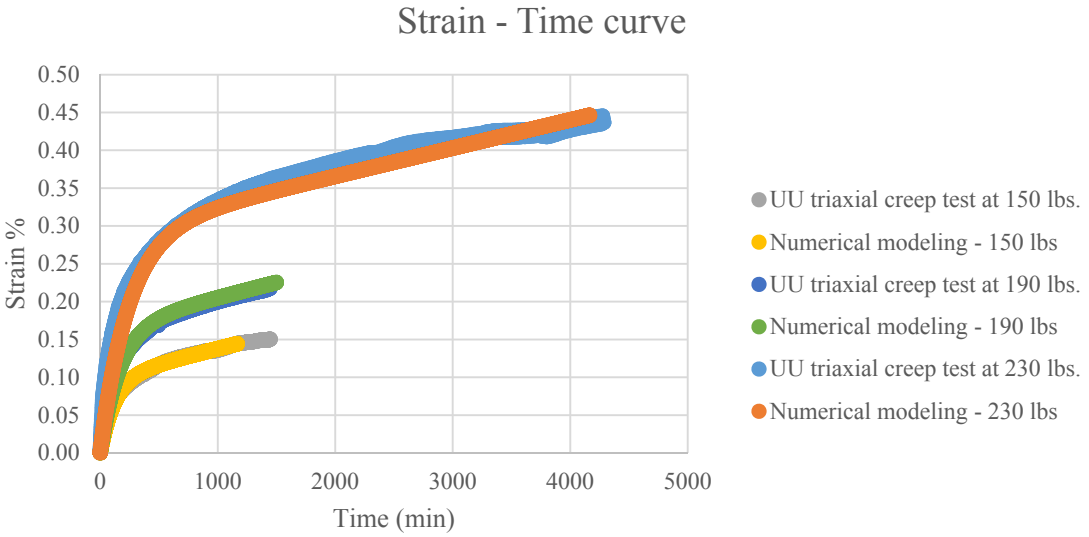

Figure 6-44. Strain-time curve for the both numerical modeling and UU triaxial creep test on the sample from the NGES-TAMU clay site at the depth of 8-10 ft.

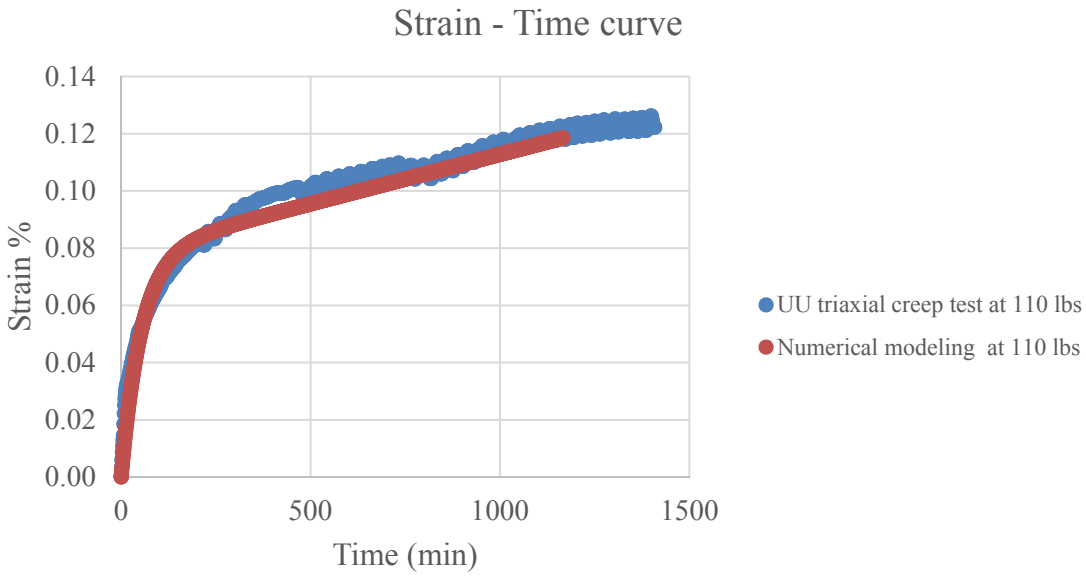

Figure 6-45. Strain-time curve for the both numerical modeling and UU triaxial creep test on the sample from the NGES-TAMU clay site at the depth of 16-18 ft.

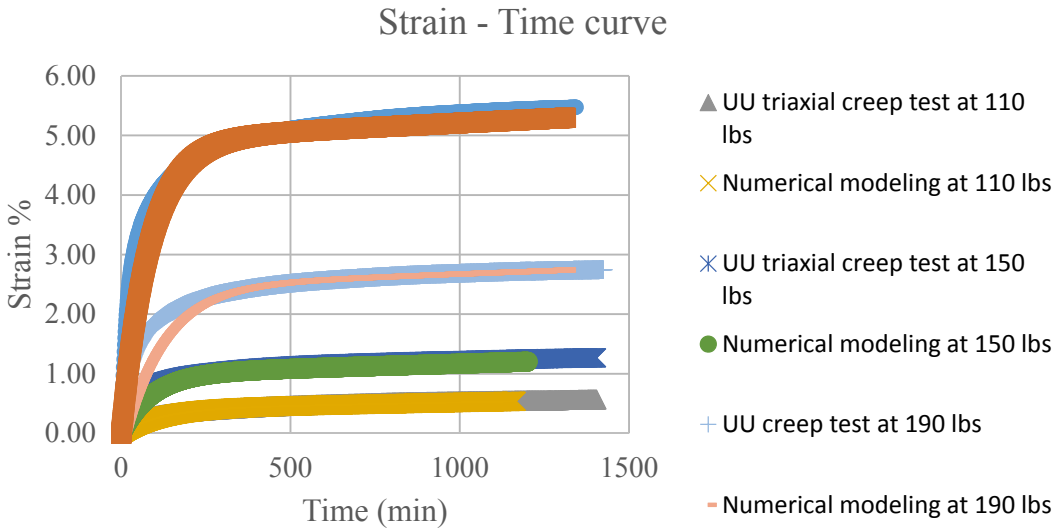

Figure 6-46. Strain-time curve for the both numerical modeling and UU triaxial creep test on the sample from the Beaumont site at the depth of 33-35 ft.

Results of the numerical modeling of the UU creep tests show that the finite difference modeling with FLAC3D can be applied to study the time-dependent behavior of the high-plasticity clay. Good agreement has been obtained from the results of the numerical modeling and laboratory test. Viscous parameters obtained from modeling of the UU triaxial creep test will be used in modeling the soil nail wall after the construction.

6.7. Simulation of Soil Nail Wall After Construction

6.7.1. Introduction

In this section, the time dependent behavior of the soil nail wall after the construction is simulated. After the construction, a soil nail wall and the soil behind it tend to deform outwards (GEC#7, 2003). For the soil nail wall project at Beaumont, at station 1+46, the maximum lateral displacement at the end of the construction took place at top of the wall and decreased towards the toe of the wall. Maximum horizontal displacement at top of the wall is 1.85 in. at the end of the construction which is 0.006 times of the height of the wall (i.e. 25 ft.). The deformation of the wall for a period of one year after the construction at top of the wall was 0.2 in. which is 10% of the deformation observed soon after construction. The creep behavior of the wall is simulated with the creep models available in FLAC3D, and the model is calibrated with the results of the post monitoring of the soil nail wall at Beaumont project. Details of modeling the wall are presented in this section.

6.7.2. FLAC3D Model – After Construction

Long-term behavior of soil nail wall at Beaumont project was simulated with FLAC3D. The in-situ stresses and displacement of the soil nail wall at the end of the construction (obtained from the numerical modeling of the soil nail wall at the end of the construction), were used as the initial condition for modeling the wall after the construction. In order to implement the rheological model (i.e. Burger mechanical model), the Mohr-Coulomb mechanical model of the soil is substituted with the Burger model to simulate the long-term behavior. The viscous behavior of the soil was taken from the results of the UU triaxial creep test on the soil samples from the Beaumont project.

The results of the horizontal deformation of top of the soil nail wall at the Beaumont project, for both creep analysis for one year and one year post-monitoring of the wall is presented in Figure 6-47. As it was discussed before, lateral displacement of the Beaumont soil nail wall at station 1+46 for one year post-monitoring was 0.18 in. which is 10% of the deformation observed soon after construction. Contours of creep deformation for one year after the construction is presented in Figure 6-48.

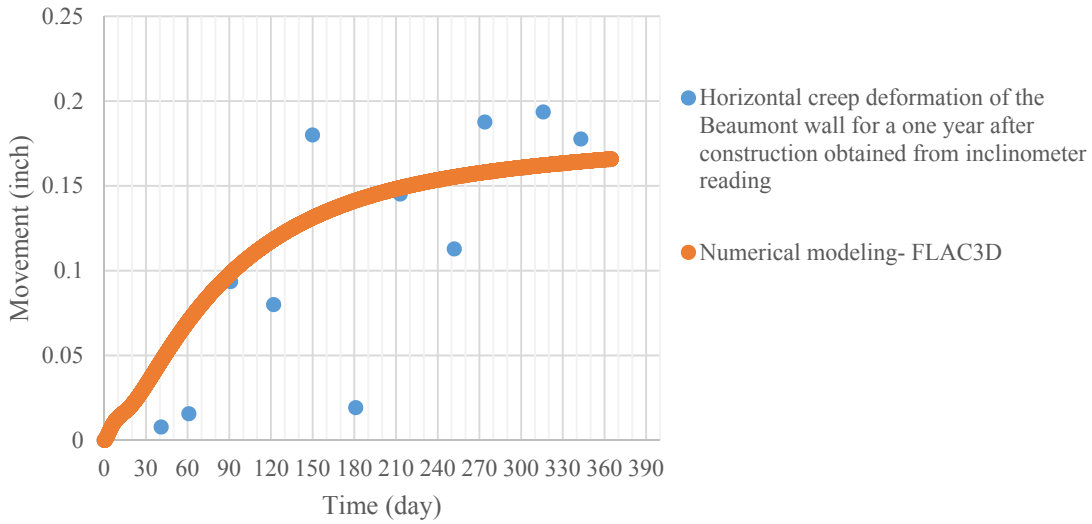

Figure 6-47. Horizontal deformation of top of the wall for one year post-monitoring of the wall and the model and (Horizontal deformation of the wall at the end of the construction reset to zero).

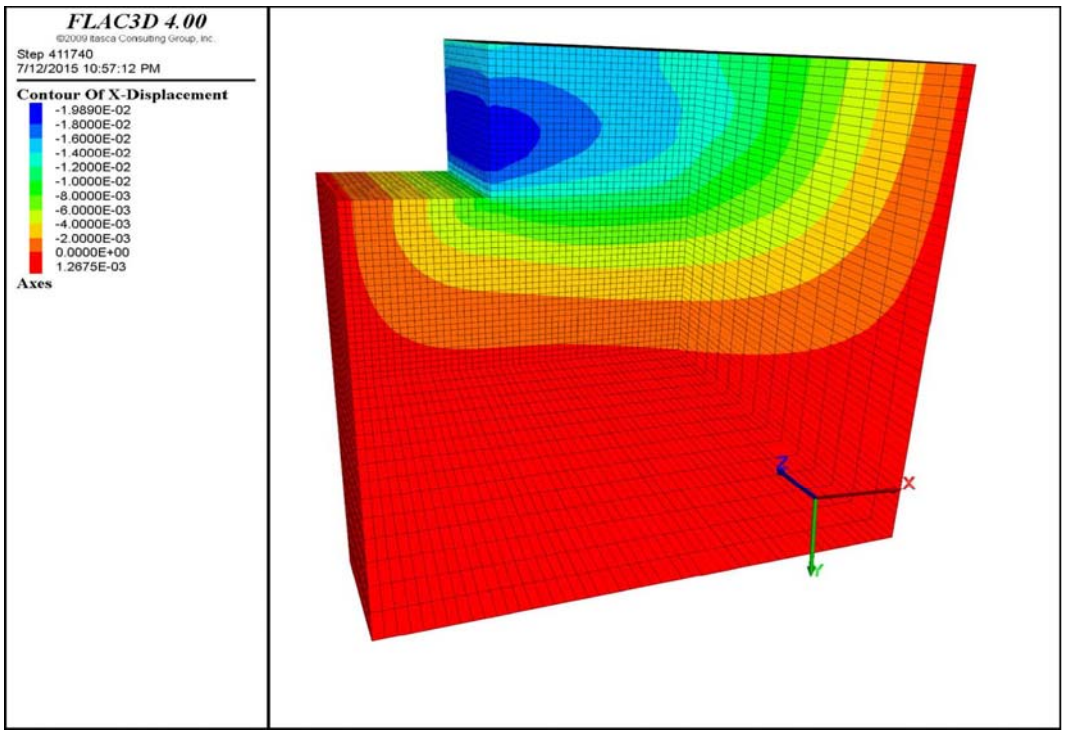

Figure 6-48. Contours of creep deformation of the Beaumont project for a period of one year after the construction

The cable structural elements were used to simulate the soil nail. The axial load in the nails for a period of one year after the construction is shown in Figure 6-49.

In Figure 6-50 to Figure 6-55, the increase in the load due to the creep movement of the wall for both numerical modeling and results of the strain gauges is illustrates. It is seen that there is very good agreement between results of the monitoring and numerical modeling.

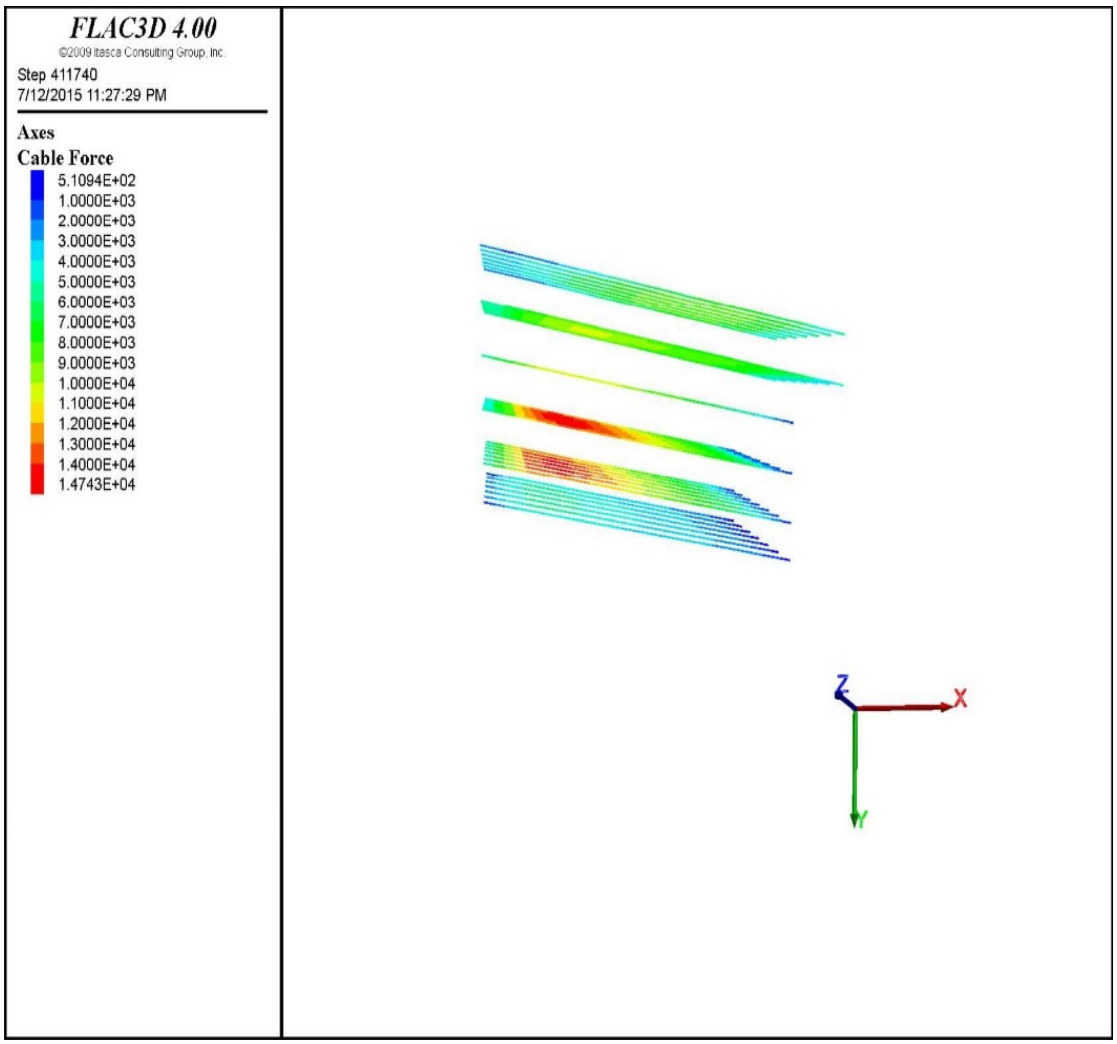

Figure 6-49. Axial load in the nails for one year after the construction.

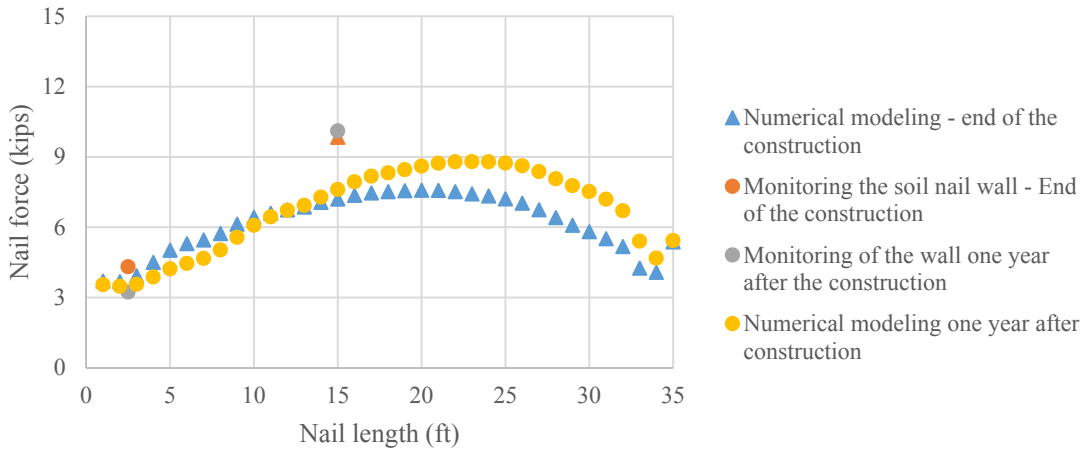

Figure 6-50. Axial load in the nails at the first row at the end and after the construction for both numerical modeling and inclinometer reading at Beaumont project.

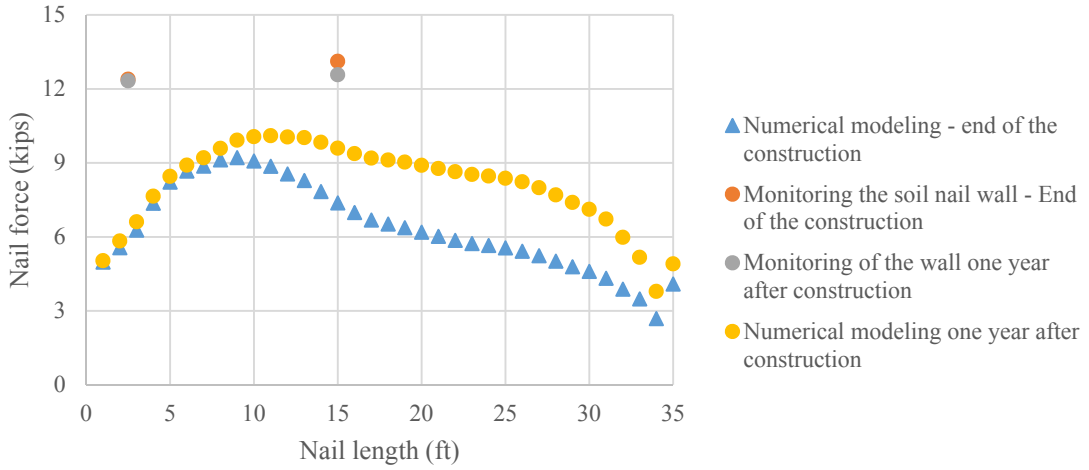

Figure 6-51. Axial load in the nails at the second row at the end and after the construction for both numerical modeling and inclinometer reading at Beaumont project.

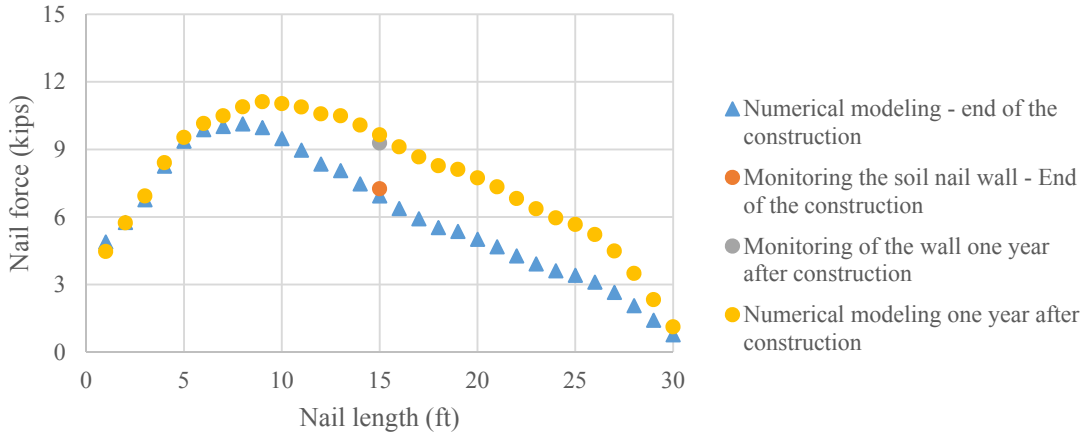

Figure 6-52. Axial load in the nails at the third row at the end and after the construction for both numerical modeling and inclinometer reading at Beaumont project.

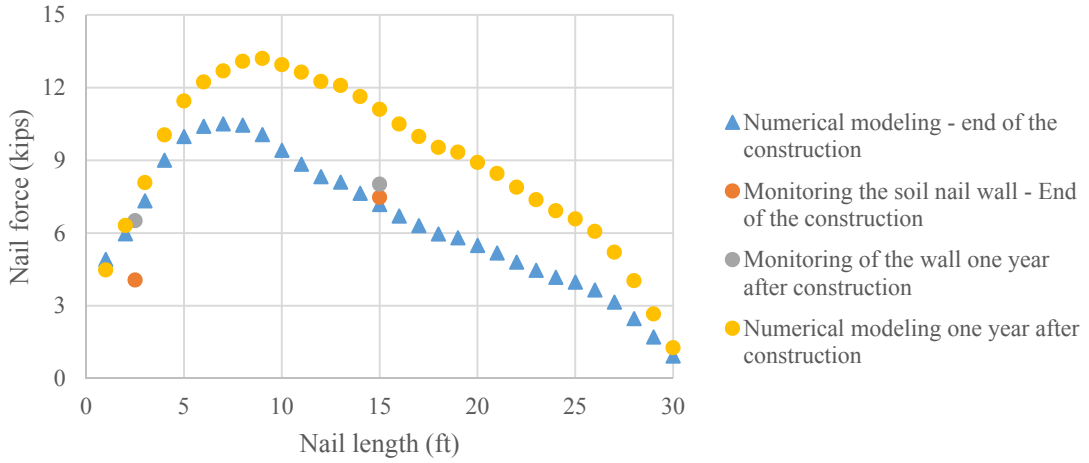

Figure 6-53. Axial load in the nails at the fourth row at the end and after the construction for both numerical modeling and inclinometer reading at Beaumont project.

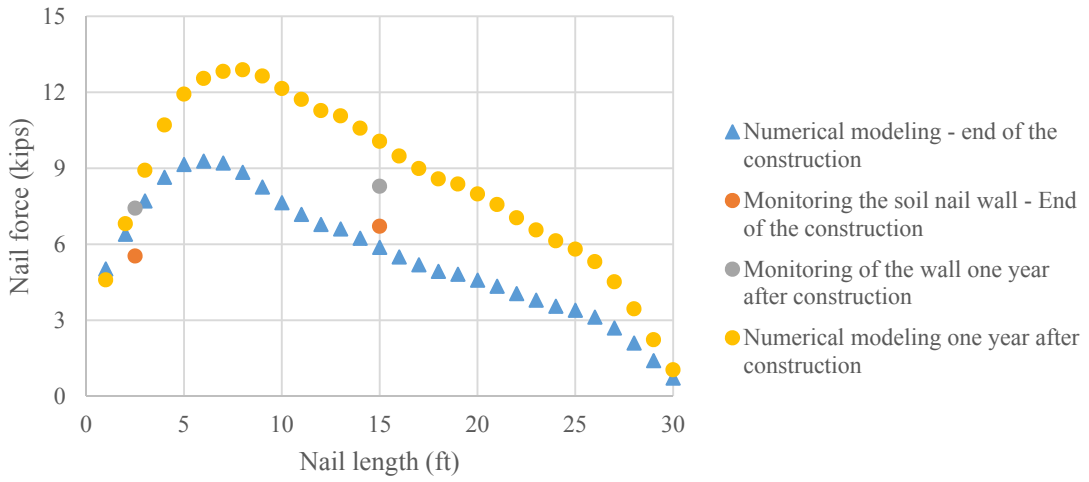

Figure 6-54. Axial load in the nails at the fifth row at the end and after the construction for both numerical modeling and inclinometer reading at Beaumont project.

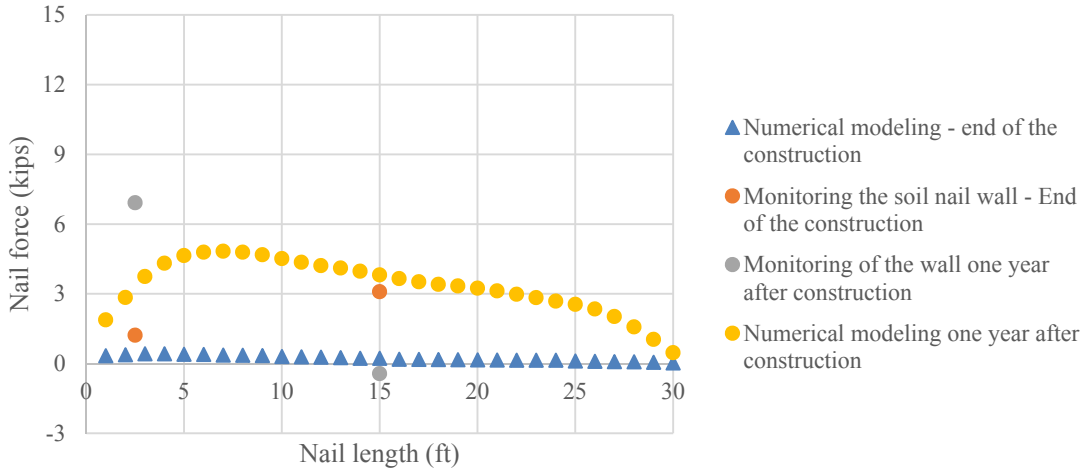

Figure 6-55. Axial load in the nails at the six row at the end and after the construction for both numerical modeling and inclinometer reading at Beaumont project.

As it was shown, the complex behavior of the soil nail wall in high plasticity clay can be modeled in FLAC3D. The adopted rheological model, the Burger model, can assess the creep behavior of the soil nail wall for a period after construction. The validated numerical code will be used to perform the parametric study. Typical Texas turn around soil nail wall was modeled and used as the base case. For the subsequent cases, one parameter at a time were changed in the base case, and influence of this particular parameter on the long-term performance of the soil nail wall were investigated.

6.8. Parametric Study

6.8.1. Introduction

The complex long-term behavior of the soil nail wall in high plasticity clay was modeled in advanced geotechnical finite difference code, FLAC3D. The model was calibrated with the results of the instrumentation and monitoring the slope repair project at Beaumont district. Parametric study was used to study the behavior of soil nails walls exploring other scenarios and cases. Since the soil nail wall at Beaumont project is not the typical soil nail wall in Texas, parametric study was performed on the typical Texas turn around soil nail wall used widely in Texas. Typical soil nail wall Texas turnaround is illustrated in Figure 6-56.

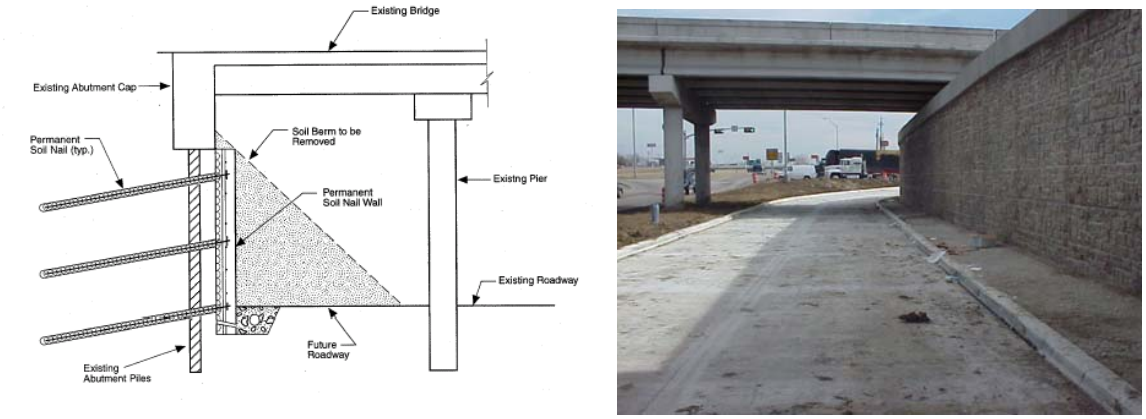

Figure 6-56. Typical soil nail wall "Texas turn around".

The soil nail wall shown in Figure 6-56 was used as the base case in parametric study. For the subsequent cases, one parameter at the time was changed respect to the base case, and influence of this particular parameter on the long-term performance of the soil nail wall was investigated.

6.8.2. Geometric Configuration of Base Case (Texas Turn Around)

Soil nail wall located at IH-40 (i.e. project 0275-01-168) was selected to use as the baseline case. Soil nail wall layout is presented in Figure 6-57 and Figure 6-58. Soil nail wall consists of five rows of the 22 ft. long nails. Table 6-7 summarizes the geometric configuration and other design details of the soil nail wall. Since the aim of this modeling is to evaluating the long-term behavior of the soil nail wall, drained strength was considered.

Table 6-7. Soil nail wall geometry and other parameters

Parameter	Value
Vertical height of the wall, H (ft.)	25
Face batter α (degree)	0
Backslope angle β (degree)	0
Yield strength of the reinforcement fy (ksi)	75
Diameter of the reinforcement d (in.)	0.86
Drill hole diameter (in.)	6
Spacing Sh x Sv (ft.)	3.5 x 3.0
Length of the nails (ft.)	22
Inclination of the nails (degree)	10
Number of rows of the nail	5
Drained cohesion c' (psf.)	0
Drained fiction angle Φ' (degree)	26
Unit weight (pcf)	125
Bond stress (psf.)	900
Surcharge (psf.)	250

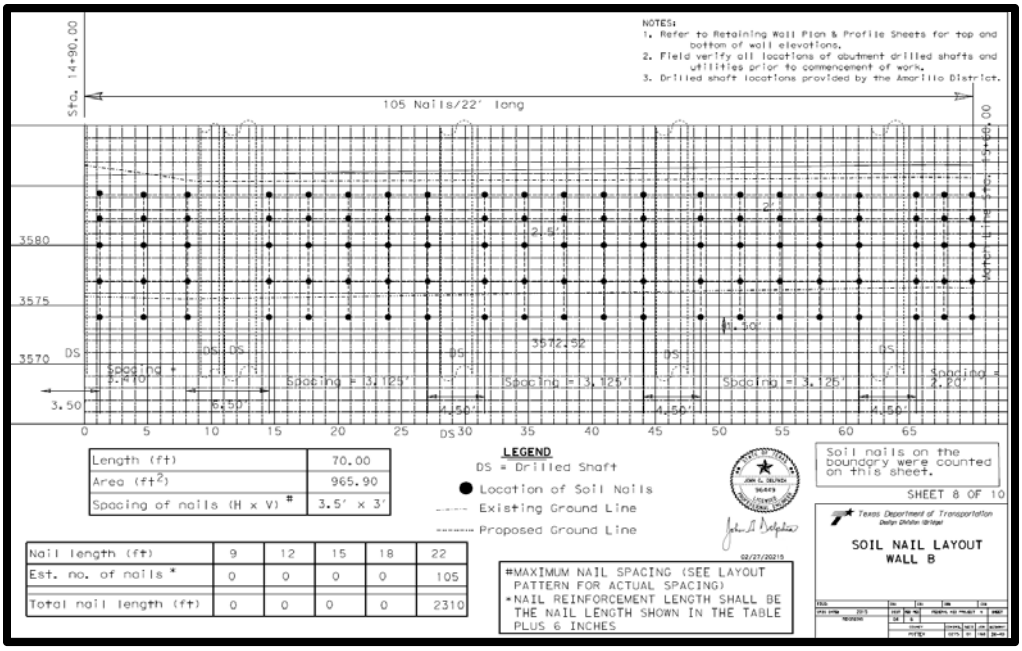

Figure 6-57. Soil nails pattern on the wall face.

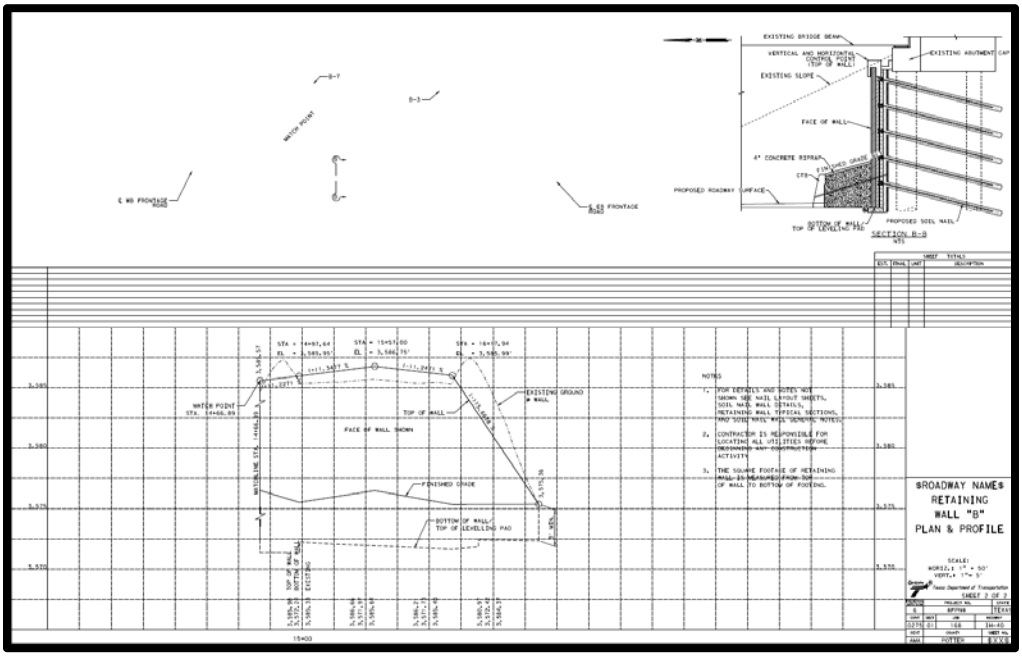

Figure 6-58. Soil nail wall cross section and details

6.8.3. Simulation of Base Case at End of Construction

Prior on simulating the soil nail in FLAC3D, the soil nail wall was modeled in ASD-based limit equilibrium slope stability program, SNAILZ. The parameters presented in Table 6-8, was entered as the input parameters. Results of the modeling the wall in SNAILZ is presented in Figure 6-59. It is noted that the ultimate pullout capacity of the nails obtained from the test on the sacrificial nail was an average of 900 psf. (6.3 psi), while the design bond stress is equal to 300 psf. Traffic load equal to 250 psf. (equal to 2 ft. of the embankment soil) was applied to top of the wall. Factor of safety and maximum load in the nails are shown in Figure 6-59 and Table 6-8, respectively.

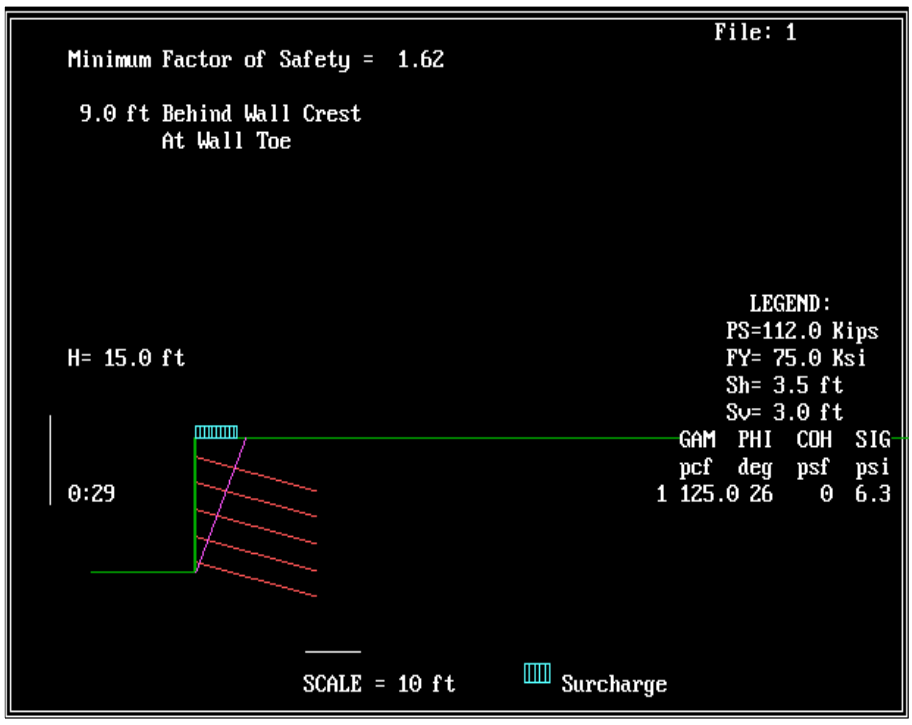

Figure 6-59. Safety factor obtained from SNAILZ.

Table 6-8. Maximum tensile load obtained from SNAILZ along the nails.

Nail #	Nail force (kips)
Nail#1 (first row)	4.8
Nail#2 (second row)	5.3
Nail#3 (third row)	5.8
Nail#4 (fourth row)	6.4
Nail#5 (fifth row)	6.9

In this phase, soil nail wall located at IH-40 (i.e. baseline case) was modeled in FLAC3D. The step by step procedures of modeling the soil nail wall with FLAC3D was presented in section 6.3 (numerical modeling). Parameters adopted in Numerical modeling with FLAC3D are presented in Table 6-9. Same geometry configuration explained in Table 6-7 was adopted.

Table 6-9. Parameters adopted for numerical simulation of the soil nail wall at IH-40 (baseline case).

Material	Constitutive model	Properties
Embankment soil	Mohr-Coulomb	Φ'=26, C'=0, Y=125 pcf, E=2.9e5 psf. , υ=0.3
Soil nails (cable element)	Elastic-perfectly plastic	E steel=4.17e9 psf (200 GPa), c_grout=1e3 psf , Φ_grout=20 degree
Shotcrete (shell element)	Elastic (isotropic)	E shot = 2.2e8 psf, υ=0.25, thickness=4 in.

Contours of horizontal movement of top of the wall and load distribution along the nails at the end of the construction is presented in Figure 6-60 and Figure 6-61.

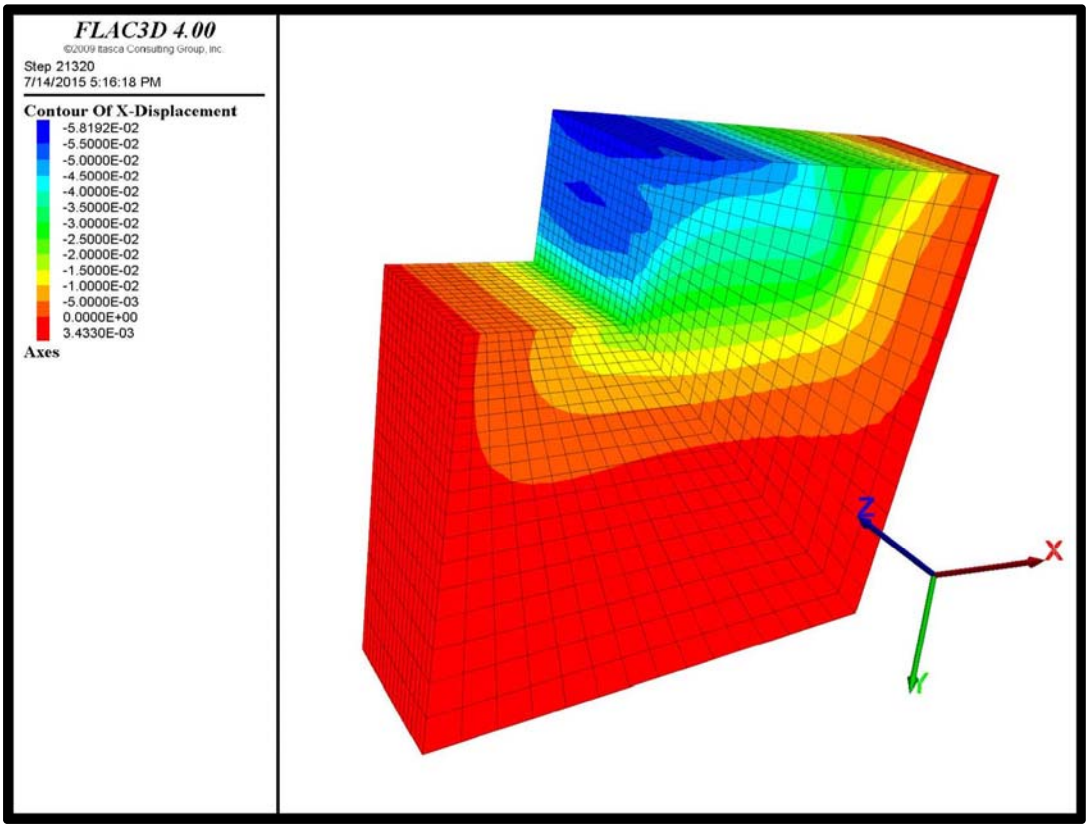

Figure 6-60. Horizontal deformation of the baseline wall at the end of the construction (unit of the x-displacement presented in this figure is ft.)

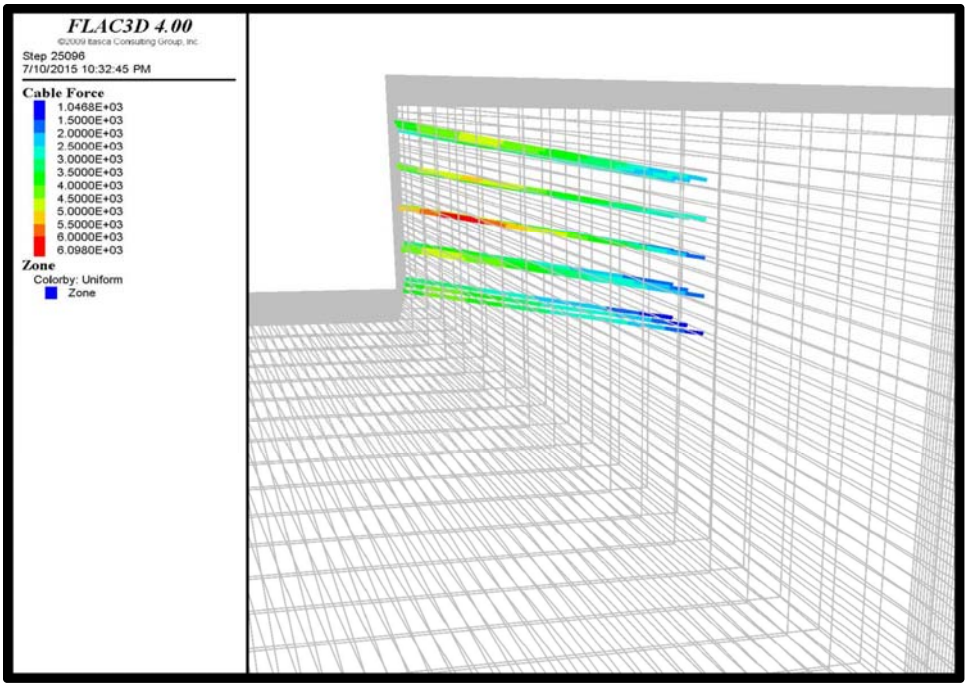

Figure 6-61. Force in the nails for the base case after the construction (unit of the cable force presented in this figure is lb.)

A very good agreement between results of modeling in SNAILZ and FLAC3D was observed. Except the axial load in the bottom row of the nail. Monitoring the soil nail wall at Beaumont project was shown that the significant portion of the axial load in the nails occurs at the subsequence stage of excavation. Since after installing the last row of the soil nail, there is no more excavation takes place, axial load in nails in this row is not developed until the soil nail wall experiences some movement.

6.8.4. Simulation of Base Case after Construction

The in-situ stresses and displacement of the soil nail wall at the end of the construction were used as the initial condition for modeling the wall after the construction.

In order to implement the rheological model (i.e. Burger mechanical model), the Mohr-Coulomb mechanical model of the soil is substituted with the Burger model to simulate the long-term behavior.

Horizontal displacement at the top of the wall and additional service load in the nails due to the creep of the soil nail wall obtained from numerical modeling is shown in Figure 6-62 and Figure 6-63, respectively.

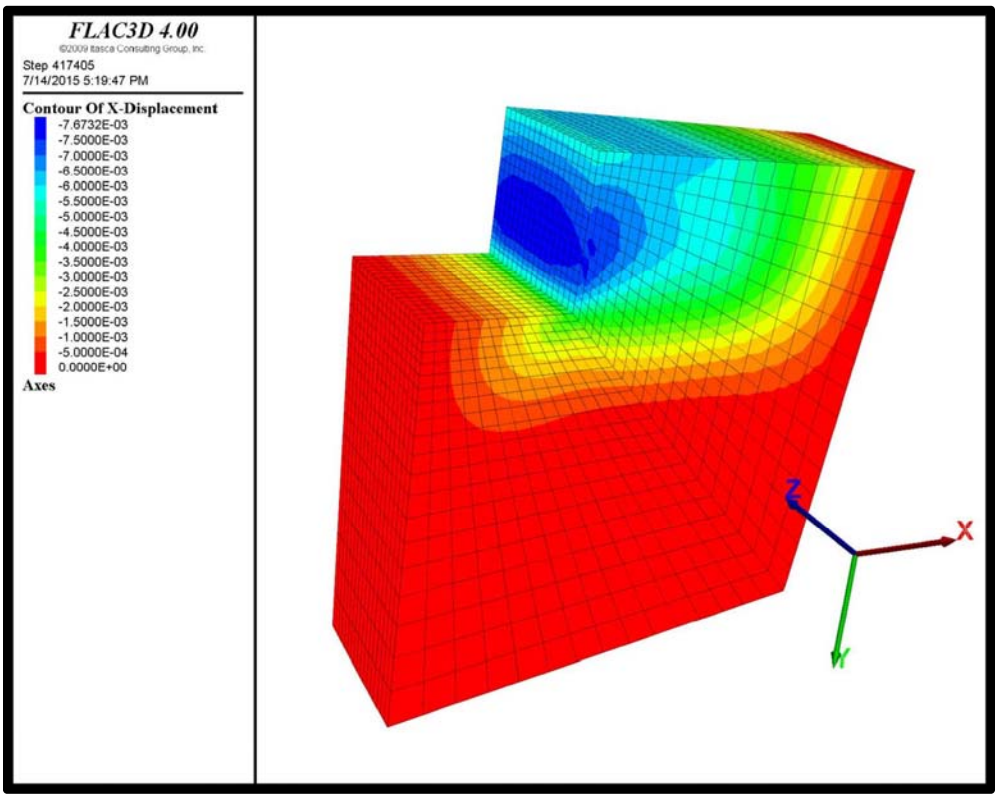

Figure 6-62. Horizontal deformation of top of the wall obtained from modeling (Horizontal deformation of the wall at the end of the construction reset to zero-unit of deformation in plot is ft.).

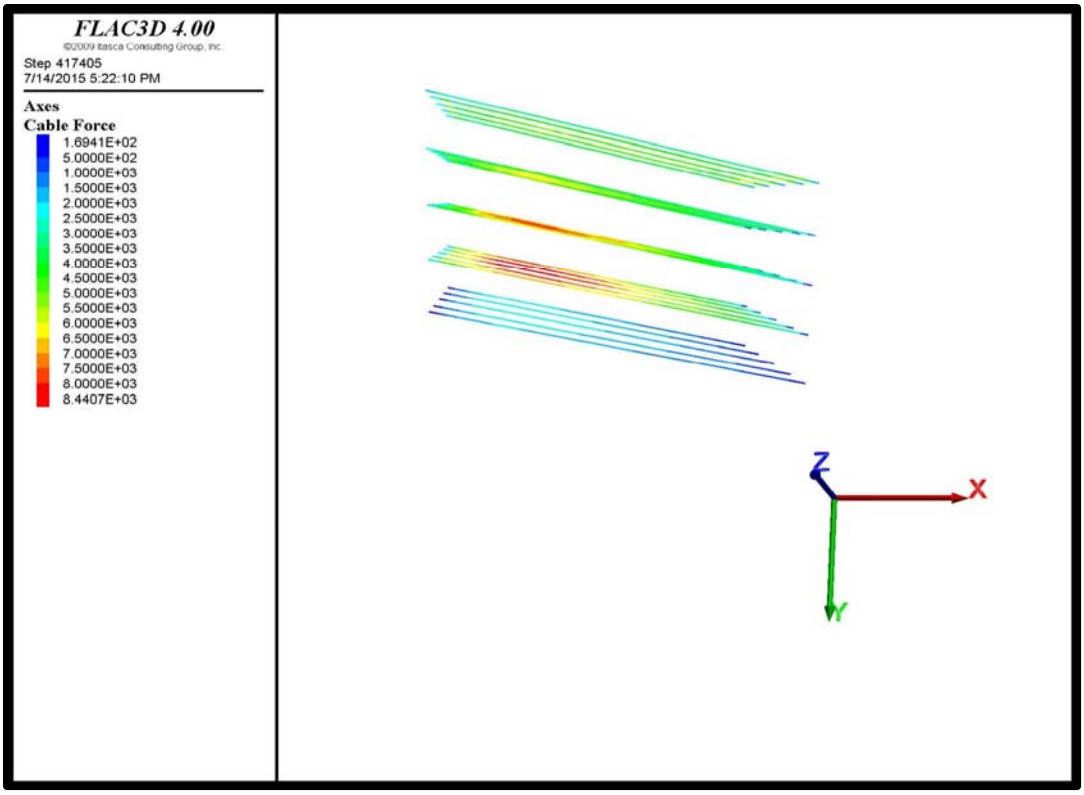

Figure 6-63. Additional axial load in the nails due to the extra horizontal displacement of the wall after construction obtained from modeling (unit of force in plot is lb.)

Figure 6-64 illustrates the profile of the horizontal movement of the wall at end of the construction along with one year after the construction. Movement of top of the wall for a period of one year after construction is shown in Figure 6-65. Rate of the movement is increased gradually and reach to the constant rate. In the word, soil nail wall exhibit more creep deformation and gradually the rate of the creep movement is decreased.

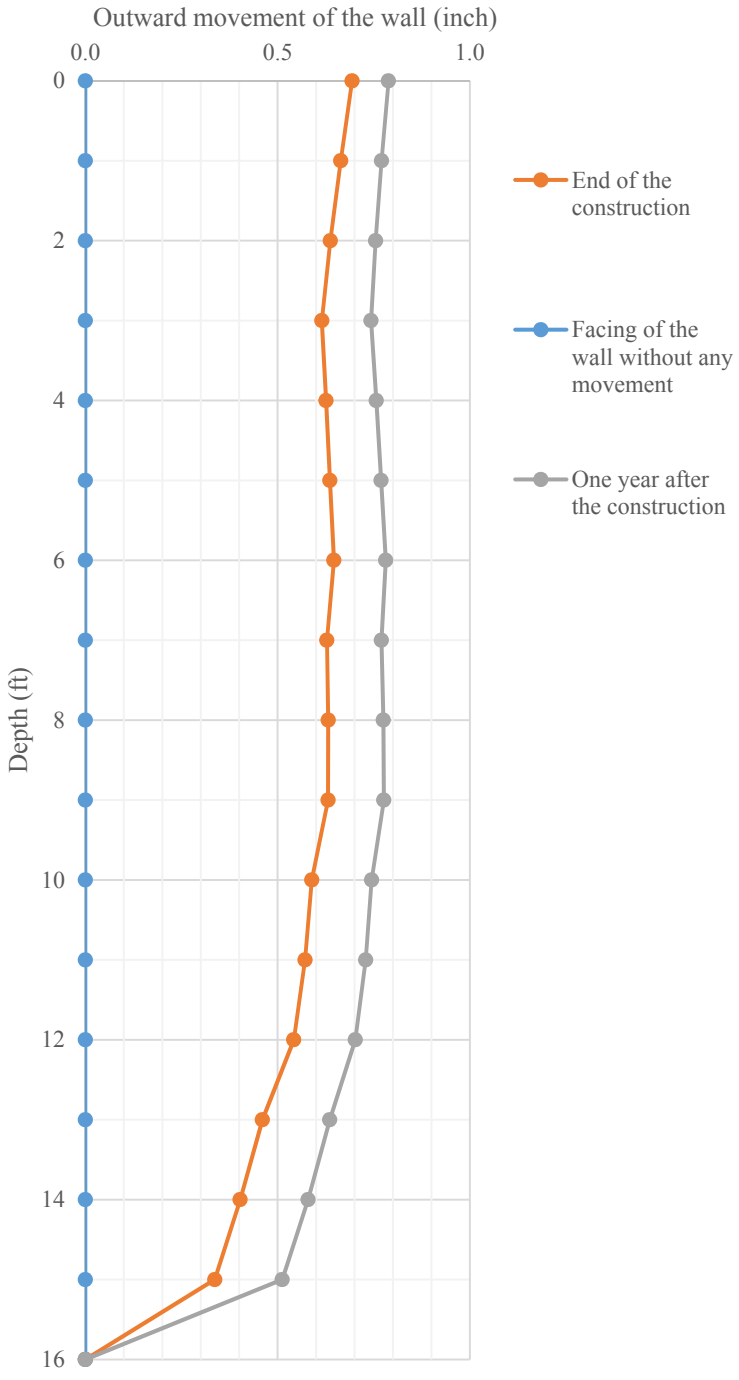

Figure 6-64. Profile of the horizontal movement of the soil nail wall for one year after the construction.

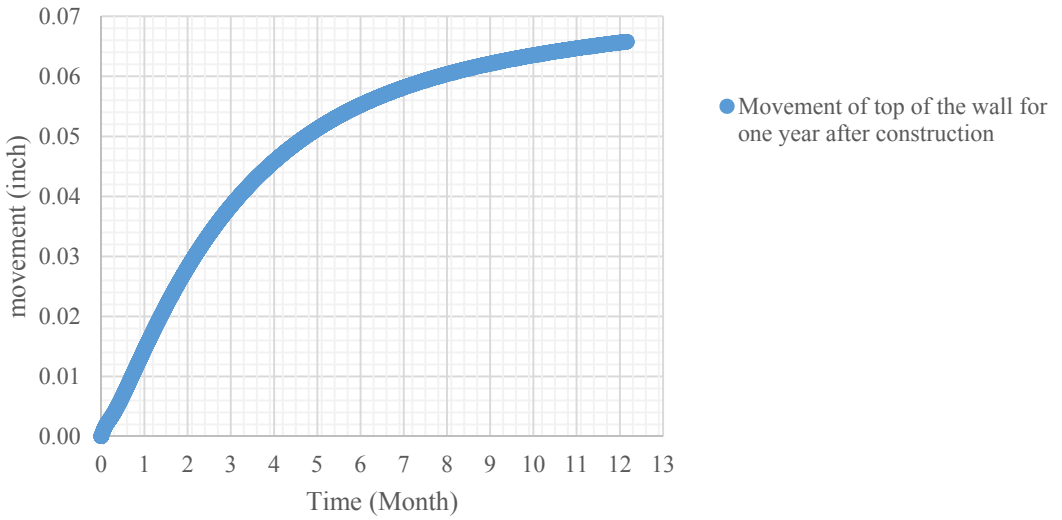

Figure 6-65. Movement of top of the wall for one year after construction (movement of the wall was rezeroed at the end of the construction)

6.9. Outline of Parametric Study

All the subsequent cases included in this parametric study are listed in Table 6-10. The height of the wall in the base line case is 15 ft., Uniform 22 ft. long nails pattern with 3.5 ft. (Horizontal spacing, Sh) by 3ft. (Vertical spacing, Sv) spacing are used in the base case design. Effect of the different parameters on the long-term behavior of the soil nail wall in high plasticity clay are presented as follows.

Table 6-10. Parametric study cases

Material	Properties
Embankment soil	E=2.9e5 psf.*, Drained friction angle Ø'=22, 26*, 30, 36
Soil nail wall height (ft.)	12, 15*, 21
Soil nails length (ft.)	15, 22*, 30
Viscosity	$0.02 < n < 0.04$, $0.05 < n < 0.07$*, $0.07 < n < 0.09$

Note: * indicates the base case parameters

6.9.1. Embankment Soil

As it was discussed in section 6.2.1, since the underline aim of this research is to investigate the long-term behavior of the soil nail wall in high plasticity clay, the drained parameters of the embankment soil are considered. The proper laboratory test (i.e. CU triaxial test) should be performed to obtain these parameters. The drained shear strength of the soil is defined as:

$$\tau = \sigma' \tan(\theta') + c' \quad (6.8)$$

Where σ' is the effective stress, θ' is the drained friction angle, and c' is the drained cohesion. In this parametric study drained cohesion is assumed to be zero.

Horizontal deformation of the soil nail wall at the end of the construction for four different drained friction angle (i.e. 22, 26, 30, and 36 degree) are shown in Figure 6-66.

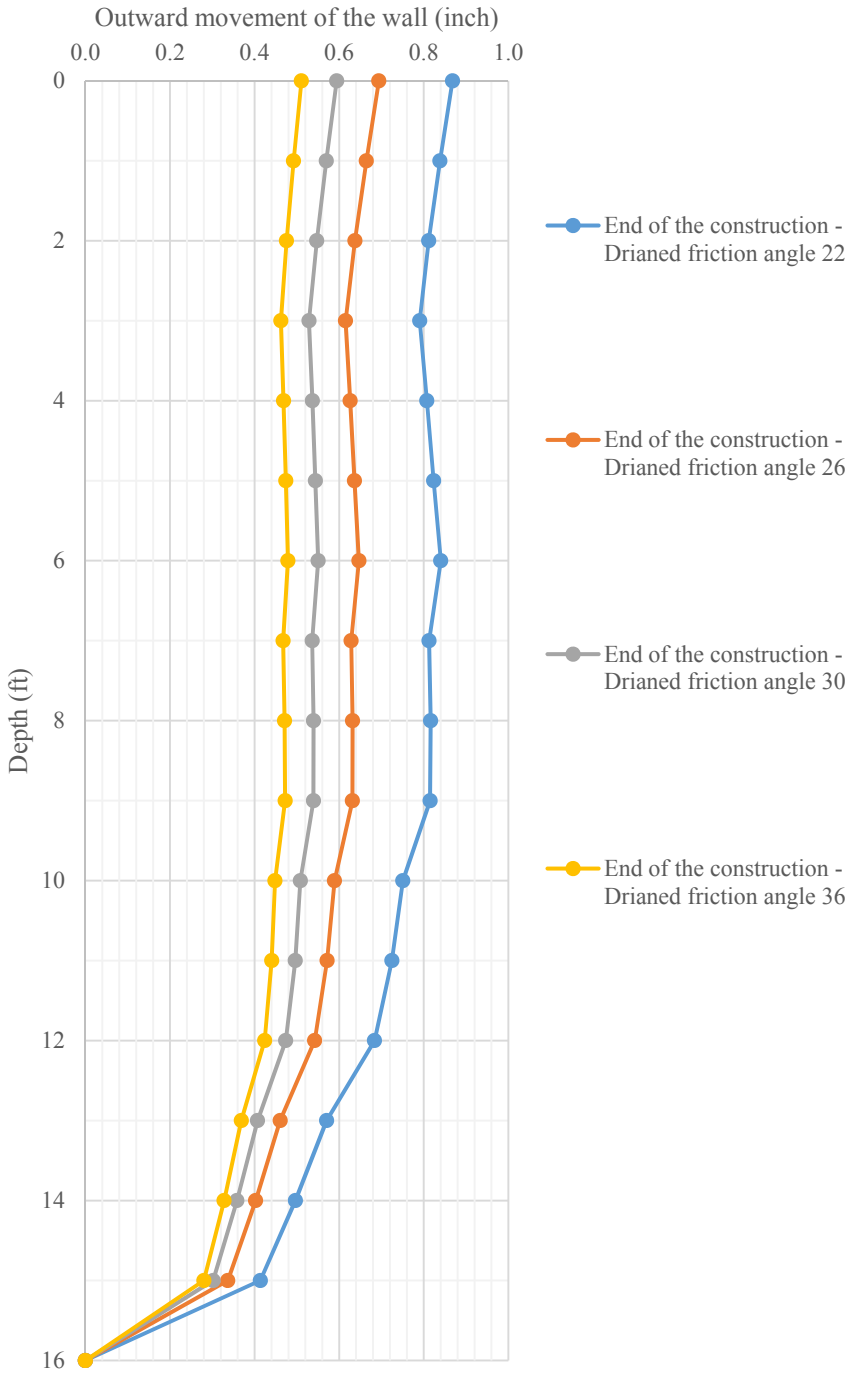

Figure 6-66. Horizontal deformation of the wall at the end of the construction for four different drained friction angle (22, 26, 30, and 36).

It is clear that the movement of the soil nail wall at the end of the construction is smaller than the low drained friction angle. Figure 6-67 present the creep movement of the wall for a period of one year after construction for four different drained friction angle. It is concluded that the creep behavior of the soil nail wall does not depened on the mechanical soil strength parameters such as drained friction angle.

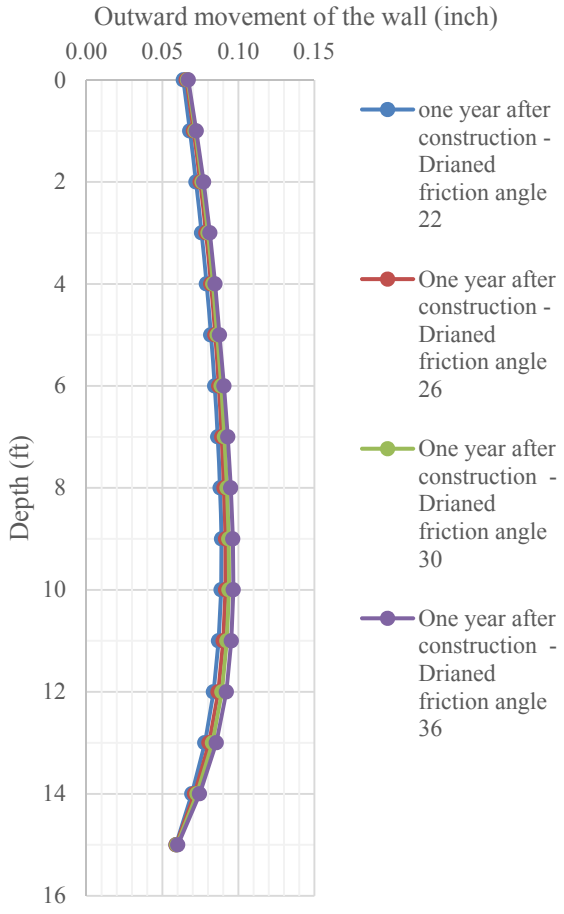

Figure 6-67. Additional axial load in the nails due to the creep of the wall for a period of one year after the construction for different drained friction angle.

6.9.2. Soil Nail Wall Height

Usually the height of the soil nail wall for the Texas turn around varies between 10 and 20 ft. In this parametric study, three different soil nail wall with 12, 15, and 21 ft. height were studied. It is noted that the same soil nails pattern was used in designing the soil nail wall with different height. Same ratio of the length of the soil to the height of the wall was adopted to designing the soil nail walls with different height. Table 6-11 presents the designing for the soil nail walls with different height.

Table 6-11. Soil nail wall design parameters for different height

Height of the soil nail wall (ft.)	L/H (ratio of length of the nails to the height of the wall)	Rows of soil nails	Length of the nails (ft.)	Spacing (Sh x Sv) (ft. x ft.)
21	1.47	7	31	3.5 x 3
15	1.47	5	22	3.5 x 3
12	1.47	4	17	3.5 x 3

The higher soil nail wall (i.e. 21 ft.) exhibit more deformation at the end of the construction (Figure 6-68). Figure 6-69 presents the horizontal deformation of the wall for both at the end and one year after the construction for 12, 12, and 21 ft. height soil nail wall.

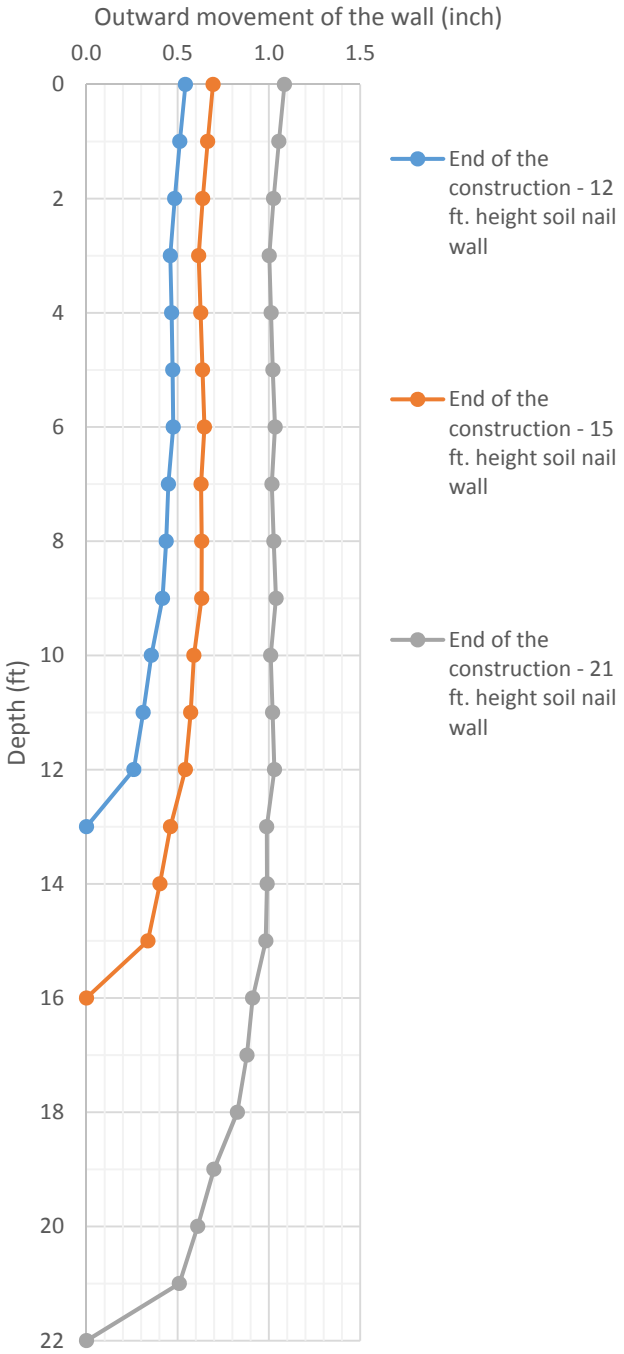

Figure 6-68. Horizontal deformation at the end of the construction for 12, 15, and 21 ft. height soil nail wall

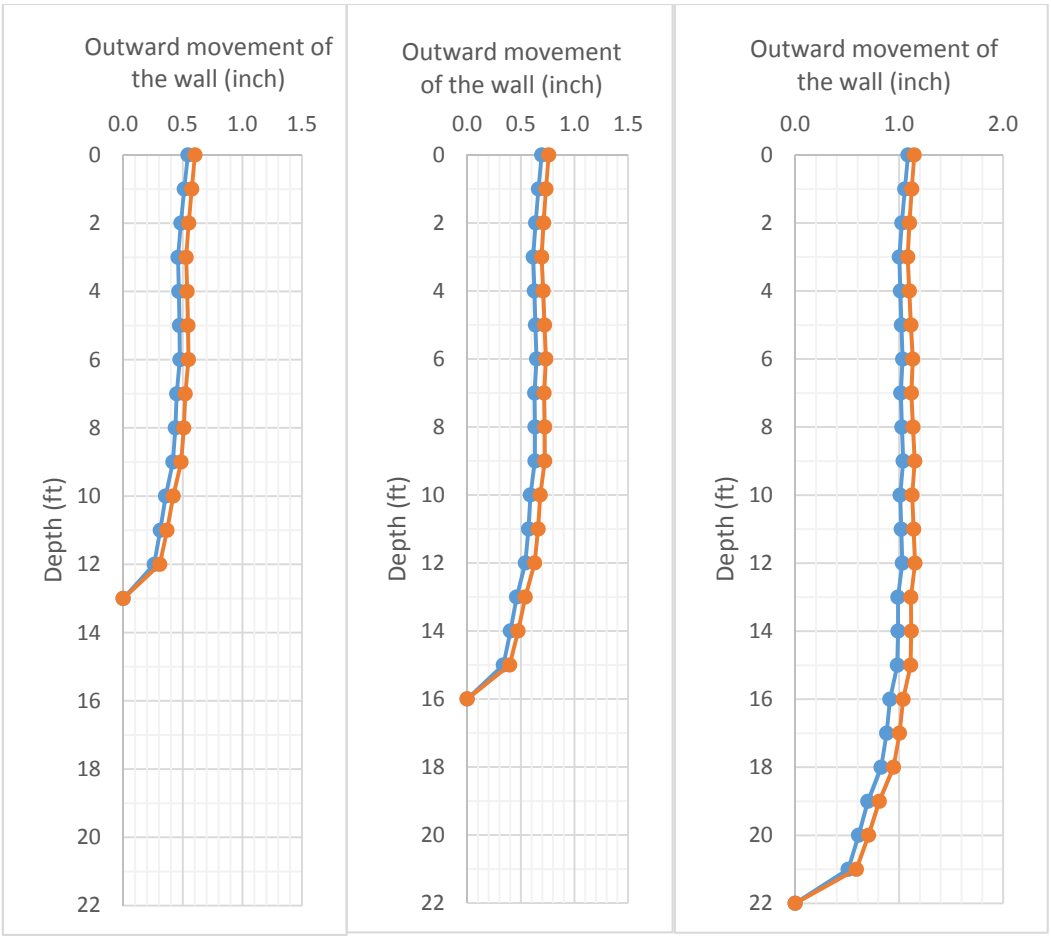

Figure 6-69. Horizontal deformation for one year after the construction for the 12, 15, and 21 ft. soil nail wall (height of the wall from left to wright is 12, 15, and 21 ft.)

It can be seen that the creep behavior of the soil nail wall is the same for all three cases. With the same ratio of the nail to the height of the wall, higher soil nail wall exhibits more creep deformation. Table 6-12 summarizes the ratio of the creep movement respect to the height of the soil nail wall. It is concluded that for all the cases, the maximum creep

movement for one year post-construction was 5e-4 times of the height of the wall, and takes place at the half bottom of the soil nail wall.

Table 6-12. Normalized creep movement of the wall respect to the height of the wall

Depth (ft.)	21 ft. wall	15 ft. wall	12 ft. wall
	creep movement / height of the wall	creep movement / height of the wall	creep movement / height of the wall
0	2.36E-04	3.65E-04	4.14E-04
1	2.66E-04	3.92E-04	4.38E-04
2	2.95E-04	4.16E-04	4.59E-04
3	3.21E-04	4.37E-04	4.75E-04
4	3.44E-04	4.55E-04	4.87E-04
5	3.65E-04	4.70E-04	4.95E-04
6	3.86E-04	4.84E-04	5.01E-04
7	4.06E-04	4.95E-04	5.00E-04
8	4.25E-04	5.03E-04	4.93E-04
9	4.43E-04	5.09E-04	4.77E-04
10	4.58E-04	5.09E-04	4.45E-04
11	4.73E-04	5.01E-04	3.93E-04
12	4.87E-04	4.82E-04	3.27E-04
13	4.97E-04	4.49E-04	-
14	5.04E-04	3.96E-04	-
15	5.07E-04	3.28E-04	-
16	5.05E-04	-	-
17	4.94E-04	-	-
18	4.72E-04	-	-
19	4.37E-04	-	-
20	3.83E-04	-	-
21	3.15E-04	-	-

Table 6-13 presents the axial load at the end and one year after the construction. In all three cases, the maximum load was increased with 50% of the load at the end of the construction.

Table 6-13. Axial load in the nails end and after the construction

Soil nail wall height (ft.)	Max load in the nails at end of the construction (kips)	Max load in the nails one year after the construction (kips)	Increase in the axial load due to the creep (kips)	Increase in the axial load due to the creep (%)
12	4.52	6.5	1.98	43.81
15	5.7	8.44	2.74	48.07
21	8.52	12.5	3.98	46.71

6.9.3. Soil Nail Length

Next parameter to be studied is the length of the soil nail. Horizontal movement of the wall at the end of the construction for 15, 22, and 30 ft. long nails are illustrated in Figure 6-70. It is clear that by increasing the length of the soil nail, the horizontal movement of the wall at the end of the construction is decreased.

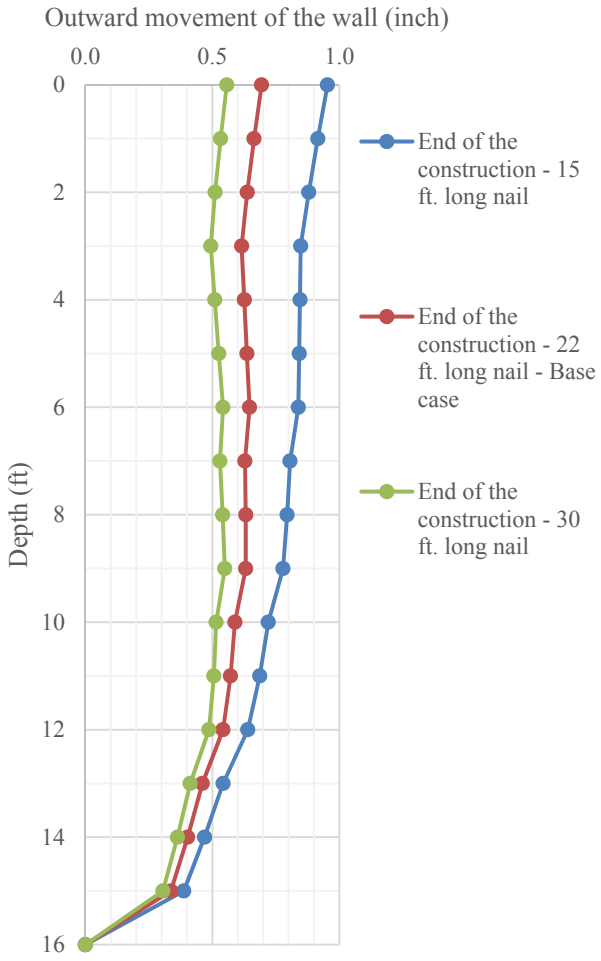

Figure 6-70. Horizontal deformation of the wall at the end of the construction for 15, 22, and 30 ft. long soil nails.

Creep simulation were performed on the soil nail wall with different nails. Figure 6-71 shows the horizontal deformation of the wall for one year after the construction for 15, 22, and 30 ft. long soil nails. It is noted that in order to show the creep deformation after one year, the deformation at the end of the construction was rezeroed.

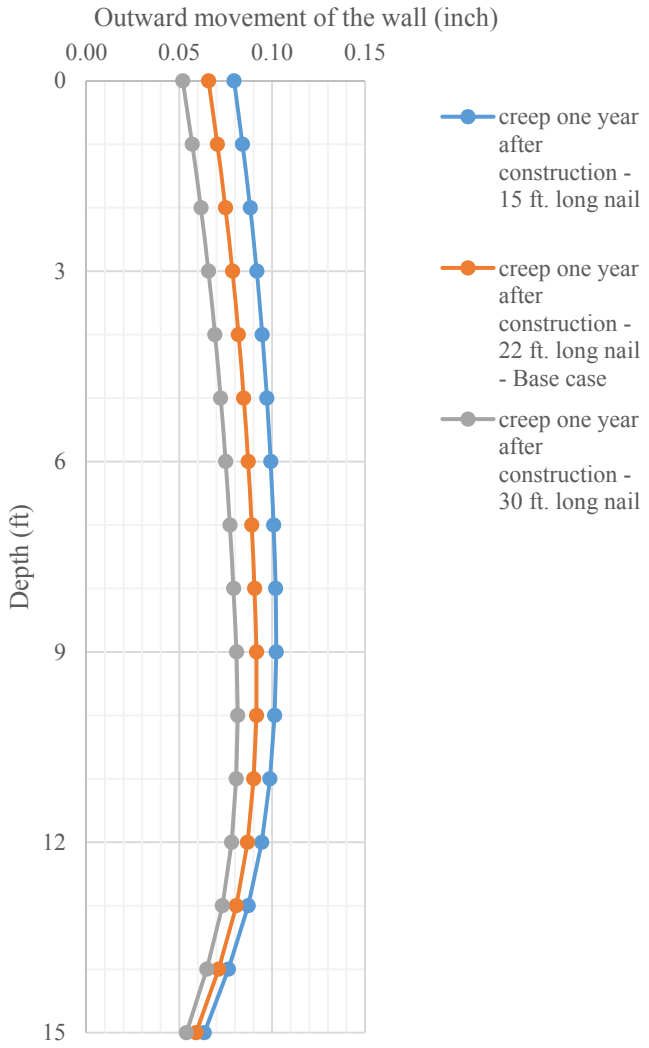

Figure 6-71. Creep deformation of the wall for a period of one year after the construction (horizontal deformation of the wall was rezeroed at the end of the construction).

It can be concluded from Figure 6-71 that the creep movement of the soil nail wall with longer nails is smaller than the shorter nails. However, in all the cases the creep

movement one year after the construction was less than 10% of the horizontal movement soon after the construction. Table 6-14 to Table 6-16 present the axial load in the nails at the end, and one year after construction due to the creep for 15, 22, and 30 ft. long nails.

Table 6-14. Axial load in the nails at the end and after construction for 15 ft. long nail.

Nail#	Max load in the nails at end of the construction (kips)	Max load in the nails one year after the construction (kips)	increase in the axial load due to the creep (kips)	Increase in the axial load due to the creep (%)
	15 ft. long nail	15 ft. long nail	15 ft. long nail	15 ft. long nail
1	3.9	4.18	0.28	7.18
2	4.6	6.2	1.6	34.78
3	5.4	7.3	1.9	35.19
4	5.5	8.3	2.8	50.91
5	0	2.8	2.8	-

Table 6-15. Axial load in the nails at the end and after construction for 22 ft. long nail.

Nail#	Max load in the nails at end of the construction (kips)	Max load in the nails one year after the construction (kips)	Increase in the axial load due to the creep (kips)	Increase in the axial load due to the creep (%)
	22 ft. long nail	22 ft. long nail	22 ft. long nail	22 ft. long nail
1	4.6	5	0.4	8.70
2	4.9	6.2	1.3	26.53
3	5.6	7.8	2.2	39.29
4	5.5	8.3	2.8	50.91
5	0	2.4	2.4	-

Table 6-16. Axial load in the nails at the end and after construction for 30 ft. long nail.

Nail#	Max load in the nails at end of the construction (kips)	Max load in the nails one year after the construction (kips)	increase in the axial load due to the creep (kips)	Increase in the axial load due to the creep (%)
	30 ft. long nail	30 ft. long nail	30 ft. long nail	30 ft. long nail
1	4.7	5	0.3	6.38
2	5.1	6.4	1.3	25.49
3	5.7	8	2.3	40.35
4	5.5	8.3	2.8	50.91
5	0	2.4	2.4	-

It is concluded that maximum load at the end of the construction is almost the same in three different cases. For the period of after the construction, the maximum axial load in the 15, 22, and 30 ft. long nails was increased by 50% of the load at the end of the construction. Therefore, regardless of length of the soil nails, the maximum load due to the creep of the soil nail wall is increased by 50%. In the studied cases, the service load in the fourth nail (for all three cases) at the end of the construction was 5.5 kips, while the maximum load one year after the construction was 8.3 kips.

6.9.4. Viscosity

The key parameter which affects the long-term behavior of the soil nail wall is the viscosity of the soil. The soil with high plasticity Index has the potential to creep, but the true creep behavior of the high plasticity clay depends on the current water content of the soil. LI of the soil at NGES-TAMU clay site and the Beaumont site are less than 0.2. In the context of this research, UU triaxial creep tests were performed on the soil samples

from NGES-TAMU clay site and the Beaumont site. The correlation obtained between n value and viscosity of the soil was used to adopt the viscos parameters for the soil nail wall. In this section, effect of different n value is investigated on the creep behavior of the soil nail wall. Table 6-17 presents the different n value and viscos parameters adopted in this parametric study. It is noted that the viscos behavior of the soil nail wall system is different from the viscos behavior of the soil samples. This behavior can be explained as the effect of the size of the soil sample compare to the height of the soil nail wall (i.e. height of the soil sample is 7 inch, while height of the soil nail wall is 25ft.). The numerical model is calibrated with the result of the UU creep test on the soil sample from the Beaumont project and instrumentation and post-construction monitoring the soil nail wall.

Table 6-17. Different viscosity parameters adopted in this parametric study.

N value
$0.02 < n < 0.04$
$0.05 < n < 0.07$*
$0.07 < n < 0.09$

*Indicates the behavior of the soil at the Beaumont project

Figure 6-72 illustrates the creep deformation of the soil nail wall for one year after construction for three different cases. The creep movement of top of the wall for one year post-construction is plotted in Figure 6-73.

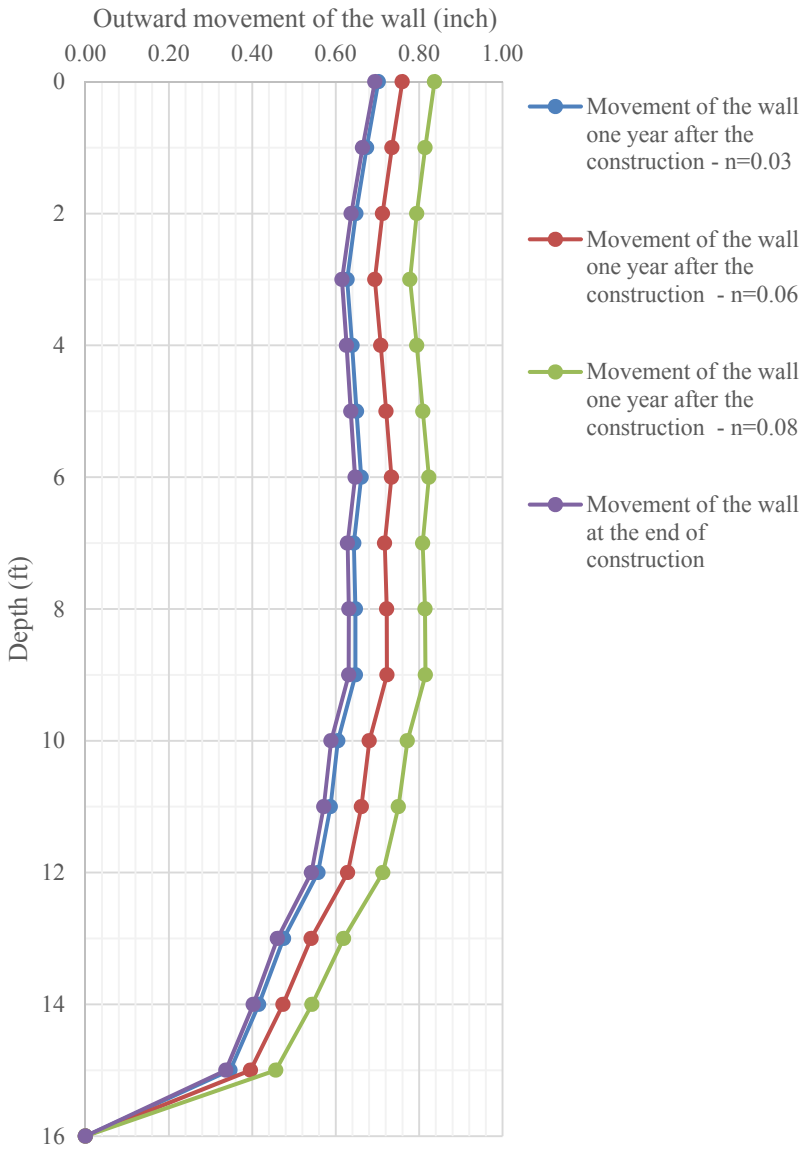

Figure 6-72. Creep deformation at top of the soil nail wall with different viscosity

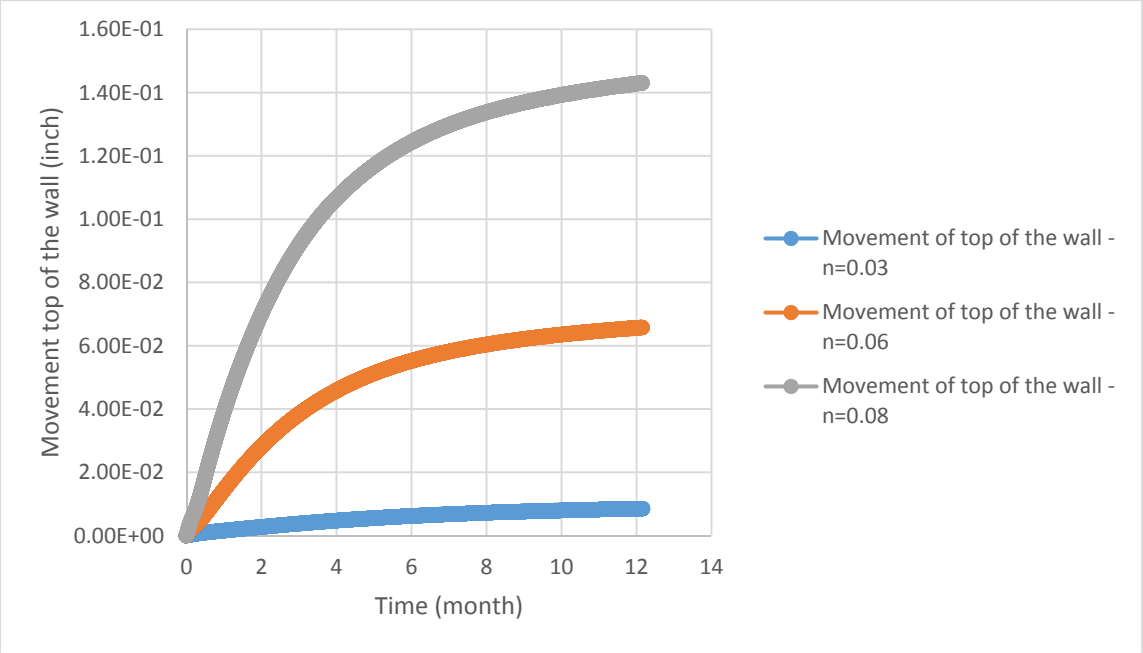

Figure 6-73. Creep deformation at top of the wall of the soil nail wall with different viscosity

It can be seen that the n value (i.e. viscosity of the soil) plays a significant role in the long-term behavior of the soil nail wall. Soil nail wall includes the soil with higher n value exhibits more creep behavior. It is worth mentioning that the n for the soil at NGES-TAMU clay site is between 0.02 and 0.04, while the n from the Beaumont project varies between 0.05 and 0.07. Typical range of n value for clay varies between 0.02 and 0.08 (Briaud, 1985).

7. CONCLUSION AND PROPOSAL FOR FUTURE WORK

7.1. Summary and Conclusion

An aspect of particular concern in the soil nail wall manual and construction guideline, Geotechnical Engineering Circular No. 7 on Soil Nail Walls, is the creep behavior of soil nail systems in high-plasticity (HP) clays. Since there were not enough information on creep behavior of soil nail systems in high-plasticity clay, this matter was addressed in this manual based on some practices in fine-grained soil with Plasticity Index (PI) more than 20 which exhibited unfavorable creep. This research is aimed to gain a better understanding of the long-term behavior of the soil nail walls in fine-grained soil with plasticity index more than 20. Therefore, this research combined experimental and numerical studies to investigate the performance of the soil nail wall in high plasticity clay.

Two different kinds of tests were performed at NGES-TAMU clay site. Tests on existing anchors installed more than 20 years ago (with a very well-known load history), and tests on new soil nails constructed in the context of this research. These tests mainly focus on studying the effect of the load level on creep behavior of soil nails in HP clays. Results of the pullout test at the NGES-TAMU clay site can be summarized as:

- The ultimate pullout capacity of the anchors in 2013 increased by almost 60%, when compared against the corresponding value measured in 1997. The comparison of the tests results on anchors tested in 1991 and in 1997 shows that there was a gain of 20% on the strength, and between 1997 and 2013 there was a gain of 60% of the strength. This gain in strength could be due to long term aging effects and past loading history.

- It is concluded that the load threshold for creep failure is about 90% of the ultimate pullout capacity of the nails. The range of the creep movement for all the tested nails indicate that the creep movement for the load less than 90% of the ultimate load is remarkably below the acceptance criteria. Creep movement higher than the acceptance criteria happens just at failure load or at the loads greater than 90% of the failure load.
- The maximum friction between grout and the soil obtained from the tests in dry season (low water content) is significantly higher than the corresponding value obtained from the tests in wet season (high water content). Variations in water content of the soil in different season change the in-situ undrained shear strength of the soil and consequently the maximum friction between grout and the soil.
- Viscous exponent *n* obtained from the tests on the nails varies between 0.01 and 0.02 for the load less than 90% of the pullout capacity of the nails. It is concluded that the creep behavior of the soil below the failure load is almost constant and well below the acceptance criteria.
- Results of cyclic loading tests on the nails indicate that the creep behavior of the soil nails is influenced by the cyclic loading. Creep movement during the first cycle is greater than the other cycles.
- The cracking strain for the grout is assumed to be 100 $\mu\varepsilon$ (100 x 10^{-6} in/in). The measured strains showed that most of the grout surrounding the threadbare was cracked. Since the measured strain exceeds the cracking strain in grout, the load on the nails is related directly to the measured tensile strain of the threadbar.

An emergency slope repair at the Beaumont District was selected to instrument monitor the time-dependent behavior of the soil nail wall in high plasticity clay. The PI of the embankment material is around 50; which made this project a very unique for the field tests and monitoring. Inclinometer casings and tiltmeters were installed to track the wall deformation during the time. A total of nine production nails were instrumented and installed at two different sections. Three of them were instrumented with load cells at the nail head. Water content probes were installed at different depths.

Furthermore, six sacrificial nails were installed at three different depths. Three of them were instrumented with foil strain gauges. Verification and modified creep tests were performed on the sacrificial nails. Following conclusion can be made from the instrumentation of the soil nail wall at Beaumont project:

- Factor of safety for design bond stress at top of the soil nail wall is 2.5 (i.e. maximum friction between the grout and the surrounding soil is 2.5 times of the design friction between the grout and the surrounding soil), while for the nails at bottom of the wall the factor of safety is almost 4.
- For the tested sacrificial nails at Beaumont project, creep rate is increased with increasing the load level. The creep rate is significantly below the acceptance criteria for the load less than 90% of the failure load.
- Maximum lateral displacement takes place at top of the wall and decrease towards the toe of the wall. Maximum horizontal displacement at top of the wall at the end of the construction was 1.85 inch which is 0.006 times of the height of the wall (i.e. 25 ft.).

- The results of the inclinometer showed the creep deformation of top of the wall for a period of one year after construction was 0.2 inch. which is 10% of the deformation observed soon after construction (1.85 inch).
- The service load (load at the end of the construction) in the nails is maximum 60% of the design load and maximum 22% of the maximum pullout capacity of the nails.
- Significant portion of the axial load in the nails takes place in the subsequent excavation. Therefore, the axial load in the last row of the soil nails at the end of the construction is remarkably low compare to the axial load in the other production nails.
- The soil nail wall exhibited the extra horizontal deformation after the construction (i.e. due to the creep). As a results of this movement, additional tension load was developed in the nails. The maximum additional load in the nails was maximum 30% of the service load. . But even with the additional load in the nail due to the creep behavior of the soil nail wall, the service load of the nails for a period of one year after the construction is 80% of the design load of the nails, and less than 30% of the maximum pullout capacity.
- It is concluded from the results of the water content probes installed at the Beaumont project at different depth of the wall that the variation of the moisture content of the embankment soil is almost 4- 5% during the wet season and dry season.

The performance of soil nail walls depends on the interaction between the soil, nails and facing. Additionally, many other parameters affect the performance of soil nail walls such as nail inclination, method of nail installation, grouting and construction. Numerical modeling using FLAC3D was carried out to determine the performance of the

wall. The model was calibrated using the information obtained from monitoring the Beaumont project. The viscoelastic model (Burger) available in FLAC3D was adopted to simulate the long-term behavior of the soil nail wall. The rheological model parameters were obtained from modeling the UU triaxial creep tests. The validated model used to perform the parametric study on the typical Texas turn around. It is concluded from the results of the parametric study that the key parameter influencing on long-term behavior of the soil nail wall is the viscous behavior (n value) of the embankment soil.

High plasticity clay exists in many areas of Texas. Texas clay has the potential of creep if the moisture content of the soil is increased. In normal conditions, the natural moisture content of this kind of soil is very close to plastic limit of the soil. The results of the laboratory tests show that the measured liquidity index of the soil at NGES-TAMU clay site and the Beaumont project is less than 0.1. Post-construction monitoring of the natural moisture content of the soil at Beaumont soil nail wall shows that the water content of the embankment soil is changed by 5% in the wet season. Even with increasing the water content of the embankment, LI of the soil is less than 0.2. Monitoring the Beaumont wall and the numerical modeling revealed that the maximum horizontal deformation of the wall due to the creep one year after the construction is less than 10% of the horizontal deformation of the wall soon after the construction. According to GEC#7, the horizontal deformation of the wall after construction usually increases up to 15% compared to the deformation observed soon after construction, and this movement is already considered in the safety factors applied in designing the soil nail wall.

As a results of this movement (i.e. due to the post-construction creep movement of the wall), additional tension load is developed in the nail. According to the Beaumont wall inspection and the numerical modeling, the maximum additional axial load is developed in the row before the last row of the soil nails. The maximum additional load is 50% of the axial load in the nails at the end of the construction for the bottom third of the wall. Even with additional 50% axial load, the service load (load in the nail after creep) of the nails in the bottom third of the wall is less than 30% of the maximum pullout capacity of the nails.

In order to investigate the creep behavior of the high plasticity soil, performing the UU triaxial creep test is recommended. The soil with *n* value between 0.02 and 0.06 was studied in this research.

7.2. Proposal for Future Works

In this work, long term behavior of soil nail wall in high plasticity clay with liquidity index less than 0.2 has been studied. There are many different aspects associated with the short-term and long-term behavior of the soil nail wall in high plasticity clay which requires careful attention. This study addressed some of those problems, and some possible solutions were proposed. However, there are still many problems in this area which should be thoroughly investigated.

Results of the pullout test on the nails installed at NGES-TAMU clay site (i.e. section four) showed that the maximum pullout capacity of the nails or bond stress at the interface of soil-grout was different at the different season. The friction of the soil-grout interface per unit of the length was two times more than the corresponding value in wet

season. Further study is needed to gain a better understanding of the physical phenomena, and appropriately select this parameter in designing the maximum pullout capacity of the nails.

In this research, to investigate the creep behavior of the soil, UU triaxial creep tests were performed on the soil samples from NGES-TAMU clay site and the Beaumont project. However, further UU triaxial creep tests on different soil sample with different liquidity index is needed to generate the relation between the *n* value and liquidity index of the soil.

Many researchers have studied the viscous behavior of the soil with higher liquidity index. The shear viscosity for the soil with water content higher than liquid limit can be determined with viscometer, but there is no standard method to determine the shear viscosity of the soil with low water content (LI<0.5). Future study to determine the shear viscosity of the high plasticity clay with LI<1 should be carried out.

REFERENCES

Akhavan, M., Ghareh, S., & Naeini, M. B. (2011). "Comparing the Results of Numerical Analysis and Monitoring about the Behavior of Cracks Occurred Nearby Soil-Nailing Walls". Electronic Journal of Geotechnical Engineering, 16.

Babu, G. S., & Singh, V. P. (2009). Simulation of Soil Nail Structures Using PLAXIS 2D. Plaxis Bulletin. Plaxis.

Banerjee, S., Finney, A., Wentworth, T. & Bahiradhan, M. (1998). "Evaluation of Design Methodologies for Soil-Nailed Walls, Volume 1. Report No. WA-RD 371.1.Washington State Department of Tranportation.

Barrows, R. J. (1994). "Two Dimensional Finite Element Modeling of Swift Delta Soil Nail Wall by ABAQUS" (Doctoral Dissertation, Portland State University, Oregon).

Briaud, J.L., & Garland, E. (1985). "Loading Rate Method for Pile Response in Clay". J. Geotech. Engrg., 111(3), 319–335.

Briaud, J.L., & Gibbens, R. (1999). "Behavior of Five Large Spread Footings in Sand. J. Geotech. Geoenviron". Eng., 125(9), 787–796.

Briaud, J.L., Griffin, R., Yeung, A., Soto, A., Suroor, A., & Park, H. (1998) "Long-Term Behavior of Ground Anchors and Tieback Walls". Report No. FHWA/TX-99/1391-1. August, 1998.

Briaud, J.L., Lim, Y. (1997). “Soil Nailed Wall Under Piled Bridge Abutment: Simulation and Guidelines”. Journal of Geotechnical and Geoenvironmental Engineering, 123(11), 1043-1050.

Briaud, J.L., Powers, W.F., Weatherby, D.E. (1998) “Should Grouted Anchors Have Short Tendon Bond Length?”. J. Geotech. Geoenviron. Eng., 124(2), 110–119.

Bingham, E. C. (1917). An Investigation of the Laws of Plastic Flow (Vol. 13, No. 2). Govt. Print. Off.

Byrne, R. J., Cotton, D., Porterfield, J., Wolschlag, C., & Ueblacker, G. (1996). Manual for Design and Construction Monitoring of Soil Nail Walls (No. FHWA-SA-96-069,).

Bryne, R. J. (1998). “Manual for Design & Construction Monitoring of Soil Nail Walls”. US Department of Transportation, Federal Highway Administration.

Chu, L. M., & Yin, J. H. (2005). “A Laboratory Device to Test the Pullout Behavior of Soil Nails”. Geotech. Test. J., 28(5), 1–15.

Chu, L.-M., & Yin, J. H. (2006). “Study on Soil-Cement Grout Interface Shear Strength of Soil Nailing by Direct Shear Box Testing Method”. Geomech.Geoeng. 1(4), 259–273.

Dornfest, E.M., Nelson, J.D. & Overton, D.D. (2007). “Case History and Causes of a Progressive Block Failure in Gently Dipping Bedrock”. Proceedings of the First North American Landslide Conference, Colorado.

Eckardt, H. (1982). “Creep Tests with Frozen Soils Under Uniaxial Tension and Uniaxial Compression”. Proceedings of the 4th Canadian Permafrost Conference, Calgary, Alberta, National Research Council of Canada, 365–373.

Fakher, A., Jones, C. J., & Clarke, B. G. (1999). Yield Stress of Super Soft Clays. Journal of Geotechnical and Geoenvironmental Engineering, 125(6), 499-509.

Fan CC, & Luo JH (2008). “Numerical Study on the Optimum Layout of Soil Nailed Slopes”. ComputGeotech 35(4):585– 599

Feda, J. (1992). Creep of Soils and Related Phenomena. Elsevier.

FHWA, Federal Highway Administration, (1998) "Manual for Design and Construction Monitoring of Soil Nail Walls." Publication No. FHWA-SA-96-069R. Revised October 1998. pp. 35. Department of Transportation

Galvan (2012). “TxDOT Bridge Division, Proposal Meeting RMC5 - 0-6784”.

GEC#7, FWHA, Federal Highway Administration, (2003) “Geotechnical Engineering Circular No. 7: Soil Nail Walls”. Report No: FHWA0-IF-03-017, Department of Transportation.

Geoguide 7 (2008). “Guide to Soil Nail Design and Construction - Geoguide 7”. Geotechnical Engineering Office; Civil Engineering and Development Dept., Government of Hong Kong Special Administrative Region, Hong Kong

Havel, F. (2004). “Creep in Soft Soils”. Ph.D. Thesis, Norwegian University of Science and Technology.

Hunter, G. & Khalili, N. (2000). “A Simple Criterion for Creep Induced Failure of Over-Consolidated Clays”. Pro.GeoEng 2000 Conference, Melbourne.

Itasca, (2006) , FLAC3D v.4.0 Manual , “Fast Lagrangian Analysis of Continua in 3D Dimension Version4.0, Online Maanual.”

Jeong, S.W. (2013). Determining the Viscosity and Yield Surface of Marine Sediments Using Modified Bingham Models. Geosciences Journal 17(3), 241–247.

Juran, I., Baudrand, G., & Farrag, K. (1990). “Kinematical Limit Analysis for Soil Nailed Structures.” J. Geotech. Engeg. Div., ASCE, 116(1), 54-73.

Keedwell, M. J. (1984). Rheology and Soil Mechanics. London: Elsevier Applied Science.

Li, J., Tham, L.G., Junaideen, S.M., Yue, Z.Q., & Lee, C.F. (2008). “Loose Fill Slope Stabilization with Soil Nails: Full-Scale Test”. J GeotechGeoenvironEng 134(3):277–288.

Locat, J., & Demers, D. (1988). Viscosity, Yield Stress, Remolded Strength, and Liquidity Index Relationships for Sensitive Clays. Canadian Geotechnical Journal,25(4), 799-806.

Ludwig, H., Weatherby, D.E. & Schnabel, H. (1985). “Research on Tiebacks Anchored in Cohesive Soils”. Proceedings of the 11th International Conference on Soil Mechanics and Foundation Engineering, San Francisco, 1721-1724.

Ludwig, H. (1984). “Short-Term and Long-Term Behavior of Tiebacks Anchored in Clay”. Ph.D. Thesis, McGill University.

Mahajan, S. P., & Budhu, M. (2006). Viscous Effects on Penetrating Shafts in Clays. Acta Geotechnica, 1(3), 157-165.

Maric, B., Kvasnička, P., Radaljac, D., &Mavar, R. (2001). “An Example of a High Soil Nailed Wall in Plastic Clayey Soil”. International Symposium on Earth Reinforcement.

Martinez-Vasques, J.J. & Diaz-Rodriguez, J.A. (2009). “Creep Behavior of an Undisturbed Lightly Overconsolidated Clay”. Proceedings of the 17th International Conference on Soil Mechanics and Geotechnical Engineering: The Academia and Practice of Geotechnical Engineering, Egypt, Volume 1, 229-232.

Menkiti, M. C., & Long, M. L. M. (2008). “Performance of Soil Nails in Dublin Glacial Till”. Canadian Geotechnical Journal, 45(12), 1685-1698.

Mitchell, J.K. (1993). “Fundamentals of Soil Behavior,” Second Edition, Wiley, New York.

Mitsoulis, E. (2007). Flows of Viscoplastic Materials: Models and Computations. Rheology Reviews, 135178.

O'Donovan, E. J., & Tanner, R. I. (1984). Numerical Study of the Bingham Squeeze Film Problem. Journal of Non-Newtonian Fluid Mechanics, 15(1), 75-83.

ODOT (1999). “Monitoring of Soil Nailed Walls at the Highway 217 and Highway 26 Interchange Final Report”. Oregon Department of Transportation.

Ohtsuki, H., Nishi, K., Okamoto, Z. & Tanaka, S. (1981). “Time Dependent Characteristics of Strength and Deformation of a Mudstone”. Proceedings of the Symposium on Weak Rock, Tokyo, 1, 119-124.

Olia, A., & Liu, J. (2011). "Numerical Investigation of Soil Nail Wall During Construction". 2011 Pan-Am CGS Geotechnical Conference, Oct 2-6, 2011, Toronto, Canada.

Oral, T., & Sheahan, T. C. (1998). The Use of Soil Nails in Soft Clays. In Design and Construction of Earth Retaining Systems (pp. 26-40).ASCE.

Ostermayer, H. (1975). "Construction, Carrying Behavior and Creep Characteristics of Ground Anchors". Proc. Diaphragm Walls and Anchorages Conference, Institute of Civil Eingeers, London, 141-151.

Pestana, J. M., & Whittle, A. J. (1995). "Compression Model for Cohesionless Soils." Geotechnique, 45(4), 611–631.

Pestana,J.M., & Whittle, A. J. (1998). "Time Effects in the Compression of Sands." Geotechnique, 48(5), 695–701.

Plaxis 2D Manual (2012). "Material Models Manual". Plaxis 2012

Powers, W.F. (1993) "Behavior of 10 full-scale Ground Anchors Installed in Stiff Clay". MS Thesis, Texas A&M University.

Plumelle, C., Schlosser, F., Delage, P., & Knochenmus, G. (1990) ''French National Research Project on Soil Nailing: Clouterre.'' Design and Performance of Earth Retaining Structures, P. C. Lambe & L. A. Hansen, eds., Geotechnical Special Publication No. 25, ASCE, Reston, Va., 660–675.

Pradhan, B., Yue, Q. Z. Q., Tham, L. G., & Lee, C. F. (2003). "Laboratory Study of Soil Nail Pullout Strength in Loosely Compacted Silty and Gravelly Sand Fills". 12th

Panamerican Conf. on Soil Mechanics and Geotechnical Engineering, 39th U.S. Rock Mechanics Symp.,VerlagGluckauf Essen, Germany, 2139–2146.

Recommendations Clouterre, (1991). English Translation of the: "French Soil Nailing Recommendation -1991. For Designing, Calculating, Constructing and Inspecting Earth Support System Using Soil Nailing (by Plumelle, Schlosser et al., 1990). Federal Highway Administration.FHWA-SA-93-026.

Sakr, C.T. & Kimmerling, R. (1995). "Soil Nailing of a Bridge Fill Embankment". Report N° OR 89-07.Oregon Department of Transportation.

Sanzeni, A., Whittle, A., Germaine, J., & Colleselli, F.(2012) "Compression and Creep of Venice Lagoon Sands". J. Geotech. Geoenviron. Eng., 138(10), 1266–1276.

Segalini, A., Giani, G. P., & Ferrero, A. M. (2009). Geomechanical Studies on Slow Slope Movements in Parma Apennine. Engineering Geology, 109(1), 31-44.

Shiu, Y. K., & Chang, G. W. K. (2006). "Effects of Inclination, Length Pattern and Bending Stiffness of Soil Nails on Behaviour of Nailed Structures". Geotechnical Engineering Office, Civil Engineering and Development Department.

Singh, V.P. & Babu, G.L.S. (2010). "2D Numerical Simulations of Soil Nail Walls". Geotech Geology Engineering, 28, 299 – 309.

Smith, T.D. (1993). "A Numerical Investigation into the Performance of the Soil Nail Wall and Pile Foundation at the Swift Delta I-5 Interchange". Report No. FHWA-OR-RD-95-15.Oregon Department of Transportation.

Su, L. J. (2006). “Laboratory Pullout Testing Study on Soil Nails in Compacted Completely Decomposed Granite fill”. Ph.D. Thesis, Hong Kong Polytechnic Univ., Hong Kong.

Su, L. J., Chan, T. C. F., Shiu, Y. K., Cheung, T., & Yin, J. H. (2007). “Influence of Degree of Saturation on Soil Nail Pullout Resistance in Compacted Completely Decomposed Granite Fill”. Can. Geotech. J., 44(11), 1314–1428.

Su, L.,Chan, T., Yin, J., Shiu, Y., & Chiu, S. (2008). “Influence of Overburden Pressure on Soil–Nail Pullout Resistance in a Compacted Fill”. J. Geotech. Geoenviron. Eng., 134(9), 1339–1347.

Taib, S.N.L. & Craig, W.H. (2006). “Modeling Construction and Failure of Soil Nailed Structures in Clay”. Physical Modelling in Geotechnics. Proceedings of the Sixth International Conference on Physical Modelling in Geotechnics, 6th ICPMG '06, Hong Kong, 577-583.

Tavenas, F. & Leroueil, S. (1981). “Creep and Failure of Slopes in Clays”. Canadian Geotechnical Journal, 1981, 18(1): 106-120

Tian, T. (2011). “Numerical Study of Different Creep Models Used for Soft Soils”. MS Thesis, Chalmers University of Technology.

Tuozzolo, T. (2003). “Soil Nailing: Where, When and Why. A Practical Guide”. 20th Central Pennsylvania Geotechnical Conference Hershey, PA.

Turner, J.P. & Jensen, W.G. (2005). “Landslide Stabilization Using Soil Nail and Mechanically Stabilized Earth walls: Case Study”. J. Geotech. Geoenviron. Eng.,131(2), 141–150.

Turner, L.L. & Parnell, J. (2006). “CalNail – A Design Tool for Soil Nail Projects Using Field Case Histories. Report No. F/CA/IR-2006/05”. California Department of Transportation.

TxDOT (2006). “Geotechnical Manual”. Texas Department of Transportation, Texas.

Vermeer, P. A., & Neher, H. P. (1999). “A Soft Soil Model that Accounts for Creep”. In Proceedings of the International Symposium: Beyond 2000 in Computational Geotechnics(pp. 249-261).

Vulliet, L., Desai, C.S. (1989). “Viscoplasticity and Finite Elements for Landslide Analysis”, XII ICSMFE.

Vyalov, S. (1986). “Rheological Fundaments of Soil Mechanics”. Developments in Geotechnical Engineering Vol. 36. Elsevier.

Weatherby, D.E. (1982). “Tiebacks”. Report No. FHWA/RD-32/047, U.S. Department of Transportation, Washington, D.C.

Weatherby, D.E. (1998). “Design Manual for Permanent Ground Anchor Walls”. Report No. FHWA/RD-97/130, U.S. Department of Transportation, Washington, D.C.

Whitman, R. V. (1957). The Behavior of Soils Under Transient Loadings. In Proc. 4th International Conference on Soil Mechanics and Foundation Engineering (Vol. 1, p. 207).

Yong, R. N., & Japp, R. D. (1967). A Flow Law for Clays in Dynamic Compression. McGill University, Soil Mechanics Laboratory.

Yelti, N. (2011). “Analysis and Design of Soil Nail Walls in High Plasticity Clays”. MS. Thesis, Dept. of Civil and Environmental Engineering, The University of Texas at San Antonio.

Yin, J.-H., Su, L.-J., Cheung, R.W.M., Shiu, Y.-K., & Tang, C. (2009). “The Influence of Grouting Pressure on the Pullout Resistance of Soil Nails in Compacted Completely Decomposed Granite Fill”. Geotechnique, 59(2), 103 –113.

Yin, J. H. & Su, L. J. (2006). “Innovative Laboratory Pull-Out Boxes for Study of Soil Nail Pull-Out Shear Resistance”. Geotech. Test. J., 29(6), 451–461.